ENDOCANNABINOID-BASED NANOPARTICLES TARGETED TO THE SYNOVIUM FOR THE TREATMENT OF ARTHRITIS

by

Nicola Barrie

A thesis submitted in fulfilment of the requirements for the degree of Doctor of Philosophy in Medicine

UNIVERSITY OF SYDNEY

SYDNEY MEDICAL SCHOOL, DEPT OF RHEUMATOLOGY

SYDNEY, AUSTRALIA

2019

DECLARATION

The work contained within this thesis is original research performed at the research laboratory of Department of Rheumatology, University of Sydney, located at Westmead Hospital, Sydney, Australia and at Manufacturing, CSIRO, North Ryde, Sydney, Australia.

In-vivo experiments conducted at the Kolling Institute's Kearn's Animal Facility located within Royal North Shore Hospital, Sydney were performed in accordance with Sydney Northern Area Health Animal Ethics Guidelines (Ethics Approval Number: RESP 15/15). *In-vivo* experiments conducted at Westmead Hospital Animal House, were performed under a protocol approved by the Westmead Hospital's Animal Ethics Committee (Ethics Approval Number: 5105.08.12.)

I hereby declare that this submission is my own work, and that to the best of my knowledge and belief, contains no material previously published or written by another person except where due reference is made in the text, nor has this work been submitted for the award of a higher degree at any other institution.

Nicola Barrie

30th April 2019

DEDICATION

I dedicate this thesis, and all that I ever achieve in my life to my beloved older brother, Jayden Bronson Barrie. Your brilliance, leadership and unwavering love inspired all those around you and made me into the person I am today. My love and admiration for you is beyond anything I could ever articulate in words. You were like no one else and you will live on in all that I do. Thank you for everything.

ACKNOWLEDGEMENTS

The PhD project undertaken was a culmination of the efforts of many individuals, whom I would like to express my deepest appreciation towards.

I would firstly like to thank my supervisor, Prof. Nicholas Manolios, for his continued support and for the opportunities provided for me throughout my PhD. I am deeply indebted to Dr. Minoo Moghaddam for the opportunity to work and complete part of my PhD in her laboratory. I would also like to thank my co-supervisor Dr. Marina Ali for her encouragement, guidance and in particular her calming presence which focused me in chaotic times. The time and effort my supervisors expended on me, as well as the encouragement and on-going support both in and out of the lab I am truly grateful for.

I would also like to thank my colleagues; Beatrice Chung, Dr. Kevin Hou and Dr. Amita Limaye within the Rheumatology Department at Westmead Hospital and; Jerikho Bulanadi and Dr. Nelly Gong, from Manufacturing at CSIRO for their continued support and friendship. I am also grateful to Dr. Vera Bender for her expertise and input in the early part of this project.

I would also like to thank Dr. Suat Dervish, Dr. Hong Yu, Dr. Joey Lai, Dr. Steven Schibeci and Virginia James for their support and assistance with all experiments undertaken at the Westmead Millennium Institute; Dr. David Booth, Dr. Rosemarie Sadsad and especially Tracy Chew for their expertise and assistance with RNA-seq analysis; Dr. Jordyn Stuart and Dr. Jonathan Arnold from the Lambert Institute for their helpful discussion on the endocannabinoid system and assistance with sample processing; Dr. Liliana De Campo and Dr. Robert Knott from ANSTO for their patience and help in performing SAXS experiments; Dr. Jacinta White for cyro-TEM imaging; Dr. Raphael Dye and all the staff at both the animal holding at Weatmead Hospital and at the Kolling Institute at Royal North Shore Hospital for their support and help with the animal work undertaken herein.

Lastly, I would to thank my parents, John and Gay, for their hard-work, guidance and support. To my brothers; Keegan and Jayden, and lastly my grandma, Leela, for their support and love for all that I do. In particular I would like to thank my uncle Anandh. I am so deeply grateful for all the late night, last minute help, words of wisdom and leadership. Your dedication to your family, courage and professionalism at work inspires me and someone I hope to emulate in the future.

TABLE OF CONTENTS

PRESENTATIONS AND CONFERENCE ATTENDANCE

2017 Barrie N, Ali M, Moghaddam MJ and Manolios M. Cannabis-based nanoparticles targeted to the synovium for the treatment of arthritis. Abstract and oral presentation at 39th Annual ARA Meeting, November 2017, Wollongong, Australia.

2017 Barrie N, Ali M, Moghaddam MJ and Manolios M. Investigation of endocannabinoid lipid nanoparticles targeted to the synovium for the treatment of arthritis. Abstract and poster presented at The 46th Annual scientific meeting; The Australasian Society for Immunology, November 2017, Brisbane, Australia.

2017 Barrie N, Ali M, Moghaddam MJ and Manolios M. Investigation of novel endocannabinoid-based nanoparticles for the delivery of anti-arthritic drugs. Abstract presented as Hospital Week, Westmead Hospital, August 2017, Sydney, Australia.

2017 Barrie N, Ali M, Moghaddam MJ and Manolios M. Investigation of novel endocannabinoid-based nanoparticles for the delivery of anti-arthritic drugs. Oral presentation at Core Facility Symposium, Westmead Hospital, March 2017, Sydney, Australia.

2016 Barrie N, Ali M, Moghaddam MJ and Manolios M. Endocannabinoid-based lipid nanoassemblies targeted to the synovium for the treatment of arthritis. Abstract and oral presentation at 38th Annual ARA Meeting, November 2016, Hunter Valley, Australia.

2016 Barrie N, Ali M, Moghaddam MJ and Manolios N. Endocannabinoid based nanoparticles targeted to the synovium for the treatment of arthritis. Oral presentation at Westmead Medical School Postgraduate Research Presentations, November 2016, Sydney, Australia.

2016 Barrie N, Ali M, Manolios and Moghaddam MJ. Investigation of targeted endocannabinoid-based nanoassemblies for the delivery of anti-arthritic drugs. Poster and presentation at Nanoparticle Therapeutics Conference, November 2016, Cairns, Australia.

2016

Barrie N, Ali M, Manolios and Moghaddam MJ. Investigation of targeted nanoparticles for the delivery of anti-arthritic drugs. Abstract and poster presented at Hospital Week, Westmead Hospital, August 2016, Sydney, Australia.

2016 Barrie N, Ali M, Manolios and Moghaddam MJ. Investigation of targeting capabilities of peptide-conjugated endocannabinoid-based lipid nanoassemblies in the treatment of arthritis. Oral presentation at 40th Condensed Matter and Materials Meeting, February 2016, Wagga Wagga, Australia.

2015 Barrie N, Ali M, Moghaddam MJ and Manolios M. Peptide conjugated endocannabinoid based nanoparticles; A novel drug delivery system for the treatment of arthritis. Oral presentation at 37th Annual Australian Rheumatology Association (ARA) Meeting, November 2015, Leura, Australia.

2015 Barrie N, Ali M, Moghaddam MJ and Manolios M. Synovium targeting peptide conjugated to endocannabinoid based nanoassemblies; A novel drug delivery system for the treatment of arthritis. Abstract and poster presented at Hospital Week, Westmead Hospital, August 2015, Sydney, Australia.

PUBLICATIONS ARISING FROM THESIS

Publications

2017 Barrie N and Manolios N. The endocannabinoid system in pain and inflammation: its relevance to rheumatic disease. European Journal of Rheumatology. Sept 2017, 4(3): 210-218.

2017 Barrie N, Kuruppu V, Manolios E, Ali M, Moghaddam M and Manolios N. Endocannabinoids in Arthritis: Current views and perspective. International Journal of Rheumatic Diseases. July 2017, 20(7): 789-797.

2019 Barrie N, Stuart J, Chew T, Sadsad R, De Campo L, Knott RB, White J, Booth D, Arnold J, Ali M, Moghaddam M.J, and Manolios N. Peptide-conjugated endocannabinoid-nanoparticles: targeted therapy for inflammatory conditions. *Manuscript submitted.*

AWARDS

2017 "Best Overall Presentation" - 39th Annual ARA Meeting, November 2017, Wollongong, Australia.

2016 "Finalist and Third Place Winner" - Post Graduate Research Seminars, Sydney Medical School, Westmead Hospital, November 2016, Sydney, Australia

2016 "2016 Post Graduate Research Seminars, October Winner" – Post Graduate Research Seminars, Sydney Medical School, Westmead Hospital, October 2016, Sydney, Australia

2016 "Best Presentation Award" – Nanoparticle Therapeutics Conference, November 2016, Cairns, Australia

2016 1st Place Student Presentations – 40th Condensed Matter and Materials Meeting, February 2016, Wagga Wagga, Australia

LIST OF FIGURES

Chapter 1

Chapter 2

Chapter 3

Chapter 4

Chapter 5

Chapter 6

LIST OF TABLES

Chapter 1

Chapter 2

Chapter 4

ABBREVIATIONS

Δ9-THC	Δ9-tetrahydrocannabinol
1-D	One-dimensional
2-D	Two-dimensional
2-AG	2-arachidonoylglycerol
Ab	Antibodies
ABHD4	α/β-hydrolase domain 4
AEA	Arachidonoyl ethanolamine (anandamide)
AECA	Arachidonyl-2-chloroethylamide
AGRF	Australian Genome Research Facility
AIA	Adjuvant induced arthritis
AjA	Ajulamic Acid
AKT1	Serine/threonine-protein kinase
ANO9	Anoctamin 9
AP-1	Activator protein 1
APC	Allophycocyanin
BASF	Badische Anilin- & Sodafabrik
BSA	Bovine serum albumin
C15orf48	Chromosome 15 open reading frame 48
CAPRI	Cannabinoid profile investigation of vapourised cannabis in patients with osteoarthritis of the knee
CB1	Cannabinoid receptor 1
CB2	Cannabinoid receptor 2
CBD	Cannabidiol
CCL	C-C motif chemokine ligand
CCL2/MCP-1	Monocyte chemoattractant protein-1
cDNA	Complementary DNA
CIA	Collagen–induced arthritis
CII-IA	Collagen type II (CII)-induced arthritis
CNS	Central nervous system
COX-2	Cyclooxygenase-2
CP450	Cytochromes P450 monooxygenases
CPP	Critical Packing Parameter
CRB2	Crumbs 2, cell polarity complex component

Cryo-TEM	Cryogenic transmission electron microscopy
Ct	Cycle threshold
CXCR	C-X-C motif chemokine receptor
CXCL	C-X-C motif chemokine ligand
d4-AEA	Deuterium labelled anandamide
DAG	Diacylglycerol
DAGL	Diacylglycerol lipase
DCM	Dichloromethane
DDX3Y	DEAD-box helicase 3, Y-linked
DE	Differentially expressed
DEPDC1	DEP domain containing 1
DIC	Differential interference contrast
DiD	1,1'-dioctadecyl-3,3,3',3'-tetramethylindodicarbocyanine,4-chlorobenzenesulfonate salt
DIEA	N, N-Diisopropylethylamine
DLGAP5	Disks large-associated protein 5
DLS	Dynamic light scattering
DMARDs	Disease modifying anti-rheumatic drugs
DSC	Differential scanning calorimetry
ECS	Endocannabinoid system
EDTA	Ethylenediaminetetraacetic acid
EET-EA	Epoxyeicosatrienoyl-ethanolamide
ELOVL7	ELOVL fatty acid elongase 7
EPR	Enhanced permeation and retention
ESI	Electrospray ionisation
ERK1/2	Extracellular Signal-regulated Kinase-1/2
F	Forward primer
FAAH	Fatty acid amide hydrolase
FACs	Fluorescence activated cell sorting
FAM213B	Family with sequence similarity 213 Member B
FBS	Fetal bovine serum
FC	Fold change
FCS	Fetal calf serum
FDR	False discovery rate

FLS	Fibroblast like synoviocytes
FOXI1	Forkhead box I1
FR- β	Folate receptor B
FSC	Forward scatter
FT-NIR	Fourier transform near infrared spectroscopy
GALNT9	Polypeptide N-acetylgalactosaminyltransferase 9
GDE	Glycerophosphodiesterase
GM-CSF	Granulocyte-macrophage colony-stimulating factor
GPCRs	G-protein-coupled receptors
h-FLS	Healthy human FLS
HA	Hyaluronic acid
HAP-1	Synovium targeting peptide
HBSS	Hanks buffered salt solution
HETE-EA	Hydroxyeicosatetraenoic-ethanolamide (hydroxy-AEA)
HIG-82	Oryctolagus cuniculus, rabbit, FLS
HPLC	High performance liquid chromatography
HPLC/MS/MS	High performance liquid chromatography tandem mass spectrometry
HSPA	Heat shock protein family A
IBSP	Integrin binding sialoprotein
IDT	Integrated DNA-technologies
IFN-ɣ	Interferon gamma
IL	Interleukin
IL1RN	Interleukin 1 receptor antagonist
IPA	Ingenuity pathway analysis
IV	Intravenous
i.v.i	Intravenous injection
JAK	Janus kinase
KIF18B	Kinesin family member 18B
KIF20A	Kinesin family member 120A
LC50	Lethal concentration 50
LEA	Linoleoylethanolamide
LFC	Log fold change
LINC01539	Long Intergenic non-protein coding RNA 1539
LINC-PINT	Long intergenic non-protein coding RNA, p53 induced transcript

LN_2	Liquid nitrogen
LOX	Lipooxygenase
LPS	Lipopolysaccharide
LXR	Liver X receptor
MAGL	Monoacyl glycerol lipase
MeOH	Methanol
MEOX1	Mesenchyme homeobox 1
MIA	Monosodium iodoacetate
MKI67	Marker of proliferation Ki-67
MMP	Metalloproteinase
MS	Mass spectroscopy
MTB	*Mycobacterium tuberculosis*
MTX	Methotrexate
MRGPRX3	MAS related GPR family member X3
MYBL2	MYB Proto-Oncogene Like 2
NAAA	N-acylethanolamine-hydrolyzing acid amidase
NAEs	N-acylethanolamines
NAPE	N-arachidonoyl-phosphatidyl-ethanolamine
NAPE-PLD	N-acylethanolamine-phosphatidyl ethanol amine
NAT1	N-acyltransferase 1
NEK2	NIMA-related kinase 2
NF-κB	Nuclear factor kappa-light-chain-enhancer of activated B cells
NIR	Near-infrared spectroscopy
NLGN4Y	Neuroligin 4, Y-linked
NOS2	Nitric oxide synthase 2
NP	Nanoparticle
N-PE	N-acylation phosphatidylethanolamine
$NP_{non\text{-}targeted}$	Non-targeted nanoparticle
NP_{HAP}	HAP-1 conjugated nanoparticle
NP_{sHAP}	sHAP-1 conjugated nanoparticle
NSAID	Non-steroidal anti-inflammatory drugs
NTSR1	Neurotensin receptor type 1
OA	Osteoarthritis
OEA	Oleoylethanolamide

P450	Cytochrome P450 monooxygenases
PBS	Phosphate buffered saline
PBK	PDZ binding kinase
PCA	Principal component analysis
PCLAF	PCNA clamp associated factor
PCR	Polymerase chain reaction
PE	Phosphatidylethanolamine
PEA	Palmitoylethanolamide
PEG	Polyethylene glycol
PEG2000	Polyethylene glycol-2000
PEG-PAMAM	Poly(ethylene glycol) conjugates of anionic dendrimer
PG-EA	Prostaglandin-ethanolamide
PI	Phosphatidylinositol
PIP2	Phosphatidylinositol 4,5 biphosphate
PLC	Phospholipase C
PLCG1	Phospholipase C gamma 1
PLD	Phospholipase D
Plk1	Polo-like kinase 1
PPAR	Peroxisome proliferator-activated receptors
PTGES2	Prostaglandin E synthase 2
PTPN22	Non-receptor protein tyrosine phosphatase 22
R	Reverse primer
RA	Rheumatoid arthritis
RES	Reticulo-endothelial system
RELA	NF-κB p65 subunit
RELB	NF-κB heterodimeric p50/p52 subunit
RGD-PEG	RGD peptide-polyethylene glycol
RNSH	Royal north shore hospital
ROI	Region of interest
RP-HPLC	Reverse phase high performance liquid chromatography
RPP-HPLC	Reverse phase preparative high performance liquid chromatography
RPS4Y1	Ribosomal protein S4, Y-linked 1
RT	Room temperature
RT-PCR	Reverse transcription polymerase chain reaction

RXR	Retinoid X receptor
SA-PE	Streptavidin, R-phycoerythrin conjugate
scFv	Single-chain variable fragment
SERPINB2	Serpin family B member 2
sHAP-1	Scrambled-synovium targeting peptide
SHISA2	Shisa family member 2
sPLA2	Soluble phospholipase A2
SOCS4	Suppressor of cytokine signaling 4
SSC	Side-scatter
STAT	Signal transducers and activators of transcription
TBTU	2-(1H-Benzotriazole-1-yl)-1,1,3,3-tetramethylaminium tetrafluoroborate
TEA	Triethylamine
TFA	Trifluoroacetic acid
TFIP2	Tissue factor pathway inhibitor 2
TMN	Temperature-modulated noncovalent interaction
TNF-α	Tumor necrosis factor alpha
TLR	Toll like receptor
TROAP	Trophinin associated protein
TRP	Transient receptor potential
TRPA1	Transient receptor potential cation channel subfamily A member 1
TRPV1	Transient receptor potential vanilloid 1
TXLNGY	Taxilin gamma pseudogene, Y-linked
ZFP	Zinc finger protein, Y-linked

ABSTRACT

Chronic inflammatory joint disease represents an emerging public health issue, occupying a sizeable proportion of the adult population in the industrialized world. Currently, the therapeutic approaches for treatment of arthritis are limited due to systemic toxicity from non-specific drug accumulation and restricted efficacy of analgesic treatment. Efficient improvements in both analgesic and anti-inflammatory treatment without accompanying undesirable side effects are required to fulfil the unmet therapeutic needs of these desperate patients. Recently, there has been a resurgence of interest in marijuana and its natural and synthetic derivatives, cannabinoid receptor agonists and antagonists, as well as chemically related compounds, for their therapeutic potential as both an anti-inflammatory and analgesic. Whilst the benefits of endocannabinoid-based treatments appear promising, very few studies have investigated the use of the self-assembled nanoparticles (NPs) for targeted drug delivery. In this study, the nanostructure mesophase behaviour of a series of mixed monoethanolamide lipids of oleoylethanolamide (OEA) and linoylethanolamide (LEA) into higher order NP structures for the encapsulation and delivery of drugs was investigated. In addition to drug encapsulation, active targeting through the conjugation of a synovium-targeting peptide, HAP-1, to the surface of these NP's was used to facilitate selective accumulation of therapeutic agents the inflamed joint. The ability to deliver endocannabinoid based NPs to specific sites of the body mediating pharmacological endocannabinoid-like effects to influence key physiological pathways, provides a novel drug delivery system and medicinal potential to treat many diseases in many fields of medicine in which inflammation is a key feature of the disease.

Chapter 1 reviews the literature addressing the endocannabinoid system and its therapeutic implications in the treatment of rheumatoid arthritis, both in clinical and basic research setting. A more extensive review of the literature has been published in manuscripts entitled; "The Endocannabinoid system in pain and inflammation: its relevance to rheumatic disease" published in the European Journal of Rheumatology 2017, 4(3): 210-218, and "Endocannabinoids in Arthritis: Current views and perspective." published in International Journal of Rheumatic Diseases 2017, 20(7): 789-797.

Chapter 2 sets the foundation for the fundamental methodologies used to generate targeted NP within the thesis. The synthesis and physiochemical characterisation of monoethanolamide endocannabinoid lipids, LEA and OEA, and their ability to self-assemble into highly ordered NP was demonstrated. By adjusting the ratio of lipid building blocks, the degree of unsaturation could be tailored to achieve lypotropic liquid crystalline mesophases and stable NP in an aqueous solution at

physiological temperatures. Differential scanning calorimetry (DSC) results demonstrated a systematic shift in the melting point of the amphiphilic mixtures was achieved by increasing the percentage of OEA. In addition to thermal stability, lypotropic phase behaviour of the monoethanolamide mixes was investigated using water penetration scans by polarising optical microscopy (POM) and small angle x-ray scattering (SAXS). The phase behaviour observed was dictated by the degree of unsaturation and displayed polymorphic changes in the crystal structure at various temperatures and various ratios of the LEA to OEA. These studies demonstrated 40% OEA and 60% LEA as the optimum ratio of the mixed amphiphiles to form stable liquid crystalline mesophases at physiologically relevant temperatures. When PEGylated lipids were incorporated to stabilise the NP and allow peptide conjugation, the folding of the lipid amphiphiles in the aqueous solution was flattened, promoting the formation of more lamellar NP. The synthesised non-targeted ($NP_{non\text{-}targeted}$), peptide-targeted (NP_{HAP}) and scramble-peptide targeted (NP_{sHAP}) preparations were used in subsequent chapters to investigate *in-vitro* binding, *in-vivo* localisation and therapeutic efficacy.

Chapter 3 investigated the targeting capabilities of conjugated NP, assessing cell binding and uptake *in-vitro* and localisation and bio distribution in a normal and adjuvant induced rodent model of arthritis *in-vivo.* Conjugation of synovium-targeting peptide, HAP-1, to the NP surface resulted in specific binding and greater uptake of NP_{HAP} in both HIG-82 and human FLS cells, when compared to $NP_{non\text{-}targeted}$ *in-vitro*. In the presence of TNF-α stimulation, cell uptake of NP was comparable to that observed in non-stimulated cells, and therefore stable in inflammatory conditions. *In-vivo* localisation of fluorescently labelled NP's was tracked using NIR imager, and demonstrated the ability to actively target therapeutics to the inflamed synovium *in-vivo*. The results demonstrated selective accumulation of NP_{HAP} to the joints in both normal and arthritic treated rats. No specific accumulation was observed in $NP_{non\text{-}targeted}$ and NP_{sHAP} treated normal rats, with only slight localised deposits observed in inflamed joints in arthritic rats. In bio-distribution studies, conjugation of HAP-1 homing peptide reduced NP off-targeted effects, limiting systemic exposure. NP_{HAP} treated rats demonstrated high concentrations of OEA and LEA in the paw, with minimal deposits in the liver after 6 h. In $NP_{non\text{-}targeted}$ treated rats, non-significant accumulation to the inflamed paw coincided with pronounced accumulation at the liver after 6 h.

Chapter 4 ability of the NP to mediate anti-inflammatory effects in RA-FLS *in-vitro* was examined using next generation sequencing (RNA-seq) and RT-PCR. Assessment of the top differential expressed genes in NP treated cells showed the acquisition of genes associated with homeostasis and inflammation resolution and led to a significant reduction in genes involved in inflammation perpetuation. NP incubation was also demonstrated to down regulate highly expressed inflammatory candidate mRNA genes prominent in RA, suggesting inflammatory resolution by dampening cytokine production. NP-mediated suppression of signalling genes TLR and JAK-STAT and an increase in PPAR signalling genes were observed, suggests anti-inflammatory effects mediated by inhibition of these pathways. The ability of the NP's to downregulate inflammatory cytokines, as well signalling genes involved in inflammatory processes highlights its promising application as an anti-inflammatory agent. Furthermore NP were demonstrated to influence AEA synthesising enzymes and catabolic and oxygenation enzymes *in-vitro*, which may assist in anti-inflammatory effects by regulating endocannabinoid metabolites concentrations at the targeted site.

Chapter 5 extended previous *in-vitro* findings and investigated the NP anti-inflammatory and analgesic effects *in-vivo*. Plasma protein levels of IL-6, IL-17A, IFN-ɣ and TNF-α were reduced following NP treatment in arthritic rats. While the effects of NP_{HAP} and $NP_{non\text{-}targeted}$ were similar, suppression of IFN-ɣ and IL-6 was more pronounced in NP_{HAP} treated rats. In addition to anti-inflammatory effects, the targeted NP_{HAP} were shown to modulate pain signalling *in-vivo,* which were void of centrally mediated effects. In analgesic studies, administration of $NP_{non\text{-}targeted}$ and NP_{HAP} to normal rats elicited dose-dependent anti-nociceptive responses against mechanical pain, which were significant at high dose concentrations. In arthritic rats, improvements in animal sensitivity to pain were only observed in NP_{HAP} treated rats, demonstrating increased efficacy through peptide-conjugation. Finally, the NP were demonstrated to influence endogenous articular NAE levels of OEA, LEA and PEA *in-vivo*. Restoration of joint endocannabinoid levels that subsequently influence anti-inflammatory actions may be an alternative approach to dampening inflammatory processes which typify the arthritic joint.

Chapter 6 integrates the results noted in prior chapters and makes suggestions for further research arising from this research.

CHAPTER 1: INTRODUCTION

Whether smoked, ingested, inhaled or injected, the anxiety relieving and mood altering effects of the plant *Cannabis Sativa*, colloquially known as marijuana, have been known for over 5,000 years (Kalant, 2001; Zogopoulos et al., 2013). The main active ingredients in cannabis have the ability to alter sensory perception, enhance appetite stimulation, induce sedation, evoke elation and euphoria, as well as impair central nervous system (CNS) function related to memory and motor control. In the nineteenth and early twentieth century, marijuana and its derivatives were recommended as muscle relaxants, analgesics and anticonvulsants. However, in the 1940's with increasing global concerns about narcotic addiction, popularity of cannabis and its related drugs as therapeutic agents declined resulting in the prohibition and further prejudice of these drugs for medical use (Robson, 2005). Recently, there has been a resurgence of interest in marijuana and its natural and synthetic derivatives, cannabinoid receptor agonists and antagonists, as well as chemically related compounds, for their therapeutic potential. Very few cannabinoids are now approved for therapeutic application despite the political debate that rages.

1.1 ENDOCANNABINOID SYSTEM

The term endocannabinoid, appeared in the literature during the mid-1990's following the discovery of the endogenous receptor for the psychoactive constituent, delta 9-tetrahydrocannabinol (Δ9-THC), a main constituent of marijuana (Matsuda et al., 1990). The identification of Δ9-THC opened the way to the cloning of the G-protein-coupled receptors, the cannabinoid receptor 1 (CB1) and cannabinoid receptor 2 (CB2), and to the discovery of the important endogenous lipid signalling pathways collectively known as the "endocannabinoid system". Endocannabinoid ligands, their receptors, and the enzymes involved in ligand biosynthesis and degradation constitute the three fundamental components of the endocannabinoid system (Battista et al., 2012). The ubiquitous endocannabinoid lipid signalling system has been noted to be relevant in many physiological functions in the body including the central, peripheral and autonomic nervous system, endocrine networks, and the immune system. The investigation and application of endocannabinoids may therefore provide therapeutic potential for a wide range of human pathological conditions including obesity and associated metabolic abnormalities, CNS (Scotter et al., 2010), and movement disorders; as well as both neuropathic and chronic pain (Anand et al., 2009) as may be found in rheumatoid arthritis ((RA), and osteoarthritis ((OA), Kalant, 2001; Mouslech & Valla, 2009; Burston et al., 2013; Pacher & Kunos, 2013; Alexander, 2016; McDougall et al., 2017).

1.2 ENDOCANNABINOID LIGANDS

The endocannabinoid system is regulated by a series of lipid signalling molecules known as "endocannabinoids", belonging to the N-acylethanolamines (NAEs). Of these, the most widely investigated is anandamide (arachidonoyl ethanolamine [AEA]) which was initially isolated from porcine brain (Devane et al., 1992), and later 2-arachidonoylglycerol (2-AG), initially found in canine intestines (Mechoulam et al., 1995). AEA is responsible for maintaining basal endocannabinoid signalling, acting as a partial to full stimulator of CB1, and a partial antagonist to CB2 where it binds with low affinity leading to partial antagonistic effect (Gonsiorek et al., 2000). At elevated concentrations, AEA functions as a full agonist for the ion channel receptor transient receptor potential vanilloid 1 (TRPV1) (Smart et al., 2000), an ionotropic receptor responsible for the integration of noxious stimuli causing pain (Kelly et al., 2015). By contrast to AEA, 2-AG functions as a full agonist for both CB1 and CB2 (Starowicz & Przewlocka, 2012). A series of other biochemically similar endocannabinoids such as 2-AG ether (Parkkari et al., 2006), virodhamine (Porter et al., 2002) and N-arachidonoyl dopamine (Grabiec & Dehghani, 2017) have also been discovered, however knowledge of their function and regulatory role remain in its infancy. In addition to these compounds, bio-active NAEs such as palmithoylethanolamide (PEA), oleoylethanolamide (OEA) and linoylethanolamide (LEA) have gained much attention in recent years due to their anti-inflammatory and potentially analgesic effects. Although possessing a similar biosynthetic pathway to AEA, they have no affinity for CB1 receptor, but instead contribute to an anti-inflammatory regulation through "entourage" effects, such as regulating the synthesis of other ligands who then mediate effects through non-CB receptors (Okamoto et al., 2004; Alhouayek & Muccioli, 2014). The anti-inflammatory potential of OEA and LEA are explored in later Chapters 4 and 5. The chemical structures of the main biologically active endocannabinoids and of the endocannabinoid-like compounds is shown in Figure 1.1

1.2.1 Endocannabinoid Synthesis and Degradation

While the predominant endocannabinoids, AEA and 2-AG, are both lipid molecules generated from the breakdown of arachidonic acid, they share very few similarities in their biosynthetic pathways, as shown in Figure 1.2 (Di Marzo, 2008). Endocannabinoid synthesis is a result of enzymatic cleavage of phospholipids within the cell membrane. AEA production is stimulated by a calcium dependent hydrolysis of membrane phospholipid precursors. N-arachidonoyl-phosphatidyl-ethanolamine (NAPE) of lipids is hydrolyzed by the specific phospholipase D (PLD) enzyme to yield AEA (Sugiura et al., 2002). Synthesis of NAE's (PEA, OEA, LEA) follow a similar pathway starting first with N-acylation of phosphatidylethanolamine (PE). In contrast to biosynthesis of AEA, the production of the second major endocannabinoid, 2-AG, involves the sequential hydrolysis of phosphatidylinositol (PI) by

phospholipase C (PLC) for the generation of diacylglycerol (DAG). DAG is then directly cleaved by diacylglycerol lipase (DAGL) α or β to form 2-AG (Ueda et al., 2011). Once released, the endocannabinoid ligands diffuse, acting locally as retrograde messengers to regulate the release of multiple presynaptic messengers. Following cellular uptake, the endocannabinoid ligands are quickly transported from the synaptic space and inactivated through subsequent catabolism via specific enzymes within the intracellular environment (Chiurchiu et al., 2015). The enzymatic reaction catalysed by intracellular enzymes unique to each endocannabinoid and include fatty acid amide hydrolase (FAAH), the principal enzyme for hydrolysis of anandamide, and monoacyl glycerol lipase (MAGL) for 2-AG. Enzymatic degradation of these endocannabinoids yields arachidonic acid and ethanolamine from anandamide, and glycerol from 2-AG, respectively (Di Marzo, 2008).

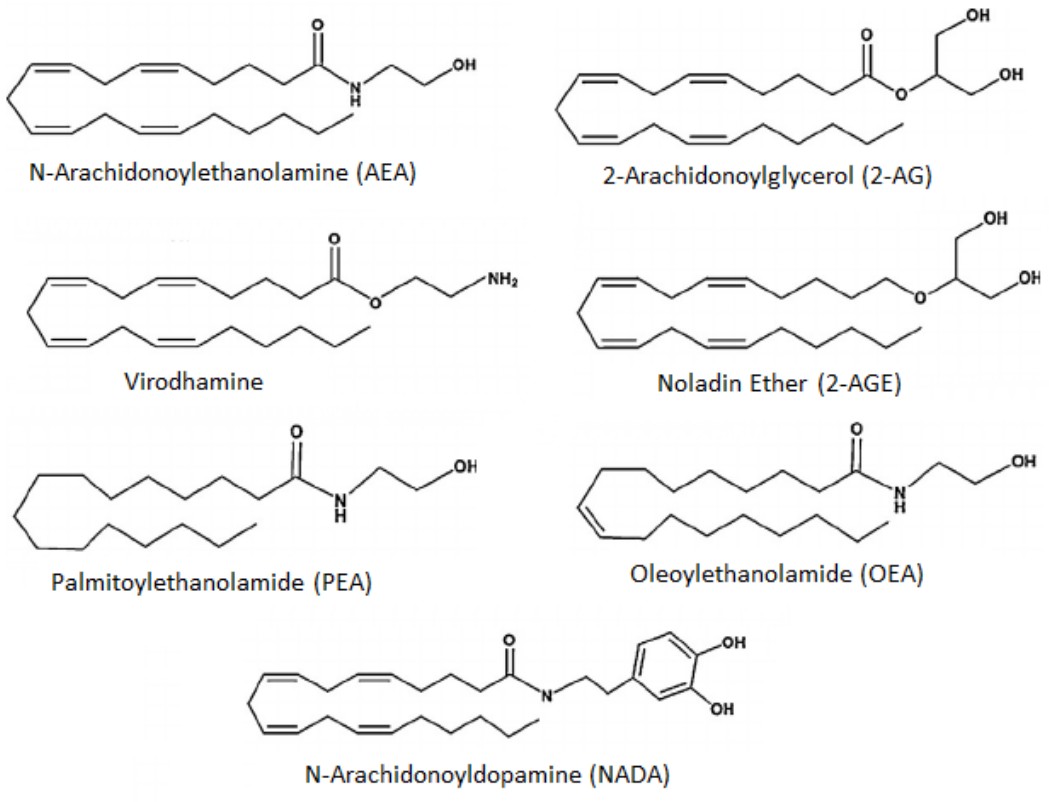

Figure 1.1. Chemical structures of biologically active endocannabinoids and of the endocannabinoid-like compounds. Figure adapted from (Battista et al., 2012).

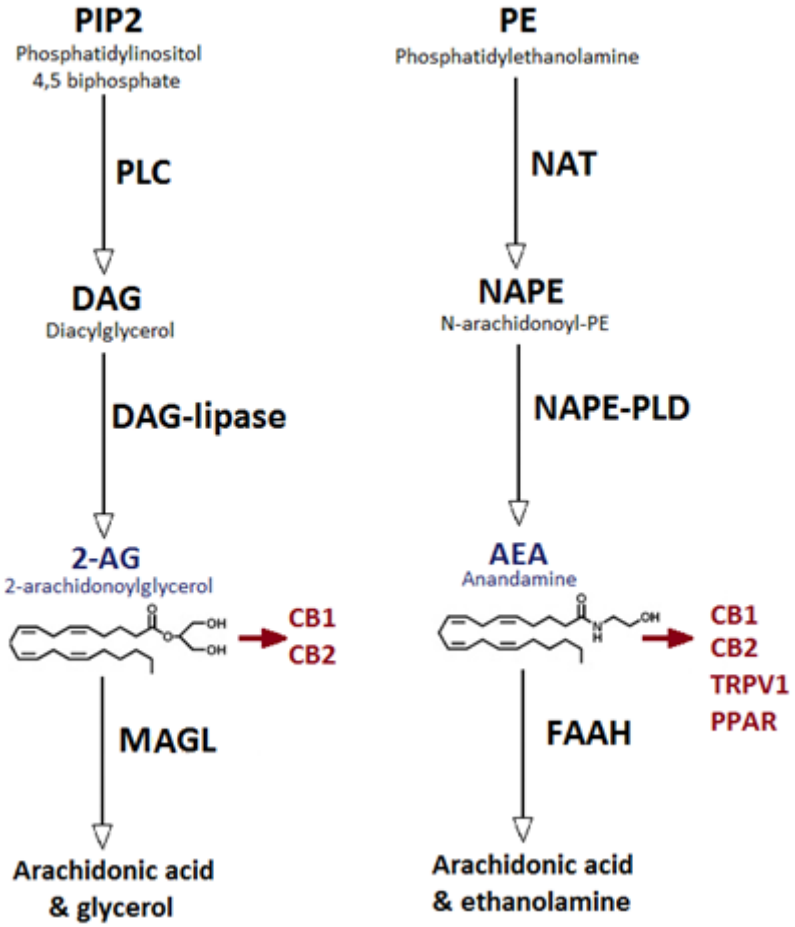

Figure 1.2. Major pathways for the synthesis and degradation of 2-AG and AEA. From membrane phospholipids, 2-AG is produced via DAGL while AEA, PEA, and OEA synthesis is enabled either directly via N-acylethanolamine-phosphatidyl ethanol amine (NAPE-PLD). The 2-AG is degraded via MAGL, whereas AEA, PEA, and OEA are hydrolyzed by FAAH.

1.3 ENDOCANNABINOID RECEPTORS

To date, two types of predominant endocannabinoid receptors have been identified; CB1 and CB2. Collectively, they are G protein coupled seven trans-membrane domain receptors, with a unique tissue density distribution suggesting that they may contribute to widely variant physiological roles (Howlett et al., 1990; Kinsey et al., 2011a). Both the CB1 and CB2 receptors are negatively coupled with adenylate cyclase via G proteins, and positively coupled to mitogen-activated protein kinase (MAPK). Accordingly, the cannabinoid receptors maintain the capacity to regulate suppression of adenylate cyclase as well as the activities of the calcium and potassium channels (Pertwee, 2006).

1.3.1 CB1

CB1 is the principle receptor of the CNS, primarily located on presynaptic as well as postsynaptic neurons (Zou & Kumar, 2018). CB1 receptors are densely expressed in several areas of the brain and supra-spinal regions involved with nociceptive transmission (Hohmann, 2002). The presence of CB1 on presynaptic neurons allows for the regulation and inhibition of neurotransmitter release. This allows for a negative feedback mechanism to develop between the anterograde and retrograde signalling pathway mediated by the endocannabinoid system. CB1 mediated suppression of neurotransmitter release in nerve terminals has been associated with the characteristic effects of cannabis including analgesia, feeling of wellbeing, catalepsy, and depression of motor activity. At the level of the spinal cord, CB1 is densely expressed at the presynaptic terminals of primary afferents and excitatory neurons and regulate the transmission of noxious stimuli to the brain by inhibiting neurotransmitter release (Pernia-Andrade et al., 2009). As well as these central effects, CB1 receptors localise on sensory terminals in the periphery, gating the propagation of pain signals, contributing to peripheral analgesia (Agarwal et al., 2007).

1.3.2 CB2

CB2 is the cannabinoid receptor immune system counterparts and unlike CB1, is almost exclusively expressed outside the CNS, being predominately found in peripheral immune and haematopoietic cells (Cabral & Griffin-Thomas, 2009). CB2 receptors mediate cannabinoid induced immunosuppression and anti-inflammatory effects by modulating cytokine release and immune cell migration (Pertwee, 2006). Furthermore, CB2 receptors extensive expression on immune cells represents a target for influencing inflammatory pain processing. CB2 receptor agonists contributed to antinociception in models of both inflammatory and nociceptive pain by suppressing the local secretion of pro-inflammatory factors by non-neural cells, which sensitise neighbouring nociceptive neuron terminals (Anand et al., 2009). Stimulation of peripheral CB2 receptors therefore mediates an antinociceptive response in settings of neuropathic pain or inflammatory hyperalgesia by acting locally on immune cells in the periphery and microglia in the CNS (Ibrahim et al., 2003; Fu & Taylor, 2015).

1.3.3 TRPV1 and the G protein-coupled receptor 55 (GPR55)

Transient receptor potential (TRP) channels are ionotropic cannabinoid receptors responsible for the detection and integration of noxious stimuli (Premkumar & Sikand, 2008). Whilst primarily expressed on sensory Aδ and C-fibres, TRPs are also located on peripheral cells and sensory neurones abundantly expressed in arthritic synovial tissue (Kelly et al., 2015). Stimulation of the TRPV1 results in cation influx and the production of an action potential that consequently results in the sensation of pain. As

such, the TRPV1 channels represent a prime focus for the development of novel analgesics. The importance of these receptors in arthritis is highlighted in TRPV1-/- knockout animals that demonstrate elevations in pain threshold and an associated reduction in joint inflammation (Szabo et al., 2005; Fernandes et al., 2011). The TRPs are thought to be involved in "cross talk" (Di Marzo, 2010) between the endocannabinoid system and endovanilloid system by existence of endogenous cannabinoids AEA, virodhamine and lysophosphatidylinositol (Ross, 2003) responsible for the activation of both endovanilloid receptors and CB1/ CB2 receptors under several pathological and physiological conditions (Wang et al., 2014). Similar to cytokines, endocannabinoid's AEA, OEA and PEA activate TRPV1 (Ambrosino et al., 2013; Redmond et al., 2014). AEA is believed to modulate synaptic plasticity, a key component in arthritic pain, through actions at both the pre and postsynaptic TRPV1 channels. On exposure, the TRPV1 channels are rapidly desensitized, resulting in reduced calcium influx and increased pain thresholds (Starowicz & Przewlocka, 2012). AEA's dual action and TRPV1 receptor co-localization with CB1 receptors in brain tissues are reviewed by (Di Marzo, 2012)

Emerging evidence has identified the GPR55 receptors as an orphan G protein coupled receptor which express an affinity and subsequent activation through endogenous cannabinoid, anandamide, 2-AG, virodhamine and noladin ether (Ryberg et al., 2007). Inhibition of GPR55 through knock-outs or pharmacological agent's correlate well with the propagation of joint inflammation and hyperalgesia, providing evidence that GPR55 is a negative regulator of inflammation (Staton et al., 2008; Bjursell et al., 2016).

1.4 THERAPEUTIC POTENTIAL OF ENDOCANNABINOIDS IN ARTHRITIS

Chronic inflammatory disease represents an emerging public health issue, occupying a sizeable proportion of the adult population in the industrialized world. Efficient improvements in both analgesic and anti-inflammatory treatment without accompanying undesirable side effects are required to fulfil the unmet therapeutic needs of these desperate patients. The primary components of the endocannabinoid signalling system, including CB1, CB2 and catabolic enzyme, FAAH, are characteristically expressed in the synovium of both OA and RA patients, with compelling evidence to demonstrate an active participation in the pathophysiology of joint pain (Richardson et al., 2008; Burston et al., 2013). A size-able number of clinical and pre-clinical studies have confirmed the potential of the endocannabinoid system in providing a number of promising therapeutic benefits for patients with chronic inflammatory diseases (Krustev et al., 2014; Salaga et al., 2014).

1.4.1 Joint Inflammation

Evidence for the endocannabinoid's anti-inflammatory effects from preclinical studies have shown that all classes of cannabinoids including phytocannabinoids (tetrahydrocannabinol, cannabidiol) and synthetic analogues such as Ajulemic acid ('Nabilone'), and elmiric acid possess anti-inflammatory effects (Burstein & Zurier, 2009). These anti-inflammatory effects may be mediated by changing the local milieu of saturated fatty acids such as ethanolamine's, that subsequently influence anti-inflammatory actions, or by directly acting on immune cells. Immune cells are able to generate and secrete endocannabinoids that lead to changes in cell migration, leucocytes generation, T-cells and macrophages cell death, reduction of pro-inflammatory cytokines, and production of other inflammatory factors that subsequently influence tissue inflammation (Maccarrone et al., 2015; Katchan et al., 2016). Therefore, by virtue of their immunomodulatory properties, cannabinoids have the potential to serve as therapeutic agents for ablation of untoward immune responses.

It has been well documented that levels of AEA and 2-AG are stimulated under inflammatory conditions (Turcotte et al., 2015). In a more recent study, Lowin *et al* (2012) showed that cannabinoid receptor CB1 and CB2 and endocannabinoids AEA and 2-AG produced by FLS are present in higher concentrations in the synovium of patients with RA and OA disease compared to normal volunteers. The regulation of the endocannabinoid system in diseased state suggesting a functional role of the endocannabinoid receptor system in the pathological effects noted in arthritic patients (Richardson et al., 2008; Lowin et al., 2012; Burston et al., 2013). With both cannabinoid receptors and endogenous ligands present in inflamed human joints, targeting this system may hold therapeutic promise for both inflammatory, as well as degenerative arthritis (Richardson et al., 2008).

In arthritis, persistent inflammation results in infiltration of immune cells and the subsequent development of hypersensitivity to noxious stimuli. Synovial fluid samples from patients with RA consistently express elevated cytokine levels such as tumour necrosis factor alpha (TNF-α), interleukin (IL)-6 and IL-1β, which act directly to sensitize joint nociceptors and stimulate the release of prostaglandins (Krustev et al., 2014). In a study by Sancho *et al*, it was shown that AEA can inhibit TNF-α induced nuclear factor kappa-light-chain-enhancer of activated B cells (NF-κB) activation by direct inhibition of the IκB kinase (Sancho et al., 2003). Similarly, synthetic cannabinoid, HU-320, ameliorating disease progression in a collagen-induced arthritis (CIA) mouse model through a comparable anti-inflammatory suppression of reactive oxygen intermediates, interferon gamma (IFN-ɣ) and TNF-α (Sumariwalla et al., 2004). Pre-clinical *in-vivo* studies examining cannabinoid anti-inflammatory effects are summarised in Table 1.1. Using a murine model of CIA, three different groups have achieved clinical improvement in CIA mice following treatment with various cannabinoids (Sumariwalla et al., 2004; Gui et al., 2015). Overall, exposure to cannabidiol (CBD) or the CB2 agonists

JWH-133 or HU-308 reduced arthritis severity, inflammatory cell infiltration, bone destruction, production of anti-collagen type II IgG1, IFN-ɣ production and TNF-α release (Malfait et al., 2000). The anti-arthritic potency of these cannabinoid agonists may be attributed to the combination of immunosuppressive responses and anti-inflammation effects through the reduction of inflammatory cytokines in the synovium, a combination that has proven successful in the past when anti-IL-12 and anti-TNF were combined to treat CIA (Butler et al., 1999).

Zurier *et al* (1998), demonstrated that a synthetic cannabinoid Ajulamic Acid (AjA), a potent anti-inflammatory in animal models of joint tissue injury (Zurier et al., 1998) suppressed cyclooxygenase-2 (COX-2), and 5 lipoxygenase activity *in-vitro* (Zurier, 2003). Oral administration of low dose of AjA suppressed joint inflammation and tissue injury in adjuvant induced arthritis (AIA) (Zurier, 2003). Similarly, AjA suppressed the release of cytokine IL-1β from peripheral blood and synovial fluid monocytes and prevented bone degradation of AIA rats by inhibition of osteoclastogenesis, osteoclast formation (in mononuclear precursor cells) and apoptosis in mature osteoclast-like cells (George et al., 2008). This activity is presumed to be initiated through peripheral CB1 receptor activation (Klein, 2005). Since AjA has weak CB1/2 receptor agonist activity, the anti-inflammatory effects may be due to the activation of other receptors that could belong to the TRPV family.

The protective effects of endocannabinoids have been noted in other inflammatory conditions such as multiple sclerosis (Patti et al., 2016; Annunziata et al., 2017) and periodontitis (Ozdemir et al., 2014). Overall, the preclinical and clinical data support the potentially effective anti-inflammatory properties of endocannabinoids/cannabinoid agonists targeting CB2 receptors. The absence of psychotropic effects and low toxicity, favour the development of cannabinoids as novel anti-inflammatory agents for the treatment of RA and OA.

1.4.2 Joint Pain

Localisation studies using receptor binding, immuno-histochemistry and *in-situ* hybridisation have mapped the distribution of the cannabinoid receptors along all levels of the pain nexus, providing a neuroanatomical framework befitting to the function of the cannabinoid system in sensory processing (Walker & Huang, 2002; Zou & Kumar, 2018). Anti-nociception is the process of blocking the detection of a painful or injurious stimuli by sensory neurons, resulting in the suppression of noxious neurotransmission. The anti-nociceptive potency of cannabinoid agonists is strongly correlated with their ability to displace binding ligands from the cannabinoid receptor, obstructing their signalling. The widespread expression of the cannabinoid receptors along the principal pain processing sites offers boundless opportunities for the development of analgesics for various pain conditions (Rani Sagar et al., 2012; O'Hearn et al., 2017).

In pre-clinical studies, anti-nociception is a prominent feature of systemically administered cannabinoids noted in studies applying various noxious agents such as chemical, mechanical and thermal stimuli (Lomazzo et al., 2015; Cajanus et al., 2016; Sun et al., 2017). Electrophysiological studies in model's arthritis have demonstrated that the facilitated nociceptive responses of peripheral nerves are attenuated in the presence of cannabinoid receptor agonists, demonstrating the capacity of endocannabinoids to act as an analgesic agent in arthritis (Schuelert & McDougall, 2008). It is suggested that both CB1 and CB2 receptors exhibit synergistic action in cannabinoid mediated anti-nociception in RA rat knee joint (Schuelert & McDougall, 2008). Pre-clinical *in-vivo* studies examining cannabinoid effects on pain are summarised in Table 1.2. Exogenously administered AEA and CB1 agonist arachidonyl-2-chloroethylamide (ACEA) have been shown to significantly reduce the firing rate of afferent nerve fibres. This effect is attenuated by the administration of CB1 antagonist AM251. Similarly, selective CB2 agonist, JWH-133, inhibited acute nociceptive responses in neuropathic rats, while systemic administration of another CB2 receptor agonist, A-796260, reversed decreases in grip strength, a surrogate measure of pain, in MIA models of RA pain (Yao et al., 2008). The peripheral localisation of CB1 on joint primary afferents and CB2 in the synovium have the potential as a promising target for arthritic pain by reducing joints nociceptors propensity to fire.

Arthritic pain is both nociceptive, primarily derived from localised inflammation; and neuropathic, resulting from a malfunction in the somatosensory nervous system (McDougall, 2006). The presence of elevated AEA, 2-AG and their synthetic precursor concentrations in synovial fluid of RA and OA patients indicates the potential for endocannabinoids to act locally in response to nociceptive stimuli to suppress nociceptive inflammatory responses (Richardson et al., 2008). The endocannabinoids anti-inflammatory effects including, suppression of cytokine and damaging proteinases secretion; and regulation of cell adhesion and migration, which collectively help slow perpetuation of disease and alleviate associated nociceptive arthritic pain primarily derived from localised inflammation (Ware et al., 2005). Similarly, systemic administration of the CB2 agonist, JWH133, suppressed pain and corrected deviation in circulating pro- and anti-inflammatory cytokines in the rat MIA model (Burston et al., 2013). While the anti-inflammatory and analgesic effects of the endocannabinoids are promising, restricted efficacy due to the rapid cellular uptake and metabolism by FAAH limits their effects (Jayamanne et al., 2006). *In-vivo* studies by Krustev *et al* reported that FAAH inhibition via URB597 can elevate tissue concentration of anandamide by inhibiting local endocannabinoid degradation and dampen inflammatory pain in rodent models of OA (Krustev et al., 2014). Similarly, URB597 suppressed inflammatory hyperaemia, as well as microvascular leukocyte rolling and adherence in a mouse model of acute arthritis highlighting the anti-inflammatory and analgesic capacity of endocannabinoids, and the modulation of the efficacy through metabolism inhibition

(Jayamanne et al., 2006; McDougall et al., 2017). In the periphery, FAAH inhibition mediates anti-inflammatory effects by down regulating cytokine production and the desensitisation of TRPV1, resulting in analgesia (Starowicz & Przewlocka, 2012). Inhibition of AEA catabolism is said to have promising effects in the management of OA pain mediated by both anti-inflammatory and anti-hyperalgesia actions (Kinsey et al., 2011a; McDougall et al., 2017).

1.4.3 Endocannabinoid Synergism with Current Therapies

In clinical use, both endocannabinoids and synthetic cannabinoids have been shown to exert synergistic anti-nociceptive effects when combined with two common nonsteroidal anti-inflammatory drugs (NSAIDs), indomethacin and flurbiprofen, in the pharmacotherapy of pain (Dani et al., 2007; Anand et al., 2009). Anti-nociceptive effects of intrathecally applied flurbiprofen were shown to be effectively inhibited by CB1 antagonism in the rat formalin test of pain (Ates et al., 2003). Similarly, reduced analgesic efficacy of indomethacin was exhibited in CB1 knockout mice suggesting involvement of the endocannabinoid system in mediating the analgesic effects of these NSAID (Guhring et al., 2002). Recent reports into NSAIDs mechanism of action demonstrates its ability to inhibit both catabolic enzymes; FAAH and COX-2, increasing concentrations of AEA and allowing indirect enhancement of cannabinoid receptor activity (Kozak et al., 2003). Reports of an interaction between cannabinoids and inhibitors of prostaglandin biosynthesis, like NSAIDs, may be partly attributed to similar chemical structure shared by the endogenous cannabinoid ligands and prostaglandins (arachidonic acid derivatives), and to the convergence of prostaglandin and endocannabinoid transduction signals (Fimiani et al., 1999). Together, therapeutic intervention in peripherally restricted CB1 antagonist and FAAH inhibition are promising strategies to ameliorate chronic inflammation and pain in RA.

Table 1.1 Pre-clinical studies examining cannabinoid anti-inflammatory effects on arthritis.

Pre-clinical model	Agent	ID[+]	ECS action	Outcome
AIA model of RA (rat)	AjA	2340729	Synthetic analog of THC-11-oic acid. CB2 agonist	Decreased joint inflammation, prostaglandin production and decreased granulocyte influx Prevented joint cartilage and bone damage (Zurier et al., 1998); (Zurier, 2003)
CIA model of RA (rat)	CBD	24547	Phytocannabinoid	Decreased production of cell mediated immunity. Inhibited disease progression (Malfait et al., 2000)
CIA model of RA (mice)	HU-320	9398378	Synthetic cannabinoid acid (CB2 agonist)	Decreased production of TNF-α and cell mediated immunity. Inhibited disease progression (Sumariwalla et al., 2004)
MIA* model of RA (rat)	JWH133	5293702	Selective CB2 agonist	Suppressed pain and corrected deviation in circulating pro- and anti-inflammatory cytokines (Burston et al., 2013)
Acute model of arthritis (mice)	URB597	1156960	Selective FAAH inhibitor	Suppressed inflammatory hyperemia (Krustev et al., 2014)
CII-IA** model of RA (mice)	JWH133	5293702	CB2 agonist	Reduced the arthritis score, inflammatory cell infiltration, bone destruction, and anti-CII IgG1 production (Fukuda et al., 2014)
CIA model of RA (mice)	HU-308	8020425	CB2 agonist	Decreased joint swelling, synovial inflammation, and joint destruction, as well as serum levels of anti-collagen II antibodies (Gui et al., 2015)

***** Monosodium iodoacetate (MIA)

****** Collagen type II (CII)-induced arthritis (CII-IA)

[+]ChemSpider I.D Number (Chemistry, 2015)

Endocannabinoid system (ECS)

Table 1.2 Summary of pre-clinical use of cannabinoids for the alleviation of joint pain

Type of Study	Agent	ID[+]	ECS action	Outcome
MIA model of OA (rat)	ACEA	4470547	Selective CB1 agonist	Attenuated firing of joint afferent fibres (Schuelert & McDougall, 2008)
MIA model of OA (rat)	A-796260	9759290	Selective CB2 agonist	Improved paw grip strength (Yao et al., 2008)
MIA model of OA (rat)	GW405833	2374[++]	Selective CB2 agonist	Attenuated weight-bearing deficits Sensitized joint afferent fibres (Schuelert et al., 2010)
MIA model of OA (rat)	URB597	1156960	Selective FAAH inhibitor	Reduced weight-bearing deficits Attenuated firing of joint afferent fibres (Schuelert et al., 2011)
LPS* model of inflammatory pain (mice)	O-3223	-	Selective CB2 agonist	Reduced nociceptive behaviour in neuropathic and inflammatory mouse models of pain (Kinsey et al., 2011a) Synthesis described (Sun et al., 2004)
MIA model of OA (rat)	PF-04457845	26390839	Selective FAAH inhibitor	Reduced joint mechanical allodynia (Ahn et al., 2011)
MIA model of OA (rat)	OMDM-198	-	FAAH-TRPV1 inhibitor	Significant reversal of joint hypersensitivity (Malek et al., 2015) Synthesis described (Miller et al., 2014)
MIA model of OA (rat)	CBD	24547	Phytocannabinoid	Attenuated firing of joint afferent fibres Reduced secondary mechanical allodynia and weight bearing deficits Reduced joint inflammation Prophylactic treatment prevented nerve damage (Philpott et al., 2017)
MIA model of OA (mice)	URB597	1156960	Selective FAAH inhibitor	Acute treatment reduced joint inflammation Prophylactic treatment prevented mechanical allodynia and nerve damage can elevate tissue concentrations of AEA (McDougall et al., 2017)

*Lipopolysaccharide (LPS)

[+]ChemSpider I.D Number (Chemistry, 2015)

[++]Catalogue number from Tocris Bioscience (Missouri, USA; Bristol, UK)

1.5 CURRENT CLINICAL TRIALS

While current cannabinoid therapy has offered particular promise in the treatment of certain inflammatory and neurodegenerative conditions, there remains limited research in the use of cannabinoids in RA., Barriers to research including insufficient legally registered marijuana manufacturers and limited clinical trials have restricted its progress into the therapeutic field. Authors of three recent systematic reviews concluded that current evidence is insufficient to allow for recommendation for any cannabinoid preparation for rheumatology patients (Ware & Tawfik, 2005; Fitzcharles et al., 2016b; Walitt et al., 2016). Clinical studies examining cannabinoid effects on pain and inflammation in RA are summarised in Table 1.3.

In a study by Blake *et al*, the effect of nabiximols (phytocannabinoids extracted from cannabis and supplied as an oromucosal spray), compared to placebo in a double-blind randomized trial of 58 patients with RA on pain was examined (Blake et al., 2006). Over a 5-week period, improvements in pain, sleep quality, and Disease Activity Score in 28 joints were observed. However, while adverse events in active treatment groups were not serious, they were common with dizziness in 26%, dry mouth in 13%, light headedness in 11%, and nausea and falls in 6%, and less frequent reports of constipation, arthritis pain, and headache. The study also had a high risk of bias for 3 of the 5 key domains assessing risk for bias (Blake et al., 2006). Similarly, in another study examining endocannabinoid-based drug, nabilone, on pain in fibromyalgia, while reaching statistical significance in two studies, the clinically meaningful effects may be outweighed when efficacy and side effects are taken into consideration (Walitt et al., 2016) FAAH inhibitor, PF-04457845, showed both analgesic and anti-inflammatory effects in animal studies comparable to naproxen (Huggins et al., 2012). However, when compared to naproxen, PF-04457845 was ineffective for OA pain when compared to placebo-control in a randomised phase II clinical trial (Huggins et al., 2012). As endocannabinoids do not solely mediate their effects via the CB1/CB2 receptors, it is thought activity mediated via the TRPV channels hampered analgesic potential (Kirkedal et al., 2017).

Recent studies with OMDM-198, a dual-acting compound which simultaneously increases FAAH substrate concentrations while inactivates TRPV1 receptors, is being investigated. OMDM-198 exhibits a meaningful reversal of hypersensitivity in MIA-model of OA joint pain, representing a promising avenue in endocannabinoid pain management. The ‘Cannabinoid Profile Investigation of Vapourized Cannabis in Patients With Osteoarthritis of the Knee’ (CAPRI) study is investigating vapourized cannabis with varying levels of THC and CBD for its ability to alleviate OA pain (NCT02324777 — NIH Clinical trials database; URL: Clinicaltrials.gov). Another ongoing clinical trial is testing combinations of cannabinoids, opioids and benzodiazepines for their pain-relieving effects in a small number of OA patients (NCT03098563 — NIH Clinical trials database; URL: Clinicaltrials.gov).

Despite the studies reviewed above, the scientific evaluation of medicinal cannabis in humans is in its infancy. Further investigation on the function of the endocannabinoid system and its role in RA is required to provide a solid foundation and allow the evolution and refinement of cannabis-based medicine. Comprehensive evaluations through well-controlled randomised trials are also required to clarify the true clinical efficacy and long-term risks associated with cannabinoid therapy. Advancements in our understanding of the endocannabinoid system and cannabinoid pharmacology, has raised the hope of exciting new pharmacological entities. Cannabis-based medications which enhance endocannabinoid function may represent a novel therapeutic solution to disorders associated with chronic pain and remains a promising avenue of contemporary importance.

Table 1.3 Clinical studies examining cannabinoid effects on pain and inflammation

Type of Study	**Pharmacological agent**	**ID***	**ECS action**	**Outcome**
RA patients	Sativex1 (THC:CBD 1:1)	34983284	Phytocannabinoid	Reduced pain at rest and during movement (Short-Form McGill Pain Questionnaire), improved quality of sleep (Blake et al., 2006)
OA patients	PF-04457845	26390839	FAAH inhibitor	Well tolerated safety profile No significant changes compared to placebo in Western Ontario and McMaster Universities Osteoarthritis Index (WOMAC) pain score (Huggins et al., 2012)
Model of experimental inflammation in humans	Ultra pure AjA (JBT-101)	2340729	CB2 agonist	70% reduction in inflammation based on a decrease in neutrophil infiltration and decreased blood flow around the site of inflammation. (Burstein, 2018)

[+]ChemSpider I.D Number (Chemistry, 2015)

CHAPTER 2: NANOPARTICLE SYNTHESIS AND CHARACTERISATION

2.1 INTRODUCTION

In the last few decades, a significant amount of research into the function of the endocannabinoid system have highlighted its role in the regulation of immune responses (Pacher & Kunos, 2013; Alexander, 2016). The endocannabinoid system is regulated by endocannabinoid lipid signalling molecules belonging to the NAE's, containing long saturated and unsaturated fatty acids formed from the breakdown of phospholipids (Coulon et al., 2012). Whilst the benefits of endocannabinoid-based treatments appear promising, very few studies have investigated the use of the self-assembled NPs as novel targeted drug delivery system. NAEs amphiphilic molecules possess excellent self-assembly properties, which can form various lyotropic nanostructured mesophases and NPs at excess aqueous solution (Sagnella et al., 2009a; Sagnella et al., 2010a; Sagnella et al., 2010b). The self-assembly of the lipid amphiphile is a robust and attractive process for the spontaneous formation of diverse nanostructured NPs. The nanostructures formed are governed by various local constraints, which can be used as a reasonable measure for predicting their mesophases (Israelachvili et al., 1976). The mesophase behaviour is an important feature in determining amphiphiles use as a drug delivery and can be predicted using the Critical Packing Parameter (CPP). The CPP is defined as $v/(\int_c a_0)$, where v is the average volume occupied by the amphiphilic chain, $\int c$ is the effective length of the amphiphilic chain and a_0 is the optimal head group area. Figure 2.1 shows the predicted phase behaviour as rationalised by the CPP. Molecules with a CPP<1 will preferentially form normal phases, while those with a packing parameter greater than 1 are likely to be wedge shaped molecules and form inverse phases (Israelachvili et al., 1976).

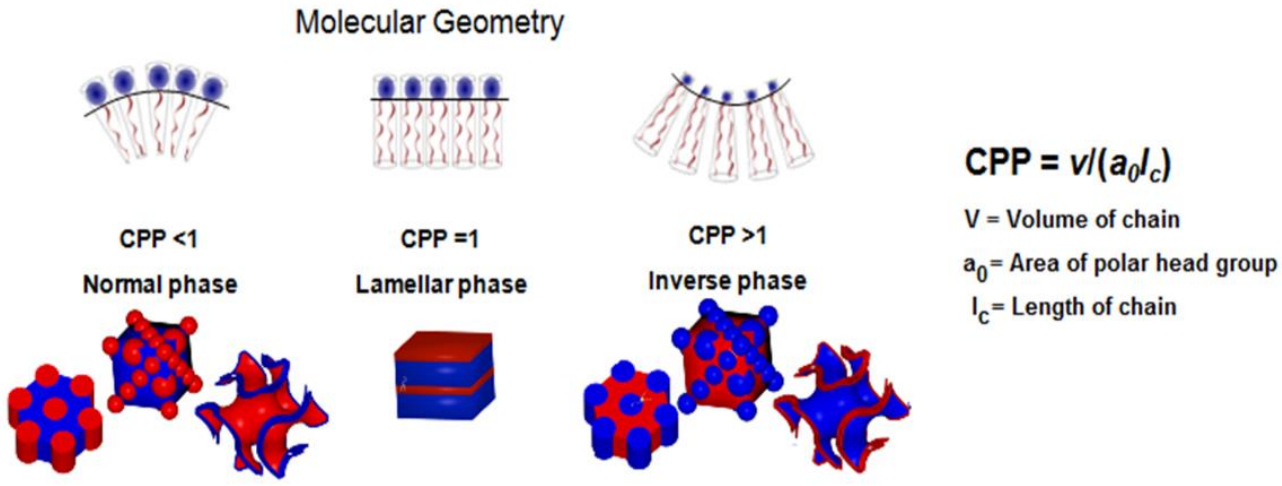

Figure 2.1: Phase behavior formed by amphiphiles rationalized by the CCP

Examples of typical lipid nanostructures formed under the CPP rule are summarised in Figure 2.2. In neat or low hydration and/or temperatures, lipids tend to form crystalline lamellar phase (L_c) due to restricted molecular motion. Increases in water content or temperatures will caused these structures to modify into various polymorphs, such as lamellar gel (L_α), fluid lamellar (L_β) or inverse micelles (L_2) (Luzzati, 1974; Cheng, 1996). The lamellear phase are a one-dimentional (1-D) nanoparticle nomenclature structure, formed by the stacking of lipid bilayers separating adjacent hydrophilic (water) layers. The common two-dimensional (2-D) structures include inverse hexagonal phase (H_2) and bicelles. The H_2 phase have water channels enclosed in a cylindrical lipid arrangement (Seddon, 1990), while the bicelles are small bilayer which are disk shaped, mediating the morphology of vesicles (Sanders, 1998). The bicontinuous cubic phases, sponge phase and micellar cubic phases form 3-D nanostructures. Bicontinuous cubic phases are comprised of two continuous, nonintersecting water channels separated by a curved bicontinuous lipid bilayer. The internal cubic phases formed have crystallographic groups such as Im3m, Pn3m and Ia3d (Seddon, 1993). Similarly, the sponge phase (L_3) is also bicontinuous in nature however is less well structured (Cates, 1991). Micellar cubic phases (such as Fd3m) consisting of two different sized micelles ordered on a cubic lattice (Seddon, 1996). Bicelles, bicontinuous cubic and sponge phases are very useful for biotechnological applications, for instance, for reconstitution and crystallization of membrane proteins.

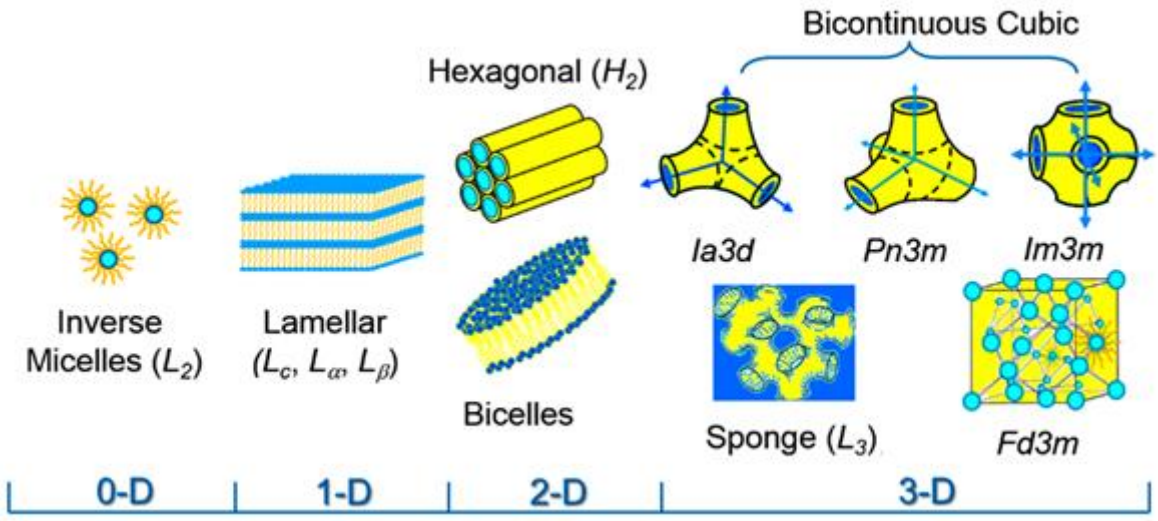

Figure 2.2. Types and schematic diagrams of thermodynamically stable self-assembled lipid nanostructures. Figure adapted from (Kulkarni, 2016). Other phases—either intermediate or metastable and not commonly found are discussed in Mulet (2010).

Research into NP drug delivery suggests that lamellar or higher order inverse liquid crystalline dispersions such as cubic and hexagonal phases formed by the amphiphilic systems have high potential for encapsulating both hydrophilic and hydrophobic drugs (Larsson, 1989; Spicer, 2005). The inverse matrices offer high internal surface area to volume ratio, and are stable against dilution making them attractive candidates for therapeutic drug delivery (Larsson, 1999; Boyd et al., 2006). The NAEs small headgroups and large volume hydrophobic tail allows for the formation of wedge shape inverse mesophases of higher ordered nanostructures such as cubic, hexagonal or reverse micellar L_2 phases making them ideal candidates for NP drug delivery.

In previous studies conducted at CSIRO, nanomedicine group, it was shown that that PEA and OEA formed crystalline NP (solid lipid NP) at room and physiological temperature, whereas the unsaturated linoleoyl (LEA) and linolenoyl (ɣ-LEA) formed molten mesophases at similar temperatures (Sagnella et al., 2010b, and 2011). The presence of an additional double bond in ɣ-LEA increases the folding capacity, as well also the thermal stability of lipid, when compared to LEA. As the phase behaviour depends on the molecular geometry of molecules, mixtures of two or more lipids, each of which separately form different phases, can be used to adjust phase behaviour. A mixed membrane of NAEs, with varying ratio of OEA and LEA was therefore hypothesised to form self-assembled lyotropic liquid crystalline mesophases and stable NP in aqueous solution at room and physiological temperatures. The amphiphilic structure of the OEA and LEA are shown in Figure 2.3. The self-assembly properties of these endogenous lipids, combined with their potential therapeutic benefits makes them attractive candidates for further study. In this chapter, previous findings were extended and the nanostructured mesophase behaviour of a series of mixed monoethanolamide lipids of OEA and LEA were investigated.

To date, liposomes have been successful as the gold standard nano-scale carriers of drugs, resulting in several NP delivery systems for cancer therapeutics (Xu et al., 2016; Ashfaq et al., 2017) and anti-fungal drugs (Weissig et al., 2014). In previous experiments, it has been shown that targeted liposomes with HAP-1 peptide carrying a therapeutic load was effective for the treatment of arthritis in animal models (Ali et al., 2011; Vanniasinghe et al., 2014). The HAP-1 peptide is a synovium targeting peptide, originally isolated from rabbit FLS cells (Mi et al., 2003).

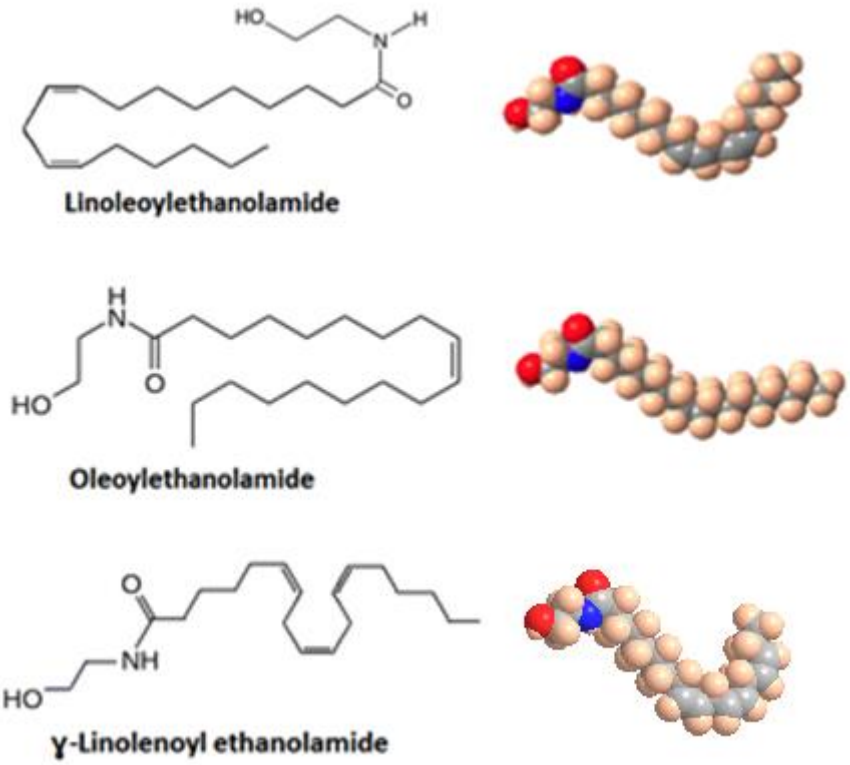

Figure 2.3. Molecular structures of linoleoylethanolamide (LEA), oleoylethanolamide (OEA) and ɣ-linolenoyl ethanolamide (ɣ-LEA) amphiphiles. 3D space-filling structures made by Chemdraw Professional (Version 15.1). Oxygen (red), nitrogen (blue), hydrogen (orange) and carbon (grey).

2.2 METHODS

2.2.1 Materials

Organic solvents were purchased from Merck (Victoria, Australia) and were either analytical or spectroscopic grade and used as received. Ethanolamine and other reagents were purchased from Sigma-Aldrich (Sydney, Australia). Oleic acid, linoleic acid and γ-linolenic acid were purchased from Nu Check Prep (Minnesota, United States of America). Polyethylene glycol-2000 (PEG2000) was obtained from Badische Anilin- & Sodafabrik ([BASF], Victoria, Australia). Targeting peptides HAP-1 (sequence: SFHQFARATLAS), and sHAP-1 (sequence: ALSRAFSHFQTA) were custom synthesised by Auspep (Victoria, Australia). Fluorescent lipid DiD (1, 1, dioctadecyl-3,3,3',3'-tetramethylindodicarbocyanine, 4-chlorobenzenesulfonate salt) was purchased from Molecular Probe (Invitrogen, Melbourne, Australia). A Milli-Q Plus ultrapure water system (Millipore, Australia) was used to filter deionized tap water to obtain high purity water.

2.2.2 Synthesis

2.2.2.1 Monoethanolamide lipid synthesis

Monoethanolamide lipids, OEA, LEA and γ-LEA were synthesised and purified as previously reported to greater than 99% purity (Sagnella et al., 2009b). Briefly, the desired fatty acids (oleic acid: 20 mmol, 5.65 g) were dissolved in dichloromethane (DCM) in a round-bottom flask and stirred vigorously on ice. Oxalyl chloride (40 mmol, 5 g) was then added to the resulting solution and the reaction stirred for a further 10 min on ice. The flask was then sealed and the reaction mixture was stirred for 2 h at room temperature (RT). The solvent and oxalyl chloride were removed under vacuum using a rotary evaporator (Rotavapor R-210; Buchi Instruments, Germany). The resulting fatty acyl chloride was dissolved in DCM and slowly added drop wise into an ethanolamine solution (40 mmol, 2.44 g) in DCM. The reaction was maintained in an ice bath with rapid stirring. After 10 min, the reaction was returned to RT and stirred for 2 h. The resulting product was filtered using Whatman 542 filter paper. The filtered solution was then sequentially rinsed with 4% citric acid, 4% sodium bicarbonate solution, and Milli-Q water. DCM was then evaporated under vacuum, leaving a white powder for OEA. Similar procedure was used for the synthesis of LEA and γ-LEA to yield an waxy residue. All NAEs synthesis had similar yields of greater than 95%.

2.2.2.2 Peptide synthesis

2.2.2.2.1 Synthesis of Ole-PEG2000-OH

Oleoyl chloride was synthesised from oleic acid and oxalyl chloride as previously mentioned. The excess solvent and oxalyl chloride were removed under vacuum using a rotary evaporator. 1-2 mL of DCM was added to the residue and removed via rotary evaporator. This process was repeated three times to eliminate any excess oxalyl chloride. The oleoyl chloride (2.1 mmol, 0.65 g) was solubilised in DCM and added to a PEG2000 (1.4 mmol, 2.7g) solution dissolved in 20 mL anhydrous DCM. The pH of the reaction was adjusted between 8-9 pH using triethylamine (TEA). The mixture was then stirred for 2 h at RT and the solvent evaporated off. The residue were stored at 4˚C prior to purification by reverse phase preparative high performance liquid chromatography (RPP-HPLC). Ole-PEG2000-OH had a total yield of 78.5%.

2.2.2.2.2 Ole-PEG2000-Succinate (Ole-PEG2000-Succ)

For succinylation of Ole-PEG2000-OH, succinic anhydride (344 mmol, 0.344 g) dissolved in 5 mL acetonitrile was added to a PEG2000-oleate (86 mmol, 1.72g) solution in 20 mL acetonitrile. TEA was added to adjust to pH 9 and the reaction stirred at RT overnight. The solvent was evaporated under reduced pressure and purified on the RPP-HPLC. Ole-PEG2000-Succ had a total yield of 76%.

2.2.2.2.3 Ole-PEG2000-Succ linkage to HAP-1 and sHAP-1

Commercially purchased HAP-1 peptide and its respective scrambled sequence, sHAP-1, were conjugated to the distal end of the PEG group. For conjugation, Ole-PEG2000-Succ (0.07465 mmols, 176.96 mg) was dissolved in 10 mL acetonitrile. 2-(1H-Benzotriazole-1-yl)-1,1,3,3-tetramethylaminium tetrafluoroborate (TBTU)**,** (0.1497 mmols, 48.1 mg)) dissolved in acetonitrile was added to a Ole-PEG2000-Succ solution and stirred for 30 min at RT. For activation, one mole equivalent of N, N-Diisopropylethylamine (DIEA), (0.07485 mmol, 48.1 mg) was added to the Ole-PEG2000-Succ solution and the reaction mixture was stirred for 2 h at RT. High performance liquid chromatography (HPLC) was then followed to monitor the reaction process. Following the activation reaction, 100 mg of protected peptide dissolved in DCM was added in a 1:1 molar ratio to the solution and stirred for 2 h at RT, while maintaining the pH >8 by addition of TEA. All the solvents were removed under vacuum using a rotary evaporator.

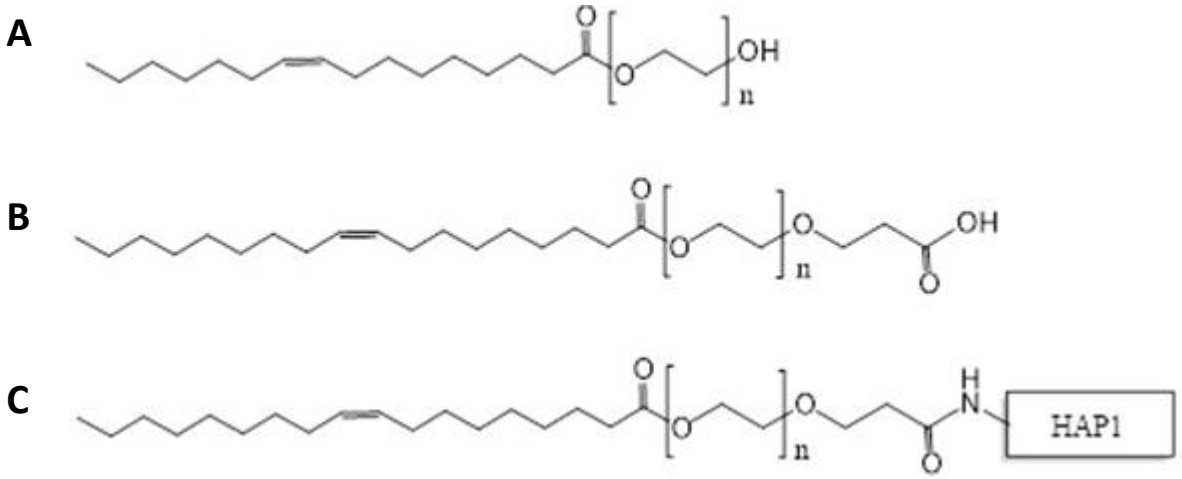

Figure 2.4. Molecular structures of **(A)** PEG2000; **(B)** Ole-PEG2000-Succ; **(C)** Ole-PEG2000-HAP-1. Molecular structures drawn in Chemdraw Professional (Version 15.1).

2.2.2.2.4 Deprotection of conjugated HAP-1 and sHAP-1

The protecting groups of the conjugated peptide were then cleaved off using a mixture of trifluoroacetic acid (TFA), water and triisopropylsilane in the ratio of 95:2.5:2.5, respectively. The solution was stirred for 2 h at RT, followed by removal of the solvents via a rotary evaporator. Ether was added and re-evaporated three times to remove any remaining TFA. The conjugated HAP-1 and sHAP-1 peptide-PEG oleates were then purified respectively using the Reveleris^{TM} flash chromatography and a C18 wide pore column (4g), applying a linear gradient solvent system: solvent A: 90% v/v water-10% v/v ethanol, and solvent B: 100% v/v ethanol. The pure fractions were pooled, evaporated to dryness and lyophilized by dissolving the residue in tertiary butyl alcohol and freeze

drying overnight. Final sample yields were 32.5% for Ole-PEG2000-HAP-1 and 41.1% for Ole-PEG2000-sHAP-1. Molecular structures of the synthesised peptides are shown in Figure 2.4.

2.2.2.3 Peptide purification

2.2.2.3.1 High performance liquid chromatography (HPLC)

Analytic HPLC was performed on Waters HPLC equipment (Waters Corporation, Milford, MA, USA), comprising a 600 solvent delivery system with a 600 automated gradient controller using a Phenomenex Gemini C_{18} column (5 uM, 4.6 x 150 mm) and an Grace 3300 evaporative light scattering detector (ELSD). The mobile phases consisted of solvent A: 50% (v/v) acetonitrile contained 50% (v/v) H_2O and solvent B: 60% (v/v) tetrahydrofuran containing 40% (v/v) acetonitrile with 0.5% (v/v) TFA with flow rate 1 mL/min. Flow rate was set at 1 mL/min to elute the samples. The ELSD detector nebulizer temperature and nitrogen gas flow were set at 103°C and 2.9 L/min, respectively. Preparative HPLC was performed on a Reveleris® Prep purification system using a semi-preparative Reveleris® C18 columns (4-40 g Reveleris®, Grace, Victoria, Australia) and using mobile phases consisted of solvent A: 90% (v/v) H_2O containing 10% (v/v) ethanol and solvent B: 100% ethanol.

2.2.2.4 Peptide purity assessment

Peptide purity was assessed by analytical HPLC using a Vydac C18 reverse-phase column on an Agilent 1100 series HPLC system as described above. LC/MS were used to assess molecular weight of final synthesised and conjugated peptides. Nuclear magnetic resonance spectroscopy (NMR) scans were then used to assess the final molecular structure of the synthesised peptides.

2.2.2.4.1 Mass spectroscopy analysis

Samples were dissolved in pure LC-MS grade methanol and analysed using a Thermo Scientific Quadrupole Orbitrap (Q-exactive plus) kindly provided on loan by Thermo Scientific Australia (Sydney, Australia). Samples were run on positive ion scan with MS range 200-6000 m/z.

2.2.2.4.2 Nuclear magnetic resonance spectroscopy (NMR)

Samples were dissolved in chloroform-d ($CDCl_3$) to a final concentration of 15 mg/mL and measured on a 400 MHz Bruker Advance 400 spectrometer (Bruker, Victoria, Australia) at 25 °C and referenced internally to the solvent. Analysis of monoethanolamide lipids for signal assignment were carried out using mNova software (MestreLab, Version 12.0.2).

2.2.3 Amphiphile Phase Behaviour

2.2.3.1 Differential scanning calorimetry (DSC)

DSC was performed using a Mettler Toledo DSC 822 system equipped with a Mettler TSO 801RO sample robot (Mettler Toledo; Melbourne, Australia). The STARe software package (Mettler Toledo; Melbourne, Australia) was used to record and analyse the thermograms. 5-10 mg of sample were placed in aluminium crucibles and cooled to -130 °C before heating at a rate of 2.5 °C min-1 up to 120 °C. Thermal calibration of the ceramic sensor was performed by integration of a standard indium sample. DSC thermograms of the monoethanolamide mixes were recorded using the STARe software package (Mettler Toledo; Melbourne, Australia).

2.2.3.2 Water penetration scans

Direct observation of the mesophase birefringence via cross-polarizing optical microscopy (POM) provide a simple and rapid assessment of the lyotropic phase behaviour of the mixed amphiphilic system. Samples of monoethanolamide amphiphile mixtures of increasing OEA to LEA ratio/content were combined in an ethanol solution, vortexed harshly and evaporated to dryness, using a rotary evaporator. Dried samples were then freeze-dried overnight. A small amount of mixed monoethanolamide amphiphile was placed onto a microscope slide and heated to melt on a hot stage to achieve an even lipid surface. A coverslip was placed on top of the melted amphiphile and then cooled to RT prior to addition of water. Water placed at the edges of the coverslip was drawn between the two glass surfaces to surround the solidified material by capillary action. This method constructs a gradient of hydration within the examined sample, ranging from fully hydrated amphiphile at the flooded margin to the neat amphiphile at the centre, exhibiting diversified mesophases formed between containing varying water content. The interaction of water and the monoethanolamide amphiphile at 25°C and 37°C was observed with an OlympusGX51 inverted optical microscope (Olympus Australia Pty. Ltd., Melbourne, Australia) in the presence and absence of polarizing lenses. The Linkam hot stage and sample temperature was controlled by a Linkam control processor PE94 (Linkam PE 94, Linkam Scientific Instruments ltd, Surrey, UK). Images were captured with an Olympus c-5060 digital camera (Olympus Australia Pty. Ltd.; Melbourne, Australia).

2.2.4 Generation of NPs

For monoethanolamide-based NP dispersions, OEA and LEA were combined in the right proportion, for example at 4:6 ratio, and dissolved in ethanol. A thin lipid film was formed by evaporating the monoethanolamide ethanol solution to dryness using rotary evaporator at 40°C. For the incorporation of the PEG stabilisers, the lipid film was then hydrated with a 15% (w/v) Ole-PEG2000-OH in PBS solution (10 mg/mL). The dispersion was then sonicated at 35°C for 1 h with intermittent probe-sonication homogenisation (Benchmark D1000 Homogeniser, PathTech, Victoria, Australia) to allow hydration of the sample and formation of NP dispersions. For HAP-1 targeted-NP (NP_{HAP}) and sHAP-1 targeted-NP (NP_{sHAP}), 7% (w/v) Ole-PEG2000-HAP or Ole-PEG2000-sHAP respectively, were dissolved in ethanol and incorporated to the phospholipid membrane via rotary evaporation prior to the hydration and sonication of lipid layers as previously described above.

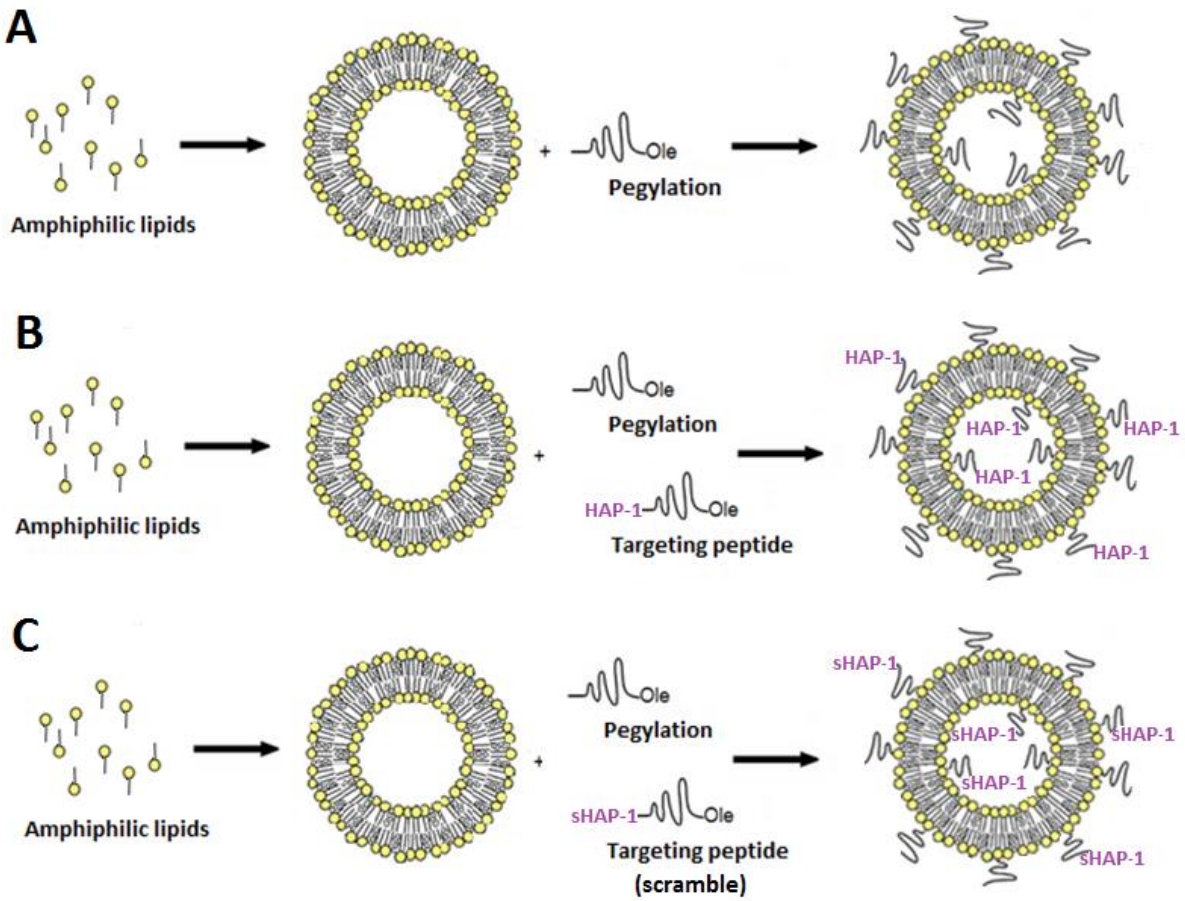

Figure 2.5. Schematic diagram illustrating the synthesis of; **(A)** $NP_{non\text{-}targeted}$; **(B)** NP_{HAP} and **(C)** NP_{sHAP}

2.2.5 NP Characterisation

2.2.5.1 Dynamic light scattering (DLS)

The physical characterisation of the of NP's was carried out using a Zetasizer nano ZS (Malvern Instruments, Worcestershire, UK) equipped with a photon correlation spectrometer. Measurements were performed at 25°C and the scattered light was detected at a scattering angle of 90°. Particle size was determined by an intensity-weighted mode and averaged over three measurements, with each measurement averaged over 14 scans.

2.2.5.2 Cryogenic transmission electron microscopy (cryo-TEM)

Cryo-TEM was employed to visualize the nanostructure of the dispersed mesophases. Samples were sonicated for 10 min prior and vortexed for 10 sec immediately before plunging. Droplets (4 μL) of NP suspensions were placed onto a 300 mesh copper grid coated with lacy formvar-carbon film (Pro-SciTech, Queensland, Australia) and gently blotted with filter paper to obtain a thin liquid film (20-400 nm). Following adhesion of NPs, the grid was plunged into ethane cooled by liquid nitrogen. Frozen grids were stored in liquid nitrogen until required. The samples were examined using a Gatan 626 cryoholder (Gatan, Pleasanton, CA, USA) and Tecnai 12 Transmission Electron Microscope (FEI, Eindhoven, Netherlands) at an operating voltage of 120 Kv, equipped with a FEI Eagle 4k × 4k CCD (FEI Co., Eindhoven, Netherlands). Samples were viewed at 100 000–150 000 times magnification.

2.2.5.3 Small angle x-ray scattering (SAXS)

Small angle X-ray diffraction measurements were used for definitive phase assignment and to obtain lattice parameters sampling regions of interest determined from the partial binary phase diagram. Samples were made up to 70% excess water content by adding a known volume of HPLC-grade water to the preweighed dry lipid. To ensure homogeneity, samples were allowed to equilibrate for a period of no less than 24 h. SAXS analysis of bulk and lyotropic mesophases at excess water (70 wt%) were performed using a NanoSTAR laboratory SAXS instrument (Bruker, Karlsruhe, Germany). The collected diffraction patterns were transmission-corrected and background-subtracted. 2-D scattering images were radially averaged to conventional scattering plots using the Bruker software. Scattering intensities I(q) were plotted as a function of the scattering vector q, where $q = (4\pi/\lambda)\sin(\theta/2)$, in which λ is the wavelength and θ is the scattering angle. Liquid crystalline mesophases gave rise to distinct diffraction patterns that were used as an unambiguous identification of each phase.

2.3 RESULTS

2.3.1 Peptide and N-Acyl Ethanolamine Analysis

HPLC, LC/MS and 1HNMR analyses were used to assess the purity, molecular mass and molecular structures of the monoethanolamide lipids, and all PEG conjugates. NMR traces of the synthesised peptides are shown in Appendix 1. The purity of the monoethanolamide proved to be >98%. The expected molecular weight of synthesised lipids, commercially purchased peptides and synthesised conjugated peptides are summarised in Table 2.1.

Table 2.1. Summary of expected molecular weight of synthesised lipids, commercially purchased peptides and synthesised conjugated peptides

Compound	Molecular Weight
OEA	325.54
LEA	323.52
ɣ-LEA	321.52
HAP-1, sHAP-1 (protected)	2259
HAP-1, sHAP-1 (deprotected)	1336
PEG2000	~2000
Ole-PEG2000	2264
Ole-PEG2000-Succ	2364
Ole-PEG2000-Peptide (protected)	4605
Ole-PEG2000-Peptide (deprotected)	3682

2.3.1.1 Assessment of Ole-PEG2000-Succ

To assist with NP stability, Ole-PEG2000-OH was synthesised and later incorporated into the NP lipid membrane. For succinylation, succinic anhydride was conjugated to Ole-PEG2000-OH to obtain Ole-PEG2000-Succ. Homing peptides was later conjugated to Ole-PEG2000-Succ and incorporated into targeted NP. Reaction mixtures of both Ole-PEG2000-OH and Ole-PEG2000-Succ were examined by HPLC and purified by RPP-HPLC for a total yield of 78.5% and 76% respectively. Assessment of the PEGylated samples by MS showed populations of correct mass to charge ratios (Figure 2.6).

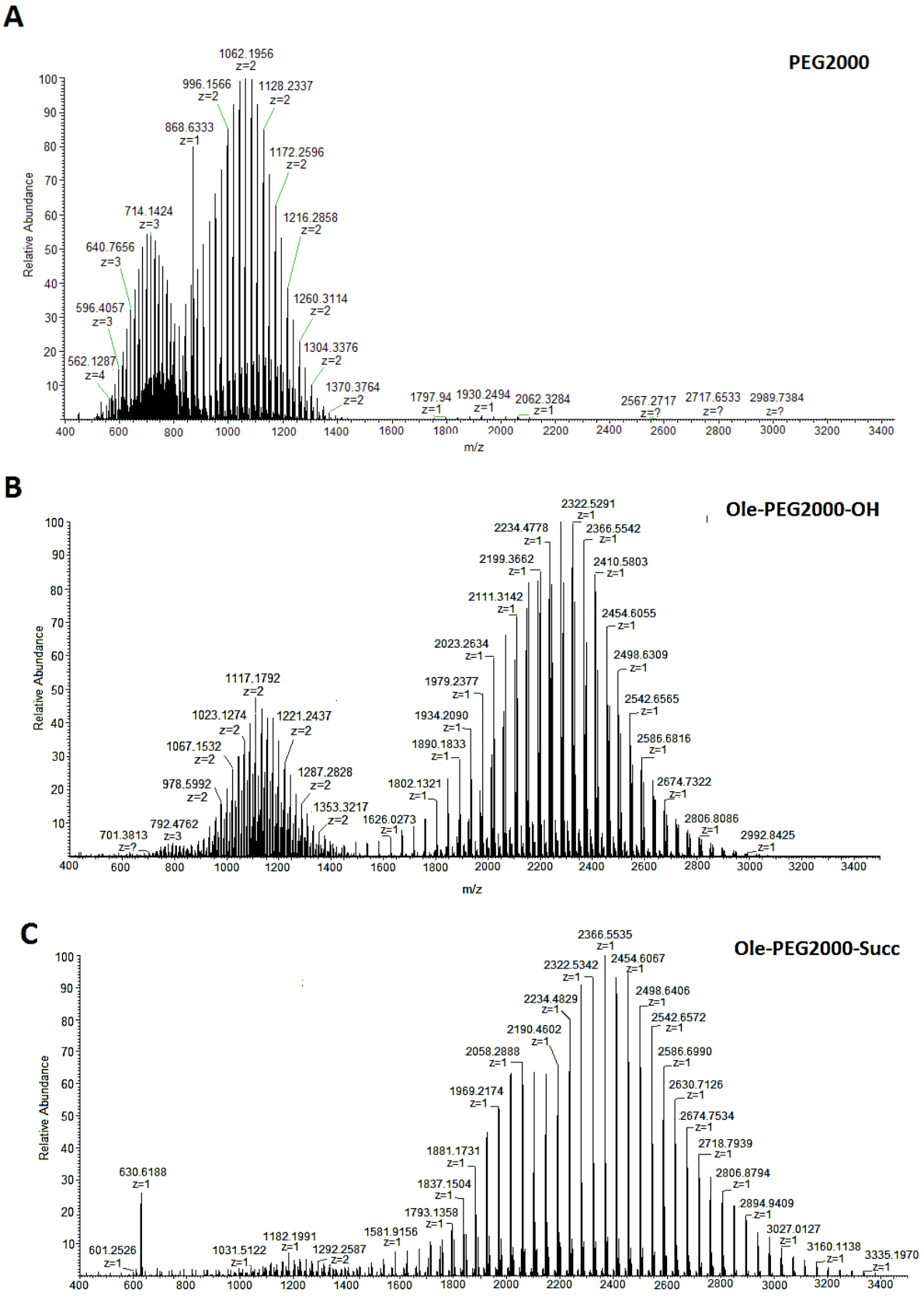

Figure 2.6. MS analysis of **(A)** PEG2000; **(B)** Ole-PEG2000-OH and; **(C)** Ole-PEG2000-Succ confirmed the correct mass of synthesized PEGylated lipids.

2.3.1.2 Assessment of Ole-PEG2000-HAP-1 and Ole-PEG2000-sHAP-1

Commercially purchased HAP-1 peptide and its respective scrambled sequence, sHAP-1, both used with temporary protected groups, were conjugated to the N-terminal of the Ole-PEG2000-Succ PEG group. This technique allowed for the formation of an amide bond between the functionalised COOH group of the PEG and free amino group on the n-terminal of the peptide. HPLC was used to monitor the reaction progress. MS confirmed the correct weight of the PEGylated lipids conjugated to their protected peptides counterparts; as shown in Figure 2.7.

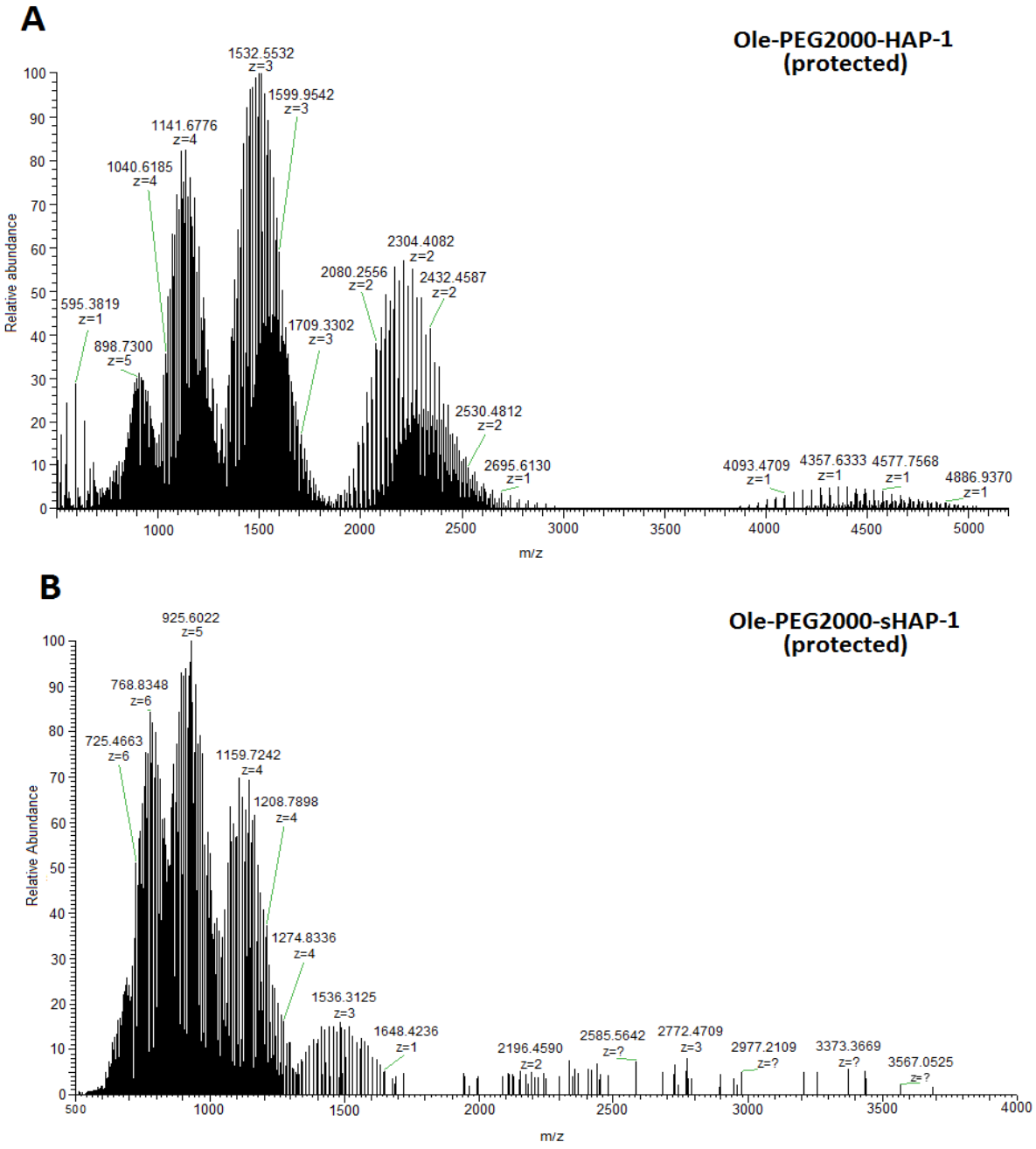

Figure 2.7. MS analysis of **(A)** Ole-PEG2000-HAP-1 and; **(B)** Ole-PEG2000-sHAP-1 confirmed the correct weight of conjugated protected peptides to Ole-PEG2000-Succ.

Following conjugation, the bound peptide was cleaved off its protecting side-chain groups. HPLC and MS confirmation of a completely deprotected HAP-1 and sHAP-1 peptide are supplied in Appendix 2. The reaction progress was monitored by HPLC and LC/MS for presence of pegylated peptide with protecting groups. Reaction mixtures of both Ole-PEG2000-HAP-1 and Ole-PEG2000-sHAP-1 were purified by RPP-HPLC, with final sample yields of 32.5% and 41.1% respectively. LC/MS and confirmed the correct weight of the deprotected peptides conjugated to PEGylated lipid counterparts (Figure 2.8).

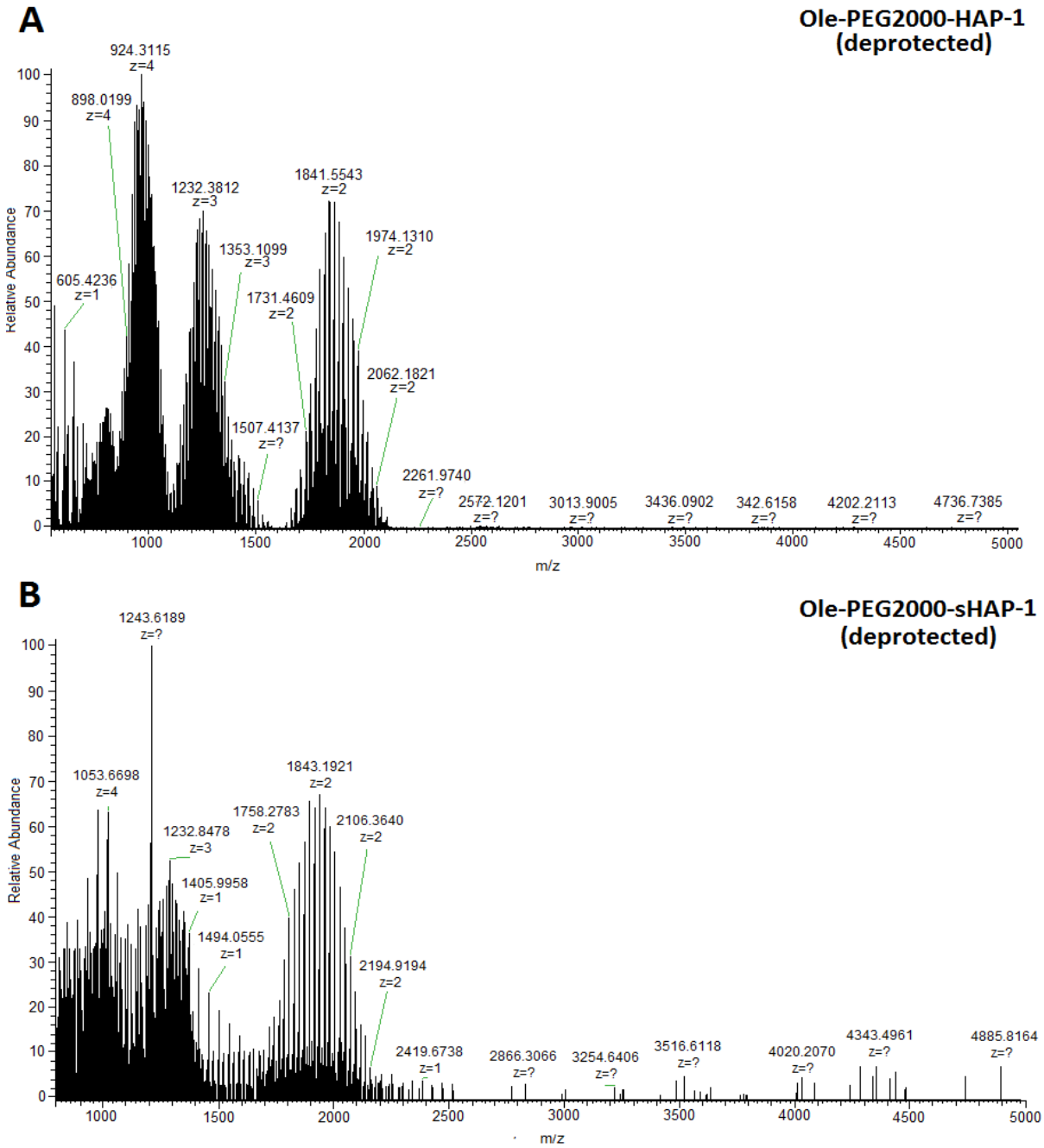

Figure 2.8. MS analysis of **(A)** Ole-PEG2000-HAP-1 and; **(B)** Ole-PEG2000-sHAP-1 confirmed the correct weight of conjugated deprotected peptides to Ole-PEG2000-Succ.

2.3.2 Synthesis of Monoethanolamide Lipids; OEA, LEA and ɣ-LEA

Synthesis of lipids were examined by HPLC and purified by RPP-HPLC. Both NAEs synthesis had similar yields of greater than 95%. Assessment of the monoethanolamides lipids by MS showed populations of correct mass ratios (Figure 2.9).

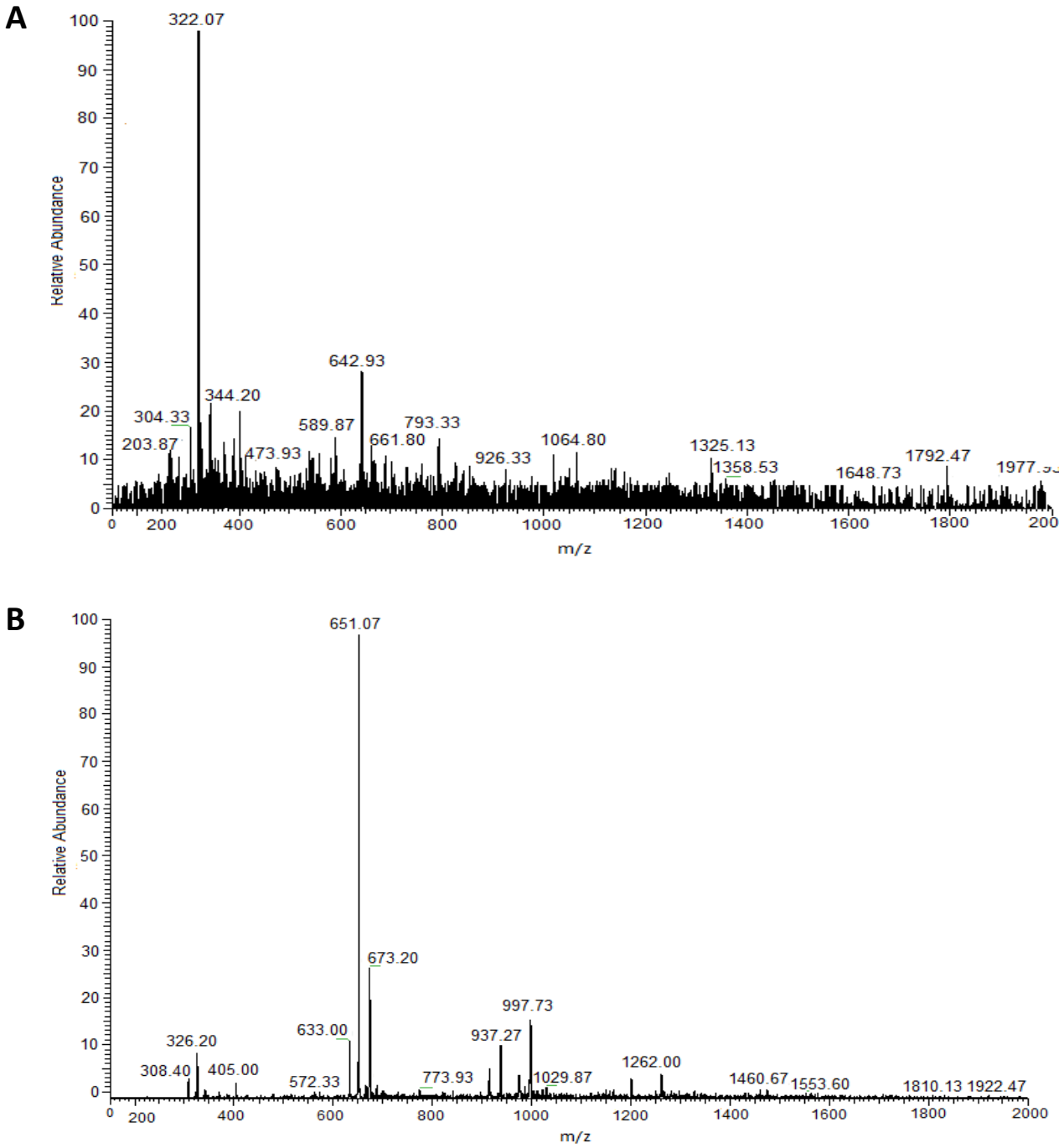

Figure 2.9. MS analysis of **(A)** LEA and; **(B)** OEA confirmed the correct weight of the synthesised lipids.

2.3.3 Amphiphile Phase Behaviour

2.3.3.1 Thermal phase behaviour of the neat endocannabinoids

To examine the thermal behaviour of the neat amphiphiles LEA, ɣ-LEA and OEA, and the influence of chain morphology in the melting behaviour of the amphiphile mix, bulk mixtures of increasing LEA to OEA ratios were prepared and DSC scans performed at 2.5 °C/min. Figure 2.10 shows the melting behaviour of amphiphile mixtures composed of LEA and OEA, representing one single melting point of each mixture. The onset of one melting point for various mixture indicates that the two amphiphiles were mixed homogenously without any phase separation. A small endothermic peak at lower temperatures was observed in most of the amphiphiles mixtures, likely due to a polymorphic transition of the unsaturated chains previously reported (Sagnella et al., 2010b).

Table 2.2 shows the transition temperatures obtained from the peak maxima of the DSC scans. LEA showed an endothermic peak with melting point at 40.4°C and OEA had a large endothermic melting point at 63.5°C. The melting behaviour of the amphiphiles was shown to be dependent on intrinsic differences in chain morphology and showed a systematic monotonic shift, which were dependent on the degree of unsaturation in the mixed hydrocarbon chains. DSC scans of OEA mixtures with ɣ-LEA, show a comparable shift in transition temperature to that seen with LEA/OEA mixtures. Table 2.3 shows the transition temperatures obtained from the peak maxima of the DSC scans. As shown, mixtures containing ɣ-LEA exhibited melting peaks at lower temperatures (Table 2.3), demonstrating the influence between the hydrogen bonding and unsaturation in dictating the melting behaviour.

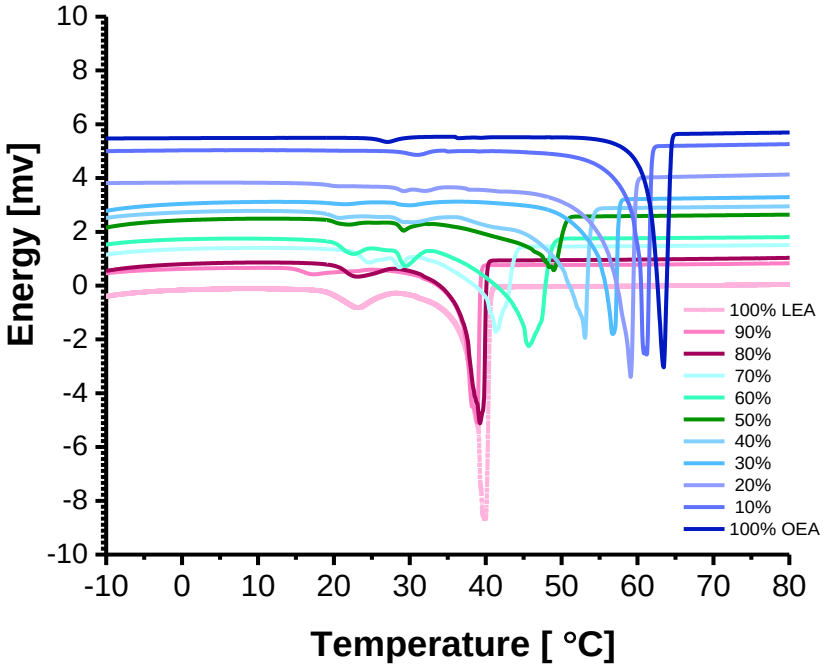

Figure 2.10. DSC of monoethanolamide lipids with increasing OEA to LEA ratio showing a shift to higher transition temperatures as OEA content increased. Scan rate 2.5°C/min.

Table 2.2. Neat monoethanolamide lipid, LEA and OEA, phase transition data determined from DSC scanned at 2.5°C/min.

Surfactant	Transitional temperatures (°C)	Transition enthalpy (kJ/mol)	Melting point (°C)
100% OEA	62.10	-115.17	63.55
90% OEA 10% LEA	60.50	-113.99	61.69
80% OEA 20% LEA	57.45	-108.15	59.40
70% OEA 30% LEA	55.53	-99.59	57.00
60% OEA 40% LEA	52.39	-89.93	54.01
50% OEA 50% LEA	46.46	-88.98	49.67
40% OEA 60% LEA	45.73	-82.98	48.38
30% OEA 70% LEA	39.53	-79.24	43.00
20% OEA 80% LEA	39.95	-93.73	41.15
10% OEA 90% LEA	39.57	-103.75	40.18
100% LEA	38.79	-100.39	40.00

Table 2.3: Neat monoethanolamide lipid's, OEA and ɣ-LEA, phase transition data determined from DSC scanned at 2.5°C/min.

Surfactant	Transitional temperatures (°C)	Transition enthalpy (kJ/mol)	Melting point (°C)
90% OEA 10% ɣ-LEA	53.96	-69.91	56.75
80% OEA 20% ɣ-LEA	51.22	-63.14	54.91
70% OEA 30% ɣ-LEA	52.25	-53.16	53.59
60% OEA 40% ɣ-LEA	44.55	-35.01	51.39
50% OEA 50% ɣ-LEA	46.88	-36.07	49.81
40% OEA 60% ɣ-LEA	36.21	-16.77	41.06
30% OEA 70% ɣ-LEA	30.82	-13.49	41.14

2.3.3.2 Lypotropic phase behaviour of monoethanolamide amphiphiles

Initially, lypotropic phase behaviour of neat amphiphilic mixes were assessed using water penetration scans under POM. Under cross polarisers, inverse structures such as cubic and micellar phases appear as dark isotropic bands while anisotropic phases such as lamellar and hexagonal phases are birefringent with well characterised textures (Rosevear, 1954). Representative POM images of the amphiphilic mixtures are shown in Figure 2.11. Inspection of the monoethanolamide lipids by POM demonstrated the ability of both OEA and LEA to self-assemble in the presence of a polar solution.

At 25°C, non-hydrated samples of both pure OEA and LEA, as well as all mixed ratios showed a crystalline structure with a distinct birefringence as indicated by the top row in Figure 2.11A. In excess water, 100% LEA amphiphile showed the formation of an isotropic molten mesophase at the flooded boundaries, perhaps an L_2 mesophase at both 25°C and 37°C. At lower water content, isotropic mesophases likely to be cubic was observed between the excess amphiphile and the neat amphiphile for 100% LEA. As the amount of OEA increased, the mesophases at the excess water boundary transformed to isotropic mesophases displaying two to three distinct bands at the water–amphiphile interface. These bands are likely to be attributed to cubic mesophases of various symmetries such as Im3m, Pn3m, and Ia3d. The full three cubic mesophases were further obvious at 37°C by three distinct isotropic bands at the water boundary. As the percentage of OEA increased to more than 80%, there was less hydration of the mixed amphiphile and the formation of either hydrated or crystalline lamellar structures became apparent. The melting point of the mixed amphiphile membrane were significantly above physiological temperature, leading to crystalline membrane at 25°C and 37°C. These results corresponded well with results obtained by DSC.

The lypotropic phase behaviour of mixtures containing triple bonded ɣ-LEA are shown in Figure 2.11B. Similarly to polymorphic changes observed in LEA and OEA mix, Figure 2.11B shows a shift in the mesophase behaviour from cubic to lamellar as OEA content is increased (Figure 2.11A). The primary defining factor which separates the two mixtures is the temperature at which the isotropic mixtures melt. In the case of LEA, the mixtures containing 60% OEA were required at achieve stable conformation at temperatures of 37°C. For ɣ-LEA, the isotropic phases formed from mixtures containing 60% OEA at 25°C were stable up to 30°C. At elevations above 35°C, the mixtures became isotropic melts. ɣ-LEA's triple bond required a greater percentage of OEA to achieve mesophases stable at physiological temperature, and so only mixtures of LEA and OEA (and not ɣ-LEA and OEA) were used for further studies.

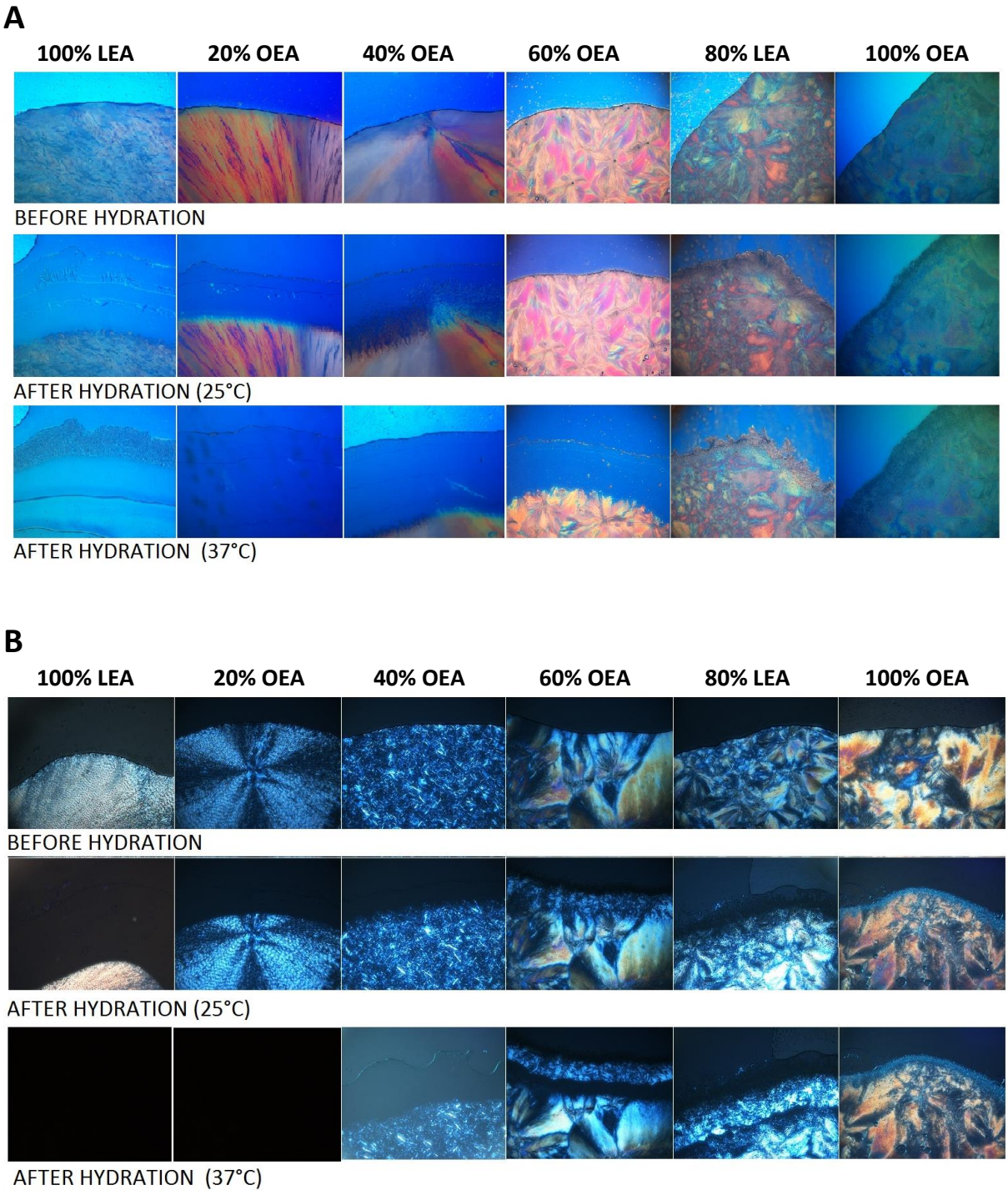

Figure 2.11. Optical microscopy of neat monoethanolamide lipids **(A)** LEA and OEA; **(B)** ɣ-LEA and OEA amphiphile mixtures at varying LEA to OEA ratios. Images acquired at 25°C and 37°C before and after hydration from a fixed position (magnification X100). Different mesophases are observed from pure water (bottom) to neat amphiphile at the top. In the 20% to 40% LEA distinct isotropic mesophases are observed. Polymorphic changes in the mesophases from cubic to a more lamellar phases were observed as the OEA to LEA ratio increased.

2.3.3.3 SAXS analysis of bulk phase

To assess the phase behaviour of the amphiphiles, SAXS analysis on the bulk and lyotropic mesophases of various LEA/OEA mixed amphiphiles was conducted to obtain a better understanding of the liquid crystalline structures of the mixed amphiphiles. Approximate partial binary phase diagrams were constructed by examining amphiphile/water mixtures over a range of temperatures. SAXS analysis also provided information into whether the two amphiphiles have been mixed well into one lyotropic mesophase.

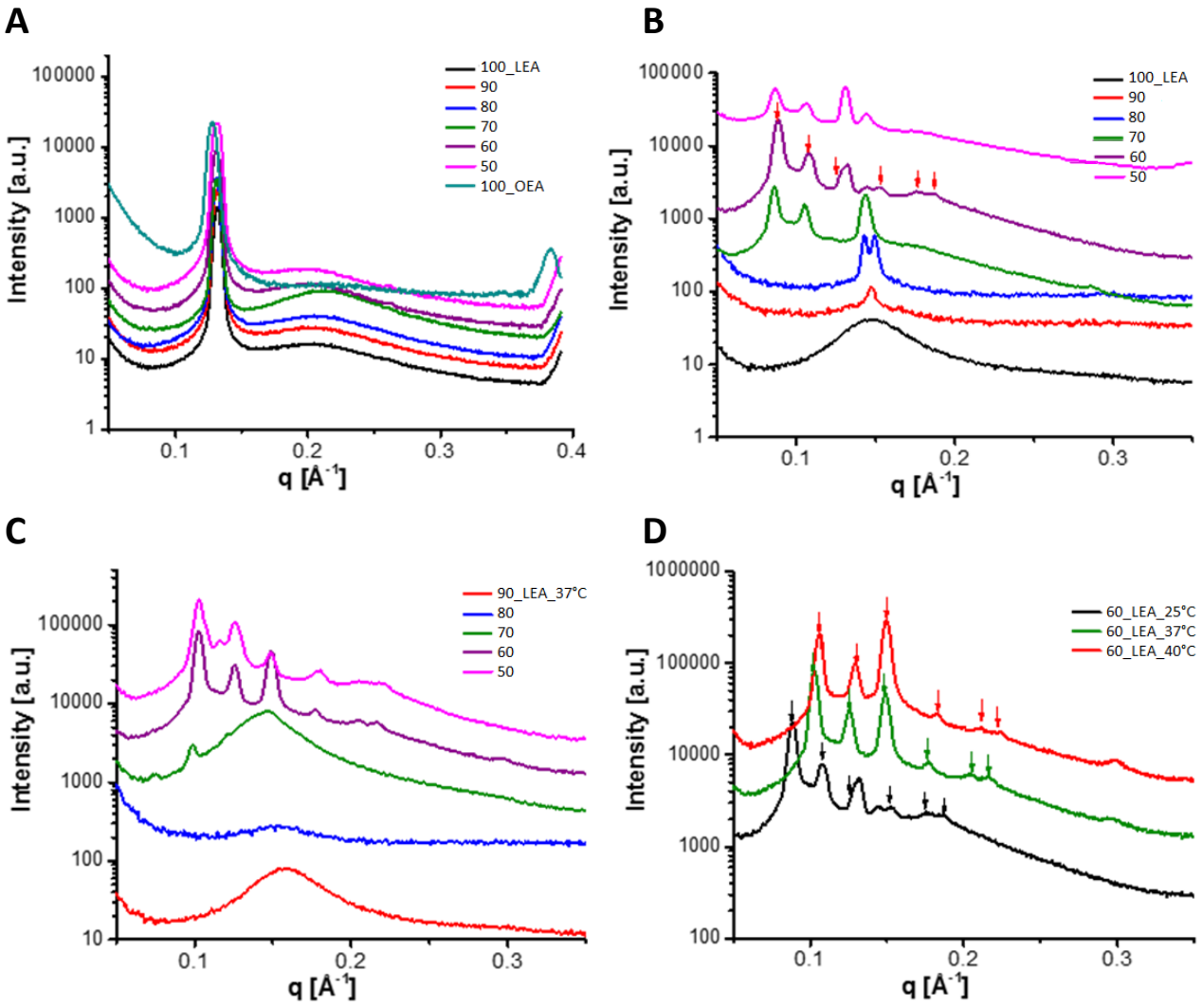

Figure 2.12. SAXS analysis of **(A)** bulk and; **(B-D)** lyotropic mesophases of mixed LEA/OEA in excess water (70 wt%). The lyotropic mesophases were equilibrated for 48 h and analysed using a laboratory SAXS instrument equipped with a Peltier temperature control chamber at; **(B)** 25°C and; **(C)** 37°C**.** Lyotropic mesophases of 60% LEA at various temperatures, showing cubic mesophase of a Pn3m space group are shown in **(D)**.

1D SAXS scattering pattern of the neat amphiphile are shown in Figure 2.12A. All the amphiphilic mixes examined showed a relatively sharp peak in addition to a broad peak. The presence of only one scattering peak suggests that the amphiphiles were well mixed, consistent with our DSC results. For 100% LEA, a sharp peak at ~0.132 Å-1 was observed and is indicative of an ordered lamellar mesophase with a lattice parameter of 47.78 Å. The lattice parameter of the lamellar phase at 100% OEA was 49.70 Å. A broader peak at 0.205 Å-1 was also observed, which is indicative of an accompanied weakly ordered mesophase. As the OEA content was increased in the mixed amphiphile, the peak progressively transformed to lower q values, indicative of a slightly larger lattice parameter.

Representative lyotropic mesophase of the hydrated mixed samples at 70wt% water (excess water) was also investigated and shown in Figure 2.12B. The SAXS of bulk mixed NAEs confirmed our observation by POM. The scattering pattern of various amphiphiles mixes ranging between 100% LEA to 50% LEA showed the formation of varying ordered nanostructures at 25°C. At 100% LEA, the lyotropic mesophase showed a broad scattering peak with maximum at 0.147 Å-1, which is different from the broad peak observed in its neat amphiphiles (Figure 2.12A). In addition, the sharp peak of the neat 100% LEA amphiphile observed in Figure 2.12A, was not observed in the hydrated 100% LEA mesophase, shown in Figure 2.12B.

The shift to a lower q value from those observed in the neat amphiphile is indicative of a swollen L2 mesophase with a weakly ordered nanostructure. As OEA ratio is increased, the molten mesophase changed slightly and a sharp peak appeared at 0.147 Å-1. At 70% LEA a mixed cubic mesophase, along with a crystalline lamellar peak at q=0.143 was observed. At 60% LEA, the cubic mesophase became more dominant. At 50% LEA the observed cubic mesophase was transformed to a mixed cubic and lamellar mesophase.

The lypotropic mesophases of the hydrated mixes was also assessed at 37°C (Figure 2.12C). Raising the temperature of the above hydrated samples to a physiological temperature resulted in more molten L_2 mesophase for 90-70% LEA amphiphile mixes. At 60% LEA, a mono cubic mesophase with the Pn3m symmetry was developed. At 50% LEA, there was a shift from sole cubic mesophases (as seen in 60% LEA), to both cubic mesophase mixed with a lamellar liquid crystalline mesophase. From the various ratios investigated here, 60% LEA mixed amphiphile showed a sole cubic mesophase of Pn3m symmetry, which was stable up to physiological temperatures. Figure 2.12D shows the shift in lattice parameter of 60% LEA / 40% OEA mix. The lattice parameter of this mesophase decreased as the temperature increased by shifting the scattering peaks towards higher q values. The results are consistent with the POM observations and shows stable NP formations obtained at 60% LEA. 60% (w/w) LEA and 40% (w/w) OEA NP composition was selected to be used in all future experiments.

2.3.4 NP Characterisation

2.3.4.1 Lipid NP dispersions size

The average hydrodynamic radii of the dispersed NP using 15% PEG2000-lipid measured by DLS was 170 d.nm with a polydispersity index of 0.124 as shown in Figure 2.13.

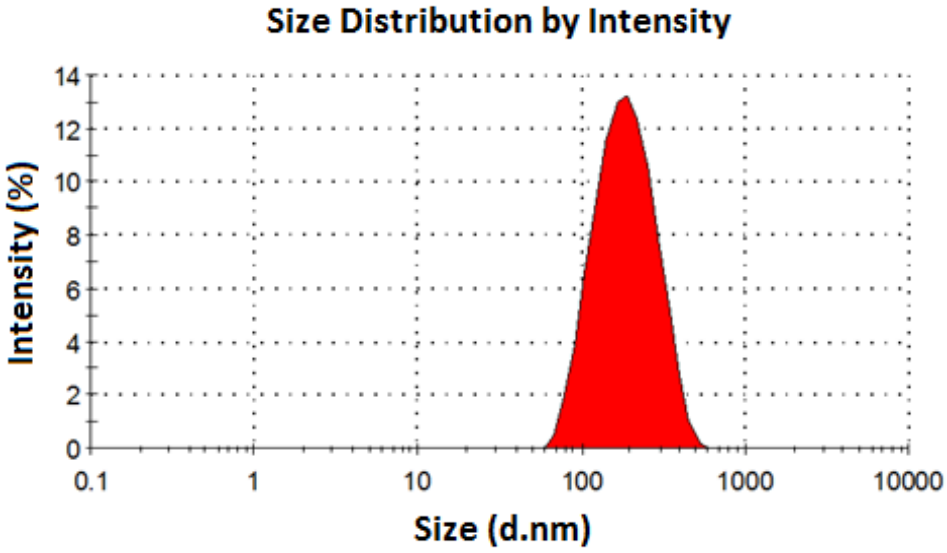

Figure 2.13. Size distribution of NP composed of 40% (w/w) OEA and %60 (w/w) LEA as distributed by intensity.

2.3.4.2 NP morphology

Cryo-TEM was used to acquire high-resolution direct images of the NP size and structure Figure 2.14 Colloidal dispersions of 40% (w/w) OEA and %60 (w/w) LEA NP's showed the production sponge-like NP's (spongosomes), co-existing with liposomal NP's. The size and uniformity of the NP, sized at 180 d.nm, in agreement with the physiochemical characterisation obtained by the Zetasizer and the number average. The size by intensity was larger to an average of 180 due to some larger NPs shown in Figure B. Observation of NP's at higher magnification highlighted the difference in structure between the synthesised spongosomes and liposomes (Figure 12.14B). Observation of the spongisomes at higher magnification showed the presence of internal water channels (shown by white arrows), appearing as small vesical inside the darkened NP. Whilst similar to cubosomes, these internal water channels were less ordered and so take on a sponge phase instead of the highly ordered inverse cubic phase. By contrast, the liposomes single dark circular boarder is the result of water encapsulated vesicle with no internal water channels.

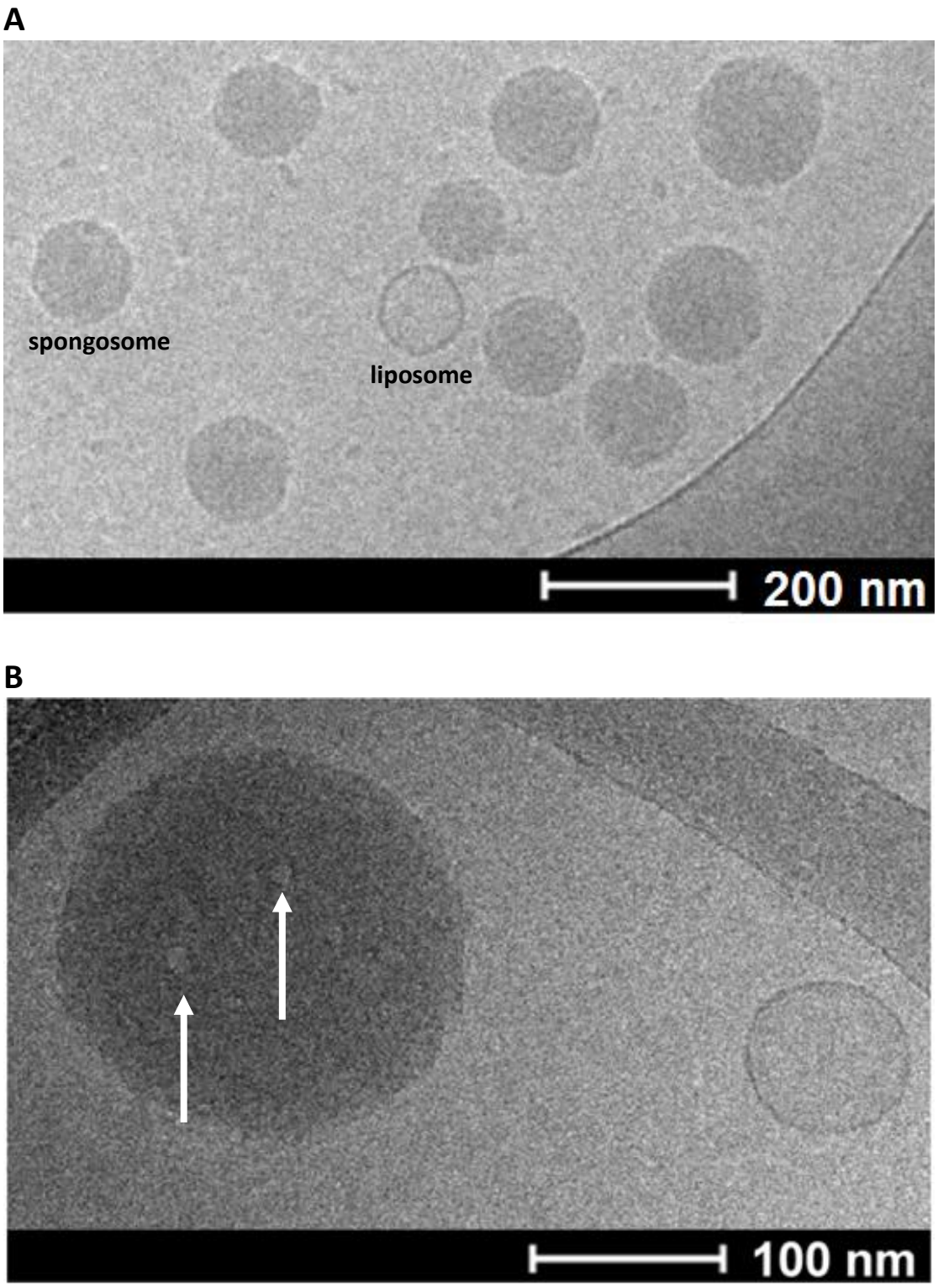

Figure 2.14. Cryo-TEM images of NP dispersions made from 40% (w/w) OEA, 60% (w/w) LEA stabilised with 15% PEG2000-OH showing the production of sponge-like NP. **(B)** NP's at higher magnification showing the formation of spongosomes.

1D SAXS scattering pattern of the NP dispersions with and without HAP-1 targeting is shown in Figure 2.15. Assessment of the NP structure by SAXS supports the formation of sponge-like NP at 40% (w/w) OEA, 60% (w/w) LEA stabilised with 15% PEG2000-OH. Both dispersions showed colloidal particles with less ordered internal nanostructures, in contrast with the bulk lyotropic phase behaviour described above. The lack of highly ordered internal nanostructure is likely due to the addition of PEG lipids at 15wt %. Less PEG-lipid led to NPs with less stability over time.

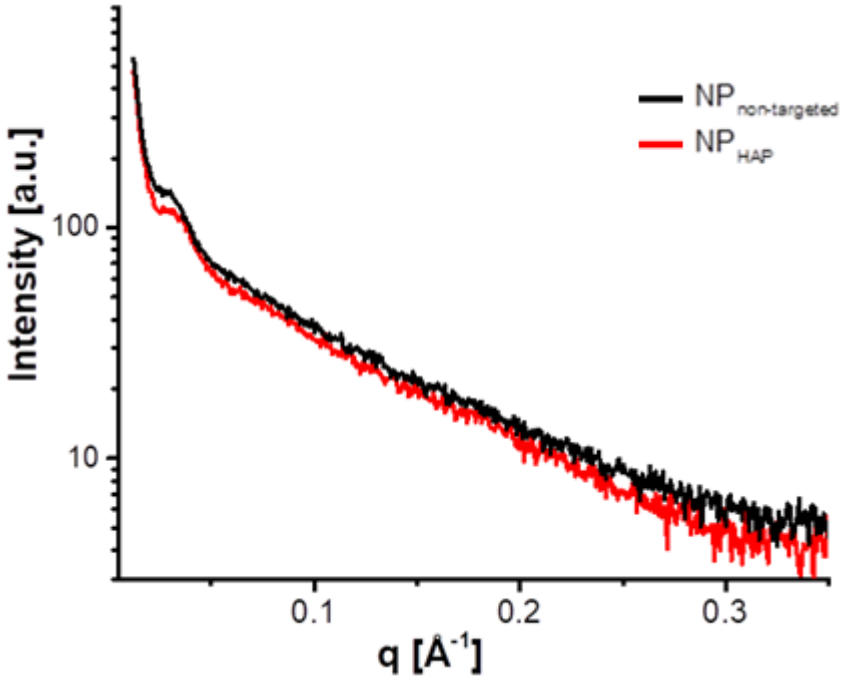

Figure 2.15. SAXS analysis of targeted and non-targeted 40% (w/w) OEA, 60% (w/w) LEA composed NP's stabilized with 15% PEG2000-OH.

2.4 DISCUSSION

The aqueous phase behaviour of amphiphilic molecules has important applications in a variety of fields such as biotechnology and drug delivery. In this study, the synthesis and physiochemical characterisation of monoethanolamide endocannabinoid lipids, LEA and OEA, and their ability to self-assemble into highly ordered NP has been demonstrated. The nanostructures formed by amphiphiles is dictated by local constraints imposed by the molecular structure, as well as external factors such as temperature, pH, ionic strength of the solution, excipient compositions and stabilising agents. For these two endocannabinoid molecules, the unsaturated hydrophobic chains were important in dictating their self-assembly behaviour. The presence of two cis-links in LEA as well as the introduction of an additional double unsaturated bond effectively shortens the amphiphiles hydrophobic chain length, leading to more splay in the membrane to accommodate its chain volume. In contrast, OEA with a single unsaturated long hydrophobic chain occupied minimal volume. By adjusting the ratio of lipid building blocks, the degree of unsaturation could be tailored to achieve lyotopic liquid crystalline mesophases and stable NP in an aqueous solution at physiological temperatures.

DSC results demonstrated a systematic shift in transition peak of the mixed amphiphilic was achieved by the increasing incorporation of OEA. By contrast, increasing LEA content decreased the melting temperature of the OEA/LEA mixes, which was more pronounced in mixtures containing Y-LEA. The primary difference between the two LEA's is due to the structure of the amphiphile molecule. LEA contains two unsaturated double bonds, while ɣ-LEA contains three. The additional double bond in ɣ-LEA further disrupts the lateral packing of the molecule, lowering the temperature at which the hydrophobic chain melts.

In addition to thermal stability, lipotropic phase behaviour of the monoethanolamide mixes was investigated using water penetration scans by POM and SAXS. Differences in refractive index of isotropic phases viewed under phase contrast allows for determination of the number of isotropic bands. The sequence of phases formed from the water–amphiphile interface along with their evident viscosity and texture formation provides indicative evidence for phase identification. Similar to results obtained by DSC, the phase behaviour observed was dictated by the degree of unsaturation and displayed polymorphic changes in the crystal structure at various temperatures and various ratios of the LEA to OEA. Assessment of phase behaviour of mixtures by POM and SAXS demonstrated the ability of a mixed ratio of 40% OEA and 60% LEA to self-assemble into highly ordered 3D cubic mesophase and form stable NPs in an aqueous solution. These structures were stable at both RT and physiological temperature, whereas LEA and OEA alone formed molten phase NPs and solid lipid NPs respectively. All other mixed samples formed either mixed mesophases that transformed to other mesophases at physiological temperature or formed mixed lamellar crystalline mesophase.

Assessment of the NP structure of by cryo-TEM showed the production sponge-like NP's (spongosomes), co-existing with liposomal NP's. While the formation of sponge-like NP is inconsistent with cubic phase liquid crystalline mesophases of the bulk amphiphiles observed in excess water under POM, it can be accounted for by the addition of 15% PEG2000-OH. Inclusion of the hydrophilic polymer chains, such as PEG, has been shown to increase both the solubility (Pasut, 2012) and molecular weight of the NP extending its half-life in circulation and improving its pharmacokinetics (Abuchowski et al., 1977). However, incorporation of PEGylated lipids have also been shown to impact the folding of the lipid amphiphiles in the aqueous solution. Consistent with this, comparison of the PEGylated system using cyro-TEM to the bulk phases observed in excess water highlights the influence of PEG2000 on the formation of liquid crystalline phase and the formation of sponge like NPs. When mixed with monoethanolamide mix, PEG's long chain promoted the formation of structures with less curvature, flattening the self-assembly and previously obtained lyotropic cubic mesophases.

Together, I have demonstrated that 40% OEA and 60% LEA is the optimum ratio of the mixed amphiphiles to form stable liquid crystalline mesophases at physiologically relevant temperatures. The ability of the monoethanolamide lipids to self-assemble into 3D NP offers a greater loading cargo, with potentially greater analgesic and anti-inflammatory effect. This mixed ratio was used in the investigation of biological activities *in-vitro* and *in-vivo* experiments.

2.4.1 Summary

This study clearly demonstrates and defines the conditions for a mix of endocannabinoid fatty acid monoethanolamides at the ratio of 40% OEA and 60% LEA to self-assemble into highly ordered 3D cubic mesophase and form stable NP at dilution in an aqueous solution. These structures are stable at both RT and physiological temperature, whereas LEA and OEA alone forms molten phase NP and solid lipid NP respectively. The ability of the monoethanolamide lipids to self-assemble into 3D cubosomes offers a greater loading cargo, with greater potential analgesic and anti-inflammatory effects.

CHAPTER 3: NANOPARTICLE LOCALISATION

3.1 INTRODUCTION

RA is a common auto-immune disorder characterised by chronic persistent inflammation of the synovial tissue that forms a pannus and ultimately leads to the destruction of articular cartilage and joints (Aletaha & Bluml, 2016). Although the exact aetiology remains unknown, it is generally accepted that RA is a multifactorial disease in which the immune cells and the FLS of the synovium play an important role (Bartok & Firestein, 2010). The identification of key players of inflammation and pathologic immune response in RA has resulted in the development of novel therapeutic strategies revolutionising the treatment of the disease. Newer agents that target FLS to the synovium could potentially improve current therapies and may provide opportunities to extend beyond the mere suppression of inflammation and to interfere with key disease processes in RA.

Traditionally, therapies for RA included a variety of drugs such as nonsteroidal anti-inflammatory drugs (NSAIDs) and disease modifying anti-rheumatic drugs (DMARDs) (Feely & O'Dell, 2010; Hoes et al., 2010). Whilst DMARDs have been shown to limit progressive joint damage and improve function, they are often associated with unfavourable side-effects limiting their application (Grove et al., 2001; Choy et al., 2008; Leon et al., 2018). More recently, the introduction of 'biologicals', which target pro-inflammatory and immunomodulatory cytokines through neutralising antibodies have demonstrated favourable disease outcomes when used in combination with DMARDs (Curtis & Singh, 2011; Inui & Koike, 2016). While the effects of cytokine-targeting/antibody therapies are encouraging, restricted efficacy due the induction of anti-drug antibody responses in chronic conditions such as RA and increased infection susceptibility at injection times remain an important limiting factor in the application of biologics (Bathon et al., 2000; Lipsky et al., 2000; Kourbeti et al., 2014). Collectively, there remains a growing unmet clinical need for the development of effective strategies that target and deliver therapeutic agents to the synovium for RA.

One such novel, strategic approach is through the use of NPs which have the potential to revolutionise the diagnosis and treatment of a variety of diseases, notably in the treatment of cancer (Davis et al., 2008; Zhang et al., 2008). Having defined the ability of a mix of OEA and LEA to form lipid NP dispersions (Chapter 2), the next few chapters investigates the NP's potential therapeutic benefits. Drug encapsulation into NPs offers numerous advantages during delivery including improved solubility, enhanced half-life and a favourable therapeutic index (Park et al., 2009; Wang et al., 2009). As the internal payload is masked, NP-encapsulated drugs are protected from early activation and degradation in circulation, thereby reducing systemic toxicity and the toxicity-benefit ratio (Zhang & Granick, 2006).

Whilst research into NP therapeutics has shown success, very few biodegradable and safe polymeric particles have been explored making the endogenous nature of these NAE-based NP's unique. NP drug encapsulation can overcome limitations such as low bioavailability and unfavourable pharmacokinetics which frequently restrict drug candidates (Petros & DeSimone, 2010). Such can be seen in the higher order lipid NP, which allows the encapsulation of both hydrophilic drugs within the internal water channels and hydrophobic drugs within the lipid bilayer (Zhang et al., 2008; Irby et al., 2017). Further to the NP's material choice, modification of NP *in-vivo* kinetic properties through surface functionalisation will help overcome biological barriers during circulation and achieve tissue targeting (Souhami et al., 1981; Alexis et al., 2008; Decuzzi et al., 2010). Incorporation of PEG2000's hydrophilic polymer chains increases both the solubility (Pasut, 2012) and molecular weight of the NP, extending its half-life in circulation (Abuchowski et al., 1977). The higher molecular weight of the pegylated NP may also benefit from enhanced permeability and retention (EPR) effect resulting in passive targeting to the inflamed joints. Finally, conjugation of a synovium targeting peptide, HAP-1, to the surface of our NP's will facilitate the delivery of therapeutic agents to the inflamed joint. It has previously been shown that conjugation of HAP-peptide facilitated the internalisation of large marker protein complexes into synovial cells in culture and *in-vivo* in a synovial cell-type-specific manner (Mi et al., 2003). In a separate study, direct linkage of HAP-1 to immunosuppressive peptide (Core peptide, CP) enhanced drug localisation and bioavailability to the inflamed joints than CP alone (Ali et al., 2011).

In this chapter, the targeting capabilities of both the $NP_{non\text{-}targeted}$ and NP_{HAP} were examined. *In-vitro* uptake of $NP_{non\text{-}targeted}$ and NP_{HAP} by human FLS and rabbit FLS cells was investigated using flow cytometry and imaged by confocal microscopy. Investigation of homing peptide, HAP-1, binding was also examined in h-FLS, RA-FLS and OA-FLS cells. *In-vivo,* localisation of fluorescently labelled $NP_{non\text{-}targeted}$, NP_{HAP} and NP_{sHAP} in both normal and arthritic rats was tracked using NIR. Finally, the pharmacokinetic profile and *in-vivo* bio-distribution of $NP_{non\text{-}targeted}$ and NP_{HAP} in arthritic rats were examined to assess their targeting capabilities and potential application as a novel drug delivery system for arthritis.

3.2 METHODS

3.2.1 Materials

Targeting and biotinylated peptides were custom made by Auspep (Melbourne, Australia). Supplied peptides were shown to be of high purity (>80%) by RP-HPLC. Human FLS cells, h-FLS, RA-FLS and OA-FLS, and synoviocyte growth medium were purchased from Cell Applications Inc (California, USA). HIG-82 cells were purchased from ATCC (Virginia, USA). Ham's F12 cell growth medium (Gibco, OK, USA), L-glutamine, penicillin, streptomycin, ethylenediaminetetraacetic acid (EDTA), 1,1'-Dioctadecyl-3,3,3',3'-Tetramethylindodicarbocyanine, 4-Chlorobenzenesulfonate salt (DiD) streptavidin-FITC and DAPI were purchased from Thermo Fischer Scientific (North Ryde, Australia). TRITC-phalloidin and other cell culture materials including fetal bovine serum (FBS), bovine serum albumin (BSA), 6-well plates, and glass coverslips were purchased from Sigma Aldrich (Sydney, Australia).

3.2.2 Generation of NPs

The NP used in this chapter were prepared as previously described in Section 2.2.2.

2.2.2.1 Fluorescent labelling of NPs

For fluorescent NPs, lipophilic fluorochrome tracer, DiD, was incorporated into the lipid membrane of the NP and used for *in-vitro* uptake and localisation studies. Briefly, the lipids 40% (w/w) OEA and 60% (w/w) LEA, and 1% (w/v) DiD were dissolved in ethanol and a thin lipid layer formed under rotary evaporator at RT as previously described in Section 2.2.2. Hydration and sonication were performed for the formation of fluorescent NP dispersions.

3.2.3 Cell Culture

Human FLS cells; healthy-FLS (h-FLS), RA FLS cells (RA-FLS), and OA FLS cells (OA-FLS) were cultured and maintained in synoviocyte growth medium at 37°C and 5% CO_2. Similarly, HIG-82 cells were cultured in Ham's F12 medium supplemented with 2 mM L-glutamine, 50 units/mL penicillin, 50 µg/mL streptomycin and 10% heat-inactivated FBS at 37°C and 5% CO_2. The cells used were from early passages (passage 3-7).

3.2.4 Immunofluorescence of HAP-1 binding

For confocal studies, FLS and HIG-82 cells were seeded at a 3 x 10^4 cells onto glass coverslips and incubated overnight at 37°C. HAP-1-biotin and sHAP-1-biotin were incubated with streptavidin-FITC. The biotinylated-streptavidin conjugates were then incubated with cells at 37°C for 3 h. Following incubation, the slides were washed with washing buffer (PBS, 1% FBS) to remove non-specific staining

and fixed with 2% paraformaldehyde for 20 min on ice. Slides were again washed and the actin cytoskeleton stained using TRITC-phalloidin (1:2000 dilution). After washing, DAPI (1:5000 dilution) was used to stain the cell nuclei. Following incubation, slides were then washed with PBS and embedded in mounting medium Fluorsave Reagent (Calbiochem, San Diego, USA). Images of cells were captured using an Olympus FV confocal laser scanning microscope (Olympus, Victoria, Australia)

3.2.5 Confocal Imaging of NP_{HAP} and $NP_{non\text{-}targeted}$ in FLS Cells

The cellular binding of DiD-labelled $NP_{non\text{-}targeted}$ and NP_{HAP} with h-FLS was evaluated using confocal microscopy. h-FLS cells were seeded at 5 x 10^6 cells onto glass coverslips and incubated overnight at 37°C. Adherent cells were then washed with PBS and incubated for 3 h with either DiD labelled $NP_{non\text{-}targeted}$ or NP_{HAP} (30 µg/mL) at 37°C. Following incubation, cells were washed three times with PBS (4°C) and fixed with 2% paraformaldehyde. After washing with PBS, slides were embedded in mounting medium Fluorsave Reagent and NP cell-uptake captured using an Olympus FV confocal laser scanning microscope.

3.2.6 Fluorescence Assisted Cell Sorting (FACs)

Flow cytometry was used to assess the NP *in-vitro* cellular binding in culture models. h-FLS and HIG-82 cells were seeded at a density 5 x 10^5 into 6 well plates and grown to confluence. After 48 h, medium was replenished and replaced with medium containing 30 µg/mL fluorescently labelled $NP_{non\text{-}targeted}$ or NP_{HAP}. Cells were then incubated for 1 h, 3 h and 18 h at 37°C. To assess if NP uptake was affected in inflammatory conditions, confluent cells were stimulated with TNF-α (10 ng/mL) for 24 h at 37°C prior to the addition of NPs. For assessment of NP dye leakage, NP were incubated with h-FLS cells for 3 h at 4°C. Untreated cells and free DiD dissolved in DMSO were used as controls. Following incubation, medium was removed and the cells washed three times with FACs buffer (PBS supplemented with 1% BSA) to remove surface-associated NPs. Cells were then detached using trypsin/EDTA (0.5 mM) and fixed in 1 mL of 4% paraformaldehyde in PBS solution for 1 h. The stained and fixed cells were stored in the dark at 4°C and the NP uptake measured as fluorescence intensity was analysed on a flow cytometer.

3.2.6.1 Quantification of NP-cell complexes by flow cytometry

The method used for flow cytometry in this chapter was modified from that published by Snipstad *et al* (2017). Fluorescence from cells was measured using BD FACS Cantroll analytic flow cytometer (BD Bioscience, San Jose, CA) and acquired with FACSDiVa v.6 software. DiD-NP were excited at 644 nm, and fluorescence emission detected at 665 nm using a 20-nm band-pass filter. A minimum of 500,000

cells were counted per sample. Selective exclusion of cellular fragments and debris from analysis was achieved by the subjective collection gating from distribution in the side-scatter (SSC) versus forward scatter (FSC) dot plot. To determine the extent of DiD uptake by the cells, a histogram was drawn with the x-axis set for cell fluorescence (detection of DiD) and the y-axis set to cell count. Settings for the flow cytometry machine were kept constant between the incubation times for both cell lines to ensure that mean intensity acquired by the gated peaks were constant. Collected data was analysed using FlowJo Software (Version 10.2).

3.2.7 Animals

Female Wistar rats (240 – 250 g, 8 to 9 weeks old) were purchased from Animal Resources Centre (Perth, WA, Australia). Rats were housed three per cage and provided with standard lab chow and water *ad libitum*. Rats were left to acclimatise for 2 weeks prior to any experiment. For *in-vivo* localisation experiments, rats were housed in Kolling Institute's Kearn's Animal Facility located within Royal North Shore Hospital (RNSH), Sydney. Animal experiments were performed at RNSH because the near infrared (NIR) machine was located in the facility. Experiments performed at the Kolling Institute were in accordance with Sydney Northern Area Health Animal Ethics guidelines (Ethics Approval Number: RESP 15/15). All other *in-vivo* work was conducted at the Westmead Animal Housing facility, located within Westmead Hospital, Sydney. Experiments performed at Westmead were in accordance with Western Sydney Local Health District Animal Ethics guidelines (Ethics Approval Number: 5105.08.12).

3.2.7.1 Adjuvant induced arthritis (AIA)

To induce arthritis, a single subcutaneous injection of lyophilised *Mycobacterium tuberculosis* (MTB) suspended in 100 µL of squalene was administered at the base of the tail as previously described (Manolios N, 1997). On average, arthritis developed 11-14 days post MTB injection. During this time, rats were monitored for any changes in wellbeing and pain and 0.05 mg/kg Temgesic (buprenorphine, 324 µg/mL) administered subcutaneously every 8-12 h when signs of pain or distress were shown. Rats were deemed to be arthritic when redness and swelling was present in the same joint(s) over two consecutive days.

3.2.8 *In-vivo* Localisation of NPs

To assess NP localisation *in-vivo*, fluorescently labelled $NP_{non\text{-}targeted}$, NP_{HAP} and NP_{sHAP} were intravenously injected (i.v.i) into the tail vein of both normal and arthritic rats and localisation tracked using a NIR imager. Rats were divided into three groups of five rats and administered either $NP_{non\text{-}targeted}$, NP_{HAP} or NP_{sHAP}, i.v.i. Rats were anaesthetised under isoflurane/oxygen (2% v/v isoflurane in 1 litre/min O_2) and NP (24 mg/kg) administered once, i.v.i. The animals remained anaesthetised and placed prone on a gamma camera (Siemens Medical Systems, IL, USA) equipped with a low energy high resolution collimator. NP *in-vivo* localisation was captured 24 h for 10 min using Fourier Transform Near Infrared Spectroscopy (FT-NIR) spectrometer (Bruker, Victoria, Australia). The images were acquired using matrix: 256 x 256 and zoom: 2.29. For optimum DiD intensity, emission was taken at 700 nm with a corresponding excitation of 650 nm. Program 'Image J' (Version 1.51) was used on the region of interest (ROI) on the chosen arthritic joint of each rat for each time point. X-rays were used to confirm the anatomical position of the region for a single case (Figure 3.1). The values reported were obtained by first averaging the signal value determined in the joints then by subtracting its background value from the signal obtained at each time-point for each joint.

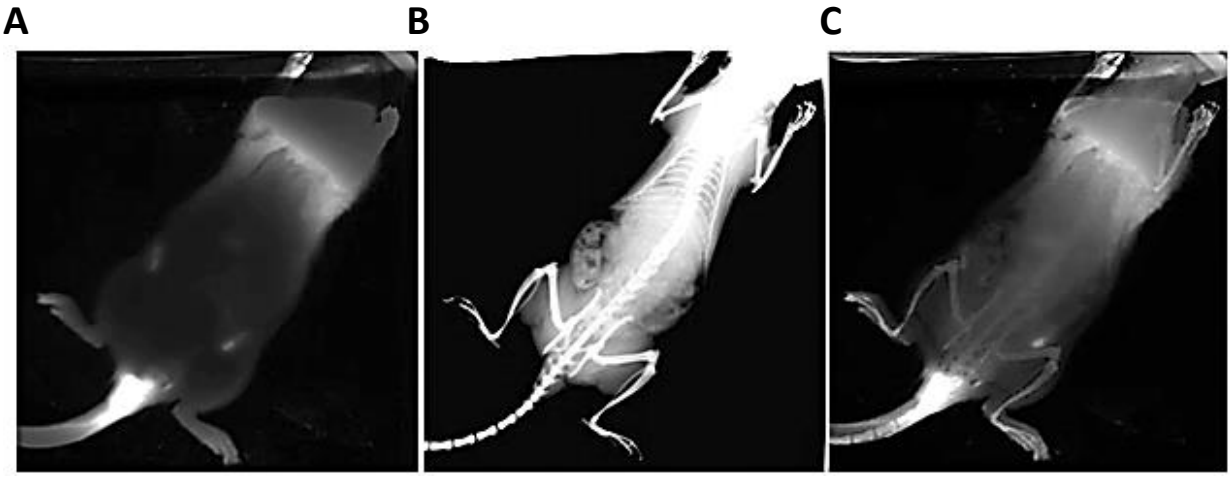

Figure 3.1. NIR localisation screening of **(A)** NIR capture of whole body**; (B)** X-ray capture of the same rat and; **(C)** A and B overlay.

3.2.9 *In-vivo* Pharmacokinetics and Bio-distribution

For assessment of NP pharmacokinetics and *in-vivo* biodistribution, arthritis was induced as stated in Section 3.2.7.1. Arthritic rats were then divided into four groups of five rats and treated as follows; untreated control (ART-CON); vehicle control (PEG/PBS, ART-PBS); $NP_{non\text{-}targeted}$ (ART-$NP_{non\text{-}targeted}$) and; NP_{HAP} (ART-NP_{HAP}). NP treated rats received an exact dose of 24 mg/kg administered i.v.i. The control groups received 500 µL injections of either normal saline or PEG/PBS. Following injection, blood samples were collected at various time intervals (0, 45 min, 1.5 h, 3 h, 6 h) via a temporary cannula in the lateral tail vein. Collected blood was centrifuged and the rat plasma separated, snap frozen in liquid nitrogen and stored -80^{o}C for analysis. After 6 h the animals were sacrificed and the kidneys, liver, spleen and paw were harvested, snap frozen in liquid nitrogen and stored -80^{o}C for analysis.

For tissues, lipid extractions were adapted from the methods by Stuart *et al* (2013). Samples were weighed and HPLC grade methanol (MeOH) was added to each tube to make a 100 mg/mL solution. For plasma, 3 mL of cold acetonitrile was added to precipitate proteins. Internal standard, deuterium labelled anandamide (d4-AEA), was added to tissue samples (100 µL of 1 µM) and plasma samples (10 µM of 1 µM) and incubated on ice for 2 h (plasma) to 12 h (tissues). Tissues were homogenised on ice for approximately 2 min using a tissue tearer, except for the paw joints which were bead beaten (glass beads 2.5 mm) for 2 min at 35,000 oscillations per min. The samples were then centrifuged at 19,000 x *g* for 20 min at 24°C. Tissues were extracted in duplicates of 500 µL (spleen, liver) or 1 mL (kidney, paw) of each supernatant. HPLC-grade water was then added to make the final supernatant (tissue and plasma) solution 25% organic. Samples were extracted through The Extrahera (Biotage, Uppsala, Sweden), an automated extraction robot through 500 mg C18 solid phase extraction columns. The columns were conditioned with 5 mL of HPLC MeOH (170 sec of 0.5 bar) and 3 mL of HPLC grade water (80 sec of 0.5 bar). 25% of organic supernatant solution was then loaded into its corresponding column. Wash steps of 1.5 mL of HPLC water, 40% MeOH 65% MeOH, and 85% MeOH (90 sec each at 0.5 bar) were then added in succession. 1.5 mL of 100% HPLC grade MeOH (105 sec at 0.1 bar, with plate dry) was then added to elute the ethanolamides which was collected in amber autosampler vials. Vials were then put straight into the autosampler (24^{o}C).

3.2.9.1 Quantification of endocannabinoids by HPLC/LC/MS

20 µL injections of each sample were rapidly separated using a C8 Zorbax guard column in conjunction with a C18 Zorbax reverse-phased analytical column by a gradient of 20% ultrapure HPLC MeOH, 80% filtered HPLC water with 1 mM ammonium acetate (mobile phase A) and 100% ultrapure HPLC grade MeOH and 1 mM ammonium acetate (mobile phase B). Two Shimadzu LC-30AD pumps (Rydalmere, NSW, Australia) were then used to create a pressurized gradient elution (200 µL/min). A Shimadzu 8030 triple quadrupole MS was used to ionize the sample using positive electrospray ionization through a multiple reaction monitoring method. Synthetic standards of PEA, OEA, LEA and d4-AEA (Cayman Chemical, Ann Arbor, MI, USA) were used to generate calibration curves for quantification by LabSolutions software (Shimadzu, Rydalmere, NSW, Australia). The concentration of each analyte was then converted to moles per gram tissue (using the weights obtained). Statistical analysis was performed using GraphPad Prism (Version 7).

3.3 RESULTS

3.3.1 *In-vitro* NP Cell Interactions

3.3.1.1 *In-vitro* assessment of HAP-1-binding peptide

Immunofluorescence was used to validate the binding of the homing-peptide, HAP-1, to human FLS cells. Since the HAP-1 sequence was originally isolated using HIG-82 cells, HAP-1-binding to HIG-82 cells (Figure 3.2A) were used as a positive control and run in parallel when testing the binding of HAP-1-biotin to h-FLS groups (Figure 3.2B). Representative confocal images of HAP-1-binding to HIG-82 and h-FLS cells are shown in Figure 3.2. Cells treated with HAP-1-biotin showed positive binding indicated by the green fluorescence, with internalisation into the cytoplasm. A similar staining pattern was noted with normal h-FLS RA-FLS and OA-FLS cell types (Figure 3.2B), with positive binding present in HAP-1-biotin treated groups. The binding pattern of HAP-1 was consistent across the h-FLS cell types with positive staining present on both the surface (yellow); and cytoplasmic internalisation (green). Cells incubated with either media or sHAP-1-biotin showed no green FITC-stain demonstrating the binding specificity of the HAP-1 sequence.

A

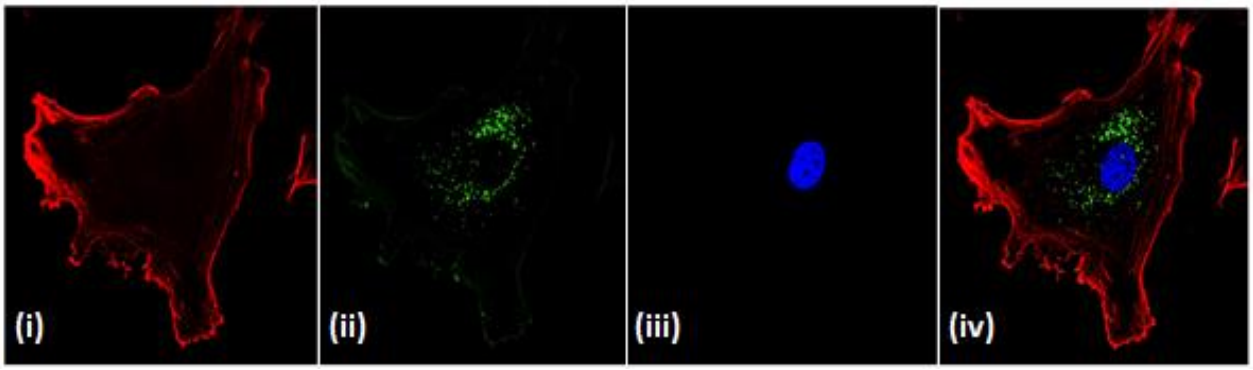

B

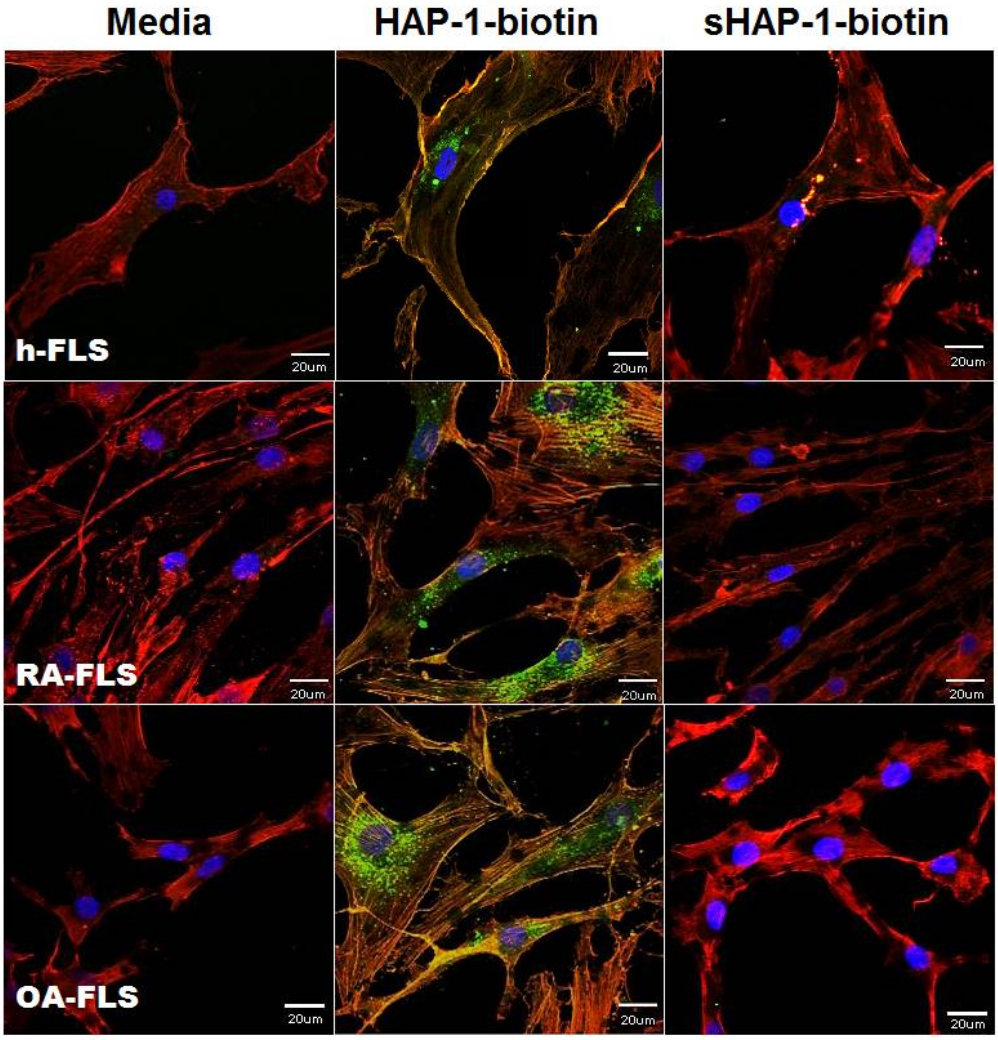

Figure 3.2. Confocal fluorescent microscopy images of positive HAP-1-binding to **(A)** HIG-82 cells and; **(B)** h-FLS, RA-FLS, and OA-FLS cells. Fluorescence labelling shown in; **(A)** using HIG-82 as a positive binding sample. Actin was labelled with TRITC-phalloidin (red (i)); HAP-biotin binding labelled with streptavidin-FITC (green (ii)); nuclei labelled with DAPI (blue, (iii)), overlay of (i-iii) shown in (iv). Scale bars represent 20 µm. HAP-1 binding was observed in all FLS cell types **(B)** incubated with HAP-1-biotin-avidin-FITC, indicated by the green fluorescence.

3.3.1.2 *In-vitro* NP cell binding confocal

Figure 3.3A, shows the fluorescent image of DiD-labelled $NP_{non\text{-}targeted}$ (yellow) following incubation with h-FLS cells. The corresponding differential interference contrast (DIC) image of the same section is shown in Figure 3.3B. Similarly, confocal microscopic image of NP_{HAP} uptake by h-FLS is shown in Figure 3.3C with corresponding DIC image in Figure 3.3D. Both images show NP uptake around the nucleus, with intracellular localisation predominately within the cytoplasm in the h-FLS cells.

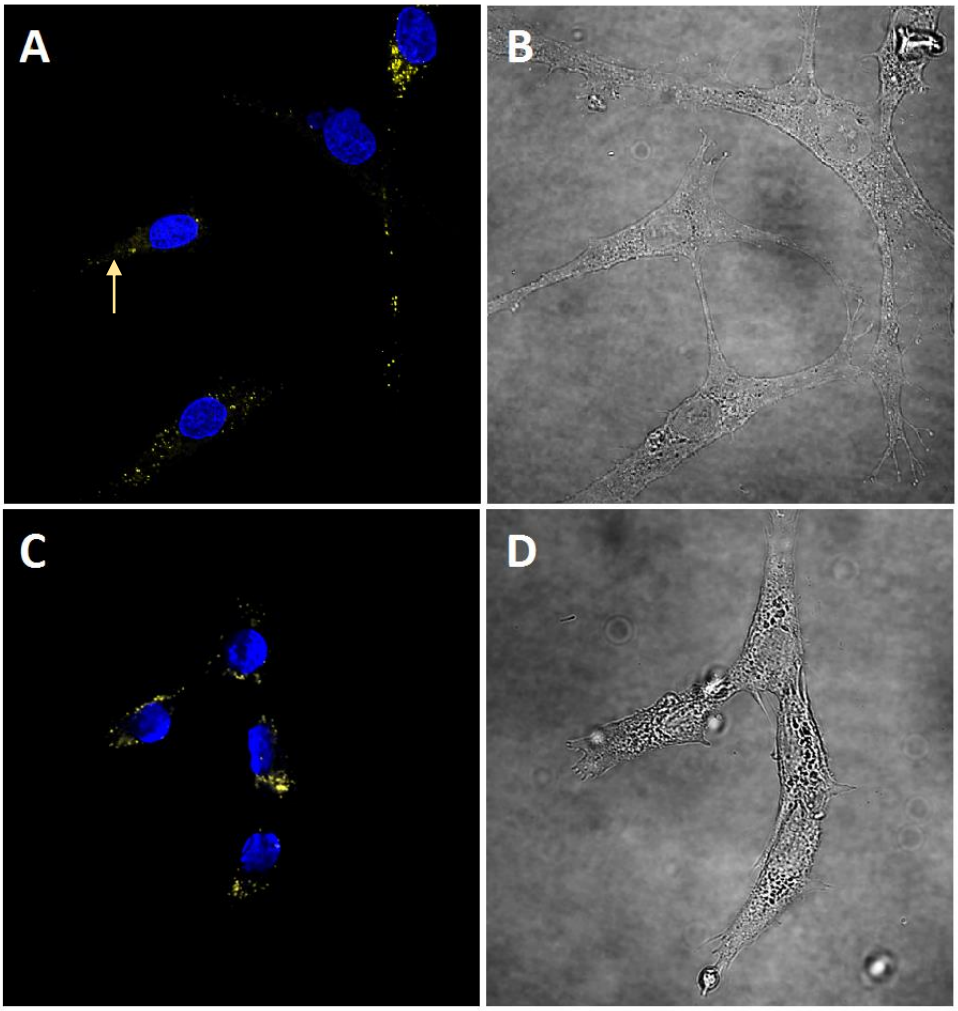

Figure 3.3. Confocal microscopy images of h-FLS cell uptake of DiD-labelled $NP_{non\text{-}targeted}$ and NP_{HAP} following 6 h incubation. Cell nucleus is stained with DAPI (blue). Yellow staining (yellow arrow) corresponds to fluorescently labelled NP uptake. Images B and D are the phase contrast view of the same cells. **(A)** Fluorescent microscopic image of $NP_{non\text{-}targeted}$ binding to h-FLS cells; **(B)** Transmitted light image of the same section as in A; **(C)** Fluorescent microscopic image of targeted NP_{HAP} binding to cells; **(D)** Transmitted light image of same section as C.

3.3.1.3 *In-vitro* NP quantitative uptake

To evaluate the cellular uptake of the $NP_{non\text{-}targeted}$ and NP_{HAP}, fluorescently labelled NPs were incubated with h-FLS cells at 37˚C. NP uptake was measured as the intensity of the fluorescence signal using flow cytometry. Figure 3.4 shows the flow cytometry analysis of (A) h-FLS cells and; (B) HIG-82 cells following incubation with either $NP_{non\text{-}targeted}$ or NP_{HAP} for 1, 3 NP_{HAP} 18 h at 37°C. As shown in Figure 3.4A no detectable dye was recorded for $NP_{non\text{-}targeted}$ and NP_{HAP} following a 1 h incubation in h-FLS cells, indicating minimal NP uptake by the cells. Following 3 h incubation, there was uptake of both NP's indicated by a shift in the cell fluorescence peak along the x-axis to the right. NP_{HAP} were internalised more efficiently than $NP_{non\text{-}targeted}$ with the percentage of cells that took up detectable dye recorded as 69.1% for NP_{HAP} and 33.2% for $NP_{non\text{-}targeted}$ (Figure 3.4A 3h). Increasing NP incubation to 18 h slightly improved uptake of both $NP_{non\text{-}targeted}$ and NP_{HAP} to 44.8% and 74.5%, respectively, when compared to 3 h incubation time.

Similarly, uptake of $NP_{non\text{-}targeted}$ and NP_{HAP} following a 1 h incubation in HIG-82 cells was minimal (Figure 3.4B), with $NP_{non\text{-}targeted}$ uptake recorded as 10.6% and NP_{HAP} uptake slightly more efficient at 16.5%. Higher levels of detectable dye were recorded for NP_{HAP} (78.5%) when compared to $NP_{non\text{-}targeted}$ (32.7%) following 3 h incubation. Cell fluorescence following 18 h incubation with both the NP_{HAP} and $NP_{non\text{-}targeted}$ was only slightly higher than 3 h exposure, recording 82.3% and 34.4% respectively. NP uptake by the h-FLS and HIG-82 cells was comparable between the two cell lines at the respective time points.

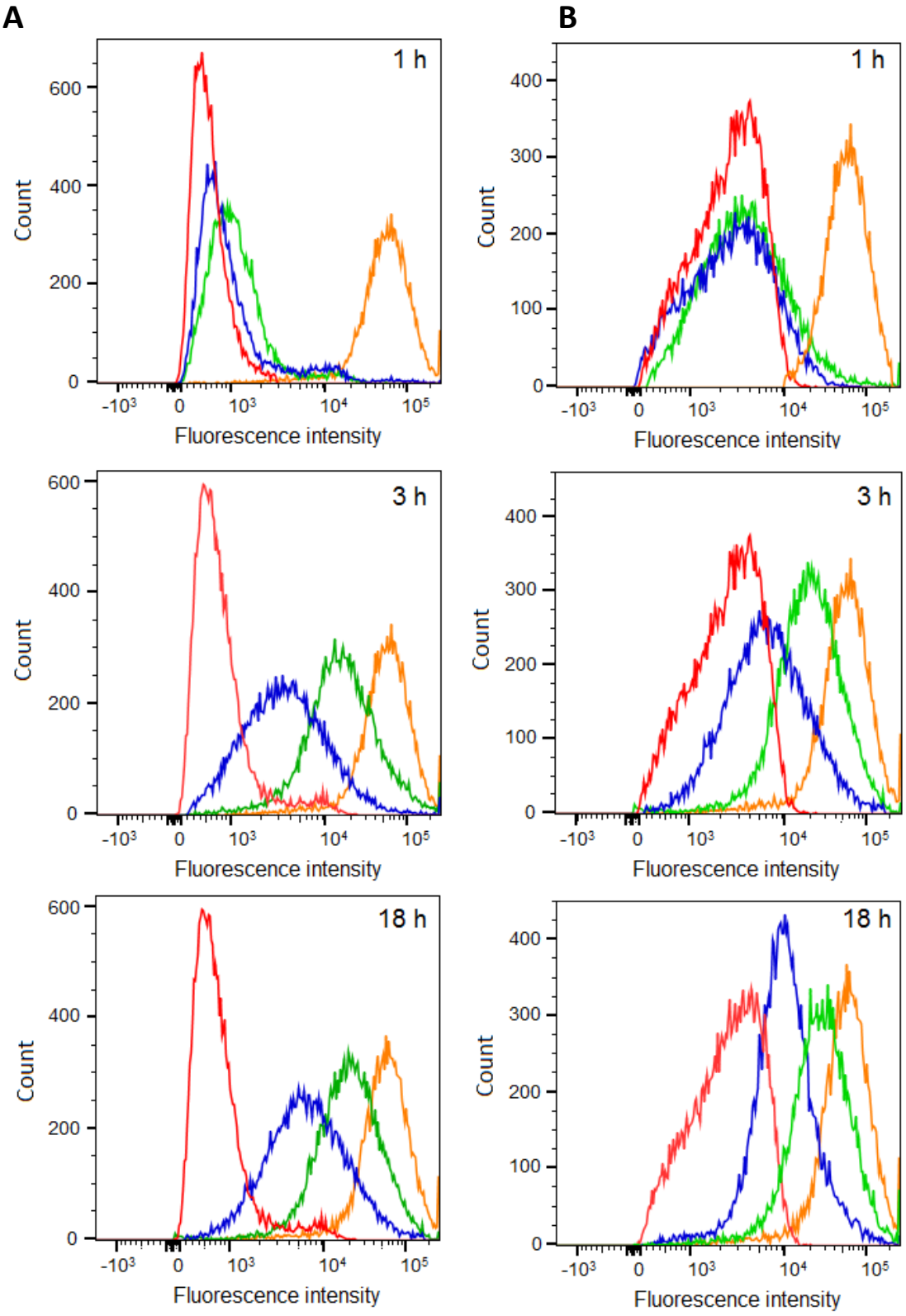

Figure 3.4. Flow cytometry histograms illustrating uptake of $NP_{non\text{-}targeted}$ and NP_{HAP} in **(A)** h-FLS or; **(B)** HIG-82 cells as indicated by a shift in cell fluorescence. Cells were incubated for 1 h, 3 h and 18 h at 37°C. Autofluorescence (red), incubation with $NP_{non\text{-}targeted}$ (blue), NP_{HAP} (green) and free DiD dye (orange). The experiment was repeated three times. The shown histograms are a representative example of results.

3.3.1.4 *In-vitro* NP uptake following TNF-α stimulation

To investigate whether NP uptake is influenced by inflammatory conditions, h-FLS and HIG-82 cells were stimulated with (10 ng/mL) TNF-α for 24 h prior to NP treatment. Flow cytometry histograms of uptake in stimulated and non-stimulated cells is shown in Figure 3.5. In h-FLS cells, uptake of $NP_{non\text{-}targeted}$ was neither hindered nor improved following TNF-α stimulation (Figure 3.5A). Similarly, cell fluorescence remained unaffected for NP_{HAP} in inflammatory conditions when compared to non-stimulated cells, suggesting uptake of NP_{HAP} was unaffected despite TNF-α stimulation (Figure 3.5B). Taken together, the data suggest that's NP uptake is not influenced by TNF-α stimulation.

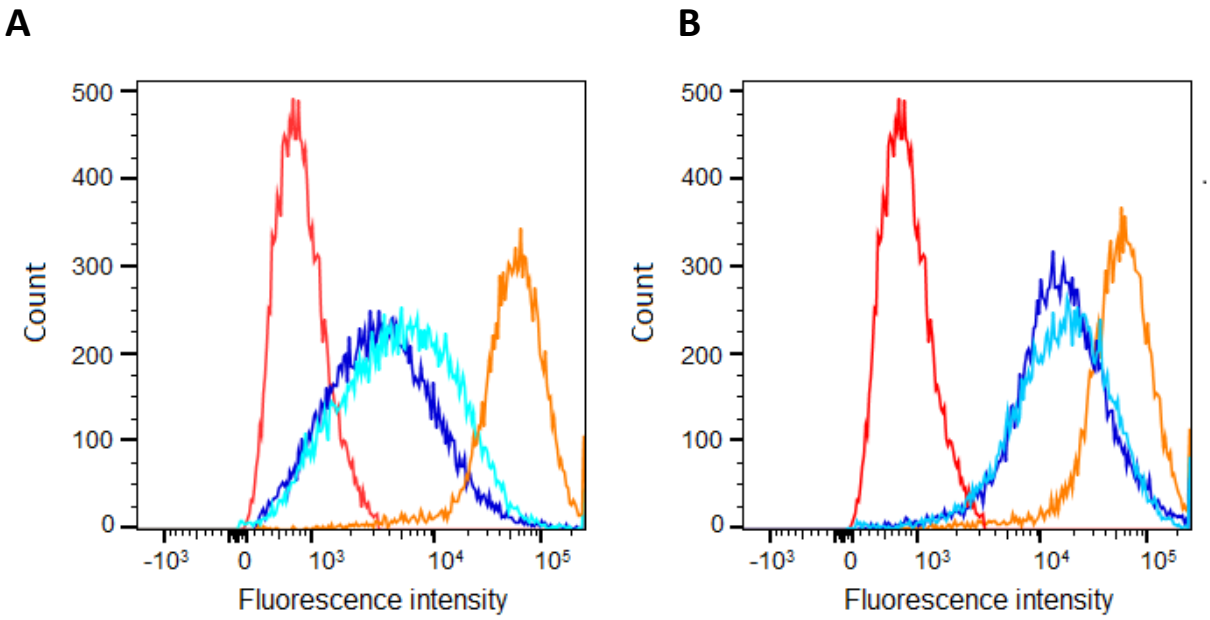

Figure 3.5. Flow cytometry histograms illustrating uptake of **(A)** $NP_{non\text{-}targeted}$ and; **(B)** NP_{HAP} in h-FLS cells before (dark blue) and after TNF-α stimulation (light blue). NP uptake by the cells is indicated by a shift in cell fluorescence intensity. Autofluorescence (red) and incubation with free DiD dye (orange). Uptake of both $NP_{non\text{-}targeted}$ and NP_{HAP} remained the same in both non-stimulated and TNF-α stimulated cells. The experiments were repeated three times. The shown histogram is a representative example of results.

3.3.2 NP Dye Retention

To evaluate the ability of NP to retain encapsulated dye, DiD labelled NP were incubated with h-FLS cells at 37˚C and 4˚C. NP uptake was measured as fluorescence intensity using flow cytometry. At 4˚C, endocytosis is largely eliminated allowing 'free dye' to diffuse across the cell membrane. With the assumption that encapsulated dye will not be endocytosed by the cell at 4˚C, this methodology allows for the assessment of the NP dye retention. Non-DiD labelled NP and untreated cells were also evaluated to account for any inherent auto fluorescence. Figure 3.6 shows cell fluorescence following incubation with (A) $NP_{non\text{-}targeted}$ or (B) NP_{HAP} at 4˚C and 37˚C for 3 h. At 4˚C minimal fluorescence was noted from cells incubated with either DiD labelled $NP_{non\text{-}targeted}$ or DiD labelled NP_{HAP}. Since there was no change in cell fluorescence is noted, it is implied that the encapsulated DiD dye was retained within the NP and suitable to use in *in-vitro* uptake studies. By contrast, encapsulated DiD NPs showed higher fluorescence at 37˚C than 4˚C, indicating endocytosis and/or surface binding of the NPs. While NP uptake was observed 37˚C, cells incubated with NP's at 4˚C showed no uptake and no change in fluorescence. With the assumption that free dyes enter the cell via an energy-independent process holds, the absence of fluorescence detection at 4˚C indicates successful retention of dye within the NP and therefore its suitable application in quantitative cellular uptake studies.

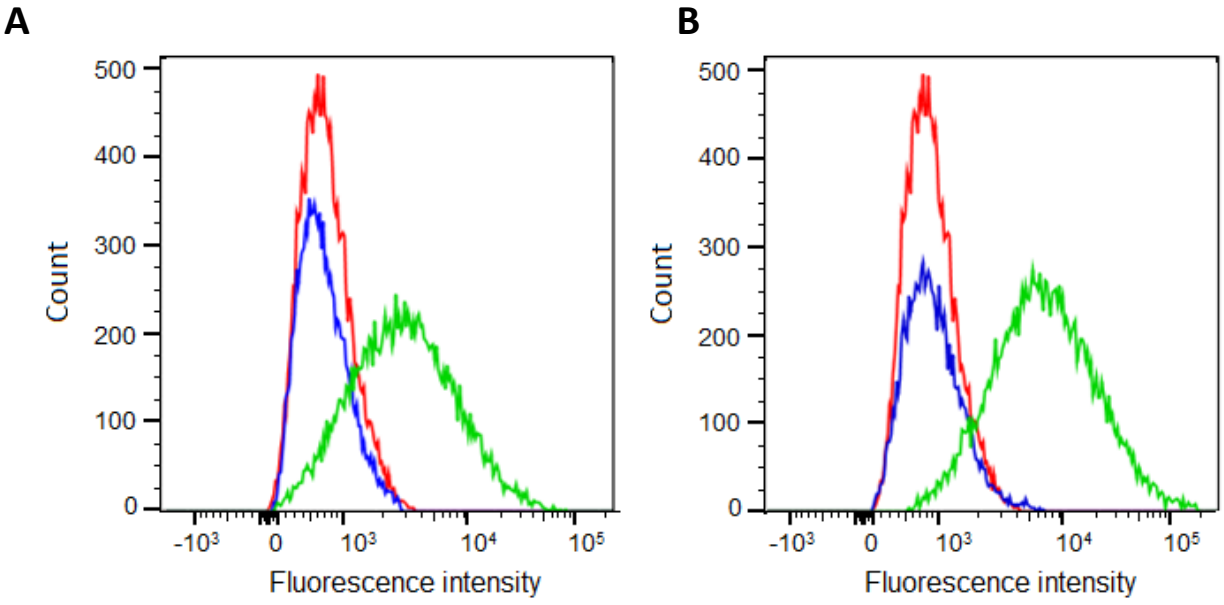

Figure 3.6. Flow cytometry histograms illustrating h-FLS cell uptake of **(A)** $NP_{non\text{-}targeted}$ and; **(B)** NP_{HAP} at 4°C (green) and 37°C (blue). NP cell uptake is indicated by the shift from the autofluorescence peak (red) to the right (x-axis), indicating higher fluorescence intensity. As no change in fluorescence intensity (when compared to the autofluorescence), was noted following NP incubation at 4°C, the dye was successfully retained within the NP. Experiments were repeated three times, the shown histogram is a representative of results.

3.3.3 *In-vivo* Localisation of NP's in Normal and Arthritic Rats

To assess *in-vivo* localisation, DiD-labelled NPs were injected into the tail vein of normal and arthritic rats. NP accumulation was measured as fluorescence intensity and captured at 1 h, 3 h, 24 h and 48 h for 10 min using FT-NIR imager. After 24 h, NIR fluorescence signals stopped increasing in intensity and remained constant. Figure 3.7A shows the NIR *in-vivo* localisation profile of normal and arthritic rats 24 h post NP injection.

In normal rats, no specific accumulation of fluorescent NP's was observed in either $NP_{non\text{-}targeted}$ or NP_{sHAP} rats, with the only minimal fluorescence noted at injection site Figure 3.7A. In arthritic rats, localisation of both the $NP_{non\text{-}targeted}$ and the NP_{sHAP} to the affected joints was increased to 62.1% (32.1 ± 8.24 signal units) and 71.2% (36.06 ± 5.57 signal units) respectively when compared to normal rats. Signal units for unaffected joints of the arthritic rats were comparable to the joints in normal rats. The restricted accumulation of $NP_{non\text{-}targeted}$ and the NP_{sHAP} to only the affected arthritic joints indicated passive targeting attributed to the leaky vasculature of the inflamed area. In contrast to the $NP_{non\text{-}targeted}$ and NP_{sHAP} treated groups, normal rats injected with the targeted NP_{HAP} localised to joints (34.37 ± 2.08 signal units). Signal at these joints was 73.6% higher than that observed in $NP_{non\text{-}targeted}$ (19.79 ± 6.04 signal units) for NPs normal rats. In arthritic rats, localisation of NP_{sHAP} to the inflamed joints increased by 58.2% (54.37 ± 13.95 signal units) compared to NP_{HAP} treated normal rats, and was 69.3% higher when compared to $NP_{non\text{-}targeted}$ injected arthritic rats.

Following whole-animal imaging at 24 h, the rats were sacrificed and the major internal organs spleen, liver, kidneys and lungs harvested for NIR imaging. As show in Figure 3.7B, minimal fluorescence was observed in the lungs for both $NP_{non\text{-}targeted}$ and NP_{HAP} treated rats. In contrast, stronger fluorescence signals were noted in both the spleen and liver of the NP treated rats suggesting retention of the NP at these sites. While the organ fluorescence were comparable between the two NP groups, fluorescence of the liver taken from the $NP_{non\text{-}targeted}$ group was significantly higher when compared to the liver of the NP_{HAP} injected group. The difference in fluorescence intensity highlights variances in NP *in-vivo* localisation between the $NP_{non\text{-}targeted}$ and $NP_{HAP,}$ and higher liver clearance of $NP_{non\text{-}targeted}$.

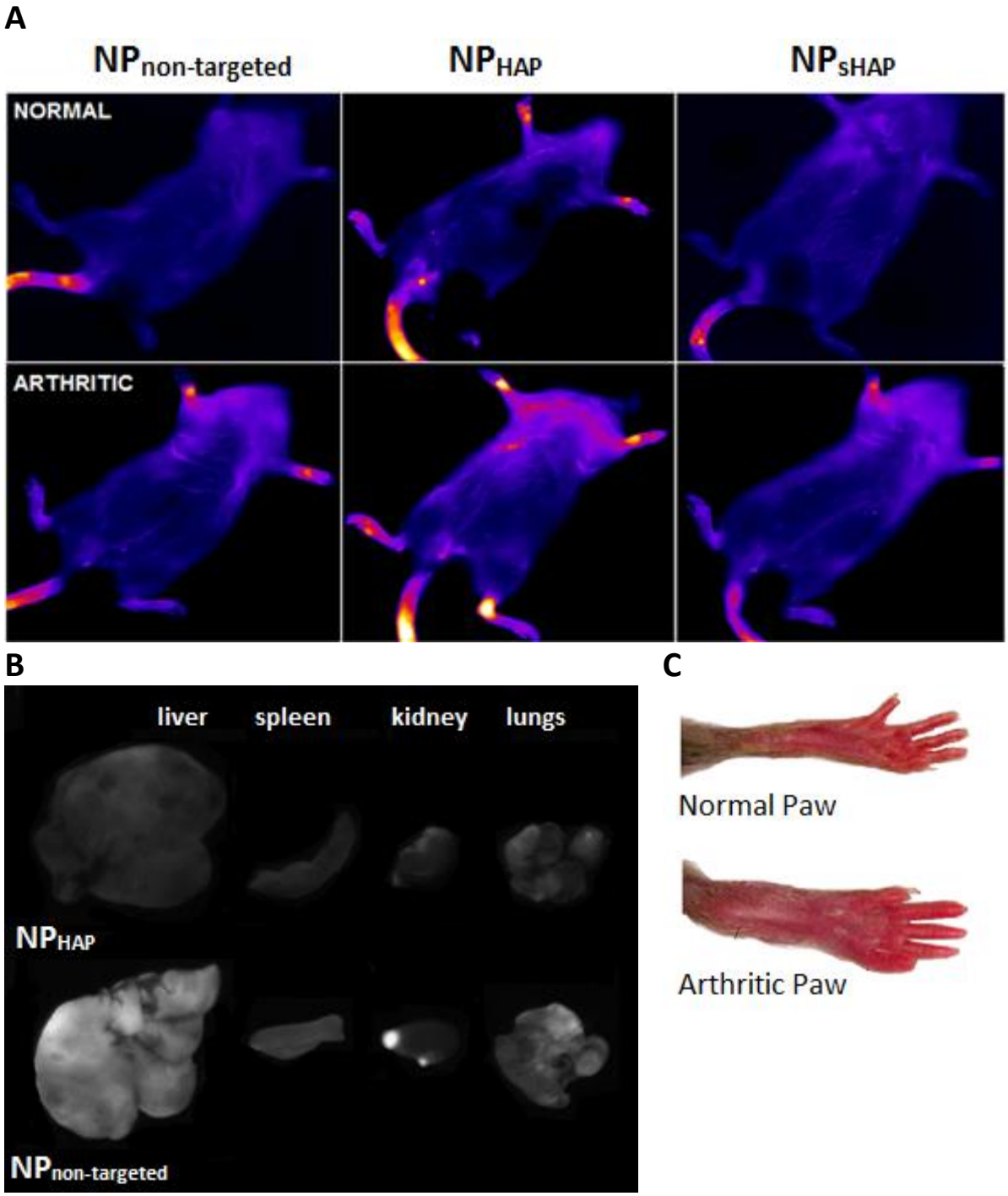

Figure 3.7. (A) *In-vivo* NIR imaging of $NP_{non\text{-}targeted}$, NP_{HAP} and NP_{sHAP} in normal and arthritic rat 24 h post-injection; **(B)** *Ex-vivo* imaging of liver, spleen and kidney $NP_{non\text{-}targeted}$, NP_{HAP} rats taken 24 h after injection. As NIR imaging has a restricted capture distance, internal accumulation to organs cannot be imaged *in-situ* and therefore not represented in the whole-animal images; **(C)** Photographic examples of normal and arthritic rat hind paws. NP_{HAP} localised to joints in both normal and arthritic joints.

3.2.4 *In-vivo* Biodistribution of $NP_{non\text{-}targeted}$ and NP_{HAP}

3.2.4.1 Plasma

Endogenous endocannabinoid levels and their entourage compounds were measured in blood plasma of normal and arthritic rats, Figure 3.8. No detectable differences were observed between OEA or LEA in normal (NORM) or untreated arthritic rats (ART CON). To assess the NP pharmacological half-life, NP were administered via the tail vein in arthritic rats and blood collected at 45 mins, 1.5, 3 and 6 h. Figure 3.8 shows the plasma concentrations of OEA and LEA over 6 h and the pharmacokinetic (PK) parameters of the injected $NP_{non\text{-}targeted}$ and NP_{HAP} are shown in Figure 3.8C and Figure 3.8D respectively. The PK profile of total NP in the plasma between 0 – 6h were fit using a one-phase decay non-linear regression curve. The initial concentration of total LEA in plasma was 214 ± 84.3 µmol/g and OEA 143.5 ± 47.2 µmol/g following injection as extrapolated from the exponential decay and decreased bi-exponentially after the 6 h sample. The terminal half-life for $NP_{non\text{-}targeted}$ was 0.16 h (LEA), 0.20 h (OEA) and 0.31 h (LEA), 0.48 h (OEA) for NP_{HAP}.

At 45 min, plasma concentrations of OEA and LEA were at their peak for both $NP_{non\text{-}targeted}$ and NP_{HAP} treated groups, with LEA being the dominant endocannabinoid. Since the NP are composed of 60% LEA and 40% OEA, the data is in agreement and reflects the composition of injected NPs components. At 45 min, concentrations of both OEA and LEA were higher in NP_{HAP} treated rats, when compared to $NP_{non\text{-}targeted}$ treated groups. Higher plasma concentration of OEA and LEA in NP_{HAP} treated rats at the same times point suggests a longer circulating time for NP_{HAP} which may be attributed to the presence of the homing peptide. At 1.5 h, circulating OEA and LEA plasma levels begin to steadily decline for both NP groups. At 3 h, plasma concentrations of both OEA and LEA were comparable, with no significant difference noted between the $NP_{non\text{-}targeted}$ and NP_{HAP} treated groups. Between 3 to 6 h, OEA and LEA plasma concentrations steadily declined towards baseline suggesting removal of NP from the blood due to clearance of joint deposits. At 6 h, OEA and LEA levels for both NP treated groups were minimal suggesting limited concentration of NP still in circulation. However when compared to baseline, OEA and LEA concentrations in NP treated groups were elevated suggesting the presence of NP still in circulation 6 h after initial injection.

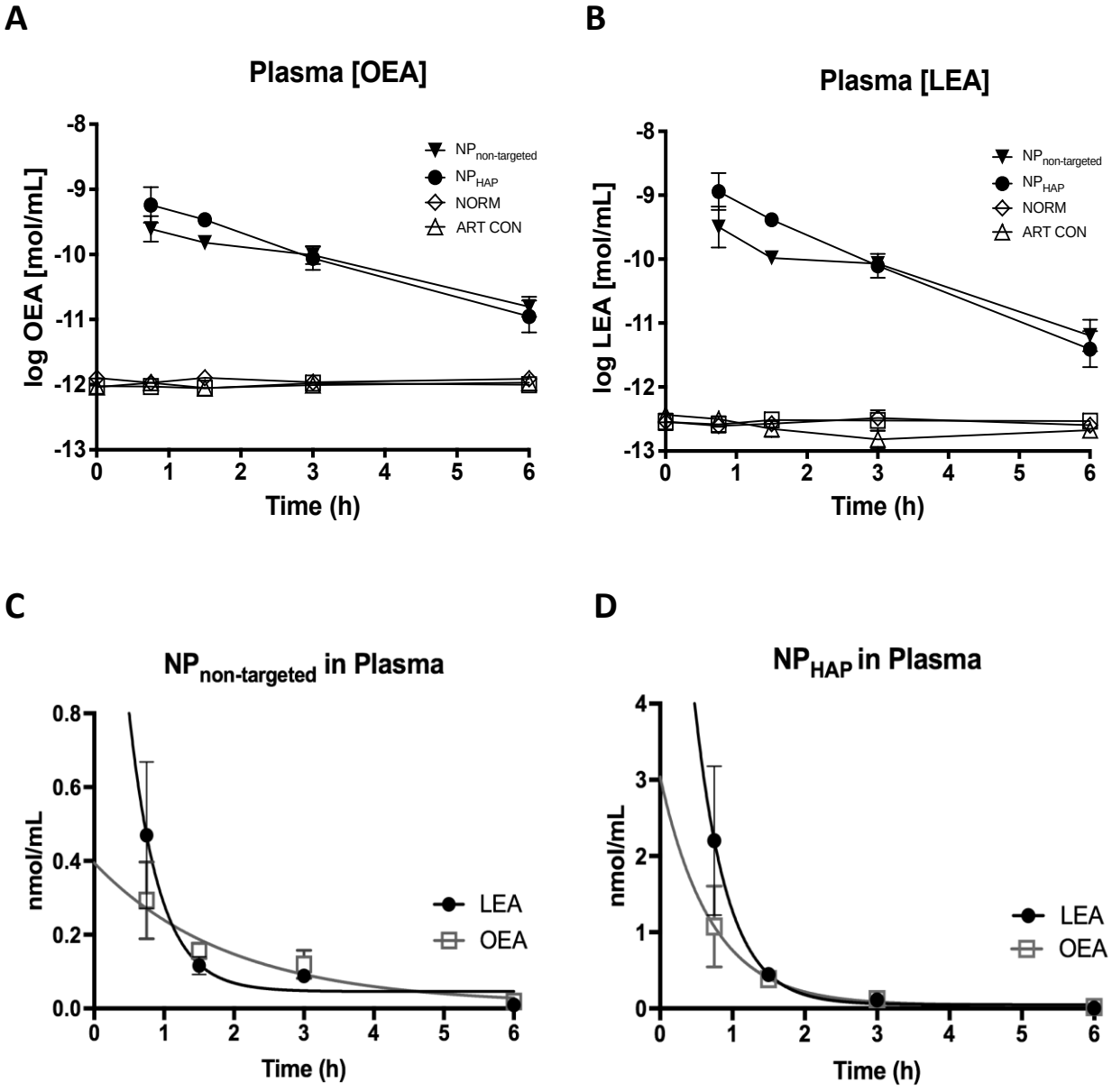

Figure 3.8. Plasma concentrations of **(A)** OEA and; **(B)** LEA in normal rats (NORM), arthritic control rats (ART CON), arthritic rats treated with $NP_{non\text{-}targeted}$ and NP_{HAP}. Plasma concentrations were calculated from blood samples collected at 0 h (baseline), 45 min, 1.5 h, 3 h and 6 h after initial treatment. Data was analysed by MS and concentration expressed as log nmol/mL (mean ± S.D, n = 5). PK for; **(C)** $NP_{non\text{-}targeted}$ and; **(D)** NP_{HAP} content vs time (up to 6 h) fitted with a one-phase exponential decay curve.

3.2.4.2 Organs

The distribution of NP into solid organs was determined at 6 h (Figure 3.9). The NP's endocannabinoid components, OEA and LEA, were measured against baseline levels of control and normal rats. For $NP_{non\text{-}targeted}$ treated rats, the liver contained the highest relative concentration of OEA (1.72 ± 0.87 pmol/g) and LEA (9.38 ± 5.2 pmol/g) when compared to endogenous ART-CON levels. Bio-distribution of $NP_{non\text{-}targeted}$ to the kidneys was minimal, with comparable concentrations of OEA (2.69 ± 1.19 pmol/g) and LEA (0.98 ± 0.29 pmol/g) to baseline control. Similarly, distribution to the spleen was also minimal, with comparable concentrations of OEA (2.56 ± 1.02 pmol/g) and LEA (0.86 ± 0.29 pmol/g) to baseline arthritis control.

While concentrations of $NP_{non\text{-}targeted}$ were high in the liver, only small amounts of OEA (0.86 ± 0.09 pmol/g) and LEA (0.59 ± 0.10 pmol/g) were recorded in the liver for NP_{HAP} treated groups. Distribution to the kidneys was shown to be OEA (2.97 ± 1.30 pmol/g) and LEA (1.29 ± 0.57 pmol/g) for NP_{HAP} groups. In the spleen, minimal concentrations of OEA (2.79 ± 1.58 pmol/g) and LEA (0.79 ± 0.219 pmol/g) were noted in NP_{HAP} groups and comparable to that seen in $NP_{non\text{-}targeted}$.

3.2.4.3 Joints

The relationship between NP concentration in the plasma and tissues at 6 h is illustrated in Figure 3.10. At 6 h, ratios of OEA and LEA were relatively low for all organs, reflecting a high concentration of NP still circulating in the plasma for both $NP_{non\text{-}targeted}$ and NP_{HAP}. In the paw, accumulation of NP_{HAP} to the inflamed joints was pronounced and was indicated by higher paw:plasma ratios for OEA (0.49) and LEA (0.55). By contrast, slightly higher plasma concentrations of OEA and LEA in the $NP_{non\text{-}targeted}$ group coincided with reduced concentrations of OEA and LEA recorded in the inflamed joints and low OEA (0.32) and LEA (0.24) paw:plasma ratios. While both the $NP_{non\text{-}targeted}$ and NP_{HAP} appeared to localise to the joints, only NP_{HAP} was significant, demonstrating a superior localisation of the targeted NP_{HAP} to the inflamed site mediated by the addition of the synovium targeting peptide, HAP-1.

A

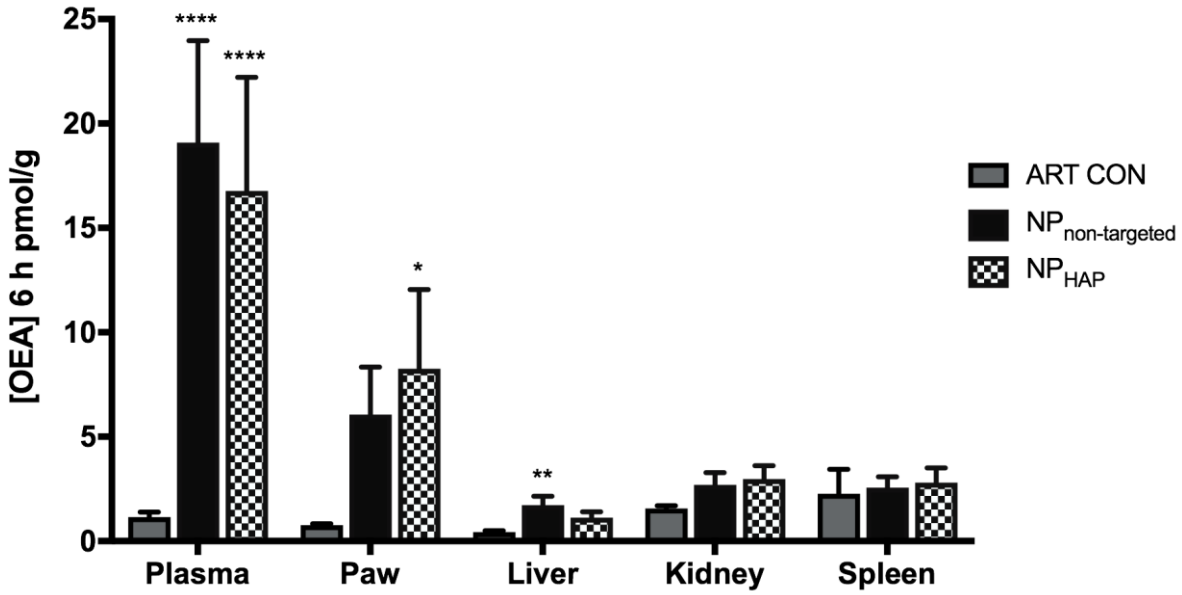

B

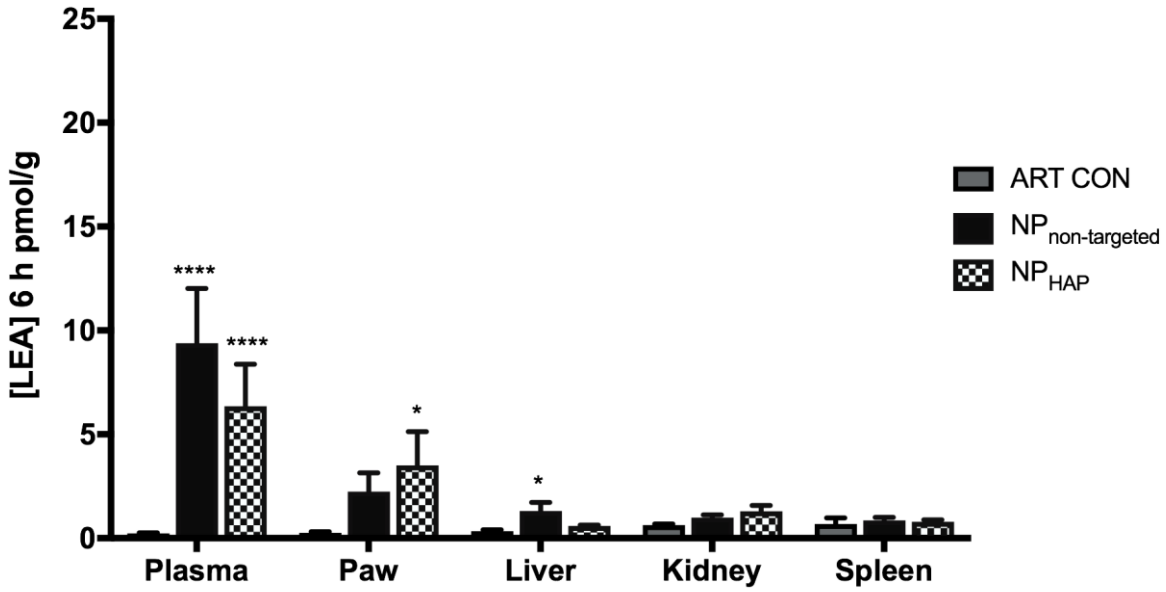

Figure 3.9. Concentrations of **(A)** OEA and; **(B)** LEA in un-treated, $NP_{non\text{-}targeted}$ and NP_{HAP} treated arthritic rats. Organs were harvested 6 h after treatment and NP distribution assessed in the arthritic paw, liver, kidney, spleen and plasma. Data analysed by MS and concentration expressed as pmol/g (mean ± SEM, n = 5). *p < 0.05, ****p < 0.0001 vs ART-CON, uncorrected Fisher's LSD, one-way ANOVA. Significant accumulation to the paw was observed in NP_{HAP} treated rats.

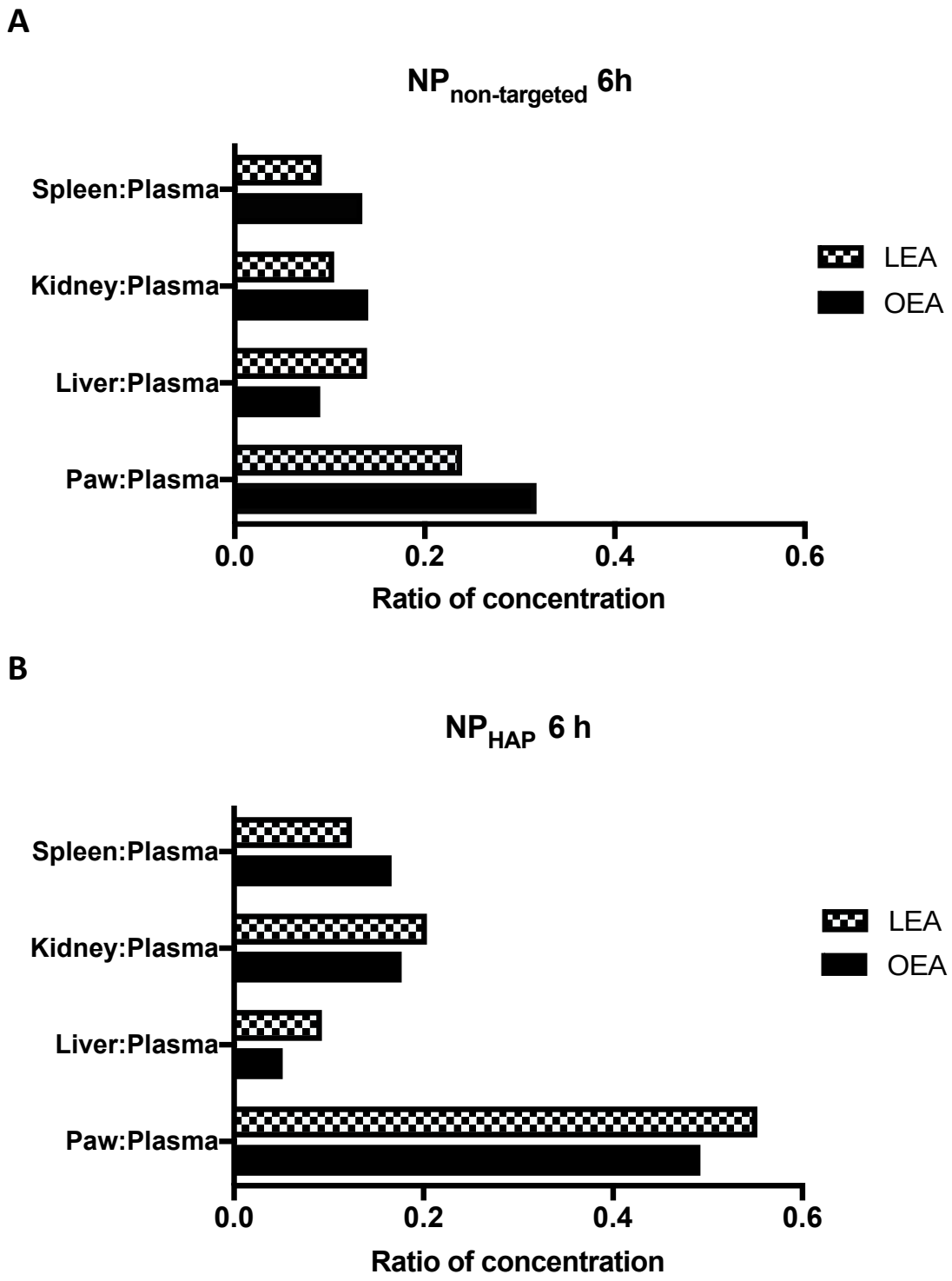

Figure 3.10. Tissue:plasma ratio of OEA and LEA in **(A)** $NP_{non\text{-}targeted}$ and; **(B)** NP_{HAP} treated arthritic rats showing accumulation of NP to the inflamed paw at 6 h (mean, n = 5).

3.4 DISCUSSION

FLS's are one of the dominant cell types in the rheumatoid synovium and play an important role in the pathogenesis of RA (Noss & Brenner, 2008; Bartok & Firestein, 2010). Currently, there are few treatment strategies aimed at targeting the FLS, with the majority of treatment options aimed at targeting the inhibition of angiogenesis, cellular contact inhibition, and cytokines, and/or immune cells that intensify the immune response (Koning et al., 2006; Yang et al., 2011). This is the first report of endocannabinoid-based NP drug delivery system which targets FLS *in-vitro* and sites of joint inflammation *in-vivo*.

In agreement with what was originally reported by Mi *et al*, (2003) for rabbit HIG-82 cells, HAP-1-binding experiments using HAP-1-biotin-streptavidin-FITC showed its intracellular localisation in all human FLS types through the use of z-stack imaging (not shown). While HAP-1 binding was noted in all human FLS types, comparison of HAP-1 binding between normal, RA and OA FLS cell types was limited to visual observation by confocal microscopy. Further quantitative binding studies using flow-cytometry are required to quantitate the binding affinity of HAP-1-binding between the cell types. Assessment of NP uptake using flow-cytometry showed that conjugation of synovium-targeting peptide, HAP-1, to the NP surface resulted in specific binding and uptake of NP_{HAP} in both HIG-82 and human FLS cells *in-vitro*. From these experiments it was evident that the targeting capability of the HAP-1 is retained following conjugation to the NP surface. In addition, NP uptake was not influenced by inflammatory condition.

In agreement with the *in-vitro* uptake data, *in-vivo* localisation of fluorescent NP using NIR demonstrated the selective accumulation of the NP_{HAP} to joints in both normal and arthritic rats. By contrast, no specific accumulation was observed for $NP_{non\text{-}targeted}$ and NP_{sHAP} treated normal rats, with only slight improvements in localisation observed in arthritic rats for these two groups. The greater localisation of NP_{HAP} to the synovium may be attributed to ligand-mediated targeting facilitated by HAP-1. In agreement with this, no specific accumulation was noted for NP_{sHAP}, suggesting that localisation of NP_{HAP} is reliant on a functioning binding sequence of the homing peptide and independent of higher molecular weight from conjugated surface peptides.

In arthritic rats, enhanced localisation to the inflamed joints was observed with all three NP's and attributed to "leaky" vasculature of the inflamed joint. During arthritis, endothelial cells within the joint lose the cellular integrity due to the activation of pro-inflammatory cytokines. As a result, gaps between the endothelial cells are widened, increasing permeability and creating a leaky vasculature around the inflamed site (Joris et al., 1990). Consequently, particles ranging from 10 to 500 nm in size

can extravasate from the vascular system to the diseased site through the abnormal endothelial gaps (Ganter et al., 2008). In agreement with this, the rats that did not develop arthritis in all paws, inflammation showed disproportionate distribution of $NP_{non\text{-}targeted}$ and NP_{sHAP} to only the inflamed sites. The uptake of NP_{HAP} was also increased in the arthritic joints and attributed partly to the greater vascular permeability as well as the specificity of HAP-1 itself. The enhanced binding of NP_{HAP} was much greater in the arthritic rats compared to $NP_{non\text{-}targeted}$ and NP_{SHAP} from baseline.

In-vivo, NP accumulation was shown to be highest in the paws in both the $NP_{non\text{-}targeted}$ and NP_{HAP} treated rats demonstrating preferential localisation to the joints. Assessment of paw and organ in bio-distribution studies, saw pronounced accumulation of NP_{HAP} to the paw, with minimal residual NP_{HAP} circulating in the plasma after 6 h. By contrast, slightly higher plasma concentrations of OEA and LEA in the $NP_{non\text{-}targeted}$ group coincided with reduced concentrations of OEA and LEA recorded in the inflamed joints after 6 h. While both $NP_{non\text{-}targeted}$ and NP_{HAP} treated rats showed preferential localisation of NP to the joints 6 h after injection, only NP_{HAP} reached significance demonstrating improved localisation through ligand mediating targeting. This data is in agreement with preliminary localisation results obtained by NIR, which indicated a significant uptake of NP_{HAP} by the arthritic joints in comparison to $NP_{non\text{-}targeted}$.

While both $NP_{non\text{-}targeted}$ and NP_{HAP} treated rat's demonstrated preferential NP accumulation to the joints, paw concentrations of OEA and LEA were relatively low. The overall lower concentrations of NP in the paw are likely due to the complexity of the paw joint (muscle, bone, ligaments, and synovial fluid) which created difficulties reaching full homogenisation during processing. In addition, plasma levels of of OEA and LEA in NP injected rats were elevated when compared to baseline un-treated rats at the 6 h mark, suggesting that the NP's were still in circulation when the tissues were collected for the bio-distribution study. Collection of tissue at a later time point would allow the remaining circulating NPs to deposit out of the plasma into the tissue, providing a more accurate reflection of final NP *in-vivo* bio-distribution.

Assessment of NP bio-distribution into solid organs at 6 h accounts may also account for the differences in NP concentrations observed in the paw for $NP_{non\text{-}targeted}$ and NP_{HAP} treated rats. While concentrations of $NP_{non\text{-}targeted}$ were high in the liver, they were minimal in NP_{HAP} treated rats, demonstrating the ability to limit off target effects through peptide conjugation. In the current study, it was found that the liver contained the highest organ concentration of $NP_{non\text{-}targeted}$ after 6 h as shown by HPLC/MS/MS. In contrast, concentrations of NP_{HAP} were minimal to none in the liver, and are in agreement with the higher fluorescence noted in the liver from $NP_{non\text{-}targeted}$ treated rats imaged by NIR. Total NP localisation to the spleen and kidneys was relatively low for both $NP_{non\text{-}targeted}$ and NP_{HAP}

indicating little distribution to this area. Taken together, the low plasma concentration of NP_{HAP} may be attributed to greater accumulation to the joints and not the liver, resulting in lower plasma concentrations of NP_{HAP} at 6 h. For $NP_{non\text{-}targeted}$, lower concentrations of $NP_{non\text{-}targeted}$ at the initial time points suggests that circulating $NP_{non\text{-}targeted}$ are more efficiently removed via clearance by the liver than NP_{HAP}, contributing to $NP_{non\text{-}targeted}$ shorter half-life. Assessment of the NP's organ concentration at these earlier time points would be required to confirm the rapid clearance of $NP_{non\text{-}targeted}$ from the plasma to other organs. Successful accumulation of NP_{HAP} to the inflamed joints highlights its promising therapeutic potential in the treatment of arthritis by facilitating localised delivery of therapeutic agents to inflamed synovium.

3.4.1 Summary

In this chapter, the ability of peptide conjugated NP to target both FLS *in-vitro*, and the synovium *in-vivo* is reported. The findings demonstrate that conjugation of synovium-targeting peptide, HAP-1, to NP surface results in specific binding and greater uptake of NP_{HAP} in both HIG-82 and human FLS cells, when compared to $NP_{non\text{-}targeted}$ *in-vitro*. Using NIR tracer and bio-distribution studies, the ability to actively target NP's to the inflamed synovium *in-vivo* was demonstrated. The ability to localise targeted NP's to the inflamed synovium using endocannabinoid lipids has important therapeutic implications for the treatment of arthritis.

CHAPTER 4: BIOLOGICAL EFFECTS OF NANOPARTICLES *IN-VITRO*

4.1 INTRODUCTION

Inflammation plays an important role in the development and resolution of rheumatic diseases. In this Chapter, the response of human FLS cells to inflammatory stimuli and interplay of NP *in-vitro* is examined. In RA, pro-inflammatory cytokines play a crucial role in the generation of inflammation, which results in the sensitization of peripheral nerve terminals, infiltration of immune cells and subsequent development of pain and inflammation (Alunno et al., 2017). Among the pro-inflammatory cytokines, TNF-α is a principal cytokine which regulates the activation of other inflammatory mediators, as well as mediating the destruction of bone and cartilage via the activation of chondrocytes and osteoclasts to produce matrix-metalloproteases (MMPs) in the synovial tissue (El-Kady & El-Masry, 2008). Other pro-inflammatory cytokines such as IL-6, IL-1 and IL-17A, are involved in the pathogenesis of RA by mediating formation of chemokines, inducible nitric oxide synthase, osteoclasts differentiation and the expression of cell adhesion molecules.

A sizeable number of clinical and pre-clinical studies have confirmed the potential of the cannabinoid system in providing a number of promising therapeutic benefits for patients with chronic inflammatory disease (Farrell et al., 2014; Fitzcharles et al., 2016b; Barrie et al., 2017). While the anti-inflammatory effects of AEA are well established, lesser-known NAEs such as LEA, OEA and PEA have recently gained much attention due to their anti-inflammatory and analgesic properties (Ishida et al., 2013; Lowin et al., 2015; Zhou et al., 2017b; Zhao et al., 2018). These compounds do not bind CB1, but instead contribute to an anti-inflammatory regulation through “entourage” effects (Okamoto et al., 2004; Alhouayek & Muccioli, 2014). These anti-inflammatory effects may be due to direct effect on immune cells, or by changing the local milieu of saturated fatty acids that subsequently influence anti-inflammatory actions.

OEA is structurally similar to AEA and exerts its effects through the PPAR-α receptors (Zhao et al., 2018) or GPR119 (Overton et al., 2006). PPAR activators have been shown to inhibit the activation of inflammatory response genes by inhibiting the NF-κB, STAT and AP-1 signalling pathways thereby playing a role in the regulation of inflammatory responses (Chinetti et al., 2001). In healthy tissue, PEA and OEA are present at relatively high concentrations, which are thought to be of sufficient concentration to activate local PPAR-α receptors. Marked decreases in OEA and PEA tissue content are observed at sites of inflammation and are correlated to inflammatory symptoms (Bonezzi et al., 2016). *In-vitro*, OEA has been shown to exert potent anti-inflammatory effects by reducing the levels of pro-inflammatory cytokines and enhancing PPAR-α expression (Yang et al., 2016). Similarly, OEA pre-treatment significantly suppresses the expression of TNF-α, IL-1B and IL-6 in the lung, liver, brain

and spleen *in-vivo* of LPS-treated mice by enhancing PPAR signalling, inhibition of Toll like receptor 4 (TLR4)-mediated NF-κB signalling pathway, and interfering with the extracellular signal-regulated kinase-1/2 (ERK1/2)-dependent signalling cascade (TLR4/ERK1/2/ activator protein 1 [AP-1]/ signal transducers, and activators of transcription [STAT3]) (Yang et al., 2016).

Similar to OEA, LEA has been shown to exert anti-inflammatory effects. *In-vitro*, LEA inhibits activation of TLR4 signalling and NF-κB p65 and suppresses LPS-induced inflammation in macrophages (Ishida et al., 2013). NF-κB is a pivotal transcription factor in the regulation of pro-inflammatory genes, and therefore plays important role in mediating cellular functions via the inflammatory response (Liu et al., 2017). In an *in-vivo* model of contact dermatitis, application of LEA to affected skin ameliorated 2,4-dinitrofluorobenzene-induced contact dermatitis and pro-inflammatory cytokine expression at inflamed sites (Ishida et al., 2013). Taken together, the ability of the endocannabinoids OEA and LEA to regulate NF-κB signalling pathway may be a promising candidate target to inhibit the inflammatory pathway.

As yet, the effects of N-acylethanolamines, LEA and OEA on the production of inflammatory mediators in primary synoviocytes have not been described. In this chapter, the effects of endocannabinoid NP on RA-FLS cells *in-vitro* was examined using next generation sequencing (RNA-seq) and RT-PCR. RNA-seq measures expression across the transcriptome to obtain highly accurate gene expression data, useful for exploring changes in diseased states or responses to therapeutics. Genome-wide association studies, pathway explorers and protein interaction databases also help provide insight into the mechanisms of action and contribute to the discovery of novel molecular targets that can be explored in experimental studies. Comparison of NP treated and non-treated RA-FLS stimulated with TNF-α in this study has identified transcriptome changes, novel genes, and the exploration of novel transcription factors involved in acute inflammatory regulation. As these cells were sourced from a patient with RA, they are in an aggressive phenotype state and represent inflammatory regulation present in a chronic state. Using pathway analysis, overlaps in regulatory pathways in which NP treatment may have therapeutic application was examined.

4.2 METHODS

4.2.1 Materials

Hanks buffered salt solution (HBSS), 6-well and 96-well culture plates (Corning Inc, NY, USA), WST-1 solution assay (Roche Australia, Sydney, Australia), Trypan blue and RNAse-free DNAse I were purchased from Sigma-Aldrich (Sigma-Aldrich Pty, Sydney, Australia). RNA and PCR kits including Isolate II RNA Mini Kit, SensiFast cDNA synthesis kit and SensiFast SYBR Green No-ROX kit were purchased from Bioline (Bioline, Sydney, Australia).

4.2.2 Generation of NP's

The NP's used in this chapter were prepared as previously described in Section 2.2.2.

4.2.3 Cell Culture

Cells used in this culture were maintained as previously described in Section 3.2.3.

4.2.4 Cytotoxicity Studies

4.2.4.1 Trypan blue

To assess effect of NP on the viability of FLS cell lines, a trypan blue dye exclusion test was performed. Briefly, FLS cells were seeded at a density 1 x 10^5 into 6-well plates and cultured over night at 37°C. After seeding, the medium was replaced and the cells treated with varying concentration of NP (5, 10, 30, 50, 80, 110 and 140 µg/mL) and maintained at 37°C for 24 h. Cells were then detached using trypsin/EDTA (0.5 mM), pelleted and resuspended in fresh medium. An aliquot (50 µL) of the cell suspension was then diluted 1:1 (v/v) with 0.4% trypan blue in HBSS solution and incubated for 5 min at RT. With a coverslip in place, and a small volume of trypan-blue cell suspension was loaded into the haemocytometer chambers and the viable cells counted. Cell viability (%) = total viable cells (unstained) ÷ total cells (stained and unstained) × 100.

4.2.4.2 WST-1 assay

NP cytotoxicity was also assessed using WST-1 assay, performed according to manufacturer's instructions. RA-FLS cells were seeded at 1 x 10^4 into 96-well plates and cultured overnight (80% confluence) prior to treatment. After seeding, the medium was replaced and various concentrations of NP (5, 10, 30, 50, 80, 110 and 140 µg/mL) were added to the wells and incubated at 37°C for 24 h. Following incubation, 10 µL of WST-1 was then added and incubated at 37°C for 4 h and the absorbance measured using an ELISA plate reader (Victor^3 model 1420-040, Perkin Elmer, Sydney, Australia). The percentage of viable cells was determined by the absorbance at 450 nm with a

reference wavelength at 630 nm. Control values (wells without NP stimuli or PBS vehicle control) were set to 100% viable. The relative cell viability (%) related to control wells was calculated by [A]test/[A]control × 100. Where [A]test is the absorbance of the test sample and [A]control is the absorbance of control sample. To make the background correction, a background control (blank) was provided for every treatment group in order to preclude the potential interference of the NP and medium with the spectrophotometric measurement. Samples were run in triplicates and repeated n = 3. Respective lethal concentration 50 (LC50, concentration inducing 50% cell mortality) was calculated by regression analysis using GraphPad Prism software (Version 7).

4.2.5 Stimulation of Human RA-FLS and OA-FLS Cells and RNA Isolation

To study the effects of NP on inflammatory cytokine production, RA-FLS cells were stimulated with TNF-α alone (10 ng/mL, RA-TNF), or in the presence of endocannabinoid-NP (30 μg/mL, RA-TNF/NP) for 48 h at 37°C. Untreated RA-FLS cells (RA-UT) and RA-FLS cells incubated with NP alone (30 μg/mL, RA-NP) were used as controls. Following incubation, cells were washed with PBS and RNA isolated. Treated groups were run using three biological replicates. Total RNA was isolated from cultured RA-FLS cells using Isolate II RNA Mini Kit according to the manufacturer's instructions. To remove any genomic DNA contamination, RNA was treated with RNAse-free DNAse I RNA purity and concentration was assessed using a Agilent 2100 Bioanalyser® (Agilent Technologies, California, USA). The mean RNA concentration of 52.92 (± 3.12) ng/μL.

4.2.5.1 RNA-seq

Illumina RNA sequencing was used to profile human RA FLS transcriptomes to gain insights into the roles of synovial fibroblasts in RA and assess the potential anti-inflammatory effects of NP. Next-Generation Sequencing was performed by the Australian Genome Research Facility (AGRF). Stranded RNA libraries were prepared and quality control from mRNA were performed using Illuminia Library Prep. HiSeq illuminia sequencing (50/100) 50 base pair (bp) single reads.

4.2.5.1.1 RNA-seq library construction and sequencing

Stranded RNA libraries were prepared from 350 ng RNA using the Illumina® TruSeq Stranded mRNA sample prep kit. The libraries were sequenced by the Australian Genome Research Facility on an Illumina HiSeq 2500 to generate 50 base-pair (bp) single-end reads. Raw sequencing reads were assessed for quality using FastQC (version 0.11.3; Babraham Bioinformatics), ensuring that Phred scores were over 30. Per base quantity scores were confirmed to be high using FastQC, and therefore no adaptor trimmings were performed. STAR (version 2.5.2a) was used to align the reads to Release 19 of the human reference genome (GRCh37/hg19), with the GENCODE (Release 28) annotation

(http://www.gencodegenes.org/) provided, using default parameters (Dobin et al., 2013). Resulting SAM files were sorted by position using SAMtools (version 1.6) (Li et al., 2009). Quality assessment, mapping and raw read counts were conducted on the high-performance computing cluster (Artemis), provided by the Sydney Informatics Hub, University of Sydney.

4.2.5.1.2 Differential gene expression analysis

Raw gene-level read counts were obtained using HTSeq (version 0.9.1) in "union" mode to exclude multi-mapping or ambiguously aligned reads (Anders & Huber, 2010). Raw counts were analysed using the DESeq2 (release 3.6) statistical package in R Studio (version 1.1.383). Data were transformed using the rlogTransformation function in DESeq2 to obtain principal component analysis (PCA) plots and sample-sample distance heatmaps. These plots were used to confirm that samples clustered within their respective treatment groups as expected. DESeq2 performed differential expression analysis on raw count data using a negative binomial distribution model. The model included implementation of normalization to correct for library size and independent filtering to exclude genes with low read counts. Differentially expressed (DE) genes were defined if had a log fold change (FC) > 2, applying a 5% false discovery rate (FDR<0.05). Gene ontologies, pathways and regulatory networks that were enriched/overrepresented in significantly differentially expressed genes were identified using the Ingenuity Pathway Analysis (IPA, QIAGEN Redwood City, www.qiagen.com/ingenuity) software (Version: 44691306).

4.2.5.2 Reverse transcription-polymerase chain reactions (RT-PCR)

RT-PCR was used to evaluate anti-inflammatory gene regulation in NP treated RA-FLS cells and confirm RNA-seq data. Treatment groups and RNA isolation were repeated as stated in Section 4.2.5. RNA purity and concentration was assessed using NanoDropTM 2000/2000c spectrophotometer (Thermo Fisher Scientific, North Ryde, Australia). Total RNA from each sample was reversed transcribed into complementary DNA (cDNA) using SensiFast cDNA synthesis kit according to the manufacturer's instructions. Briefly, a 20 µL reaction containing up to 1 µg mRNA, 5x TransAmp Buffer (4 µL) and Reverse transcriptase (1 µL) were prepared for each sample. RNA was reversed transcribed into cDNA using Thermocycler (Hybaid Omn-E, Hybaid Ltd, UK) following, primer annealing at 25˚C for 10 min, reverse transcription at 42 ˚C for 15 min, inactivation at 85˚C for 5 min and finally held at 4 ˚C. No reverse transcriptase controls were prepared with water in place of reverse transcriptase, and no template controls were prepared with water in place of RNA to indicate potential genomic DNA contamination.

Following reverse transcription, cDNA was subject to quantitative-polymerase chain reaction (q-PCR) carried out on CFX96 RT-PCR detection system (Bio-Rad, Sydney, Australia). PCR amplification were performed using specific primers (Table 4.1). Primer sets were design using the Primer3web software and supplied by Integrated DNA-Technologies (IDT, Baulkham Hills, Australia). PCR amplification was performed with SensiFast SYBR Green No-ROX kit according to established protocols. Briefly, 10 µL of 2x SensiFAST SYBR No-ROX mix, 0.8 µL 5' sense primer and 0.8 µL 3' antisense primer (10 µM, final concentration 400 nM), RNAse free water and cDNA template were prepared in a 20 µL reaction. Samples were heated at 95°C for 3 min and cycled for a maximum of 39 times. Each cycle included denaturation at 94°C for 30 sec, annealing at 60-65°C for 10 sec, and extension at 72°C for 2 min. The PCR process was optimised at various cycle numbers with cDNA. The constitutively expressed housekeeping gene encoding GAPDH was used as an internal control to normalise the amounts of mRNA in each sample. Quantification of mRNA levels were performed using the ΔΔCt method. The value of each control sample were set at one and used to calculate the fold change of target genes.

Table 4.1 Summary of primer set sequences, base pairs and annealing temperatures used in RT-PCR.

Primer	Sequence	Base pair	Annealing Temp (°C)
GAPDH	*F: GAAGGTCGGAGTCAACGG #R: GGAAGATGGTGATGGGAT	18 18	60
β-actin	F: CTACGCCGAATATGCCATCTC R: GTACGGGATTGCCCCTCTG	21 19	61
IL-8	F: ACTGAGAGTGATTGAGAGTGGAC R: AACCCTCTGCACCCAGTTTTC	23 21	62
IL-6	F: GTGGG CGCCCCAGGCACCA R: CTCCTTAATGTCACGCACCATTTC	22 25	61
NF-κB	F: GGTGCGGCTCATGTTTACAG R: GATGGCGTCTGATACCACGG	20 20	62
MMP-1	F: GGGGCTTTGATGTACCCTAGC R: TGTCACACGCTTTTGGGGTTT	21 21	62
MMP-3	F: TATGGACCTCCCCCTGACTCC R: AGGTTCAAGCTTCCTGAGG	21 19	60
MMP-13	F: GCTGCCTTCCTCTTCTTGA R: TGCTGCATTCTCCTTCAGGA	19 20	61

*F = Forward sequence

#R = Reverse sequence

4.3 RESULTS

4.3.1 NP cytotoxicity

NP *in-vitro* cytotoxicity was assessed using Trypan blue exclusion method and WST-1 colorimetric assay. The LC50 was 40 µg/mL after a 24 h incubation period (Figure 4.1).

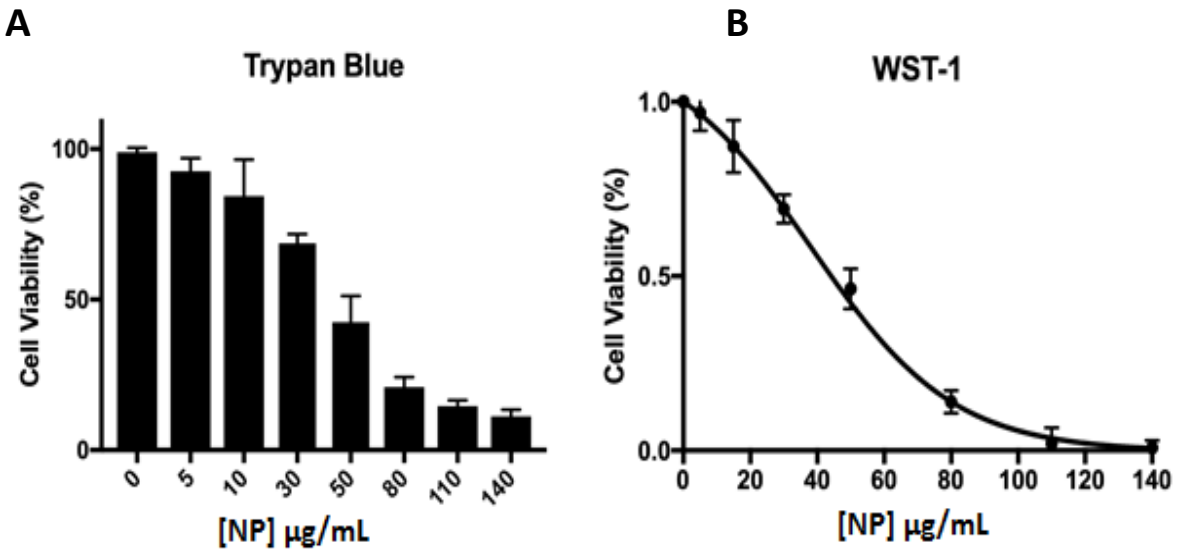

Figure 4.1: NP *in-vitro* cytotoxicity in RA-FLS cells as assessed by **(A)** Trypan blue exclusion method and; **(B)** WST-1 colourmetric assay. FLS cells were incubated for 24 h with increasing concentrations of NP and compared to untreated cells. The data represents the mean of three independent experiments (n=3 ± SD). NP LC50 = 40 µg/mL

4.3.2 RNA-seq

Illumina RNA-seq was performed to investigate the effect of NP on gene expression using human RA and OA-FLS cells. Treatment groups were performed in three biological replicates and included; untreated cells (RA-UT), NP treated cells (RA-NP), TNF-α stimulated cells (RA-TNF) and TNF-α stimulated cells with NP treatment (RA-TNF/NP). Effects on OA-FLS cells were also investigated, OA-UT, OA-NP, OA-TNF and OA-TNF/NP groups treated as above, respectively. Differences in gene expression between TNF and TNF/NP treated groups for both cell types were compared to assess NP regulation of inflammatory genes in an acute inflammatory state. In addition, differences in gene expression between UT and NP were compared to assess NP regulation of inflammatory genes present in a chronic state. Summarises of the raw read count and gene expression statistics for significant and non-significant gene counts are supplied in Appendix 3.

4.3.2.1 Sequence and alignment quality assessment of RNA-seq data

Raw read and quality metrics of RNA-seq data that was aligned to the GRCh37/hg19 reference genome using STAR are summarised in Table 4.2. DE analysis of raw counts by DESeq2 implemented normalisation to correct for library size and independent filtering to exclude genes with low read counts. Between 0% - 0.12% of the reads were excluded due to low quality before mapping to the reference genome began. Total map reads were 98.29 – 99.06%, where 80.12 – 86.65% were uniquely mapped. A total of 28,288 and 27438 genes with non-zero total read counts were identified for RA-FLS and OA-FLS groups respectively (log_2 FC ≥1; FDR ≤0.05). MA plot is a scatter plot whose y-axis and x-axis respectively display M=log2(Ri/Gi) and A=log2(Ri*Gi) where Ri and Gi represent the intensity of the ith gene in R and G samples. MA scatter-plots of microarray spot statistics for each gene across the treatment groups showed a normal, un-biased distribution with low biological variability. Low biological variability was to be expected as the primary cell lines were harvested from a single source. Plot symmetry about the x-axis (mean) indicated normalisation was fine with equal number of upregulated and downregulated genes (shown in Appendix 3).

PCA plots and sample-sample heat distance heat maps provided by DESeq2 were used to assess quality of the RNA-seq replicates. As shown in Figure 4.2, replicates within each of the four treatment groups could be clearly distinguished for RA-FLS cells. The number of clusters, along with the percentage variance between the clusters confirmed that the samples clustered within their respective treatment groups, as expected (Figure 4.2A, Figure 4.2C). By contrast, two of the three OA-NP replicates grouped together in one quadrant, while the third replicate clustered away (Figure 4.2B). The poor clustering of the OA-NP replicates highlights in-consistency within the OA-NP sample replicates. Furthermore, the shared genetic similarity between the clustered OA-NP and OA-UT suggests that these two OA-FLS groups were either not exposed to NP, or had poor NP uptake during treatment. The poor clustering of OA-NP was confirmed in sample distance heat map (Figure 4.2D) and hence OA-NP group were excluded from further analysis.

Table 4.2. Raw read and quality metrics of RNA-seq data that was aligned to the GRCh37/hg19 reference genome using STAR

	Replicate	Number of reads	Total mapped reads (%)	Uniquely mapped reads (%)	Multi-mapped reads (%)	Per base sequence quality with score > 30
RA-UT	1	10888740	98.55%	84.00%	14.55%	50
	2	11576222	98.70%	84.98%	13.72%	50
	3	11190454	98.63%	84.34%	14.29%	50
RA-TNF	1	11449253	98.29%	86.13%	12.16%	50
	2	10455644	98.75%	86.65%	12.10%	50
	3	11921803	98.85%	86.58%	12.27%	50
RA-NP	1	11064780	98.80%	84.67%	14.13%	50
	2	11199571	98.95%	84.72%	14.23%	50
	3	11110842	98.88%	84.80%	14.08%	50
RA-TNF/NP	1	11602864	98.68%	83.98%	14.70%	50
	2	11649019	99.04%	84.41%	14.63%	50
	3	11903358	99.05%	84.15%	14.90%	50
OA-UT	1	10226420	98.63%	83.00%	15.63%	50
	2	10652763	98.85%	82.98%	15.87%	50
	3	10666266	98.79%	82.34%	16.45%	50
OA-TNF	1	13828969	99.06%	85.51%	13.55%	50
	2	10787373	99.01%	85.39%	13.62%	50
	3	10768148	98.88%	84.65%	14.23%	50
OA-NP	1	10606142	98.91%	85.75%	13.16%	50
	2	11162818	98.63%	82.92%	15.71%	50
	3	10950970	98.70%	80.12%	18.58%	50
OA-TNF/NP	1	10308568	98.31%	84.07%	14.24%	50
	2	10922988	98.86%	84.47%	14.39%	50
	3	10396049	98.95%	84.52%	14.43%	50

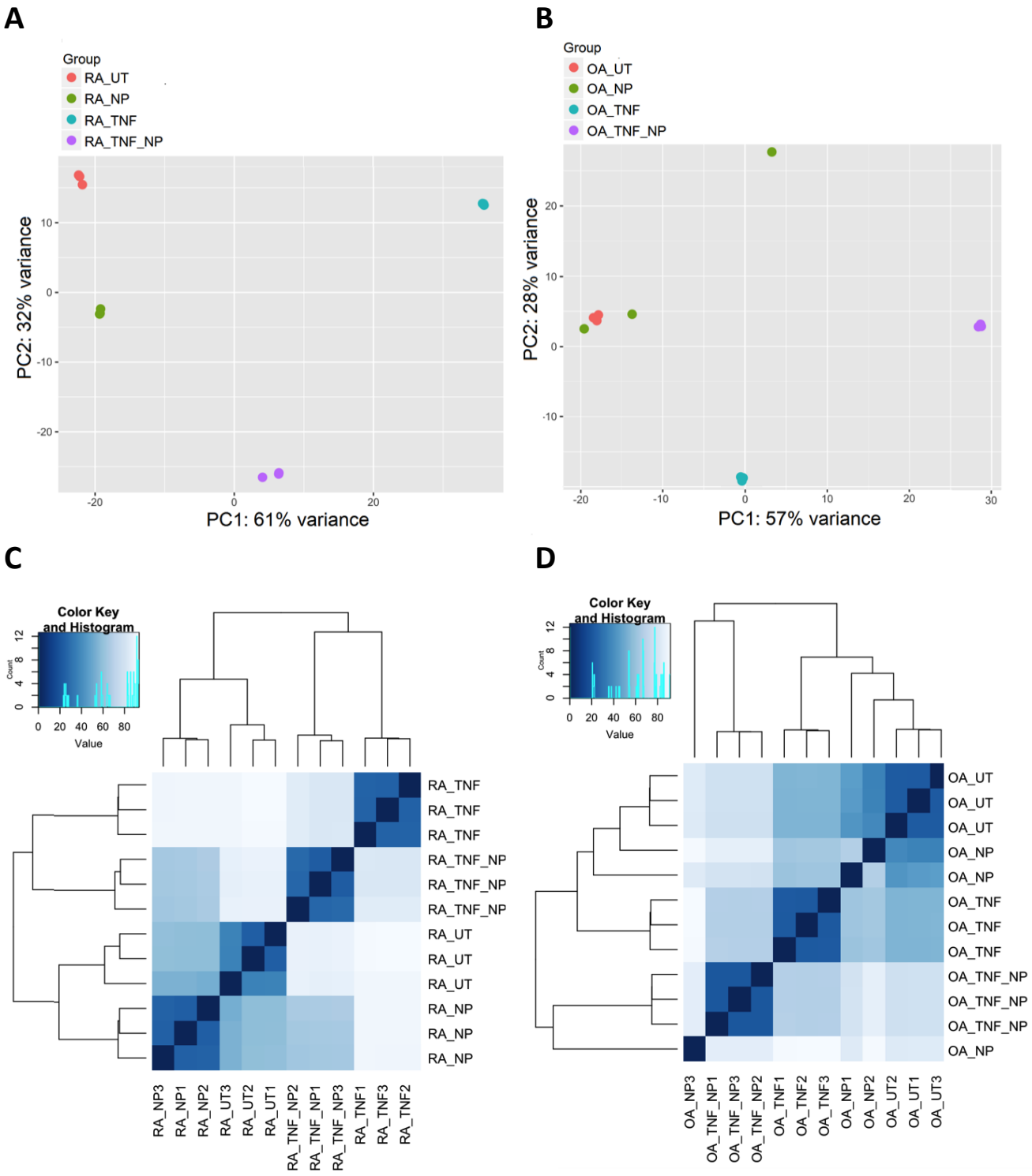

Figure 4.2. PCA plots of **(A)** RA-FLS and; **(B)** OA-FLS groups. Sample-sample heat distance heat maps of RNA-seq data from **(C)** RA-FLS cells and; **(D)** OA-FLS cells. Sample clustering met quality assurance quality for RA-FLS treated groups.

4.3.2.2 Top DE genes

In the present study, Illumina RNA sequencing was used to profile human RA FLS cells transcriptomes to gain insights into the regulatory role of NP on FLS cells in RA. Statistical analysis of DE genes was carried out using IPA software. DE genes were identified if their log fold change was greater than a magnitude of two fold and if FDR < 0.05. A heat map of the top DE expressed genes in RA-FLS treated groups are shown in Figure 4.3. Table of the top DE expressed in the discussed RA-FLS treatment groups are supplied in Appendix 4.

4.3.2.2.1 Top DE genes following TNF-α stimulation, (RA-TNF vs RA-UT)

TNF-α was used to stimulate RA-FLS cells. It was found that 7968/17912 of genes which were upregulated (>2 fold) by TNF-α reached statistical significance when compared to untreated controls (FDR <0.05). Table of the top DE expressed in the RA-TNF vs RA-UT treatment groups are supplied in Appendix 4.

Assessment of the top DE genes in RA-TNF cells showed the acquisition of genes associated with inflammation and joint erosion. As shown, the upregulated chemokines CXCL5,8,10; CCL20, CXCR4, were elevated and are important in the recruitment of inflammatory mediators and angiogenesis (Kokkonen et al., 2010). In addition to the chemokines, a pronounced recruitment of genes involved in inflammatory signalling TRPA1, IL23A, NOS2, nociceptive signalling TRPA1, MRGPRX3 and bone remodelling IBSP were also observed. These include genes involved in osteoclastogenesis CXCL8, CCL20, IL-23, and breakdown of extracellular matrix proteins MMP-3, all which collectively contribute to inflammation and degenerative joint function associated with RA.

4.3.2.2.2 Top DE genes following NP treatment, (RA-TNF/NP vs RA-TNF)

By comparing TNF-α treated cells to TNF-α and NP treated cells, the influence of NP in acute inflammation was examined. Analysis showed 7874/18430 of genes which were DE (>2 fold) in RA-TNF/NP reached statistical significance when compared to RA-TNF (FDR <0.05). Table of the top DE expressed in the RA-TNF/NP vs RA-NP treatment groups are supplied in Appendix 4.

As shown in Figure 4.3, assessment of the top DE genes in TNF/NP showed a significant reduction in inflammatory and bone remodelling genes, previously upregulated in RA-TNF. In addition to reduction of these genes, NP treatment promoted the acquisition of SERPINB2, Hsp70; HSPA6, HSPA7, TFPI2, IL1RN genes, which are associated with homeostasis and inflammation resolution. Increase in SHISA2 would also decrease wingless/integrated (WNT) signalling, and increase in anti-nociceptive signalling NTSR1. By contrast, CXCLorf48, MMP-3 and CXCL3,6 genes appeared to be largely unaffected by NP treatment, whilst CXCL5,8 was slightly upregulated. Overall, assessment of top DE genes in each group

highlight an immunological shift from highly pro-inflammatory acute inflammatory environment to a less inflammatory environment mediated by NP treatment.

4.3.2.2.3 Top DE genes following NP treatment in untreated cells (RA-NP) vs (RA-UT)

Differences in gene expression between untreated RA-FLS (RA-UT) and NP treated RA-FLS (RA-NP) were compared to assess the effect of NP on RA-FLS cells. It was found that 5941/15839 of genes which were DE (>2 fold) in RA-NP reached statistical significance when compared to RA-UT (FDR <0.05). Table of the top DE expressed in the RA-NP vs RA-UT treatment groups are supplied in Appendix 4.

As shown in Figure 4.3, an upregulation of interstitial collagenase MMP-1 in RA-NP was observed, which degrade type II collagen in cartilage and are crucial in the progression of RA and OA (Vincenti & Brinckerhoff, 2002). However, increase in tissue factor pathway inhibitor 2 (TFPI-2), helpful in reducing extracellular matrix degradation by inhibiting a variety of serine proteases including MMPs was increased in RA-NP. Increases in Interleukin 1 receptor antagonist (IL1N) in RA-NP, may also assist in mediating anti-inflammatory effects by Inhibiting IL-1 by binding activation (Dinarello, 2011). Similarly, increased expression of long intergenic non-protein coding RNA, P53 induced transcript (LINC-PINT) and neurotensin receptor type 1 (NTSR1) have been linked to anti-inflammatory and angiogenic effects were positively DE expressed in RA-NP (Mirsafian et al., 2016; Li et al., 2014). Other DE genes included those involved in ATP binding, RNA binding and hydrolysis (DDX3Y), ribosome formation (RPS4Y1) and pseudogene (TXLNGY). Collectively, the upregulation of DE with potentially anti-inflammatory regulatory properties (IL1N, LINC-PINT, NLGN4Y, TFP1-2) suggests NP may be beneficial in mediating inflammatory responses through the expression of these genes.

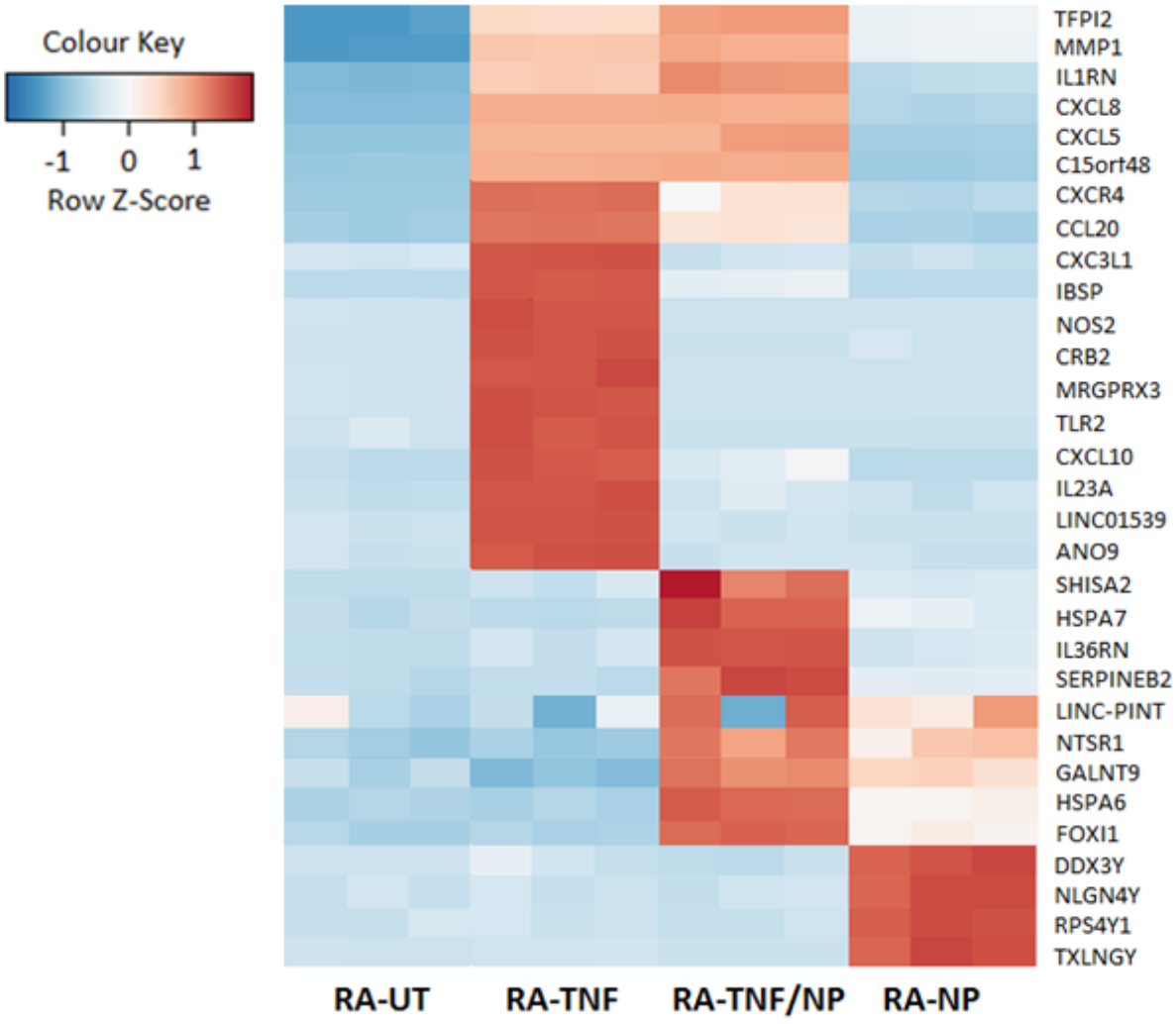

Figure 4.3. Heat map of the top DE genes based on comparison of RNA-seq data between TNF-α and NP treated cells (RA-TNF/NP), and TNF-α treated (RA-TNF) RA-FLS cells. The normalized RNA-Seq data is in log2 scale, where red is highly expressed genes and blue is low expression. To be included in the heat map, genes were required to have at least 1000 counts (reads), totalled over all samples, where the standard deviation of log2 expression differences had to exceed two. The heatmap highlights an immunological shift from highly pro-inflammatory environment to a non-inflammatory environment, mediated by NP. Abbreviations: Tissue factor pathway inhibitor 2 (TFPI2); Matrix metalloproteinases-1 (MMP-1); Interleukin 1 receptor antagonist (IL1RN); Chemokine C-X-C motif ligand 1 (CXCL, 8,5); Chromosome 15 open reading frame 48 (C15orf48); C-X-C chemokine receptor type 4 (CXCR-4); Chemokine (C-C motif) ligand 20 (CCL20); Integrin binding sialoprotein (IBSP); Nitric oxide synthase 2 (NOS2); Crumbs 2, cell polarity complex component (CRB2); Mas-related G-protein coupled receptor member X3 (MRGPRX3); Toll like receptor 2 (TLR2); Interleukin-23A (IL-23A); Long Intergenic non-protein coding RNA 1539 (LINC01539); Anoctamin 9 (ANO9); Shisa family member 2 (SHISA2); Heat shock protein family A member 6/7 (HSPA6, HSPA7); Interleukin 36 receptor antagonist (IL36RN); Plasminogen activator inhibitor-2 (SEPINB2); Long intergenic non-protein

coding RNA, P53 induced transcript (LINC-PINT); Neurotensin receptor type 1 (NTSR1); Polypeptide N-Acetylgalactosaminyltransferase 9 (GALNT9); Forkhead Box I1 (FOXI1); DEAD-Box Helicase 3 Y – Linked (DDX3Y); Neuroligin 4 Y-linked (NLGN4Y); Ribosomal protein S4 Y-linked 1 (RPS4Y1); Taxilin gamma pseudogene (TXLNGY).

4.3.2.3 NP regulation of candidate inflammatory markers

To examine the influence of NP in regulating published key mediators of inflammation expressed in RA, logfold changes of prominent RA genes were compared between RA-TNF/NP and RA-TNF, as well as, RA-UT and RA-NP treated groups, respectively. The expression of key mediators in arthritis are represented as a heat maps in Figure 4.4. This panel of candidate mRNA were specifically selected and screened for their importance in inflammatory and disease progression in RA.

TNF-α is a potent pro-inflammatory cytokine that regulates immune and inflammatory responses (Jacque et al., 2005). To confirm the pro-inflammatory effects of TNF-α on gene regulation, untreated RA-cells (RA-UT) and TNF-α stimulated cells (RA-TNF) were first compared. As expected, clustering based on the expression pattern of the chosen genes resulted in a clear separation between RA-UT and RA-TNF as indicated by opposite colour scoring in z-score. Highly expressed pro-inflammatory genes IL-6, IL-8, IL-1B, IL-1A, represented by red in the RA-TNF were oppositely expressed in the RA-UT group (blue). Similarly, IL-12A – IL-2 genes highly expressed in RA-UT were down regulated in RA-TNF and confirmed an effective alternative inflammatory model as induced by TNF-α stimulation.

Comparison of RA-TNF/NP and RA-TNF groups were then examined to assess NP regulation of key inflammatory genes in a TNF-α induced acute inflammatory response *in-vitro*. As shown in Figure 4.4, highly expressed pro-inflammatory cytokines IL-1B, IL-1A, IL-6, IL-8 and IFN-ɣ in RA-TNF cells, were shown to be down regulated in RA-TNF/NP groups. Similarly, TNF-α induced up regulation of MMP-1 and MMP-3 were also shown to be suppressed following NP incubation in RA-TNF/NP groups. NF-κB dimers, RELA appeared largely unaffected by NP incubation, while RELB was suppressed in RA-TNF/NP. In contrast, CCL2/MCP-1 genes were shown to be more highly expression in RA-TNF/NP when compared to RA-TNF alone. These genes are involved in the innate immune system and are upregulated in the synovium of RA patients (Koch, 1992; Choy, 2001). The up-regulation of these particular genes in RA-TNF/NP group was dependent on the presence of TNF-α and not shared by the RA-NP group. This suggests an alternative NP effect on the regulation of acute inflammatory responses. While there is clear evidence that NP can influence inflammatory markers, the data is still limited, and the pathway of activation for CCL2 and MMP-13 requires further investigation. Similarly, to RA-TNF/NP, highly expressed inflammatory in RA-UT were downregulated following NP treatment in RA-NP, in particular IL-4, IL-12B, IL-13, IL-2, IFN-ɣ and CCL2. In contrast, expression of collagenases

MMP-1 and MMP-3, while downregulated in RA-TNF/NP, where upregulated in RA-NP when compared to RA-UT.

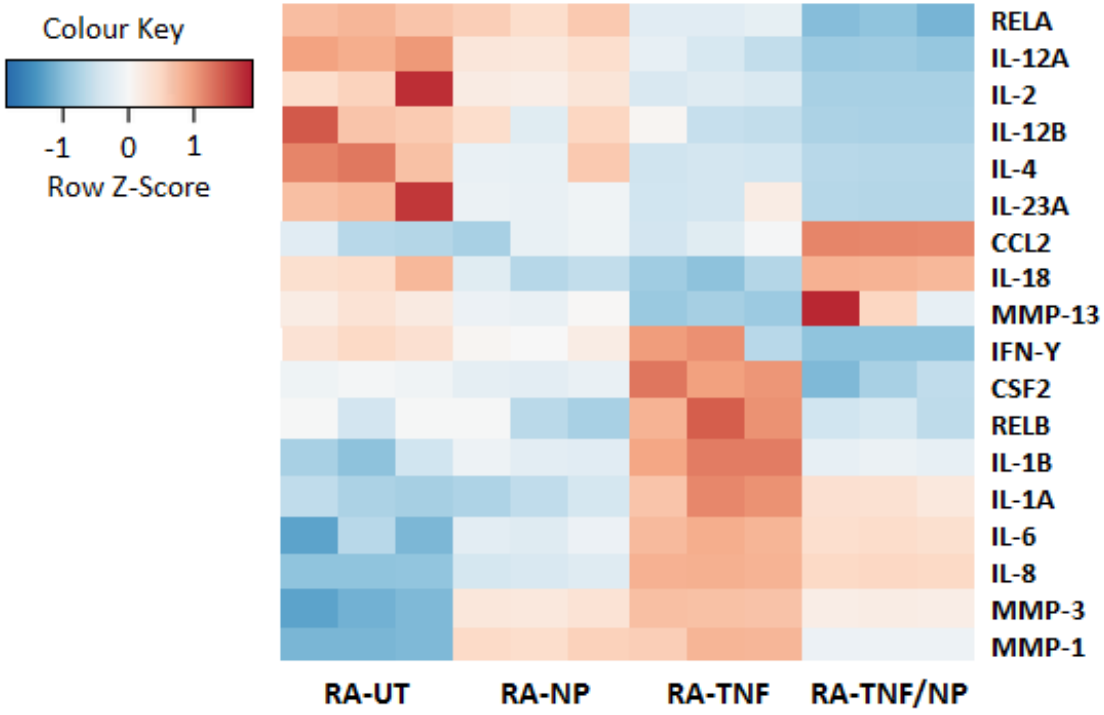

Figure 4.4: Heat map of DE candidate genes prominent in arthritis progression in RA-FLS cells. Groups include; untreated RA-FLS cells (RA-UT), TNF-α stimulated cells (RA-TNF), NP and TNF-α stimulated cells (RA-TNF/NP) and NP treated cells (RA-NP). The normalised RNA-seq data is in log2 scale, where red is highly expressed genes and blue is low expression. To be included in the heat map, genes were required to have at least 1000 counts (reads), totalled over all samples, where the standard deviation of log2 expression differences had to exceed two. The heatmaps highlights anti-inflammatory effects of NP in TNF-α induced pro-inflammatory cytokine expression. Abbreviations: NF-κB subunits (RELB, RELA); Interferon (IL-[12A, 12, 12B, 4, 23A, 18, 1B, 1A, 6, 8]); Matrix metalloproteinases (MMP-[13, 3, 1]); Chemokine ligand 2 (CCL2); colony-stimulating factor 2 (CSF2).

4.3.2.4 NP pathway signalling regulation of candidate signalling genes

To explore the potential pathways involved in the NP mediated suppression of inflammatory markers, connector molecules produced by pathway analysis were employed by integrating RNA-seq DE genes to show signalling in RA-FLS cells. The activation status of the genes and the pathway flow was predicated by a corrected log expression, comparing RA-TNF/NP to RA-TNF. The predicated influence of NP on FLS gene induction is shown in Appendix 5. To assess the mechanisms mediating the NP's anti-inflammatory effects, candidate mRNA signalling genes were compared between NP treated and non-treated cells. This panel of candidate mRNA were specifically selected and screened because of their importance in inflammation and disease progression in RA. Logfold changes and FDR values for Figure 4.5 are supplied in Appendix 4.

Figure 4.5 illustrates the regulation of candidate mRNA genes involved in inflammatory signalling, abbreviations are supplied in legend. As expected, clustering based on the expression pattern of the chosen signalling genes resulted in a clear separation between RA-TNF and RA-UT as indicated by opposite colour scoring in z-score. In RA-TNF, high expression of JAK, STAT, PPAR and TLR2, and to a lesser degree AKT1 were found to be upregulated when compared to RA-UT. The increase in signalling genes following TNF-α are consistent with the pro-inflammatory stimulatory effects of the cytokine. By contrast, TLR3 remained largely unaffected, while TLR4 were downregulated. For NP treated cells, there was a significant shift in gene regulation, with highly expressed genes in RA-TNF oppositely expressed in RA-TNF/NP. In particular TLR, STAT, RXR and PPAR-ɣ genes were significantly downregulated, while PPAR-δ, SOCS4, AKT1 and LXR genes were significantly upregulated and suggests anti-inflammatory effects are mediated by regulation of these genes. Comparison of RA-NP to RA-UT showed a shift in gene regulation consistent to that seen in RA-TNF/NP when compared to RA-TNF, however to a lesser degree and suggests effects mediated by a similar pathway. In particular, TLR and RXR genes which were highly regulated in RA-UT, were downregulated in RA-NP. Note the marked inhibitory effect of JAK/kinases in TNF/NP stimulated cells.

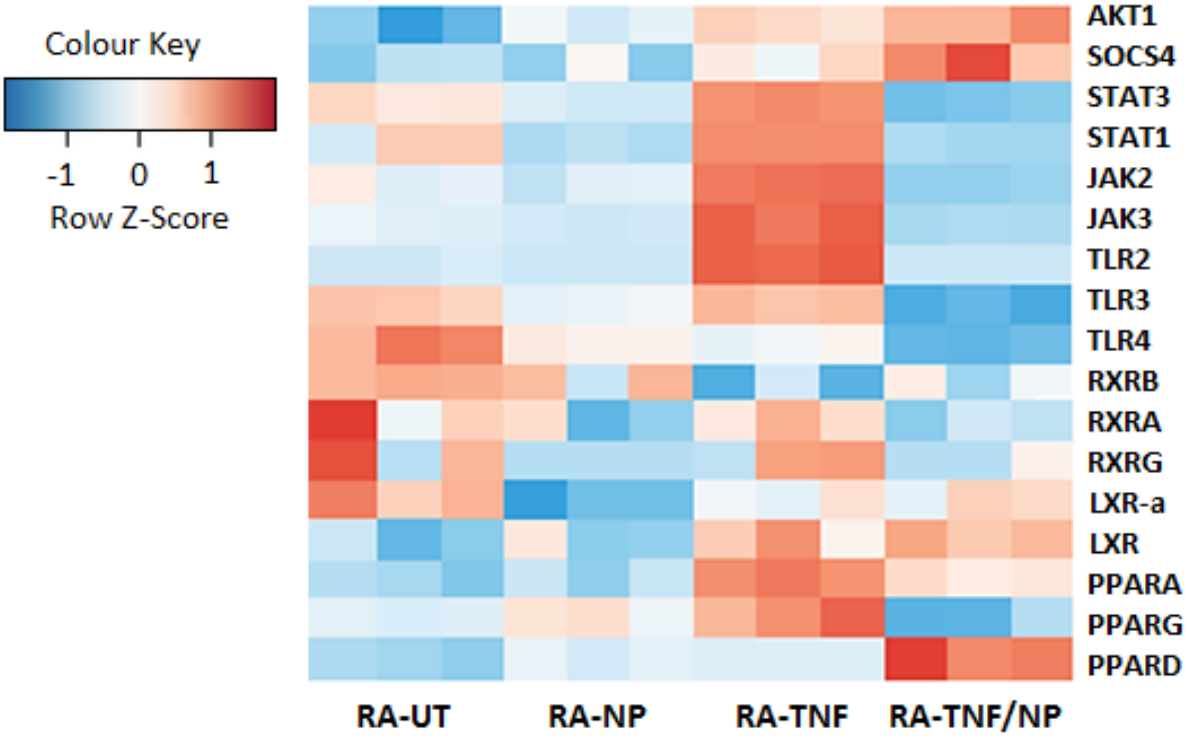

Figure 4.5. Heat map of DE candidate signaling genes. Groups include; untreated RA-FLS cells (RA-UT), TNF-α stimulated cells (RA-TNF), NP and TNF-α stimulated cells (RA-TNF/NP) and NP treated cells (RA-NP). The normalised RNA-seq data is in log2 scale, where red is highly expressed genes and blue is low expression. To be included in the heat map, genes were required to have at least 1000 counts (reads), totalled over all samples, where the standard deviation of log2 expression differences had to exceed two. The heatmaps highlights shift in gene expression following NP treatment. Abbreviations: Serine/threonine-protein kinase (AKT1); Suppressor of cytokine signalling 4 (SOCS4); Janus kinase (JAK-[2,3]); Signal transducers and activators of transcription (STAT-[1,3]); Toll like receptor (TLR-[2,3,4]); Liver X receptor (LXR-[α]); Retinoid X receptor (RXR); Peroxisome proliferator-activated receptors (PPAR [A,G,D]-[α, ɣ, δ]).

4.3.2.5 Effect of NP on the biochemistry of endocannabinoid synthesis

Since LEA is a FAAH inhibitor, the effect of NP regulation of genes involved in the synthesis and metabolism of endogenous endocannabinoids was examined. Figure 4.6 illustrates the regulation of candidate mRNA genes involved in the synthesis, degradation and oxidation of AEA. Logfold changes and FDR values for Figure 4.6 are supplied in Appendix 4. Following TNF-α stimulation there is an overall decrease in both synthesising enzymes, in particular ABHD4/GDE1 and NAT1/NAPE-PLD, and catabolic enzymes LOX and FAAH in RA-TNF when compared to RA-UT. In contrast, COX-2 was upregulated in RA-TNF.

In NP treated cells, synthesising enzymes were increased in RA-TNF/NP when compared to RA-TNF, suggesting a shift in genes to a more active synthesising state following NP treatment. In particular, FAM213B, PTPN22, PLG1, PTGSG2 were upregulated, while ABHD4 and GDE1 were downregulated/not affected. For catabolic enzymes, LOX and FAAH were downregulated, while CP450 and COX-2 were upregulated in RA-TNF/NP. Similarly, comparison of RA-NP to RA-UT showed increase a similar expression pattern consistent to that seen in RA-TNF/NP. In RA-UT, highly expressed PTGSG2 and GDE1 were downregulated following in RA-NP.

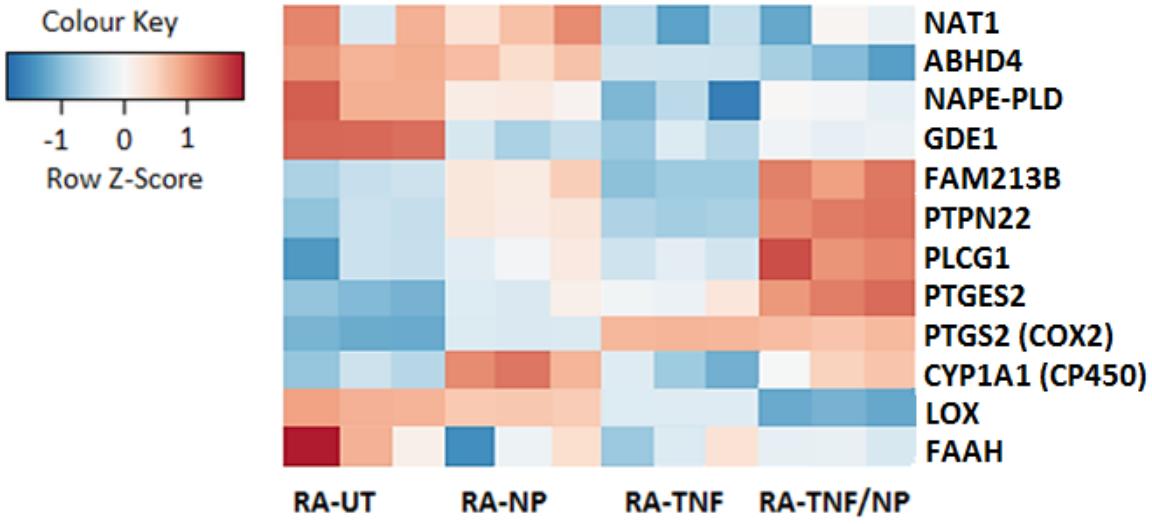

Figure 4.6. Heat map of DE candidate mRNA genes involved in endocannabinoid synthesis and degradation. Groups include; untreated RA-FLS cells (RA-UT), TNF-α stimulated cells (RA-TNF), NP and TNF-α stimulated cells (RA-TNF/NP) and NP treated cells (RA-NP). The normalised RNA-seq data is in log2 scale, where red is highly expressed genes and blue is low expression. To be included in the heat map, genes were required to have at least 1000 counts (reads), totaled over all samples, where the standard deviation of log2 expression differences had to exceed two. An increase in synthesizing enzymes was observed in NP treated cells. Abbreviations: N-acyltransferase 1 (NAT1); α/β-hydrolase domain 4 (ABHD4); N-acyl phosphatidylethanolamine phospholipase D (NAPE-PLD); Glycerophosphodiesterase-1 (GDE1); Family with sequence similarity 213 Member B (FAM213B); Non-receptor protein tyrosine phosphatase 22 (PTPN22); Phospholipase C gamma 1 (PLCG1); Prostaglandin E synthase 2 (PTGES2); Cyclooxygenase-2 (COX-2); Cytochrome P450 monooxygenases (P450s); Lipoxygenase (LOX); Fatty acid amide hydrolase (FAAH).

4.3.2.6 Network and pathway analyses of DE genes

Pathways analysis of DE genes was performed using IPA. The percentage overlap represents the number of genes in the canonical pathway that were influenced by the following treatment. The top canonical pathways induced in the TNF-α stimulated RA-FLS cells are summarised in Table 4.3A. In TNF-α inflammatory model, DE genes significantly expressed following stimulation with TNF-α led to enrichment of cytokine-rich ontologies and were consistent to top biological functions involving inflammation. The top canonical pathways activated following NP treatment in TNF-α stimulated and non-stimulated RA-FLS cells are summarised in Table 4.3B and C respectively. For RA-TNF/NP, the pathway activated were heavily involved in immune cell trafficking as well as lipid metabolism. Similarly, for RA-NP immune cell trafficking was a common biological feature of the activated pathways, with particular regulation in osteoarthritic conditions.

Table 4.3. Top Canonical Pathways based on comparison of RNA-seq data between **(A)** RA-TNF and RA-UT; **(B)** RA-TNF/NP and RA-TNF; **(C)** RA-NP and RA-UT.

A

Top canonical pathway	p-value	overlap
Hepatic Fibrosis / Hepatic Stellate Cell Activation	6.85E-11*	21.9% (40/183)
Granulocyte Adhesion and Diapedesis	7.65E-10	21.7% (36/166)
Dendritic Cell Maturation	1.34E-09	20.5% (38/185)
Agranulocyte Adhesion and Diapedesis	4.08E-09	20.5% (36/176)
Neuroinflammation Signalling pathway	2.25E-08	16.3% (49/301)

B

Top canonical pathway	p-value	overlap
Granulocyte Adhesion and Diapedesis	3.32E-11	21.1% (35/166)
Hepatic Fibrosis / Hepatic Stellate Cell Activation	3.36E-11	20.2% (37/183)
Agranulocyte Adhesion and Diapedesis	2.93E-09	18.8% (27/121)
Role of Macrophages, Fibroblasts & Endothelial Cells in RA	8.23E-08	14.2% (33/176)
LXR/RXR Activation	1.56E-09	22.3% (43/303)

C

Top canonical pathway	p-value	overlap
Granulocyte Adhesion and Diapedesis	3.59E-08	10.2% (17/166)
Agranulocyte Adhesion and Diapedesis	8.52E-08	9.7% (17/176)
Role of Osteoblast, Osteoclasts and Chondrocytes in RA	1.57E-07	8.3% (19/228)
LPS/IL-1 mediated Inhibition of RXR function	2.04E-07	8.6% (18/209)
Osteoarthritis Pathway	8.12E-07	8.3% (17/206)

*E- equals E to the power of the next numeral.

4.3.3 RNA-seq Gene Expression in OA-FLS Cells

4.3.3.1 Top DE genes following TNF-α stimulation (OA-TNF vs OA-UT)

TNF-α was used to stimulate OA-FLS cells. It was found that 13766/15779 of genes which were upregulated (>2 fold) by TNF-α reached statistical significance when compared to untreated controls (FDR <0.05). Assessment of the top DE genes in OA-TNF cells showed the acquisition of genes associated with inflammation and joint erosion, Table 4.4. As shown, the upregulated chemokines CXCL5,8,10 and CCL5,20 were elevated and are important in the recruitment of inflammatory mediators (CCL5, CCL20) and angiogenesis (CXCL8; Scanzello, 2017). In addition to the chemokines, a pronounced recruitment of genes involved in nociceptive signalling (TRPA1) and bone remodelling (IBSP, MEOX1) were also observed. These include genes involved in osteoclastogenesis such as CXCL8 and CCL20, all of which collectively contribute to inflammation and degenerative joint function associated with OA). The top canonical pathways induced in the TNF-α stimulated OA-FLS cells are summarised in Table 4.5. In TNF-α inflammatory model, DE genes significantly expressed following stimulation with TNF-α led to enrichment of cytokine-rich ontologies and were consistent to top biological functions involving inflammation.

4.3.3.2 Top DE genes following NP incubation (OA-TNF/NP vs OA-TNF)

By comparing TNF-α treated cells to TNF-α and NP treated cells the influence of NP in inflammation was assessed. Analysis showed 12846/16781 genes which were DE (>2 fold) in OA-TNF/NP cells reached statistical significance when compared to OA-TNF cells (FDR <0.05). As shown in Table 4.6, assessment of the top DE genes in OA-TNF/NP cells shows the downregulation of genes involved with mitotic processes, MKI67, KIF20A, DEPDC1, KIF18B, NEK2, DLGAP5, MYBL2, PCLAF, retrograde vesicular trafficking from the golgi apparatus, KIF20a, KIF18B, and protein binding, TROAP. In agreement with this data, assessment of OA-TNF/NP's top canonical pathways highlight pathways involved in both mitotic regulation and immune cell trafficking (Table 4.7).

Table 4.4. Top 10 DE genes based on comparison of RNA-seq data between TNF-α treated (OA-TNF) and non-treated (OA-UT) OA-FLS cells.

Gene	Name	Log2FC	FDR
CXCL8	C-X-C motif chemokine ligand 8	9.237	9.81E-64
TRPA1	Transient receptor potential cation channel subfamily A member 1	9.183	7.53E-17
CXCL10	C-X-C motif chemokine ligand 10	9.050	7.74E-12
CCL5	C-C motif chemokind ligand 5	9.048	3.22E-24
C15orf48	Chromosome 15 open reading frame 48	8.777	4.27E-11
IBSP	Integrin binding sialoprotein	8.385	6.86E-10
MEOX1	Mesenchyme homeobox 1	7.819	6.51E-12
CCL20	C-C motif chemokind ligand 20	7.748	7.87E-24
ELOVL7	ELOVL fatty acid elongase 7	7.450	2.42E-08
CXCL5	C-X-C motif chemokine ligand 5	7.194	2.36E-107

Table 4.5. Top canonical pathways based on comparison of RNA-seq data between TNF-α treated (OA-TNF) and non-treated (OA-UT) OA-FLS cells.

Top canonical pathway	FDR	overlap
Granulocyte Adhesion and Diapedesis	1.079E-15	15.0% (25/167)
Agranulocyte Adhesion and Diapedesis	3.39E-13	13.0% (23/177)
Role of IL-17F in Allergic Inflammatory Airway Diseases	1.12E-11	28.6% (12/42)
Atherosclerosis Signalling	1.83E-10	13.7% (17/124)
Role of Macrophages, Fibroblasts and Endothelial Cells in RA	1.18E-09	8.1% (25/310)

Table 4.6. Top 10 DE genes based on comparison of RNA-seq data between NP treated (OA-TNF/NP) and non-treated (OA-TNF) TNF-α stimulated OA-FLS cells.

Gene	Name	Log2FC	FDR
MKI67	Marker of proliferation Ki-67	-10.769	6.32E-11
KIF20A	Kinesin family member 20A	-10.684	2.11E-10
DEPDC1	DEP domain containing 1	-9.3266	7.54E-11
PCLAF	PCNA clamp associated factor	-8.9747	2.22E-10
PBK	PDZ binding kinase	-8.8419	3.01E-10
TROAP	Trophinin associated protein	-8.7708	1.74E-05
KIF18B	Kinesin family member 18B	-8.7094	2.50E-08
NEK2	NIMA-related kinase 2	-8.3465	7.55E-09
DLGAP5	Disks Large-Associated Protein 5	-8.0457	2.34E-09
MYBL2	MYB Proto-Oncogene Like 2	-7.8215	2.66E-07

Table 4.7. Top Canonical Pathways based on comparison of RNA-seq data between NP treated (OA-TNF/NP) and non-treated (OA-TNF) TNF-α stimulated OA-FLS cells.

Top canonical pathway	FDR	overlap
Mitotic Roles of Polo-Like Kinase	1.149E-07	22.2% (14/63)
Cell Cycle Control of Chromosomal Replication	1.39E-06	21.4% (12/56)
Hepatic Fibrosis / Hepatic Stellate Cell Activation	3.11E-05	12.0% (22/183)
Granulocyte Adhesion and Diapedesis	3.15E-05	11.4% (19/167)
Agranulocyte Adhesion and Diapedesis	7.01E-05	10.7% (19/177)

4.3.4 RT-PCR Effect of NP on RA-FLS Cells

To replicate and confirm findings obtained by RNA-seq, RT-PCR was used to confirm NP effects in the regulation of anti-inflammatory genes. RNA purity and an evaluation of suitable housekeeping genes were assessed prior to testing primers of interests.

4.3.4.1 RNA purity and concentration

RNA purity and concentration was assessed using a Nanodrop spectrophotometer and summarised in Table 4.8. The ratio of the readings at 260 nm and 280 nm (A260/A280) provided an estimate of the purity of RNA. Pure RNA had an A260/A280 ratio of 1.9-2.1. RNA isolated from all groups had a pure RNA ratio between 1.9-2.1

Table 4.8. RNA purity and concentration of RA-FLS cells as assessed by Nanodrop spectrophotometer.

Cell Line	Treated Groups	A260/A280	A260/A230	[RNA] ng/µL
RA-FLS	RA-UT	1.925	1.920	138
	RA-TNF	1.983	1.844	152
	RA-TNF/NP	1.945	2.025	160
	RA-NP	1.977	1.852	104

4.3.4.2 Assessment of house-keeping genes

House-keeping genes GAPDH and β-actin, were used to normalise gene expression data and correct sample-to-sample variation. The ideal control gene is consistently expressed regardless of treatment. Stable expression was defined as cycle threshold (Ct) = 0-0.05 between treatment groups. Two house-keeping genes, GAPDH and β-actin, were assessed for stability before testing primers of interest. Figure 4.7 compares the relative mRNA expression of GAPDH and β-actin, as well as their respective melting peaks. It was found that GAPDH was consistently expressed at a comparable level between groups and was therefore selected as the house-keeping gene for normalisation in all subsequent PCR experiments.

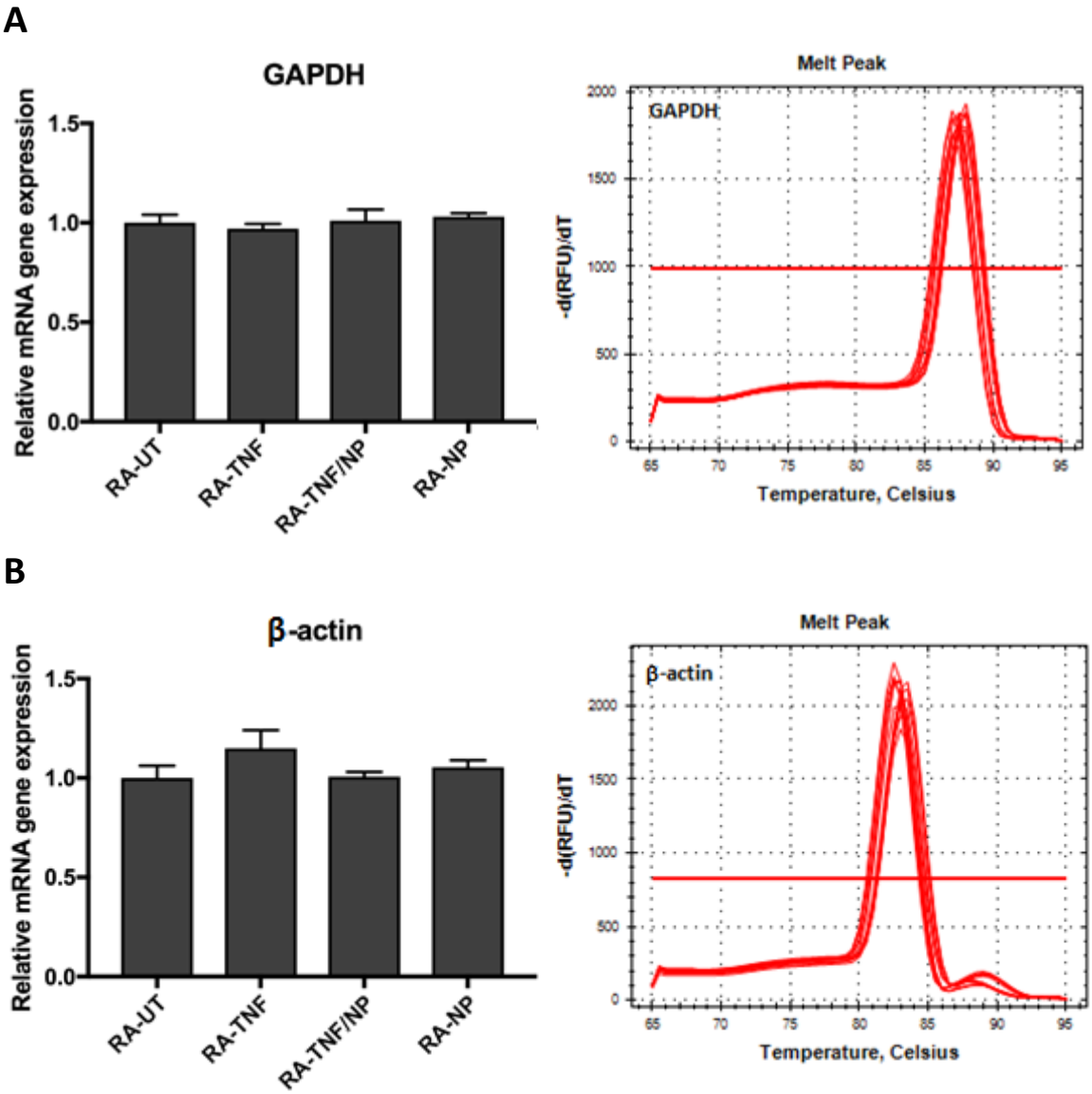

Figure 4.7. Comparison of house-keeping genes **(A)** GAPDH and; **(B)** β-actin mRNA between RA-FLS treatment groups. Melting curves of the house-keeping genes are represented alongside and show one single melt peak. GAPDH was shown to be consistently expressed and used to normalise subsequent mRNA runs.

4.3.4.4 NP effects on TNF-α induced IL-6, IL-8, and NF-κB mRNA

RT-PCR was carried out to investigate whether NP treatment could regulate TNF-α stimulated changes in the gene transcription levels of three target genes; NF-κB, IL-6 and IL-8. Changes in gene regulation are expressed as a fold change to control groups and normalised against GAPDH. Consistent with previously documented pro-inflammatory actions of TNF-α, incubation of cultured RA-FLS with recombinant TNF-α (10 ng/mL) induced marked increases in the gene transcription for all 3 genes tested. As shown in Figure 4.8, RA-TNF cells exhibited a fold change increased NF-κB by 2.832 ($p < 0.0001$, n=3), IL-6 by 47 ($p < 0.0001$, n=3) and IL-8 by 53 ($p < 0.0001$, n=3). In contrast, all three pro-inflammatory genes were significantly supressed in TNF-α stimulated cells which were NP treated. RA-TNF/NP cells significantly decreased expression of NF-κB by 0.64 ($P < 0.0001$, n=3), IL-6 by 0.5-fold ($P < 0.0001$, n=3) and IL-8 by 0.8-fold ($P < 0.0001$, n=3) when compared to RA-TNF. These results are consistent with the data observed in RNA-seq analysis.

4.3.4.4 NP effects on TNF-α induced MMP-1, MMP-13, and MMP-3 mRNA

Similarly, to investigate whether NP treatment could regulate TNF-α stimulated changes in collagenases, the gene transcription levels of MMP-1, MMP-3 and MMP-13 were compared using RT-PCR. Changes in gene regulation are expressed as a fold change to control groups and normalised against GAPDH. As shown in Figure 4.9, TNF-α induced marked increases in the gene transcription for all MMP genes tested. RA-TNF cells exhibited increased MMP-1 by 10.17-fold ($p < 0.0001$, n=3), MMP-3 by 2.086-fold ($p < 0.01$, n=3) and MMP-13 by 1.884-fold ($p < 0.001$, n=3) mRNA levels, respectively. Similar to data obtained by RNA-seq, NP treated cells showed a marked decrease in all three genes following TNF-α stimulation. As shown in Figure 4.11, RA-TNF/NP cells demonstrated significantly decreased expression of MMP-1 from 10.2 to 1.1 ($p < 0.0001$, n=3), MMP-3 from 2.1 to 1.2 ($p < 0.0001$, n=3) and MMP-13 from 1.9 to 0.8 ($p < 0.0001$, n=3) when compared to RA-TNF. These results are consistent with the data observed in RNA-seq analysis. Interestingly, NP incubation in untreated cells (RA-NP) increased the expression of MMP-3. This expression was four fold greater than unstimulated/untreated RA-FLS cells.

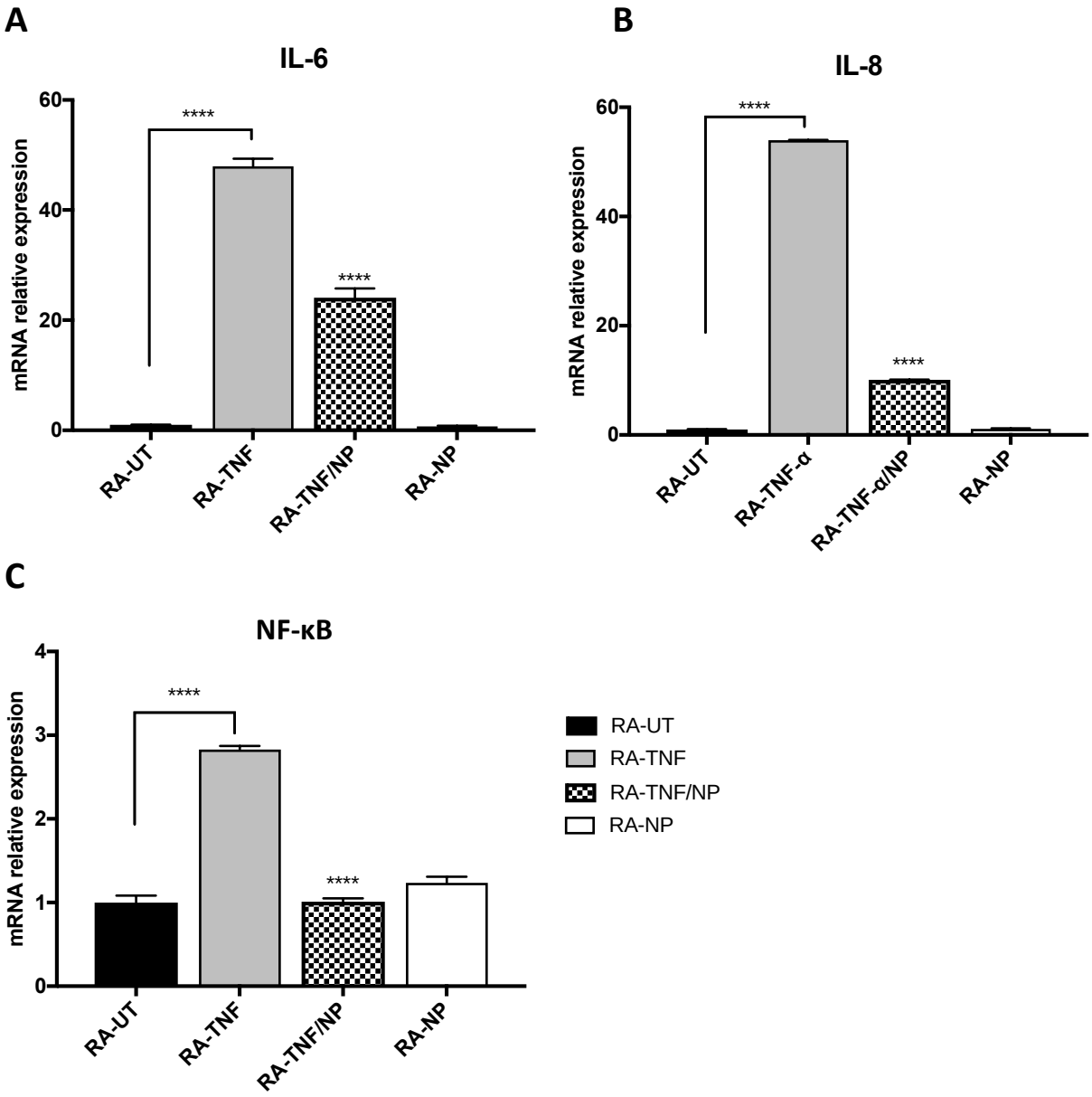

Figure 4.8. NP suppressed pro-inflammatory upregulation of NF-κB, IL-6 and IL-8 mRNA in RA-FLS cells. Cultured RA-FLS stimulated with either alone TNF-α (10 ng/mL) or in the presence of NP (30 μg/mL) for 24 h. Expression levels of mRNA were assayed by quantitative real-time RT-PCR. The mRNA levels of each gene were standardised against GAPDH levels. Data are expressed as the mean ± S.D, n = 3. *p < 0.05; **p < 0.01, ***p < 0.001, ****p < 0.0001 vs TNF-α alone, analysis using one-way ANOVA, followed by Turkey's multiple comparison test.

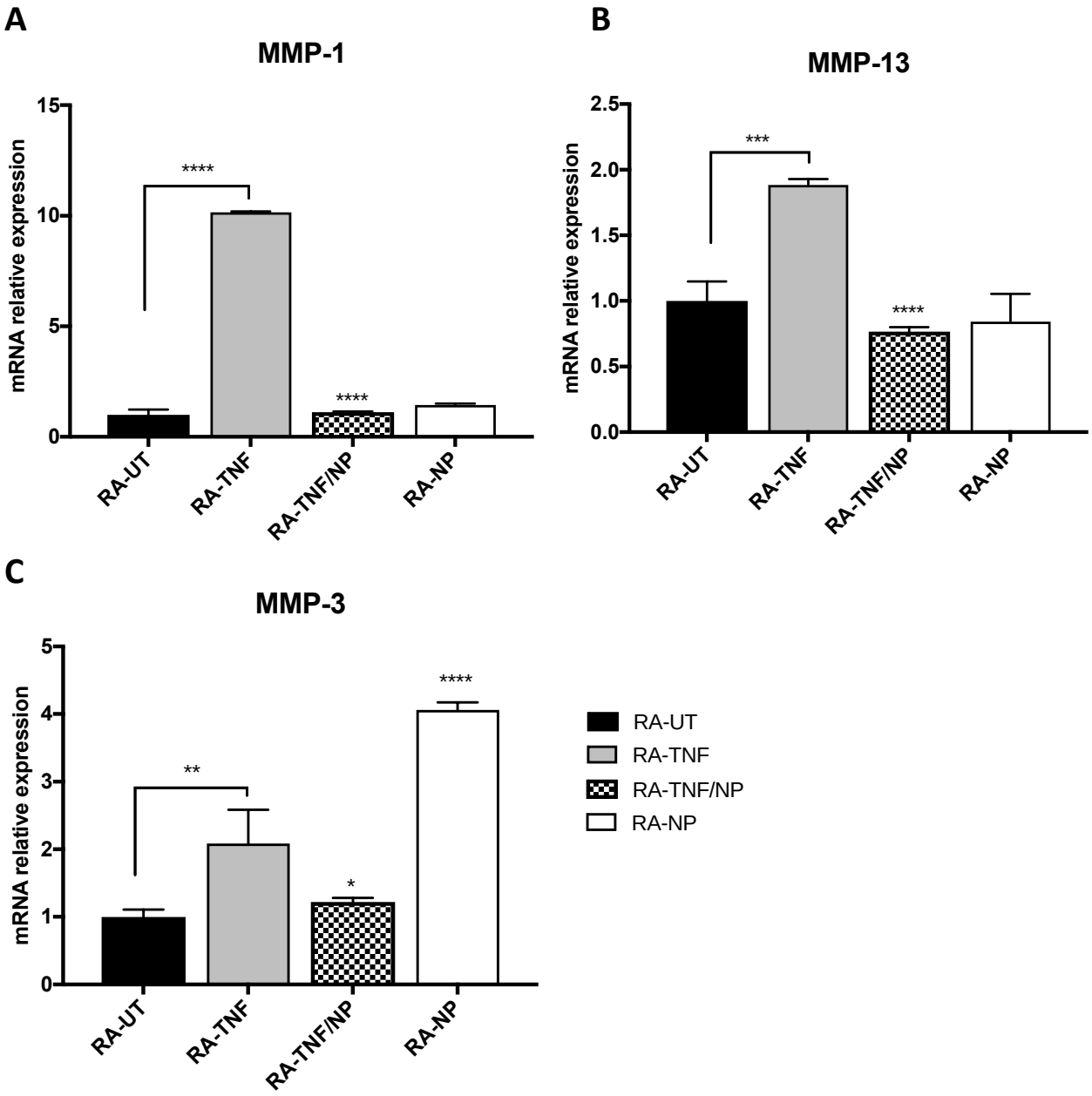

Figure 4.9. NP suppresses pro-inflammatory upregulation of collagenases MMP-1, MMP-3 and MMP-13 mRNA in RA-FLS cells**.** Cultured RA-FLS stimulated with either alone TNF-α (10 ng/mL) or in the presence of NP (30 μg/mL) for 24 h. Expression levels of mRNA assayed by quantitative real-time RT-PCR. The mRNA levels of each gene were standardised against GAPDH levels. Data are expressed as the mean ± S.D, n = 3. *p < 0.05; **p < 0.01, ***p < 0.001, ****p < 0.0001 vs TNF-α alone, analysis using one-way ANOVA, followed by Turkey's multiple comparison test.

4.4 DISCUSSION

With the rapidly growing interest in NP research, the toxicity of NP is becoming an increasingly important issue to resolve. To ensure consistency in screening, the cytotoxicity of the endocannabinoid-based NP's were evaluated using two means, the Trypan blue exclusion method and the WST-1 colorimetric assay. To minimise inaccurate toxicity measurements due to variables such as temperature, size and cell lines which can affect NP toxicity (Warheit, 2010), NP's were sized prior to cytotoxicity testing to ensure size consistency and stability at temperatures upwards of 37˚C. The effective concentration needed to reduce cell viability by 50% (LC50) in tested FLS cells was 40 µg/mL and consistent between the two assays. NP concentrations of 30 µg/mL showed 75% viability, NP were used at 30 µg/mL for all future *in-vitro* experiments.

The effects of LEA and OEA on FLS cells under various conditions has not been previously described. Consistent with previously described effects of TNF-α, assessment of the top DE genes in RA-TNF showed upregulation and acquisition of genes associated with inflammation and joint erosion (Bek et al., 2017). For NP treated cells, assessment of the top DE genes in RA-TNF/NP indicated that NP promoted the acquisition of genes associated with homeostasis and inflammation resolution and led to a significant reduction of pro-inflammatory genes. Highly expressed pro-inflammatory cytokines IL-1B, IL-1A, IL-6, IL-8 and IFN-ɣ in RA-TNF cells were down regulated in RA-TNF/NP groups indicating inflammatory resolution by decreasing cytokine production. Similarly, low expression of MMP's in the TNF/NP group suggests a protective role of NP in preventing cartilage destruction by limiting the production of collagenases. The up-regulation other genes involved with the innate immunity that can stimulate NK cells suggests an alternative NP effect on the regulation of inflammatory responses.

Activation and release of factors from macrophages, FLS and endothelial cells involved in RA pathogenesis are principally initiated by four main signal transduction pathways, ERK/MAPK pathway, NF-κB pathway, WNT pathway and JAK-STAT pathway. Activation of these pathways are regulated by upstream receptors such as TLR, PPAR-α, TNF-R as well as DAG/PKC signalling. Previous experiments have demonstrated OEA and LEA ability to interrupt pro-inflammatory signalling. OEA exerts anti-inflammatory effects by enhancing PPAR-α signalling, inhibiting the TLR4-mediated NF-κB signalling pathway, and interfering with the ERK1/2-dependent signalling cascade (TLR4/ERK1/2/AP-1/STAT3; (Yang et al., 2016). Similarly, LEA has been shown to suppress LPS induced expression of TNF-α, IL-1B, IL-6, COX-2, and PE2, by inhibition of NF-κB signalling in macrophages *in-vitro* (Ishida et al., 2013). Consistent with published literature, analysis of candidate mRNA signalling genes showed suppression of TLR (2,3,4) in NP treated cells, when compared to non-treated cells (Yang et al., 2016). TLRs are

highly expressed in patients with RA, and have been shown to contribute to the pathogenesis of the disease (Huang & Pope, 2009; Duffy & O'Reilly, 2016). Activation of NF-κB and MAPK signalling pathways through TLR results in expression of pro-inflammatory cytokines and activation of cells of the innate immune system. Inhibition of the TLR pathways may be mediated by changes in PPAR signalling. PPAR and LXR are both members of the nuclear receptor family which regulate metabolic and inflammatory signalling. These receptors heterodimerize with RXR to regulate gene transcription. Activation of RXR has been linked to increased production of chemokines, resulting in increase in leucocyte recruitment and an inflammatory response (Nunez et al., 2010). By contrast, LXR-dependent repression of inflammatory genes induced by LPS/TLR4 signalling has been noted in macrophages (Ogawa et al., 2005). NP induced increases in PPAR-ɣ, LXR genes and decrease in RXR (α, ɣ, δ) genes could therefore help mediate the anti-inflammatory effects by enhanced PPAR signalling, and interrupted TLR signalling.

In addition to the known effects of OEA on TLR and PPAR signalling, expression of JAK-STAT signalling mRNA was also shown to be suppressed in NP treated cells. In recent years, numerous studies have established that the JAK/STAT signalling pathway is important in the synovium of RA patients and in animal models of arthritis (Ahmad et al., 2015). In addition to JAK-STAT suppression, expression of STAT inhibitor SOCS4 was increased in NP treated cells. Given that many JAKs are associated with cytokine receptors, the JAK-STAT signalling pathway is an emerging target for RA therapy. Novel oral JAK inhibitor, tofacitinib, has been suggested as a new first line monotherapy, having superior efficacy over methotrexate (MTX) in the treatment of RA (Lee et al., 2014a; Onuora, 2014). In tofacitinib-treated patients, clear reductions in synovial STAT1 and STAT3 phosphorylation levels were observed and strongly correlated with 4-month clinical responses (Boyle et al., 2015). Dampening of JAK-STAT signalling by NP's may suppress cytokine signalling and may offer as an alternative JAK inhibitor in the treatment of RA.

NP effects in OA-FLS cells were also evaluated. Quality of RNA-seq treatment samples using PCA plots and sample-sample heat distance maps demonstrated poor clustering of the OA-NP replicates. The shared genetic similarity between the clustered OA-NP and OA-UT suggests that these two OA-FLS groups were either not exposed to NP, or had poor NP uptake during treatment. Due to this, OA-NP group was excluded from analysis and therefore only general remarks on the NP influence in OA can be inferred. Similar to TNF-α induced effects observed in RA-FLS treated cells, assessment of the top DE genes in OA-TNF showed the acquisition of genes associated with inflammation and joint erosion, with particular upregulation of chemokines (CXCL5,8,10; CCL5,20). Following NP treatment, assessment of the top DE genes in RA-TNF/NP cells showed the downregulation of genes involved in mitotic processes, retrograde vesicular trafficking from the golgi apparatus and protein binding. In

agreement with this, evaluation of the top canonical pathways influenced in OA-TNF/NP shows the downregulation of mitotic roles of polo-like kinase 1 (Plk1). Further analysis of the NP effects on OA-FLS cells should be further evaluated in the presence of OA-NP group.

NP influence on endogenous endocannabinoid synthesis and degradation was also examined. Unlike OEA, the anti-inflammatory effects of LEA may be mediated by the CB receptors. In previous experiments, LEA has been demonstrated to be an endogenous ligand for the CB receptors, although affinity is relatively low (Lin et al., 1998). LEA has also been shown to inhibit FAAH (Maccarrone et al., 1998), increasing the life-time of AEA, which then mediates its anti-inflammatory effects by the CB receptors. Analysis of candidate mRNA genes involved in AEA synthesis and degradation, demonstrated an increase in AEA synthesising enzymes following NP treatment in both non-stimulated (RA-NP), and TNF-α stimulated (RA-TNF/NP) cells. The higher bioavailability of synthesising enzymes may increase endogenous AEA levels mediated by the ABHD4/GDE1 and NAT/NAPE-PLD pathway. In addition to enhancing synthesising enzymes, a shift in catabolic enzymes following NP treatment was observed. Metabolism of AEA into AA and ethanolamine depends on multiple enzymes, including oxygenation by COX-2, LOXs and several cytochrome P450 monooxygenases. In NP treated cells, oxygenation enzymes LOX was downregulated, while CP450 was upregulated. Down regulation of LOX would decrease metabolite production of hydroxyl-AEA (HETE-EAs), while an upregulation in CP450 would increase EETs-EA (epoxyeicostrienoyl-ethanolamides). EETs-EA are shown to be potent CB2 (Snider et al., 2009) and PPAR-ɣ agonist (Liu, 2005), exerting anti-inflammatory effects (Node et al., 1999; Thomson et al., 2012). In agreement with this data, increased expression of PPAR-ɣ mRNA noted in NP treated cells may correlate with elevated expression of EETs-EAs from increased metabolism of AEA by CP450s. By contrast, down regulation of LOX would decrease metabolite production of hydroxyl-AEA (HETE-EAs). Metabolic products of LOXs, such as 12- and 15-HPETEs and 5- and 15-HETEs, are capable of activating TRPV1 (Hwang et al., 2000) and PPAR-α (Kozak et al., 2002). Stimulation of TRPV is associated with increases in both neurotransmitter release (Kelly et al., 2015) and inflammatory mediators contributing to joint inflammation. A reduction in LOX metabolites may help facilitate both anti-inflammatory and analgesic potential of the NP by decreased TRPV agonists (Premkumar & Sikand, 2008; Hu & Ma, 2018). Consistent with the reported effects of LEA, NP treatment decreased expression of FAAH. Expression of FAAH is strongly correlated with AEA concentrations (Haller et al., 2013), and the ability of AEA to elicit anti-inflammatory effects. Several studies have demonstrated robust anti-inflammatory and anti-hyperalgesia phenotypes after genetic or pharmacological disruption of FAAH, and so NP anti-inflammatory effects may be in part mediated by local increases in endocannabinoid ligands (Sasso et al., 2012; Cajanus et al., 2016).

4.4.1 Summary

This is the first report examining the effects of endocannabinoid-based NP's on the production of inflammatory mediators in human FLS cells. The ability of the NP to mediate anti-inflammatory effects *in-vitro* was demonstrated. The ability of the NP's to downregulate inflammatory cytokines, as well signalling genes involved in inflammatory processes highlights its promising application as an anti-inflammatory agent. Furthermore, NP regulation of AEA synthesising enzymes and catabolic and oxygenation enzymes may have flow on therapeutic effects by regulating endogenous endocannabinoid and metabolites concentrations at the targeted site.

CHAPTER 5: NANOPARTICLE BIOLOGICAL EFFECTS *IN-VIVO*

5.1 INTRODUCTION

In previous *in-vitro* experiments (Chapter 4), NP incubation significantly suppressed pro-inflammatory markers in TNF-α stimulated RA-FLS cells. The anti-inflammatory effects included suppression of pro-inflammatory cytokines, chemokines and metalloproteinase genes. In addition to anti-inflammatory effects, NAE's have been implicated as having potentially analgesic effects, influencing pain and inflammation in the peripheral nervous system (Piomelli & Sasso, 2014; Skaper et al., 2015). Localisation studies using receptor binding, immuno-histochemistry and *in-situ* hybridisation have mapped the distribution of the cannabinoid receptors along all levels of the pain nexus, providing a neuroanatomical framework befitting the function of the cannabinoid system in sensory processing (Walker & Huang, 2002; Starowicz & Przewlocka, 2012; Corcoran et al., 2015). The widespread expression of the cannabinoid receptors along the principal pain processing sites offers boundless opportunities for the development of analgesics for the treatment of various pain conditions. Anti-nociception is the process of blocking the detection of a painful or injurious stimuli by sensory neurons, resulting in the suppression of noxious neurotransmission. Anti-nociception is a prominent feature of systemically administered cannabinoids noted in preclinical studies applying various noxious agents such as chemical, mechanical and thermal stimuli to induce pain (Lotsch et al., 2018). In addition to centrally mediated effects, endocannabinoid lipids produced and released at sites of acute tissue injury, inflammation and neuropathy regulate the flow of nociceptive signals to the CNS (Piomelli & Sasso, 2014). NAE's, OEA and PEA, have been shown to exhibit anti-hyperanalgesic effects by supporting both anti-inflammatory and neurogenic effects through PPAR-α-dependent mechanisms (Suardiaz et al., 2007; Seol et al., 2017). These PPAR-α-dependent mechanisms may include opening of calcium-activated potassium (BKCa) channels and (IKca) potassium channels and regulation of the NF-κB transcription complex. In PPAR-α–deficient mice, the anti-hyperalgesic effects of PEA are attenuated, and responses to several pro-inflammatory and proalgesic stimuli are enhanced (Devchand et al., 1996; Ruiz-Medina et al., 2012). Increased activation of peripheral entourage receptors such as PPAR-α, TLR, TRPV by local NAE's, help regulate anti-inflammatory and anti-nociceptive responses, and can be achieved by increases in NAE or peripheral FAAH inhibition.

LEA has been shown to inhibit FAAH (Maurelli et al., 1995; Maccarrone et al., 1998). In Chapter 4, NP incubation suppressed FAAH mRNA expression *in-vitro*, which can be attributed to the NP's LEA component. Selective FAAH inhibition has been linked to both anti-inflammatory and anti-nociceptive responses in several models of pain–behaviour (Huggins et al., 2012; Fichna et al., 2014; Salaga et al., 2014). In a rodent model of visceral and inflammatory pain, systemic administration of the

peripherally restricted FAAH inhibitor, URB937, selectively interrupted AEA degradation outside the brain and spinal cord (Clapper et al., 2010) causing striking anti-hyperalgesic effects (Sasso et al., 2012). The increased lifetime of AEA and other articular endocannabinoids induced by LEA could have a considerable prolonged effect on cellular signalling, and be a novel anti-inflammatory and analgesic agent (Clapper et al., 2010).

Similarly, current NSAIDs, including ibuprofen and indomethacin, prescribed for the treatment of inflammatory pain in OA and RA patients have been shown to inhibit cyclooxygenase (COX) and FAAH (Karlsson & Fowler, 2014). Since both COX2 and FAAH are involved in the degradation of endocannabinoid lipids, another mode of action maybe the accumulation of endocannabinoids and entourage compounds. Interactions between NSAIDs and the endocannabinoid ligands may be of great clinical importance in terms of multiple-target drug development having synergistic actions (Guindon et al., 2006). Together, these findings suggest that the endocannabinoid system plays an important role in pathogenesis of RA, and manipulation of this system by increasing endogenous endocannabinoid lipids, especially by combination of COX-2 and FAAH inhibitors, may be a promising strategy to reduce erosions, pain and inflammation in arthritis.

In this chapter, the previously noted *in-vitro* effects of the NP's were extended to examine if the same results would translate into an *in-vivo* system. For this, NP were administered i.v.i into arthritic rats, and the circulating plasma cytokines measured using an immune-bead based assay. The influence of NP on endogenous articular endocannabinoids was also assessed by HPLC/MS measuring levels of 2-AG, AEA, OEA, LEA and PEA in the paws of non-treated and NP injected rats. In addition, the potentially analgesic effect of NP in normal and arthritic rats was evaluated using the Randall-Selitto method. The Randall-Selitto or paw pressure test is a tool to assess response thresholds to mechanical pressure stimulation and is often considered a measure of mechanical hyperalgesia (Randall and Selitto, 1957). The test involves application of an increasing mechanical force to the surface of the paw or tail until withdrawal or vocalisation occurs. Finally, the rota-rod apparatus was used to assess any centrally mediated effects of injected NPs in normal rats. The rota-rod test is sensitive to injury of the basal ganglia and cerebellum and to drugs that affect motor function by assessing the animal's sensorimotor coordination. Treated rats must maintain their balance on a rotating rod. Animals experiencing impaired motor coordination are unable to cope with the rotating rod and will drop off when the rotation speed exceeds their motor coordination capacity. The test measures the time (latency) it takes for the rat to fall off a rod rotating at different speeds or under continuous acceleration. Together this chapter aims to assess the anti-inflammatory and analgesic potential of the endocannabinoid-based NP *in-vivo* and investigate NP influence of endogenous endocannabinoids present at the joint.

5.2 METHODS

5.2.1 Generation of NP's

The NP's used in this chapter were prepared as previously described in Section 2.2.2.

5.2.2 Animals

Female Wistar rats (240 – 250 g, 8 to 9 weeks old) were purchased from Animal Resources Centre (Perth, WA, Australia). Experiments were performed at Westmead Housing Facility in accordance with the Western Sydney Local Health District Animal Ethics guidelines (Ethics Approval Number: 5105.08.12), as previously described in Section 3.2.8.

5.2.2.1 AIA model

Arthritis was induced by single subcutaneous injection of lyophilised MTB suspended in 100 µL of squalene at the base of the tail as previously described in Section 3.2.8.1.

5.2.3 NP Treatment of AIA Rats

To investigate NP effects on circulating inflammatory cytokines in arthritic rats, $NP_{non\text{-}targeted}$ and NP_{HAP} were i.v.i administered and the plasma concentration of circulating cytokines evaluated using an LEGENDplex™ Rat Th Cytokine Panel (13-plex), immune-bead based assay (Biolegend, Australian Biosearch, WA, Australia). Arthritic rats were divided into three groups of five each and treated as follows; (a) untreated control (ART-CON); (b) $NP_{non\text{-}targeted}$ (ART-$NP_{non\text{-}targeted}$) and; (c) NP_{HAP} (ART-NP_{HAP}). NP's (24 mg/kg) were administered i.v.i once a day, for two days, for a total of two injections. The control group received 500 µL injections of normal saline. Blood was collected by the lateral tail vein 24 h after each injection. Collected blood was centrifuge for 10 mins at 1,000 x *g* and the plasma separated, snap frozen in liquid nitrogen and stored -80°C prior to analysis. The protocol for cytokine measurement is summarised in Figure 5.1.

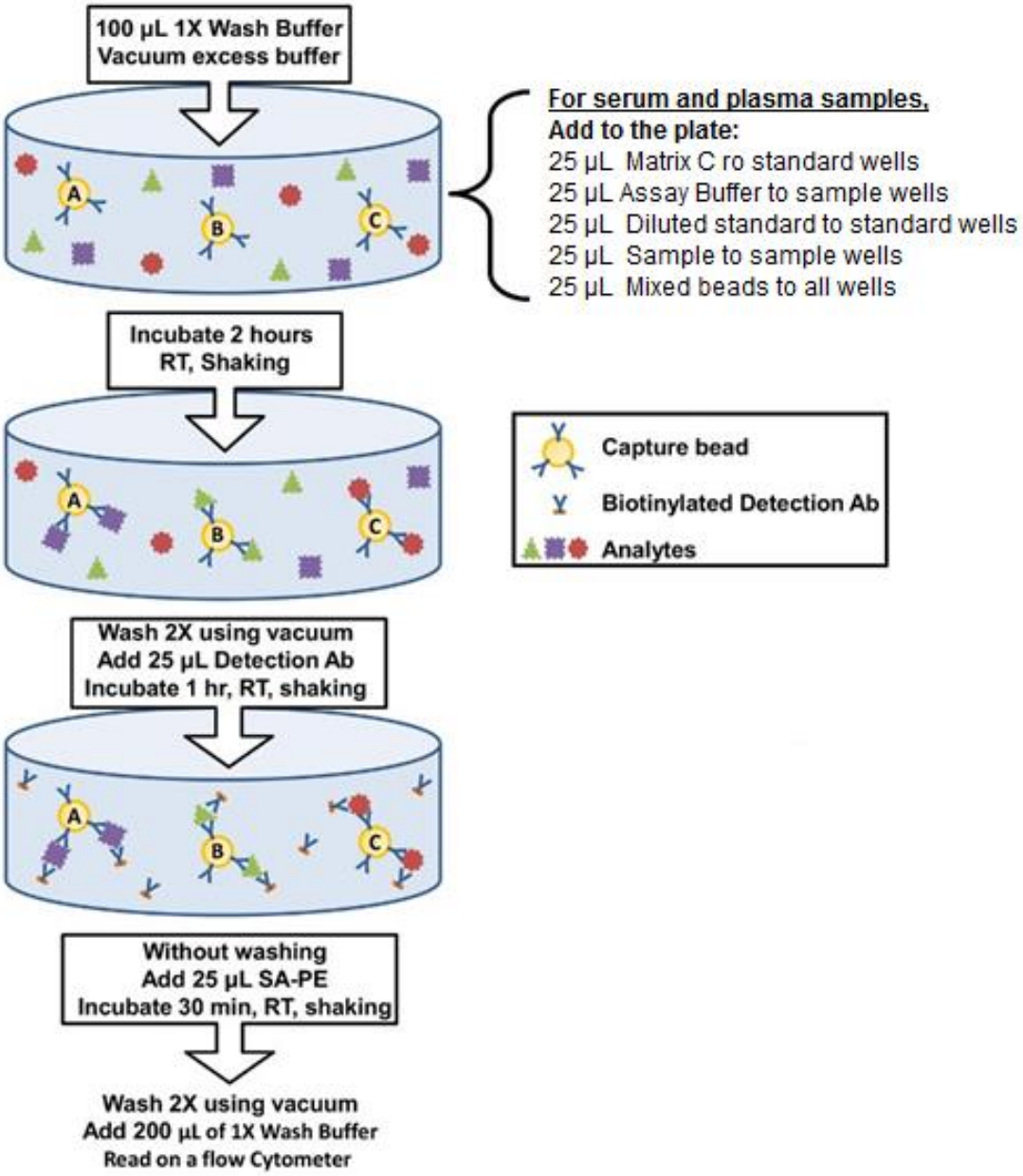

Figure 5.1. Summary of immune-bead based assay procedure for the detection of rat cytokines, using a V-bottom plate. Abbreviations; Antibodies (Ab); Streptavidin, R-Phycoerythrin Conjugate (SA-PE)

5.2.3.1 Quantification of circulating cytokines

Plasma cytokines were quantified using a LEGENDplex™ Rat Th Cytokine Panel, immune-bead based assay, detecting IL-10, IFN-ɣ, CXCL1/KC, CCL2/MCP, TNF-α, GM-CSF, IL-18, IL-12p70, IL-1β, IL-17A, IL-33, and IL-1α. Analysis was performed using BD FACS Cantroll analytic flow cytometer (BD Bioscience, San Jose, California, USA) according to the manufacturer's instructions for analysis in plasma samples. Flow cytometry voltages and gating set-ups are summarised in Figure 5.2. Reporter channel, phycoerythryn (PE), had emission 575-585 nm. Classification channel, allophycocyanin, had emission 660 nm. Standards and each sample were analysed in duplicate and the final concentration obtained from an average of values observed in 3 to 6 samples for each time point and condition. Data analysis was performed using LEGENDplex™ software, version 7.1 and presented as concentrations (pg/mL).

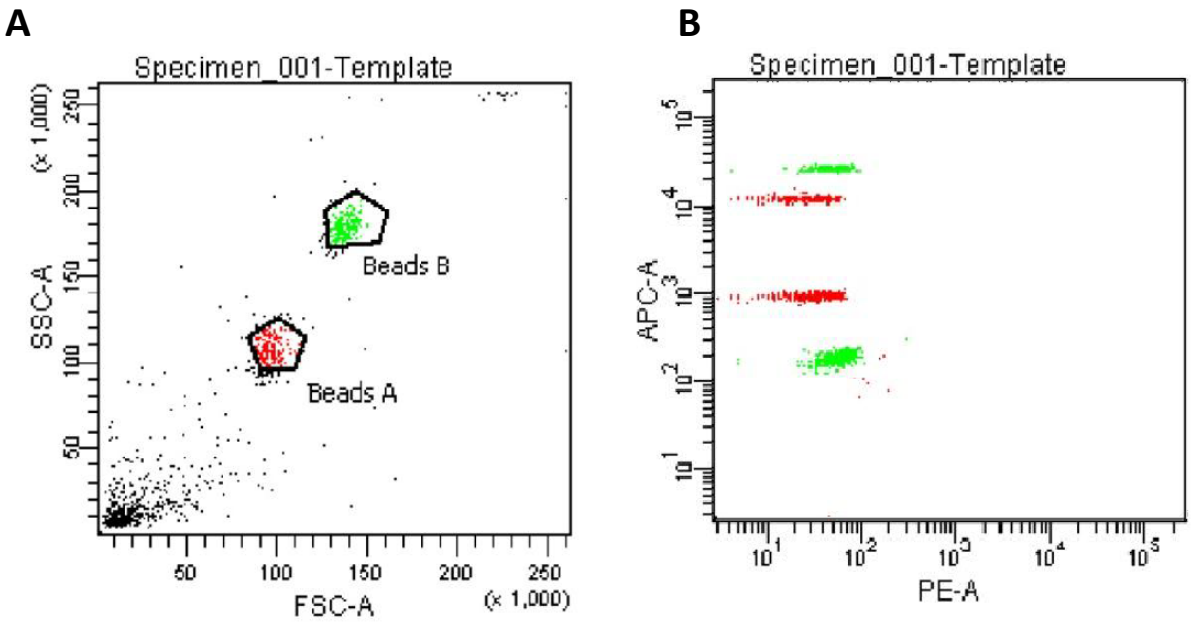

Figure 5.2. Flow cytometry setting for voltages and gating. Beads A (red) and beads B (green) were distinguished with using adjusted; **(A)** FSC (forward scatter) and SSC (side-scatter) reading of >50 (x1000); **(B)** PE signals were adjusted so the majority of the bead collections were between $1x10^1$ and $1x10^2$ on PE-A scale. Allophycocyanin signals were adjusted so the majority of the beads were between $1x10^2$ and $5\ x10^4$ on APC-A scale.

5.2.4 Quantification of endogenous endocannabinoids

To assess the NP influence on endogenous endocannabinoids in injected rats, rats were treated as previously described in Section 3.2.10. Endogenous endocannabinoids; OEA, LEA, PEA, AEA and 2-AG were quantified by HPLC/MS/MS as previously described in Section 3.2.10.1.

5.2.5 Evaluation of pain

To evaluate the analgesic effect of NP *in-vivo*, normal and arthritic rats were treated with NP and the nociceptive pressure threshold assessed using analgesy-meter (Model 37215, Ugo-Basile, VA, Italy). Rats were divided into four groups of five each and treated as follows; (a) untreated control (control); (b) Positive control, 0.05 mg/kg Temsgesic (buprenorphine, 324 µg/mL); (c) $NP_{non\text{-}targeted}$ treated; (d) NP_{HAP} treated. Treated rats received exact doses of 6 mg/kg, 12 mg/kg, 24 mg/kg and 36 mg/kg of NP, administered i.v.i once daily. Untreated control rats, received 500 µL of PBS solution. For evaluation of analgesia in arthritic rats, arthritis was induced as previously stated in Section 3.2.8.1. Arthritic rats were then divided into four groups of five rats each and treated as above. NP treated groups received an exact dose of the highest injected dose (36 mg/kg) administered i.v.i once a day, for two consecutive days, for a total of two injections. Untreated control rats, received 500 µL of PBS solution. Known analgesic Temsgesic (0.05 mg/kg) was administered as a positive control. Measurement of the nociceptive threshold in both normal and arthritic rat groups were carried out 1 h, 2 h and 4 h post NP treatment using an analgesy-meter.

5.2.5.1 Analgesy-meter (Randall–Selitto test)

Quantification of the nociceptive pressure thresholds in rat hindpaws were performed using an analgesy-meter (Model 37215, Ugo-Basile, VA, Italy). The test consisted of applying a linearly-increasing mechanical force (constant rate of 12.5 mmHg/s) to the middle portion of the rat's hindpaw (Chipkin et al., 1983) with a dome-tipped plinth, 0.7 mm in radius and curvature of 36°. Schematic diagram illustrating analgesy-meter set up is shown in Figure 5.3. The site at which the force was applied was marked prior to testing to ensure all recordings were taken from the same site. The nociceptive response was taken to be the final force upon which the hindpaw is withdrawn from the instrument. During a single testing session, the force was applied three times at intervals of 1 min between measurements. For every session, the data for each animal were calculated as a mean of all three measurements and as a value of the last measurement only. Training consisted of one session per day for the assigned number of days (Anseloni et al., 2003).

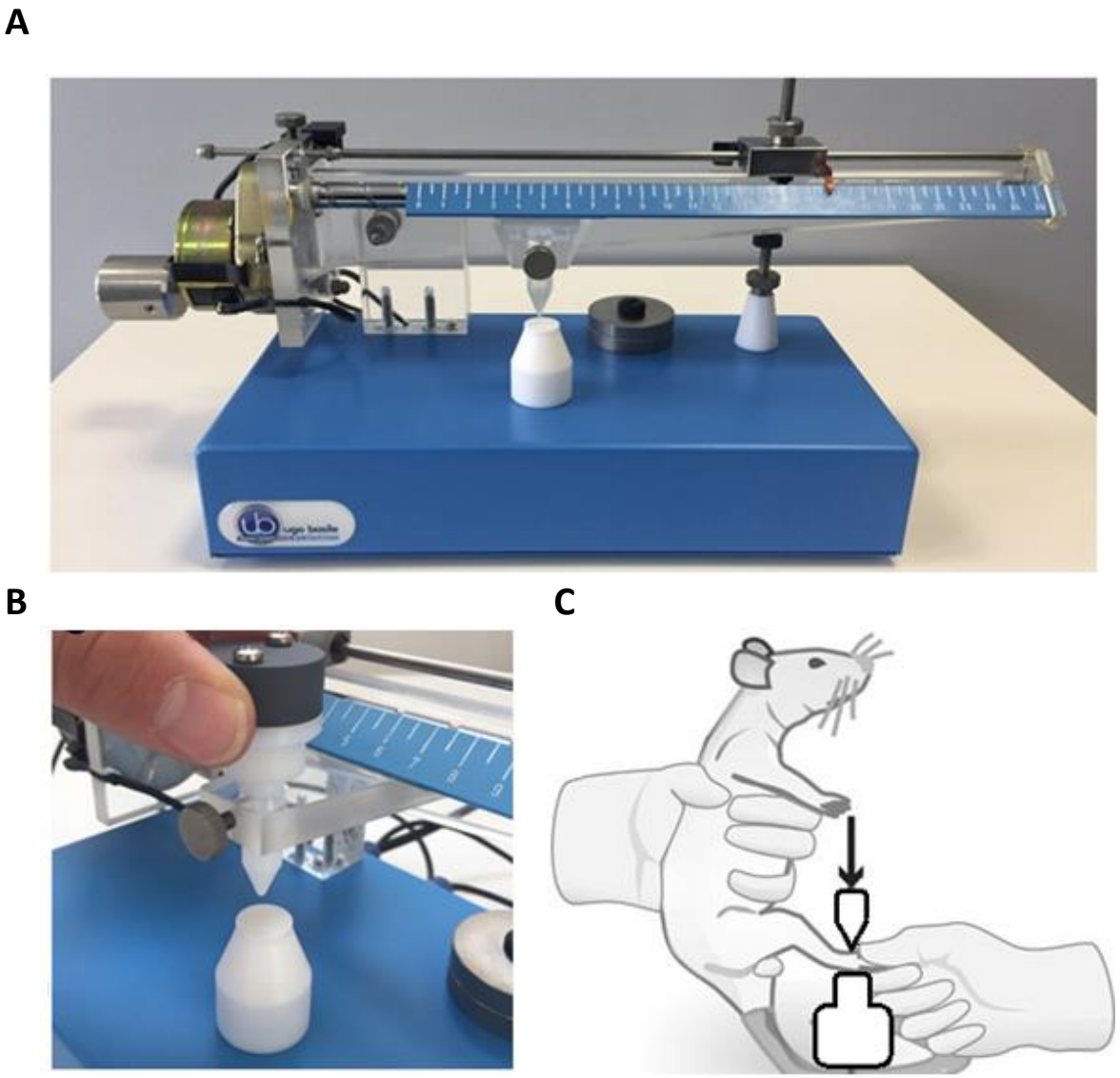

Figure 5.3. Schematic diagram illustrating analgesy-meter set up. **(A)** Ugo-Basile analgesy-meter; **(B)** dome-tipped plinth; **(C)** schematic representation of rat hind paw placed between plinth.

Percentage increase in nociceptive threshold relative to the control group was estimated for each treatment group. Comparison of the nociceptive pressure thresholds throughout training were conducted with a repeated measures one-way ANOVA followed by uncorrected Fisher's LSD test. Evaluation of the effects of different treatments were performed with Dunnett's multiple comparisons test conducted after two-way ANOVA. Percentage increases in nociceptive threshold responses for both inflamed and intact paws were calculated relative to their respective control readings.

5.2.5.2 Basal nociceptive thresholds during training

Baseline nociceptive pressure readings were analysed during training sessions prior the commencement of any treatment. Figure 5.4 shows the effect of training on baseline nociceptive pressure threshold of the right rat hindpaw. It was found that threshold values taken on the second day of treatment were 13% higher than that of the first day. This increase was apparent, independent of whether the analysis was based on the average of all three measurements made during each daily training, or using the value of the last measurement in the day's session. Following the initial increase, threshold values plateaued and remained stable for the remaining 2 days of training.

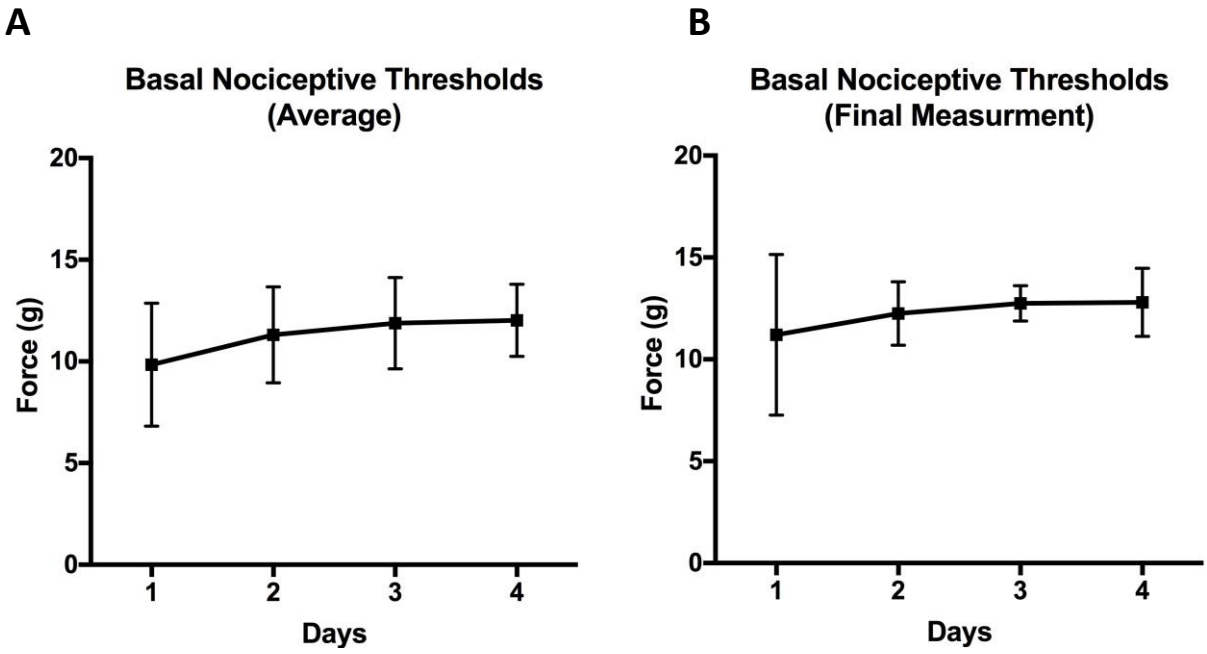

Figure 5.4. Effect of training on baseline nociceptive pressure threshold of the right rat hindpaw **(A)** Data represents averages of three measurements within a daily session; **(B)** data represents the last measurement of each session. Each point represents mean ± S.E.M, n=5. No significant differences were detected between the values obtained between second and fourth days of training.

5.2.5.3 Assessment of positive analgesia (testing experimental set-up)

Positive and negative nociceptive pressure threshold readings were analysed prior to testing agents to validate experimental design/ as an indication of positive results. 0.05 mg/kg of known analgesic drug, Temsgesic was administered for positive control, and PBS was administered for negative control. Figure 5.5 shows the effect of Temsgesic and PBS on baseline nociceptive pressure threshold of the right rat hindpaw 1 h after injection. Rats injected with the Temsgesic showed strong analgesic responses with significant improvement in nociceptive pressure readings (21.60 ± 6.37, $p < 0.05$, $p = 0.0028$) when compared to baseline (11.28 ± 1.53). By contrast, rats injected with PBS showed no improvement in nociceptive pressure readings (10.65 ± 3.62), being consistent to baseline levels (11.5 ± 2.79). The improvement in nociceptive pressure readings demonstrates the ability of the force/pressure units to reflect analgesic potential in the administered testing agents.

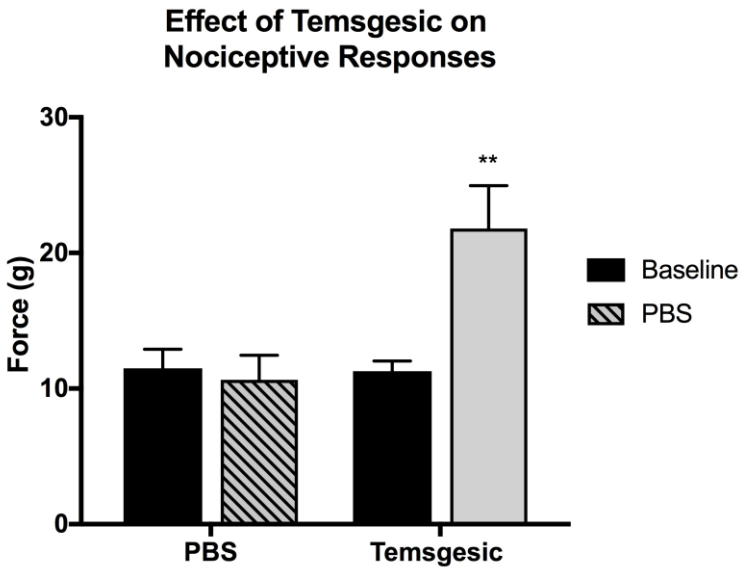

Figure 5.5. Effect of Temsgesic and PBS on baseline nociceptive pressure threshold of the right rat hindpaw 30 min after injection. Data expressed as the mean ±S.D, n=5. **p < 0.01, Student–Newman–Keuls test conducted after repeated measures ANOVA. No significant differences were detected between baseline and PBS.

5.2.6 Evaluation of NP Centrally Mediated Effects (Rota-rod)

To assess for any central CNS effects of the injected NP, motor coordination tasks were examined using an accelerating rota-rod apparatus (47600 Rota-rod, Ugo Basile, Italy). Normal rats were weighed and divided into three groups of five and treated with (a) 500 µL PBS (control); (b) $NP_{non\text{-}targeted}$; (c) NP_{HAP} once daily, one hour prior to each rota-rod testing. NP treated groups received exact doses of 6 mg/kg, 12 mg/kg and 24 mg/kg, administered i.v.i once daily.

Rat motor coordination tasks were evaluated using the rota-rod which accelerates from 4 to 40 rpm in 300 sec. Rat motor coordination was tested for 3 trials per session on three consecutive days. Prior to testing, animals were subject to two consecutive days of rota-rod training to discriminate motor endurance activity from motor skill learning. Prior to testing, rats were brought into the experimental room 20 min before testing to ensure acclimatisation. Training phase consisted of rats placed on the rota-rod at a constant speed of 4 for 300 sec. During testing phase, rats were to maintain their balance at 4 rpm constant speed for 10 sec. After 10 sec, the rods acceleration was started and the speed at which the rat falls off recorded.

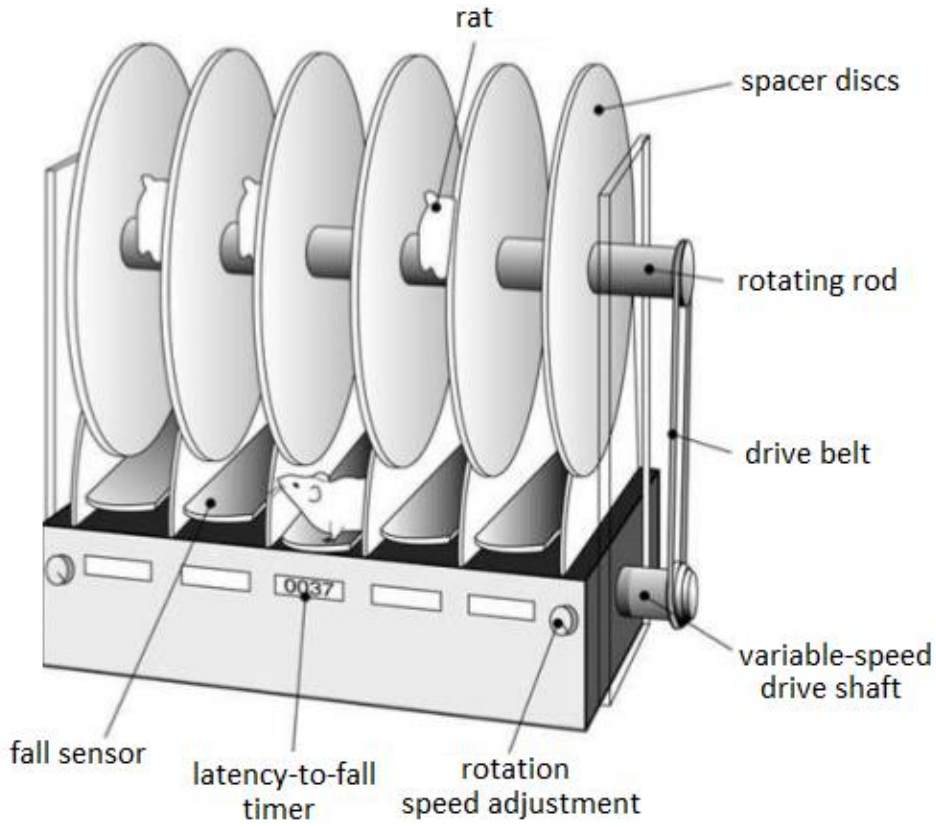

Figure 5.6. Schematic diagram illustrating rota-rod set up (Turner, 2009).

5.2.6.1 Rota-rod performance training

Prior to the injection of testing agents, rats were subject to two consecutive days of training on rota-rod equipment. Figure 5.7 shows the effect of training on the animals latency to fall. Significant improvement in sensorimotor coordination was observed after the first two trials. Following the initial increase, threshold values plateaued and remained stable for the remaining 3 days of training.

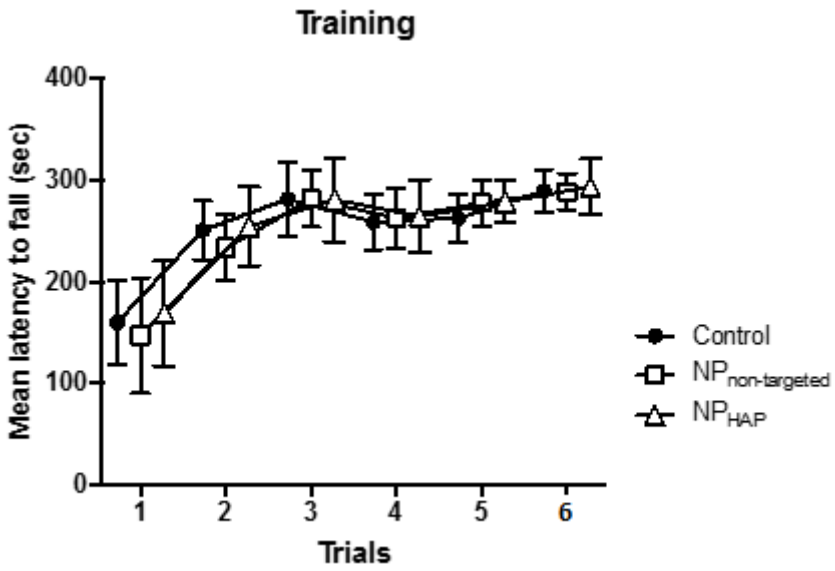

Figure 5.7. The influence of training on rota-rod performance in rats. Training consisted of three training sessions in two consecutive days.

5.3 RESULTS

5.3.1 Serum Plasma Pro-Inflammatory Cytokines in NP Treated Arthritic Rats

Measurement of plasma pro-inflammatory cytokines in treated and non-treated arthritic rats are shown in Figure 5.8 and Figure 5.9. Blood was collected 24 h after each NP injection and the cytokines quantified by flow cytometry. Plasma concentration of inflammatory/immune mediators: IL-10, IFN-ɣ, CXCL1/KC, CCL2/MCP, TNF-α, GM-CSF, IL-18, IL-12p70, IL-1β, IL-17A, IL-33, IL-6 and IL-1α are shown for; day 1 (Figure 5.8) and; day 2 (Figure 5.9). Sample concentrations for each cytokine analyte were calculated using a standard curve shown in Appendix 6.

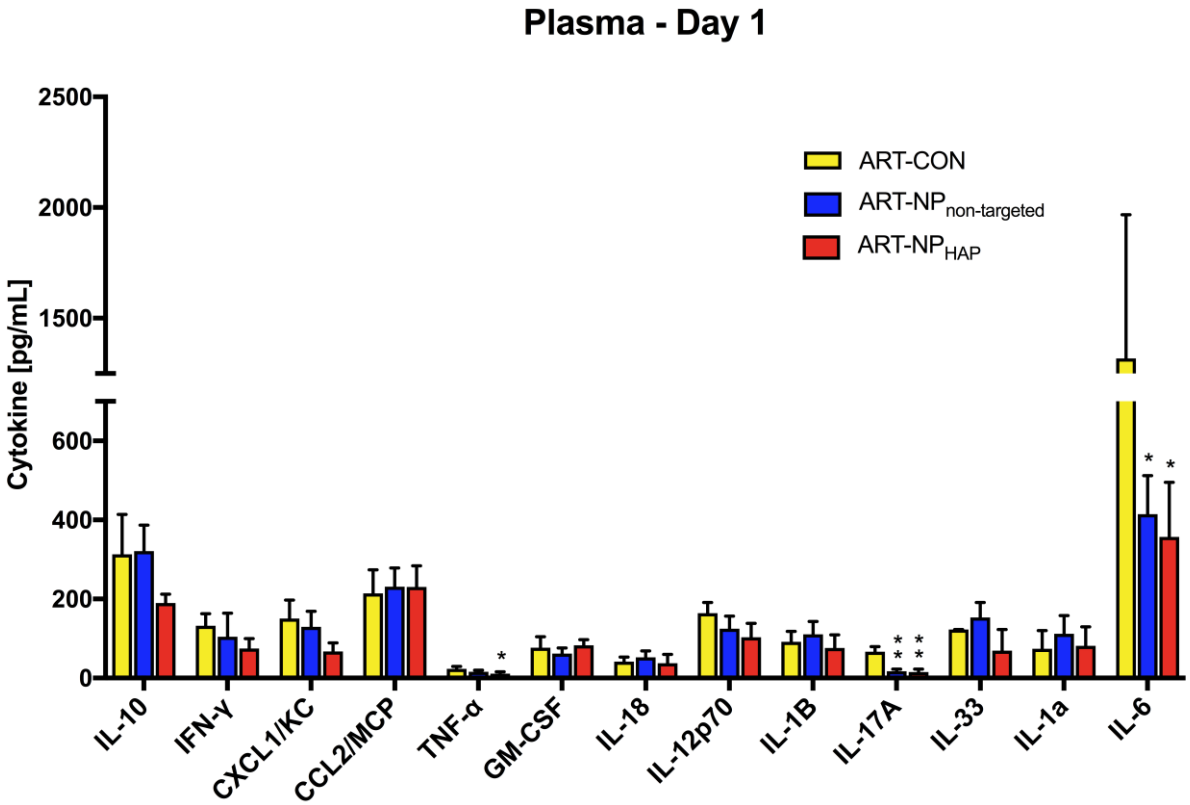

Figure 5.8. Plasma cytokine concentrations in untreated (ART-CON), $NP_{non\text{-}targeted}$ (ART-$NP_{non\text{-}targeted}$) and NP_{HAP} (ART-NP_{HAP}) treated arthritic rats. NP treated groups suppressed IL-17A, IL-6 on day 1. Data expressed as the mean ±S.D, n=5. Analysis was performed using multiple t-tests, using the Bonferroni-Dunn method with alpha = 0.05, without assuming a consistent SD. *p < 0.05, **p < 0.01 vs ART-CON. Abbreviations: Interleukin (IL-[10, 18, 12p70, 1B, 17A, 33, 1a, 6]); Interferon gamma (IFN-ɣ); Chemokine (C-X-C motif) ligand 1 (CXCL1/KC); Monocyte chemoattractant protein-1 (CCL2/MCP); Tumor necrosis factor alpha (TNF-α); Granulocyte-macrophage colony-stimulating factor (GM-CSF).

As shown in Figure 5.8, high serum concentrations of pro-inflammatory cytokines were observed in ART-CON and are a likely consequence of general inflammation. Cytokine concentrations remained relatively consistent over the two day collection period, with no significant changes noted between the ART-CON's day 1 and day 2 cytokine profile. On day 1, NP treated rats suppressed circulating cytokine levels of both IL-6 and IL-17A. IL-6 levels were significantly reduced for both $NP_{non\text{-}targeted}$ (414.86 ± 168.68 pg/ml, p = 0.03) and NP_{HAP} (357.28 ± 217.42 pg/ml, p = 0.03) groups by 68.4% and 72.8%, when compared to ART-CON (1314.20 ± 868.849 pg/mL), respectively. Levels of cytokine IL-17A were also significantly reduced in both $NP_{non\text{-}targeted}$ (17.05 ± 10.63 pg/mL, p = 0.003) and NP_{HAP} (14.98 ± 11.83 pg/mL, p = 0.005) groups by 73.4% and 77.5% when compared to ART-CON (66.56 ± 29.73 pg/mL), respectively. In both instances, no notable difference was observed between the $NP_{non\text{-}targeted}$ and NP_{HAP} groups, suggesting similar effects despite the presence of a homing peptide. No significant changes were observed for all other cytokines tested, with comparable levels measured for both the NP treated groups and the ART-CON.

A more pronounced and broad spread suppression of circulating inflammatory cytokines were observed on day 2. As shown in Figure 5.9, NP treated rats had lower circulating pro-inflammatory cytokines when compared to ART-CON. $NP_{non\text{-}targeted}$ treatment suppressed pro-inflammatory cytokines IL-6 by 73.3% (389.86 ± 416.84 pg/mL vs ART-CON 1457.95 ± 918.86 pg/mL, p = 0.03), TNF-α by 42% (17.95 ± 3.74 pg/mL vs ART-CON 30.95 ± 6.32 pg/mL, p = 0.002), IL-17A by 70.6% (20.01 ± 12.07 pg/mL vs ART-CON 68.09 ± 26.44 pg/mL, p = 0.05), and IFN-ɣ by 61.3% (49.52 ±5 34.99 pg/mL vs ART-CON 127.91 ± 67.29 pg/mL, p = 0.03).

Similar cytokine levels were observed for NP_{HAP} treated rats. In ART-NP_{HAP}, IL-6 was suppressed by 83.9% (234.45 ± 58.95 pg/mL vs ART-CON 1457.95 ± 918.86 pg/mL, p = 0.01), TNF-α by 47.4% (16.28 ± 6.57 pg/mL vs ART-CON 30.95 ± 6.32 pg/mL, p = 0.003), IL-17A by 53.8% (31.49 ± 16.89 pg/mL vs ART-CON 68.09 ± 26.44 pg/mL, p = 0.02) and IFN-ɣ by 85.3% (18.86 ± 6.74 pg/mL vs ART-CON 127.91 ± 67.29, p = 0.003) pg/mL. The suppression of IFN-ɣ was significantly more pronounced in ART-NP_{HAP}, when compared to ART-$NP_{non\text{-}targeted}$ and may be attributed to greater localised effect through ligand-mediated targeting facilitated by the HAP-1 receptor. In contrast, NP_{HAP} treated rats increased circulating concentrations of MCP/CCL2 (403.26 ± 42.52 pg/mL vs ART-CON 184.69 ± 66.67 pg/mL, p = 0.006), which was not statistically significant in ART-$NP_{non\text{-}targeted}$ treated rats (244.82 ± 48.87 pg/mL). These results are consistent with increased expression of CCL2/MCP in RA-TNF/NP when compare to RA-TNF *in-vitro*. As previously shown, exposure of NP also increased expression of PTGES2 in RA-TNF/NP when compared to RA-TNF *in-vitro*. In a study by Nakayama et al. (2006), it was shown that PGE2 dose-dependently induced MCP-1 in mast cells, identifying the PGE2/MCP-1 as a pathway underlying inflammation-associated angiogenesis. The relationship between NP and MCP-1

stimulation may be due to NP increase of PTGES2, however the mechanism of MCP-1 activation requires further investigation.

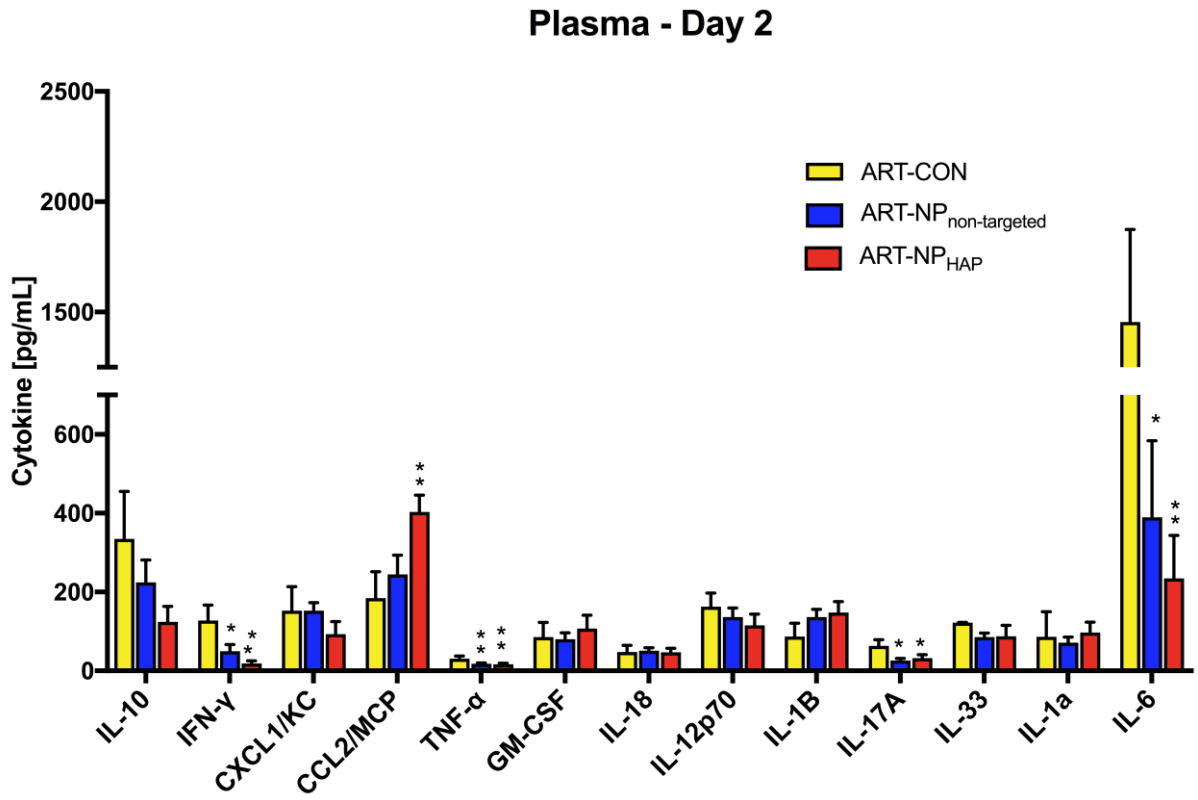

Figure 5.9. Plasma cytokine concentrations in untreated (ART-CON), $NP_{non\text{-}targeted}$ (ART-$NP_{non\text{-}targeted}$) and NP_{HAP} (ART-NP_{HAP}) treated arthritic rats. NP treated groups suppressed IL-17A, IL-6, IFN-ɣ and TNF-α on day 2. NP_{HAP} was more effective in reducing IL-6 and IFN-ɣ when compared to $NP_{non\text{-}targeted}$, but also increased CCL2/MCP expression on day 2. Data is expressed as the mean ±S.D, n = 5. Analysis was performed using multiple t-tests, using the Bonferroni-Dunn method with alpha = 0.05, without assuming a consistent SD. *p < 0.05, **p < 0.01 vs ART-CON.

5.3.2 Influence of NP on Endogenous Endocannabinoid Levels

Arthritic joints from non-treated, $NP_{non\text{-}targeted}$ and NP_{HAP} treated arthritic rats were removed and the articular endocannabinoid levels and their entourage compounds measured. AEA, 2-AG, OEA, and PEA were detected and quantified in all samples analysed. Figure 5.10 compares the concentration of OEA, LEA, PEA, 2-AG and AEA in $NP_{non\text{-}targeted}$, NP_{HAP} and non-treated arthritic control rats. As shown, arthritic rats injected with NP_{HAP} significantly increased joint concentrations of both OEA (8.26 ± 3.79 pmol/g, P = 0.03) and LEA (3.51 ± 1.62 pmol/g, p = 0.02), when compared to ART CON. Similarly, increased concentrations of OEA (6.06 ± 2.27 pmol/g, p = 0.09) and LEA (2.25 ± 0.90 pmol/g, p = 0.13) were

observed in $NP_{non\text{-}targeted}$, however failed to reach statistical significance. Assessment of endogenous PEA levels were shown to be elevated for both NP_{HAP} (12.26 ± 10.27 pmol/g, p = 0.04) and $NP_{non\text{-}targeted}$ (9.13 ± 6.85 pmol/g, p = 0.04), when compared to ART CON (1.09 ± 0.12 pmol/g). Levels of AEA were slightly increased in both NP_{HAP} (0.78 ± 0.65 pmol/g, p = 0.18) and $NP_{non\text{-}targeted}$ (0.64 ± 0.48 pmol/g, p = 0.07) treated rats when compared to ART CON (0.07 ± 0.01 pmol/g), however these levels were not significant. In contrast to PEA, endogenous levels of 2-AG remained relatively unaffected in both NP_{HAP} (38.84 ± 10.86 pmol/g) and $NP_{non\text{-}targeted}$ (41.92 ± 18.91 pmol/g) treated rats when compared to ART CON (41.68 ± 10.32 pmol/g).

Collectively, the data suggests that the NP's endocannabinoid components LEA and OEA, influence endogenous endocannabinoid levels. Significant concentrations of OEA and LEA in NP_{HAP} treated group were correlated with significant increases in PEA. While similar trends were observed for $NP_{non\text{-}targeted}$ treated rats, non-significant increases in OEA and LEA translated to non-significant elevations in endogenous PEA levels. The variation in regulation may be due to the presence of homing-peptide HAP-1, which facilitated greater accumulation of NP and therefore higher concentrations of OEA and LEA to the joint through ligand mediated targeting.

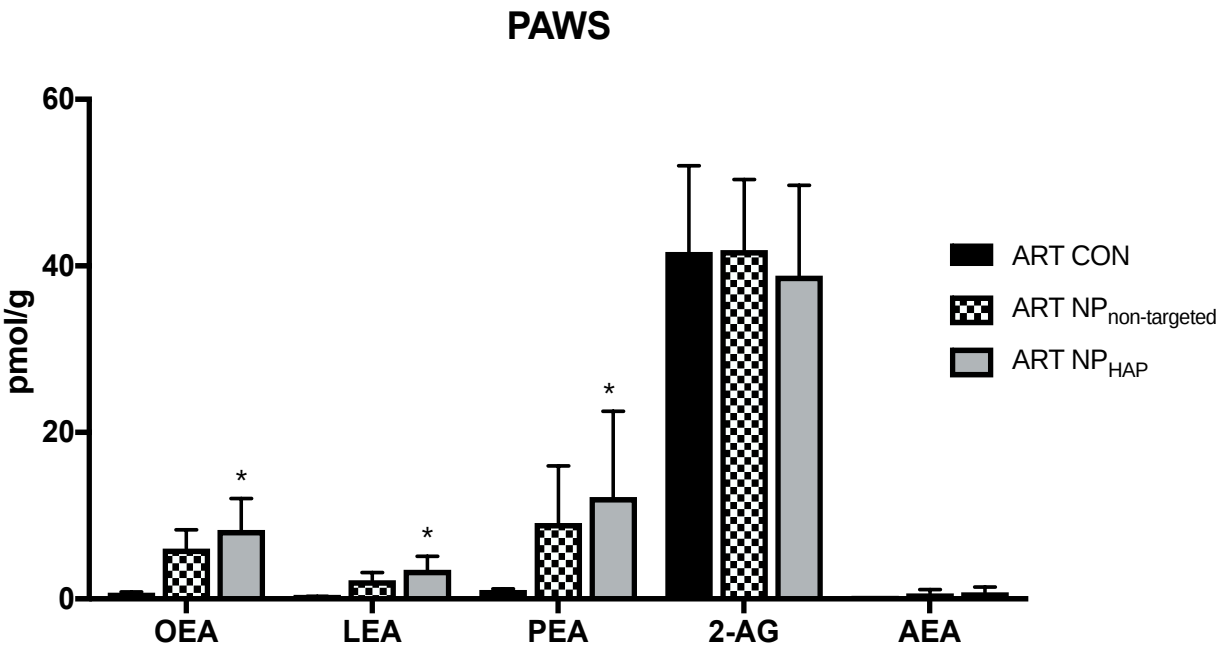

Figure 5.10. Concentration of OEA, LEA, PEA, 2-AG and AEA in the paws of untreated (ART CON), $NP_{non\text{-}targeted}$ (ART $NP_{non\text{-}targeted}$) and NP_{HAP} (ART NP_{HAP}) treated arthritic rats, harvested 6 h post i.v.i of NP. Data expressed as the mean ± S.D, n=5, in picomoles per gram. *p < 0.05 vs ART CON, analysis using one-way ANOVA, followed by uncorrected Fisher's LSD test. Significant concentrations of OEA, LEA and PEA were observed in NP_{HAP} treated arthritic rats.

5.3.3 Assessment of NP Analgesia

5.3.3.1 NP analgesia in normal rats

Normal rats were pre-treated with NP and the anti-nociceptive potential assessed using analgesy-meter. NP treated groups received exact doses of 6 mg/kg, 12 mg/kg, 24 mg/kg and 36 mg/kg, i.v.i daily, respectively. Untreated control rats received 500 µL injections of PBS/PEG solution. Figure 5.11 shows the nociceptive pressure readings of the right hind paw for each rat taken at 1 h, 2 h and 4 h after treatment. As shown, treatment of $NP_{non\text{-}targeted}$ at the starting does of 6 mg/kg (blue line) showed no significant improvement in the nociceptive readings compared to baseline values. Similarly, increasing doses to 12 mg/kg in the same rats did not improve analgesic responses. At higher doses an increase in nociceptive threshold responses was observed at both 24 mg/kg and 36 mg/kg of injected $NP_{non\text{-}targeted}$ (Figure 5.11B). Both doses followed a similar threshold pattern, peaking at 1 h with a sharp fall at 2 h before plateauing. While both 24 mg/kg and 36 mg/kg doses improved analgesic responses, only 36 mg/kg was significant when compare to untreated normal rats.

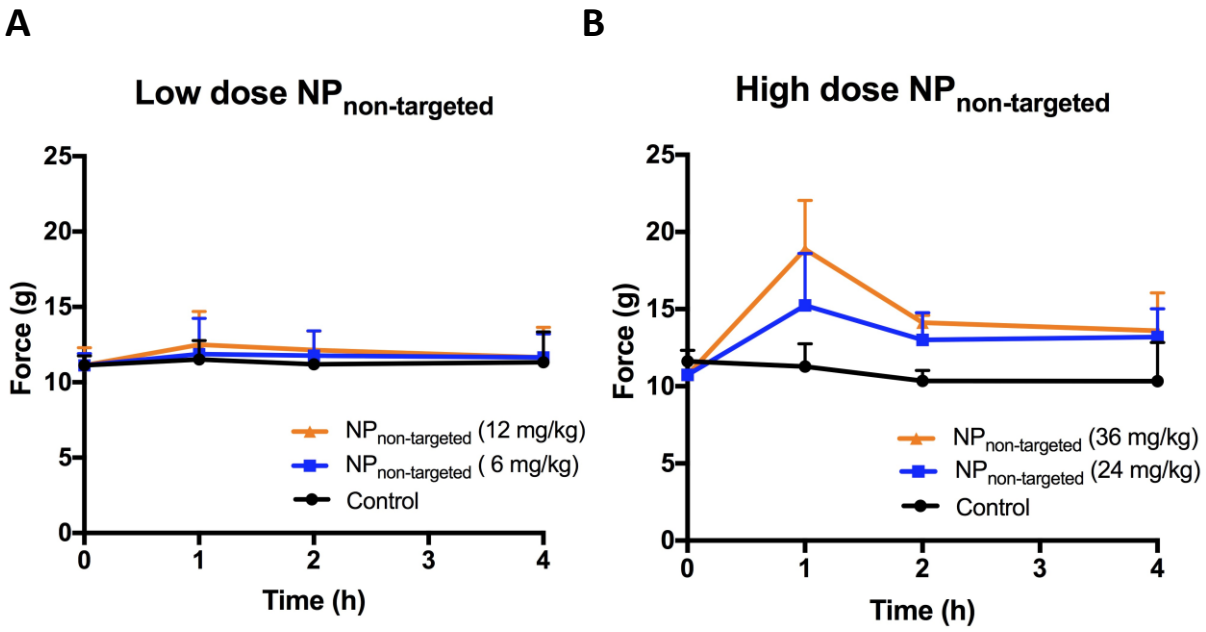

Figure 5.11. Effect of $NP_{non\text{-}targeted}$ on nociceptive pressure thresholds in normal rats. $NP_{non\text{-}targeted}$ were administered at; **(A)** 6 mg/kg, 12 mg/kg and; **(B)** 24 mg/kg and 36 mg/kg and measured 1 h, 2 h and 4 h after injection. Data expressed as the mean ± S.D., n=5. Increases in nociceptive thresholds at 1 h were observed in high dose $NP_{non\text{-}targeted}$ treated normal rats.

Similar to $NP_{non\text{-}targeted}$, no improvements in nociceptive readings were observed with NP_{HAP} treated rats at 6 mg/kg, as shown in Figure 5.12A. Increasing the injected dose to 12 mg/kg slightly improved pressure threshold readings after 1 h, however, it was not significant. At higher doses (Figure 5.12B), a significant increase in nociceptive pressure readings were observed after 2 h at both 24 mg/kg and 36 mg/kg injected NP_{HAP} concentrations. In NP_{HAP} treated groups, threshold readings peaked later at 2 h, with a slow returned to baseline around 4 h.

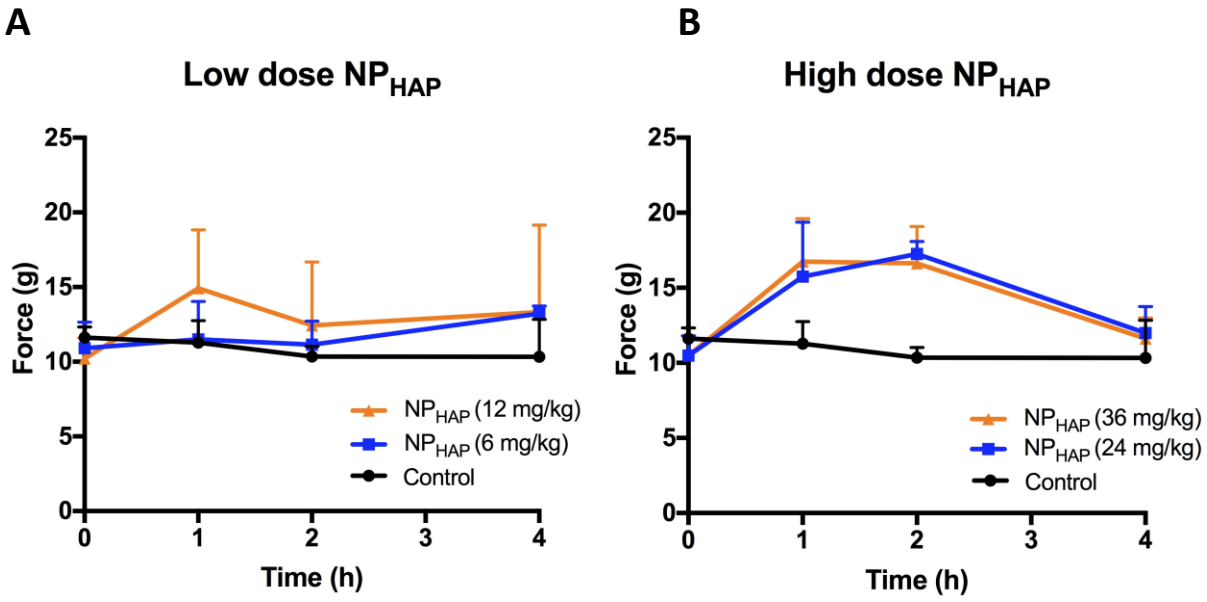

Figure 5.12. Effect of NP_{HAP} on nociceptive pressure thresholds in normal rats. NP_{HAP} were administered at **(A)** 6 mg/kg, 12 mg/kg and; **(B)** 24 mg/kg and 36 mg/kg and measured 1 h, 2 h and 4 h after injection. Data expressed as the mean ± S.D, n=5. Increases in nociceptive thresholds at 2 h were observed in high dose NP_{HAP} treated normal rats.

Comparison of the thresholds of responses in non-treated, $NP_{non\text{-}targeted}$ and NP_{HAP} treated normal rats is shown in Figure 5.13. At low doses, threshold responses were comparable between all groups with no significant difference observed between treatment and control. At 24 mg/kg, only NP_{HAP} produced an analgesic response which was significant at 2 h time point (16.63 ± 4.92). At 36 mg/kg, both the $NP_{non\text{-}targeted}$ and the NP_{HAP} treated normal rats had a significant improvement in nociceptive threshold responses, at 1 h for the $NP_{non\text{-}targeted}$ (18.88 ± 6.36) and 2 h for the NP_{HAP} (17.25 ± 1.67) These data are consistent with the nociceptive threshold trend patterns observed above and correlate with the reduced half-life of $NP_{non\text{-}targeted}$ when compared to NP_{HAP}. As positive nociceptive threshold responses were observed at 36 mg/kg for both NP groups, this concentration was used in future analgesic experiments in arthritic rats.

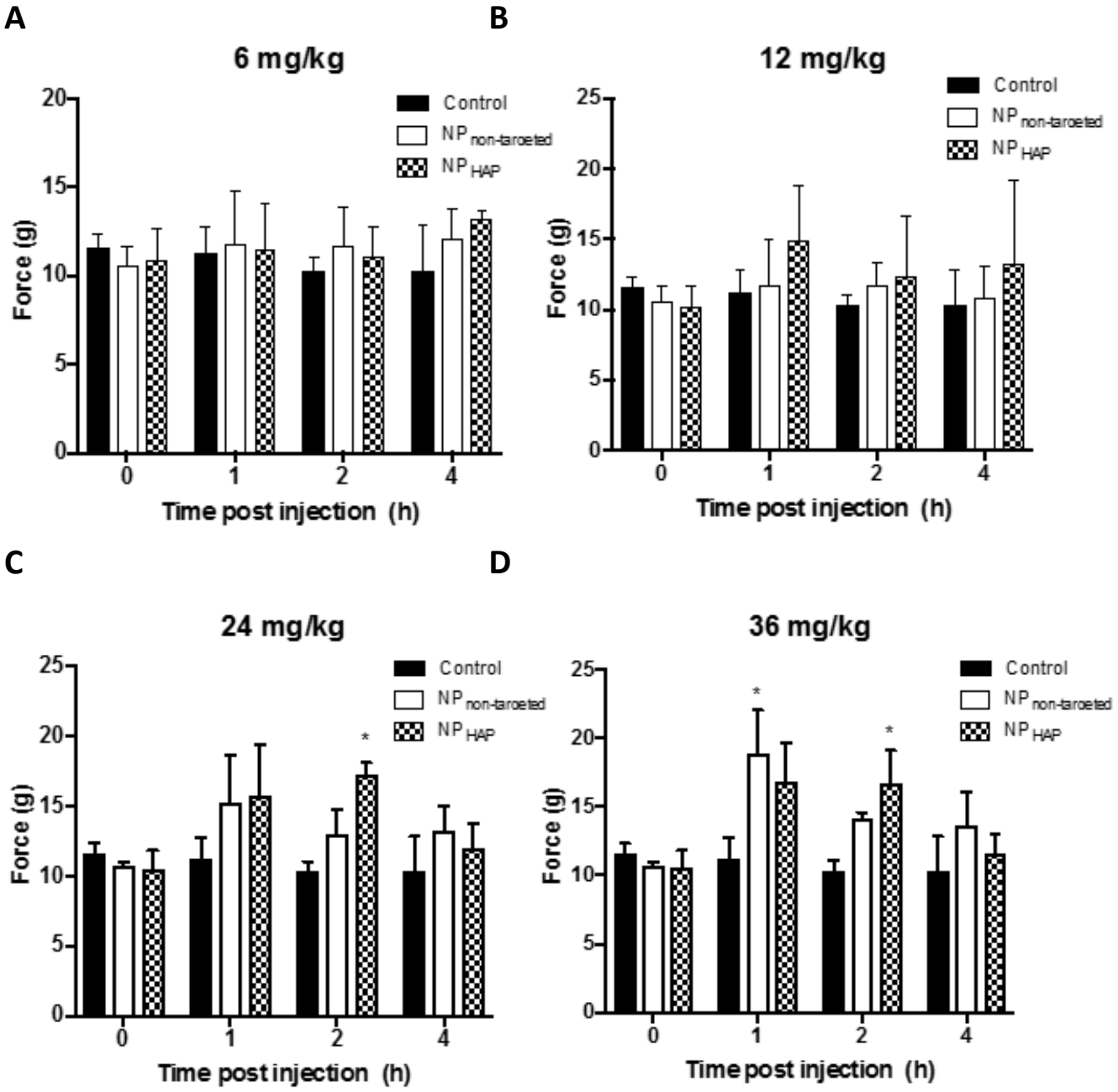

Figure 5.13. Effect of $NP_{non\text{-}targeted}$ and NP_{HAP} on baseline nociceptive pressure thresholds in normal rats. NP's were administered once daily at a concentration of **(A)** 6 mg/kg; **(B)** 12 mg/kg; **(C)** 24 mg/kg and; **(D)** 36 mg/kg and measured 1 h, 2 h and 4 after injection. Data expressed as the mean ± SEM, n=5. *$p < 0.05$ vs Control, analysis by two-way ANOVA, followed by Dunnett's multiple comparisons test. Statistically significant increase in nociceptive pressure thresholds were observed at 36 mg/kg for both $NP_{non\text{-}targeted}$ and $NP_{HAP.}$

5.3.3.2 NP analgesia in arthritic rats

To evaluate for any anti-nociceptive effects in arthritic rats, arthritic rats were treated with $NP_{non\text{-}targeted}$ and NP_{HAP} (36 mg/kg) i.v.i once daily, for two consecutive days and the nociceptive pressure thresholds recorded 1 h, 2 h and 4 h after treatment. Nociceptive effects were calculated as the percentage change from control baseline values. Figure 5.14 shows the percentage changes in nociceptive threshold responses relative to baseline after day 1 (A) and; day 2 (B). As shown in Figure 5.14A, $NP_{non\text{-}targeted}$ and NP_{HAP} treated arthritic rats showed slight improvement in nociceptive responses after 1 h, increasing thresholds responses by 27.41% and 43.71% respectively from baseline values. At 2 h, these anti-nociceptive effects were lessened, with only a 12.4% and 29.1% improvement from baseline in $NP_{non\text{-}targeted}$ and NP_{HAP} treated groups respectively. At 4 h, no improvement in nociceptive pressure threshold were observed with readings comparable to baseline untreated controls, with a close to 0 percentage change for both $NP_{non\text{-}targeted}$ (1.18%) and NP_{HAP} (-3.7%).

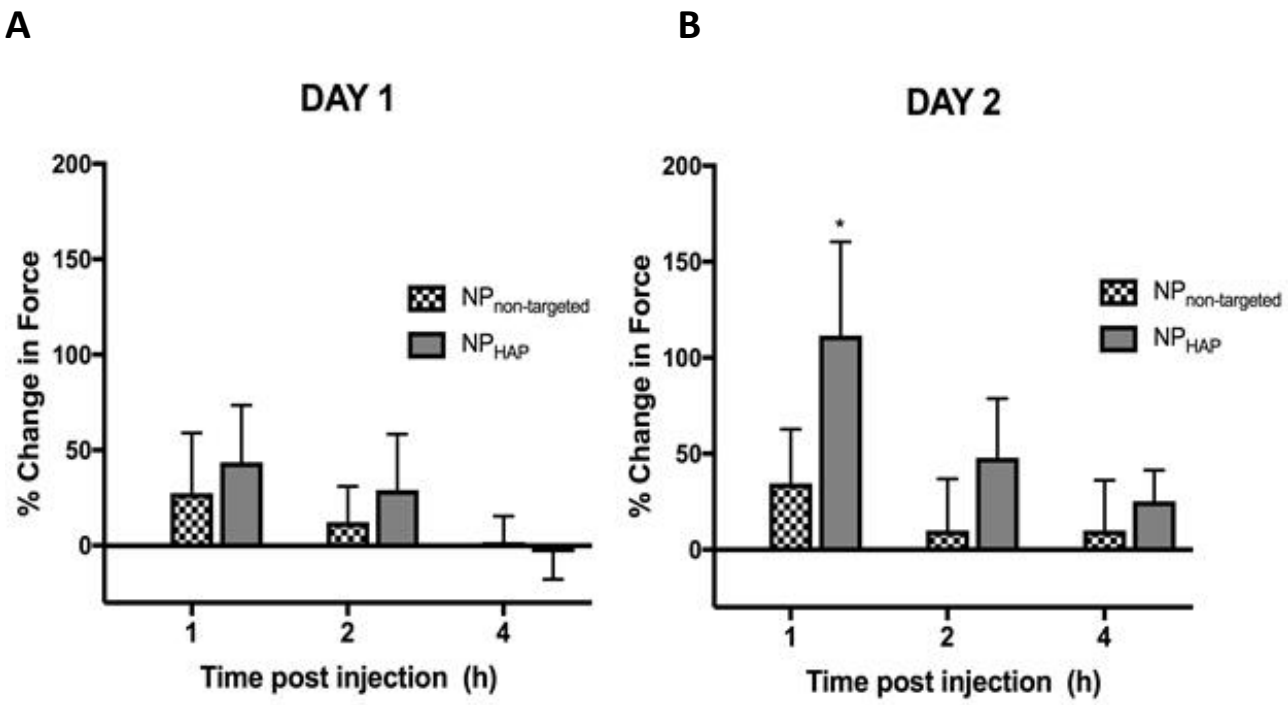

Figure 5.14. Effect of $NP_{non\text{-}targeted}$ and NP_{HAP} on nociceptive pressure thresholds in arthritic rats. Day 1 shown in; **(A)** and; day 2 **(B)**. Pressure readings were recorded 1 h, 2 h and 4 h after treatment. Data is represented as the percentage change in nociceptive pressure thresholds from baseline values, as measured in force (g). Data expressed as the mean ± SEM, n=5. *$p < 0.05$ vs control, two-way ANOVA, followed by Dunnett's multiple comparisons test. Analgesic effects were observed in NP_{HAP} treated rats after 1 h on day 2.

On the second day (Figure 5.14B) the percentage change in nociceptive thresholds were higher than that observed in day 1 (Figure 5.14A). After 1 h, rats treated with $NP_{non\text{-}targeted}$ showed a 34.6% improvement in nociceptive pressure thresholds, when compared to baseline values. By contrast, rats treated with NP_{HAP} showed a 111.6% improvement in nociceptive threshold response, which was significant compared to baseline values. At 2 h improvements in nociceptive effects were lessened, with drops in the percentage change to 10.1% in $NP_{non\text{-}targeted}$ and 47.9% in NP_{HAP} treated groups. At 4 h, only slight increases in nociceptive thresholds by 9.9% in $NP_{non\text{-}targeted}$ and 25.3 % in NP_{HAP} treated groups, suggesting lower analgesic effects at this time point and a return to baseline values.

Comparison of positive NP responses to known analgesic, Temsgesic, was also compared. Figure 5.15A shows the effect of Temsgesic and PBS on baseline nociceptive pressure threshold of the right rat hindpaw 1 h after injection. Figure 5.15B shows the percentage change in nociceptive pressure thresholds in NP, PBS and Temsgesic treated rats.

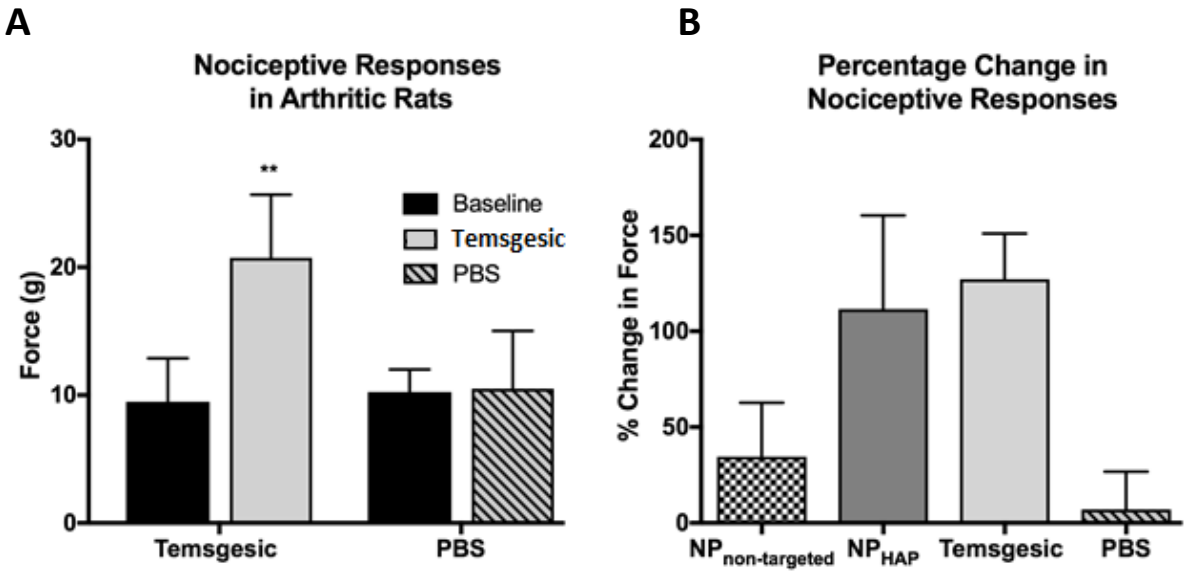

Figure 5.15. (A) Effect of Temsgesic and PBS on baseline nociceptive pressure threshold of the right rat hindpaw 1 h after injection; **(B)** Percentage change in nociceptive pressure threshold responses in $NP_{non\text{-}targeted}$, NP_{HAP}, Temsgesic and PBS treated arthrtitic rats. 1 h after injection, represented as a percentage change in force. Data expressed as the mean ± SEM, n=5. *p < 0.05, **p < 0.01 vs baseline, two-way ANOVA, followed by Dunnett's multiple comparisons test.

Arthritic rats injected with Temsgesic demonstrated strong analgesic responses with significant improvement in nociceptive pressure readings (20.75 ± 4.92, **p < 0.01, p = 0.0028) when compared to baseline (9.48 ± 3.41). By contrast, rats injected with PBS showed no improvement in nociceptive pressure readings (10.25 ± 1.78, p = 0.9949), which were comparable to baseline levels (10.5 ± 4.53). Comparison of percentage changes in nociceptive responses in Temsgesic and day 2 NP_{HAP} show similar analgesic effects after 1 h (Figure 5.15B)

5.3.4 Rota-Rod Testing for Any Centrally Mediated NP Effects

To assess the potential of centrally mediated effects of injected NPs in normal rats, NP were administered i.v.i to rats and their sensorimotor coordination evaluated using the rota-rod, shown in Figure 5.16. It was found $NP_{non\text{-}targeted}$ injected rats did not impair the animal's sensorimotor coordination at the doses given compared to respective controls. Similarly, no significant change in sensorimotor coordination was observed in NP_{HAP} injected rats, when compared to non-treated control rats. Although there was a drop in mean latency noted 1 h post injection, these values failed to reach statistical significance.

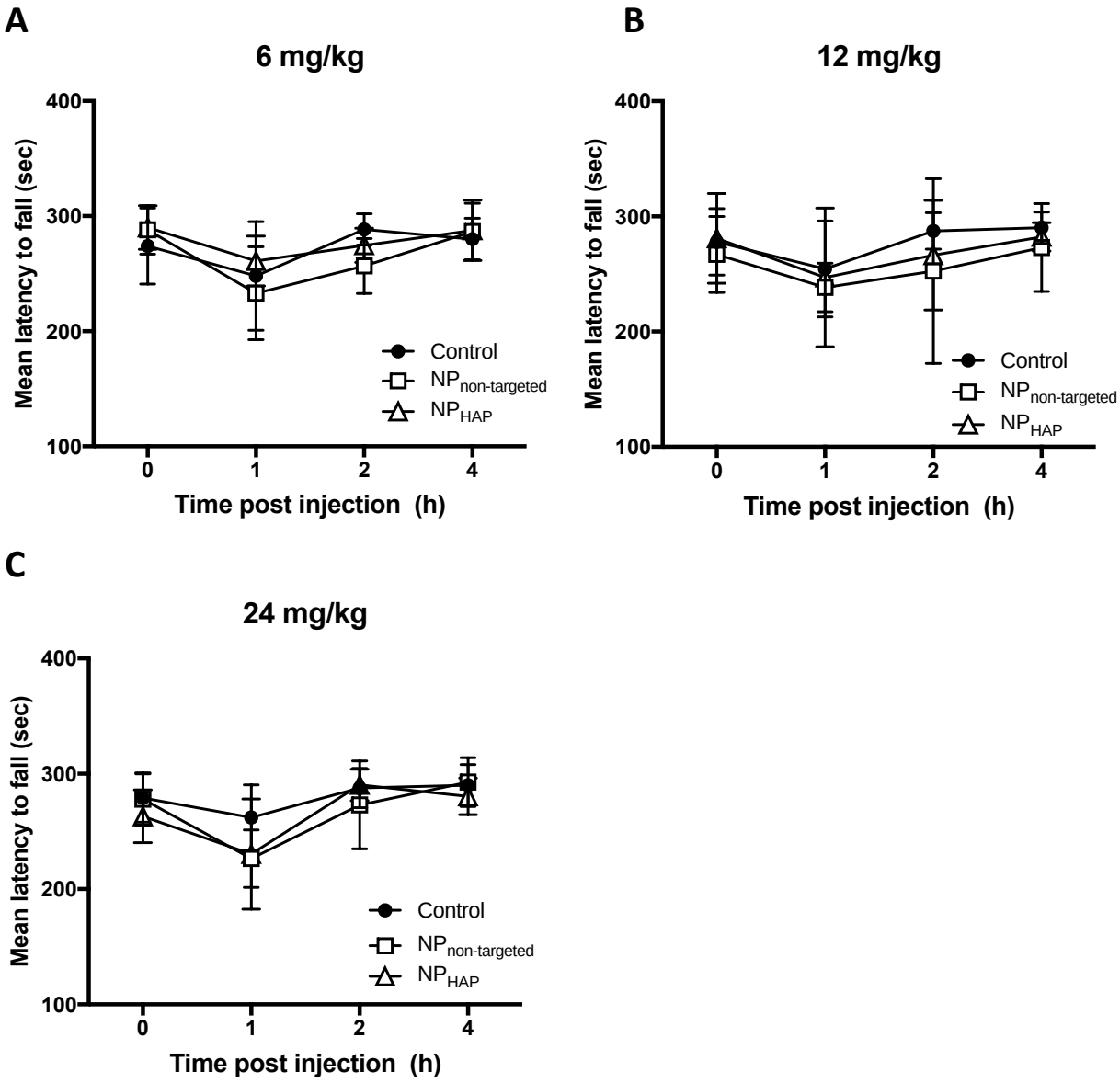

Figure 5.16. The influence of $NP_{non\text{-}targeted}$, NP_{HAP} treatment on rota-rod performance in rats, measured 1 h, 2 h and 4 h after administration. NP were administered i.v.i at **(A)** 6 mg/kg; **(B)** 12 mg/kg and; **(C)** 24 mg/kg. The sum of latencies of five trials in one day is presented. Data is presented as mean ± S.D, n=5. Analysis by two-way ANOVA, followed by Dunnett's multiple comparisons test.

5.4 DISCUSSION

Chronic inflammatory arthritis represents an emerging public health issue, occupying a sizeable proportion of the adult population in the industrialized world (Stockings et al., 2018). Efficient improvements in both analgesic and anti-inflammatory treatment without accompanying undesirable side effects are required to fulfil the unmet therapeutic needs of these desperate patients. The search for new naturally occurring analgesic and anti-inflammatory compounds is intensifying because of the need to find more effective compounds with less serious side effects. Increasing evidence from both pre-clinical and clinical studies support the therapeutic application of cannabinoids in the treatment of chronic pain. While structurally similar to AEA, OEA and LEA do not bind CB1, but instead contribute to an anti-inflammatory regulation through "entourage" effects (Okamoto et al., 2004; Alhouayek & Muccioli, 2014), and therefore lack negative psychotropic actions typified by cannabis-based medicines. In this chapter, we evaluated the anti-inflammatory and analgesic effects of our endocannabinoid-based NP and their influence of naturally occurring endocannabinoids in the arthritic joint.

NP incubation was shown to suppress TNF-α induced inflammatory cytokines *in-vitro*, mediated primarly via inhibition of the NF-κB signalling pathway (Chapter 4). Similarly, NP given to arthritic rats decreased plasma concentrations of IL-6, IL-17A, TNF-α and IFN-ɣ *in-vivo*. NP_{HAP} was more effective in suppressing IL-6 and IFN-ɣ when compared to $NP_{non\text{-}targeted}$, and may be attributed to greater localised effects mediated by the ligand-targeting. These results are in agreement with data obtained via RNA-seq (Chapter 4), and support the idea of endocannabinoid-NP's mediating anti-inflammatory effects. In RA, cytokines IL-6, IFN-ɣ, TNF- α and IL-17A are all important drivers of inflammation and are also implicated in the induction of cartilage and bone degradation in synovial and bone explants (Kokkonen et al., 2010). Inhibition of these key mediators may help alleviate arthritic progression by interrupting the induction of other cytokines, slowing inflammatory responses.

Electrophysiological studies in model's of arthritis have demonstrated that the facilitated nociceptive responses of peripheral nerves are attenuated in the presence of cannabinoid receptor agonists, demonstrating the capacity of endocannabinoids to act as analgesic agents in arthritis (Schuelert & McDougall, 2008). In this study, the ability of the $NP_{non\text{-}targeted}$ and NP_{HAP} to modulate nociceptive signalling in normal and arthritic rats was demonstrated using an analgesy-meter. Administration of NP to normal rats elicited dose-dependent anti-nociceptive responses against mechanical pain, which were significant at high dose concentrations. While the effects collectively showed slight anti-nociceptive effects against mechanical pain, the results obtained were only significant at 1-2 h suggesting short acting effects. These results are consistent with the previous PK studies (Chapter 3) which demonstrated a relatively short half-life for both NP's. As well as the analgesic effects, the

injected NP's did not significantly impair the animal's sensorimotor coordination. The peripheral lipid-mediated mechanisms offer the opportunity to develop medications that manage pain without producing negative central psychotropic effects.

While the preliminary results appear promising, several limitations of the study should be acknowledged. Evaluation of anti-nociceptive effects were measured using only the analgesy-meter, which assesses pain caused by mechanical pressure. Assessment of the analgesic potential employing other methods such as strain guages, Von-Frey filaments and inclined-plane test, would be required to validate the currently obtained results. Further to varying screening methods, experiments applying different modalities of pain such as thermal, electrical and chemical stimuli are required to further evaluate the analgesic potential of the NP's. Laboratory models for screening analgesics are reviewed by Milind & Monu (2012). In addition, the threshold nociceptive response was taken to be the final force upon which the hindpaw is withdrawn from the instrument. As the withdrawal response is detected visually by the researcher, the measurement of the threshold is subjective. Finally, over the course of the experiment, several rats appeared to anticipate pain, and react pre-maturely to the stimuli. The exhibited learned behaviour was not uniformly expressed within all treatment groups, and therefore would impact on threshold nociceptive readings obtained. Further evaluation of the efficacy of i.p administered NP on AIA-induced inflammatory pain, employing different modals of pain, is required before a conclusive statement regarding the potential analgesic effects of OEA and LEA are made. Similarly, the centrally mediated effects of the NP's were only evaluated using the rota-rod apparatus and using a single rod diameter over a specified time period. Additional methods such as water maze performance (Cain et al., 1997), static rods or beams, used to measure motor coordination (Deacon, 2013) are required to validate obtained results and gain a full profile of the NPs centrally mediated effects. Evaluation of the NPs central effects at higher doses, in particular 36 mg/kg, are required.

In the synovial fluid of healthy patients, PEA and OEA exist in high concentration, and have been shown to exert marked anti-nociceptive and anti-inflammatory effects in several animal models (Bonezzi et al., 2016). Substantial decrements in the tissue content of PEA and OEA have been noted in patients suffering from RA (Richardson et al., 2008). Changes in local joint production of PEA and OEA therefore may contribute to the control of chronic inflammation, by regulating joint endocannabinoid signalling system. In this study, the ability of the NP's NAE components LEA and OEA, to influence endogenous endocannabinoid levels of PEA, 2-AG and AEA in the joint was demonstrated. Increased concentrations of PEA correlated with significant increases in both OEA and LEA in NP_{HAP} treated rats, and may be partly mediated by LEA'S influence on FAAH. In Chapter 4, NP incubation suppressed FAAH gene expression in treated RA-FLS cells as demonstrated by RNA-seq. Given that PEA is susceptible to

metabolism by FAAH, increases in PEA in NP_{HAP} treated rats may be partly mediated LEA/NP inhibition of eicosanoid biosynthetic enzyme FAAH. Similar to PEA, levels of AEA were also shown to be elevated in NP treated groups, but failed to reach statistical significance. The overall low concentrations of AEA in the paws of animals was likely due of relatively low pre-existing endogenous levels of AEA, and difficulties homogenising the complex bone structures of the paw.

5.4.1 Summary

This is the first report showing the ability of NP's to decrease circulating cytokines *in-vivo*. In particular plasma levels of IL-6, IL-17A, IFN-ɣ and TNF-α were reduced. While the anti-inflammatory effects of NP_{HAP} and $NP_{non\text{-}targeted}$ on plasma cytokine levels were similar, suppression of IFN-ɣ and IL-6 was more pronounced in NP_{HAP} treated rats. In addition to cytokine inhibition, targeted NP_{HAP} had the ability to modulate nociceptive thresholds *in-vivo* as demonstrated by the analgesy-meter measurements. Assessment of NP on CNS showed no impairment on the animal's sensorimotor coordination for $NP_{non\text{-}targeted}$ and NP_{HAP} injected rats, suggesting the analgesic effects were not centrally mediated. Quantification of endogenous endocannabinoid concentrations of the paws in NP treated and non-treated arthritic rats, demonstrated the ability of NP_{HAP} to influence endogenous articular endocannabinoids levels. Given the anti-inflammatory and analgesic effects, NP's biological effects may be due to either direct effect on immune cells, or an entourage effect by changing the local milieu of saturated fatty acids that subsequently influence anti-inflammatory and analgesic actions, or both.

CHAPTER 6: FINAL DISCUSSION

6.1 ACHIEVEMENTS AND LIMITATIONS

The understanding and application of endocannabinoids in medical practise is ever increasing, adapting their use in many conditions and fields, ranging from pain management in cancer and chronic inflammatory disease, to intractable epilepsy in children, schizophrenia and mental disease in psychiatry. Although historically used for analgesia and pain relief, the cannabis extract based medications, rapidly fell out of favour because of the psychotropic effects and at times lack of efficacy due to many mixture combinations. In the musculoskeletal literature, the effectiveness and safety of medical marijuana to treat lupus, fibromyalgia, OA and RA came into question (Farrell et al., 2014). The predominant alert raised was the significant adverse effect of alteration in perception, motor and cognitive function, which largely outweighed any benefits which at times were viewed as minimal (Farrell et al., 2014). Most trials, which are not many, combined CBD with THC, prescribed low and likely ineffective dose, and only used a short test period of observation. Hence, it is not surprising when meta-analysis studies were completed and conclusions reached that the use of cannabis as a therapeutic in rheumatic conditions was discouraged (Fitzcharles et al., 2016a; Stockings et al., 2018). Despite these negative findings a better understanding of endocannabinoids mode of action, receptor function, mode of delivery, identification of analogues without psychotropic effects, and public pressure has resulted in a resurgence of interest. While benefits of cannabis-based medicines are promising, current drug delivery techniques are limited relying heavily on inhalation or ingestion of solutions/capsules. Due to this, therapeutics are not directed to their target areas of pain or disease, resulting in unpredictable potency and inconsistent release times. This study highlights the promising application of endocannabinoid-based NP targeted to the synovium for the treatment of arthritis. This musculoskeletal model of arthritis is not restrictive and the NPs can be targeted and applied to many other medical conditions such as epilepsy (brain), malignancies (melanoma, lymphoma), skin (psoriasis) and lung (interstitial fibrosis) to name a few. By regulating the homing-peptide, we are able to actively target and deliver cannabinoid therapeutics in the form of NP, facilitating application in a variety of illness in which cannabinoid therapy has proven successful.

The NPs generated in this study are unique and extend previous findings reported in the literature (Sagnella et al., 2010b). The mesosphere behaviour of a series monoethanolamide lipids is extended and a mixed monoethanolamide ratio of OEA and LEA with the ability to self-assemble into highly ordered 3D cubic nanostructured mesophase was defined. What was evident in this thesis was that the nanostructures formed by the amphiphiles were dictated by local constraints imposed by the molecular structure, as well as external factors, such as temperature, pH, ionic strength of the solution, excipient compositions and stabilising agents. At the ratio of 40% OEA: 60% LEA these

dispersions self-assembled into highly ordered 3D cubic structures and form stable NP within an aqueous solution which were stable at both RT and physiological temperature. However, when PEGylated lipids were incorporated to stabilise the NP and allow peptide conjugation, the folding of the lipid amphiphiles in the aqueous solution resulted in the formation of liposomal NP. The conjugation and successful incorporation of a synovium targeting peptide, HAP-1, into the NP formulation was accomplished. The development of stable endocannabinoid based NPs with an efficient targeting molecules attached is a major advancement in endocannabinoid drug delivery with many clinical applications.

This is the first report of the application of endocannabinoid-based NP targeting FLS *in-vitro* and sites of joint inflammation *in-vivo*. Despite the plethora of research suggesting the importance of FLS in RA (Bartok & Firestein, 2010; Bustamante et al., 2017), treatment strategies aimed at targeting FLS are rare. Conjugation of synovium-targeting peptide, HAP-1, to the NP surface resulted in specific binding and greater uptake of targeted NP_{HAP} in human FLS cells *in-vitro*, and corroborates results (Vanniasinghe et al., 2014). *In-vivo*, targeted NP_{HAP} increased localisation to the joint in both normal and arthritic rats, demonstrating the future potential to actively target therapeutics to the inflamed synovium. The implications of specifically targeting FLS are huge with the possibility of localised drug delivery, reduced toxicity and reduced side-effects. The high number of patients with RA who do not respond to available therapies suggests that, in some cases, therapeutic dosage might not have been reached owing to safety concerns (Bello et al., 2017). In this context, tissue-specific drug delivery might increase drug concentration in the site of interest, limit systemic exposure, increase therapeutic potency and decrease off-site effects, improvements all achieved with a single therapy. In addition to active targeting, the NPs exerted an anti-inflammatory effect at sites of localisation, by virtue of the lipid capsule constituents. This was demonstrated *in-vitro,* suppressing pro-inflammatory cytokines and MMPs in NP treated RA-FLS cells*,* and *in-vivo*, suppressing circulating cytokine levels in NP treated arthritic.

A unifying model of action of NP integrating *in-vitro* and *in-vivo* data is shown in Figure 6.1. Reflection of the RNA-seq data suggests that the anti-inflammatory effects are mediated by inhibition of a number of pathways including pro-inflammatory NF-κB cytokine pathways, TLR and PPAR signalling. In addition to known TLR and PPAR dependent-effects of the NAE's (Yang et al., 2016), the ability of NAE NPs to regulate JAK-STAT expression is demonstrated, and may be an alternative therapeutic to currently available JAK-inhibitors. These results confirm previous studies showing that OEA and LEA, have inherent anti-inflammatory and analgesic properties (Suardiaz et al., 2007; Ishida et al., 2013; Zhou et al., 2017a). NP incubation with RA-FLS cells induced the expression of endocannabinoid synthesising enzymes and enzymes involved with oxygenation of endocannabinoids. Metabolism of

AEA into AA and ethanolamine depends on multiple enzymes, including COX-2, LOXs and several cytochrome P450 monooxygenases, as shown in Figure 6.2. NP down regulation of LOX would decrease metabolite production of known TRPV1 agonists, HETE-EAs (Hwang, 2000) and therefore reduce pain. By inhibiting LOX, the upstream metabolites are shunted to the P450 system that increase metabolite production of EET-EA, which is known to exert anti-inflammatory effects by CB2 and PPAR-ɣ (Node et al., 1999; Snider et al., 2009; Liu, 2005).

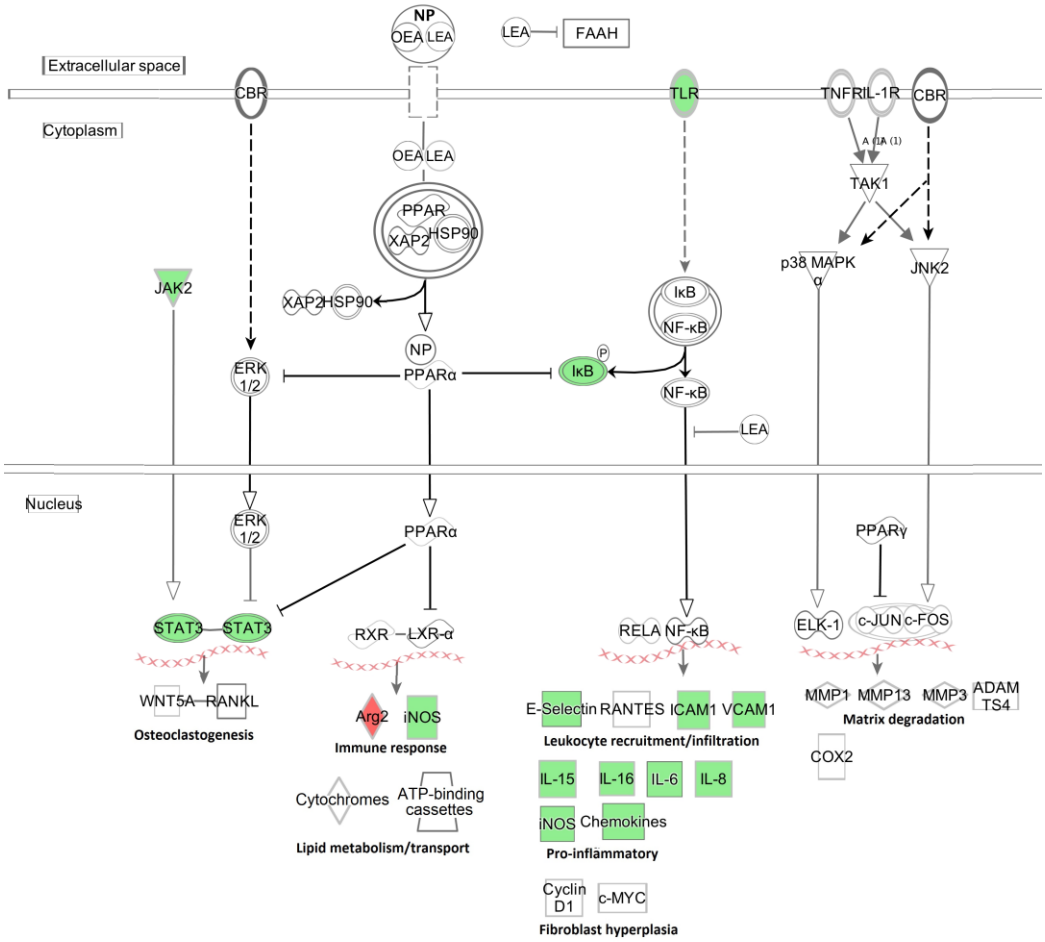

Figure 6.1 Schematic representation showing NP regulation of inflammatory signalling.

NP incubation decreased expression of FAAH mRNA *in-vitro*. Studies in the literature have demonstrated robust anti-inflammatory and anti-hyperalgesic phenotypes after genetic or pharmacological disruption of FAAH (Adamson Barnes et al., 2016; Kloza et al., 2017). The regulation of oxygenation and catabolic enzymes may help mediate the NP's anti-inflammatory and analgesic effects by regulating metabolite levels of EETs-EA and HETE-EAs, as well as FAAH substrate concentrations at the targeted site (Vandevoorde et al, 2007). The ability of the NP's to regulate metabolite levels of EETs-EA and HETE-EA, as well as down-regulate inflammatory cytokines and

transcriptional factors involved in inflammatory processes demonstrates the NP's promising application as anti-inflammatory agents.

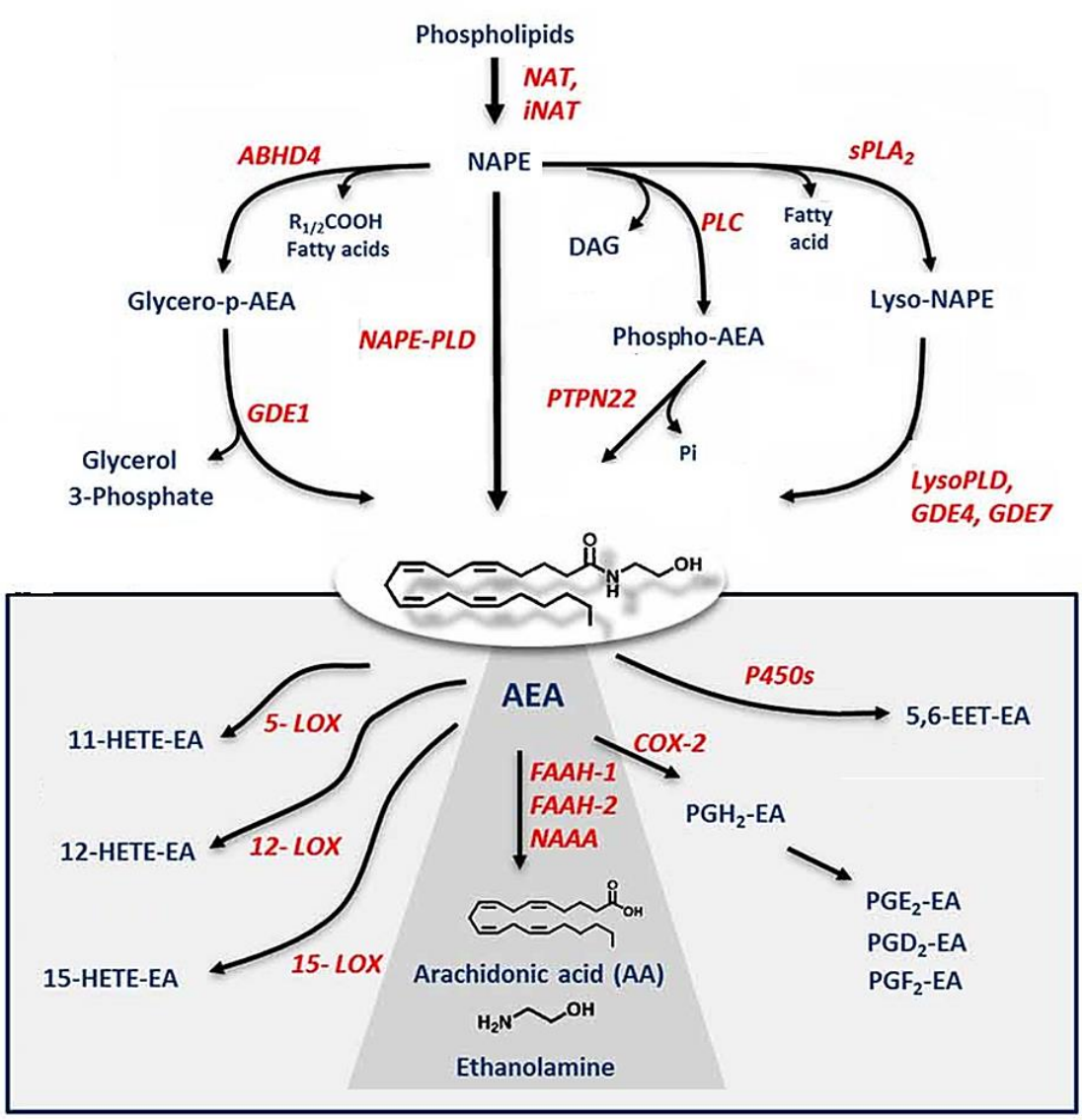

Figure 6.2: Metabolic pathways and enzymes involved with AEA synthesis, degradation and oxidation. Abbreviations: NAT, N-acyltransferase; NAPE-PLD, NAPE-specific phospholipase D; ABHD4, α/β-hydrolase domain 4; GDE, glycerophosphodiesterase; PLC, phospholipase C; PTPN22, non-receptor protein tyrosine phosphatase 22; sPLA2, soluble phospholipase A2; COX-2, cyclooxygenase-2; LOX, lipoxygenase; P450s, cytochrome P450 monooxygenases; PG-EA, prostaglandin-ethanolamide; HETE-EA, hydroxyeicosatetraenoyl-ethanolamide (hydroxy-AEA); EET-EA, epoxyeicosatrienoyl-ethanolamide. Figure adapted from Maccarrone (2017).

As well as demonstrating anti-inflammatory effects, the therapeutic potential of NAE NP's in pain was explored. Initially, research on cannabinoid-analgesics focused on CB1 mediated processes, which regulate nociceptive processing through inhibition of presynaptic gamma-aminobutyric acid (GABA) and glutamatergic transmission (Hohmann, 2002). While effects of CB1 mediated nociception were promising, the distribution of CB1 receptors along central processing sites associated CB1 mediated analgesics with negative psychoactive effects (Talwar & Potluri, 2011). While structurally similar to AEA, OEA and LEA do not bind CB1. Instead, these NAE's contribute to an anti-inflammatory regulation through "entourage" effects (Okamoto et al., 2004; Alhouayek & Muccioli, 2014), and therefore lack negative psychotropic actions typified by cannabis-based medicines. The existence of these peripheral lipid-mediated mechanisms offers the opportunity to develop medications that manage pain without producing negative central psychotropic effects. From the analgesic studies (Chapter 5), endocannabinoid-based NP treated normal rats elicited dose-dependent anti-nociceptive responses against mechanical pain, which was significant at high dose concentrations. These anti-nociceptive effects were devoid of central effects as observed. Besides centrally mediated effects, endocannabinoid lipids produced and released at sites of acute tissue injury, inflammation and neuropathy regulate the flow of nociceptive signals to the CNS. In this study, NP_{HAP} treated rats increased local joint concentrations of LEA, OEA and PEA. Since PEA and OEA, have a well-described anti-inflammatory role (Bonezzi et al., 2016), Increased local concentration of NAEs through targeted NP delivery or peripheral FAAH inhibition may alleviate nociceptive signalling and dampen local pro-inflammatory signals at the arthritic joint. The NP's demonstrated anti-inflammatory and analgesic effects may therefore be due to either direct effect on immune cells regulating cytokines, or by changing the local milieu of saturated fatty acids (OEA, LEA and PEA) that subsequently influence anti-inflammatory actions. Targeted NP delivery may be an alternative approach to increasing natural endocannabinoid ligands in the joint, offering a novel target for the treatment of arthritis.

6.2 FUTURE DIRECTION

6.2.1 Identification and Characterisation of HAP-1 Receptor

The receptor for HAP-1 binding as yet is not known. Mi *et al*., (2003) demonstrated that HAP-1 mediates internalization of a marker protein into rabbit synovial cells in a temperature dependant manner, implying receptor involvement. Understanding the HAP-1 receptor would be an important study to fully understand and utilise homing capabilities of the HAP-1 peptide. Isolation and characterisation of the HAP-1 bound complex would enhance our understanding of this ligand mediated targeting.

6.2.2 Other Targeting Peptides

There have been a number of attempts at targeted delivery of anti-inflammatory agents in RA. The selection of a suitable homing molecule is crucial to allow the specific accumulation of therapeutic agents to disease sites so as to improve drug efficacy without compromise to healthy tissues. As the bio-distribution of the target antigen contributes to target efficiency, antigens uniquely expressed at the disease site are optimal candidates for drug delivery. Future work might focus on targeting antigens that are expressed specifically in the synovium, such as the cell surface glycoprotein CD44, spliced variant isoforms CD44v4 and v6 which are associated with enhanced fibroblast invasive capacity and are important for cell migration and lymphocyte activation (Naor & Nedvetzki, 2003). Hyaluronic acid (HA) is a polysaccharide that specifically binds to the CD44 receptor. HA drug conjugates (Methotrexate-HA; Shin et al., 2014) and HA encapsulated polymeric nanoparticles (Heo et al., 2014; Lee et al., 2014b) were shown to preferentially accumulated in the inflamed joint and were significantly more potent that unconjugated drug in controlling clinical score, joint swelling and pro-inflammatory levels (Shin et al., 2014). Other antigens specifically expressed in the synovium such as folate receptor B (FR- β; van der Heijden et al., 2009) and integrin αVβ3 (Wilder, 2002) are also being explored for ligand-mediated nanoparticle targeting. Other homing sequences such as synthetic peptide (peptide 3.1, CKSTHDRLC) and isolated single-chain variable fragment (scFv) A7 selected/isolate from phage display libraries, have shown specificity for the human arthritic synovium (Lee et al., 2002). scFv A7 targets the stromal compartment of human arthritic synovium without reacting with the vasculature or other cellular components of normal human tissue from other organs (Kamperidis et al., 2011). These results indicate that scFv A7 targets an arthritic synovium-specific antigen, or one that is overexpressed in diseased tissues, as no reactivity could be detected in non-arthritic human synovium or in other inflammatory disease conditions could be used as an alternative to HAP-1.

6.2.3 Effects of NP on Clinical RA and Inflammatory Pain

While this study focused on the synthesis and characterisation of the endocannabinoid-lipids, as well as their inherit anti-inflammatory and analgesic effects, experiments focusing on the encapsulation of drugs was not explored. NP drug delivery proposes a platform to actively target and deliver therapeutic agents to the disease site, improving therapeutic index of currently available treatment. While NP drug delivery in arthritis is still in its infancy, promising results are being achieved with new patents filed world-wide (Summarised in Appendix 7). Vannasinghe *et al* (2014) convincingly demonstrated the benefits of prednisone loaded liposomes in the treatment of arthritis. Further *In-vivo* assessment of NP effects on clinical parameters, weight, inflamed joint count, paw/ankle width,

used to score joint inflammation would be required to assess the therapeutics efficacy of NPs (loaded or unloaded) and application in RA conditions. At the local joint level, immunostaining of inflamed joints would also be useful to assess the degree of active disease progression following NP treatment. Comparison of histopathological features of inflammation/disease progression and the expression levels of inflammatory markers in tissue samples from non-treated and NP treated arthritic rats, would further evaluate NP immunological potential and insight into treatment periods and effective doses.

In addition to NP effects on clinical joint inflammation, further evaluation of the NP's nociceptive potential should be assessed in formal and extensive pain studies. The current therapy of chronic pain relies heavily on opiates such as morphine and oxycodone, which primarily act on neural circuits of the brain and spinal cord. Cannabinoids have been shown act both synergistically with opioids and as opioid sparing agents, enabling reduced doses and fewer side effects from chronic opioid therapy (Ibrahim et al., 2005; Cox et al., 2007; Smith et al., 2007). Interaction of NP's endocannabinoid lipid constituents facilitate the potential for joint pain relief via local manipulation of the endocannabinoid system present in the synovium of RA patients. While the preliminary results appear promising, several limitations of the study (previously discussed in Chapter 4) limit claims on analgesic effects. Further evaluation of the efficacy of administered NP on AIA-induced inflammatory pain employing other methods, and applying different modalities of pain would be required before a conclusive statement regarding the potential analgesic effects of OEA and LEA are made. Studies focusing on the therapeutic efficacy of drug loaded NP's and the potential synergistic effects with the endocannabinoid-lipids are required to evaluate the full potential of this novel delivery system.

6.2.4 Application to Other Models of Disease

Endocannabinoids have potential application in a range diseases, with promising effects demonstrated in chronic pain, epilepsy, multiple sclerosis, neurodegenerative disorders (Parkinson's disease, Huntington's disease, Alzheimer's disease), glaucoma, cardiovascular disorders, cancer, obesity and other metabolic syndrome-related disorders (Kalant, 2001; Alexander, 2016). The ability of the endocannabinoid-based NPs to suppress key cytokines IL-6, IFN-ɣ, TNF-α and IL-17A, and regulators such as NF-κB of key canonical pathways such as granulocyte adhesion and diapedesis, macrophage activation, fibroblast and endothelial cell function, LXR/RXR activation, and neuro-inflammation suggests the potential application of the NPs in other areas of disease. 'Granulocytes (neutrophils, basophils and eosinophils) and agranulocyte (lymphocytes and monocytes) adhesion and diapedesis' pathway, is the migration of leukocytes from the vascular system to sites of pathogenic/allergenic exposure and is a key event in the process of inflammation (Nourshargh & Alon, 2014). NP regulation of key cell adhesion molecules involved in the tethering of leukocytes to the blood vessel wall (such as selectins, ICAM1, ICAM2, chemokines) would hinder leukocyte diapedesis

and migration. These NP therefore have therapeutic application in both allergic and pathogenic inflammation by regulating leukocyte migration.

Regulation of the key 'hepatic fibrosis' canonical pathway suggests the potential therapeutic application of NP's in liver fibrosis. Administration of OEA (5 mg/kg/day, i.p) significantly attenuated liver fibrosis progression in two experimental animal models by blocking the activation of hepatic stellate cells (Chen et al., 2015). These effects were suggested to be mediated by PPAR-α activation, which are abundantly expressed in the liver. Similarly, LXR/RXR is involved in the regulation of lipid metabolism, inflammation, and cholesterol to bile acid catabolism. OEA has been shown to activate lipid metabolism by decreasing neutral lipid content in hepatocytes, as well as through a decrease in serum cholesterol and triglyceride levels (Fu et al., 2005). Administration of OEA (5 mg/kg, i.p, once daily) lowered body weight and hyperlipidaemia in obese rats (Fu et al., 2005), mediated by enhanced PPAR-α signalling. In a separate study, OEA suppressed appetite by stimulating satiety (food intake, not feeding behaviour) and that its profile of action might be predictive of safer effects in humans as a novel anti-obesity treatment, by enhancing lipid utilisation (Romano et al., 2014). Together, NP's may have application in the treatment of liver fibrosis as a or as novel anti-obesity treatment through enhanced PPAR signalling mediated by OEA.

The neuro-inflammatory canonical pathway shown to be upregulated by the TNF-α, was suppressed in RA-TNF/NP cells. In separate studies, peripheral administration of OEA (20mg/kg, i.p.) was shown to cross the blood-brain barrier (Gonzalez-Aparicio et al., 2014) and reduce LPS-induced NF-κB activation, iNOS and COX-2 expression and lipid peroxidation in frontal cortex (Sayd et al., 2014). The observed anti-inflammatory effects of OEA in the brain may be a consequence of the modulation of peripheral inflammation, that is modulation of innate immune TLR4 receptors, by these acylethanolamides by the direct action in the CNS (Sayd et al., 2014). Given the importance of neuroinflammation in the physiopathology of neuropsychiatric diseases, the results suggest that OEA based NP may help delay the onset of neurodegenerative and neuropsychiatric diseases by reducing the insults to brain function, and helping those with neuroinflammatory or immune related neuropsychiatric conditions (Galan-Rodriguez et al., 2009; Melis et al., 2013). The ability of the NP to regulate these key canonical pathways offers promise in the treatment of various diseases in which these pathways play a central role.

6.3 CONCLUSION

The findings of this thesis have made an original contribution towards our knowledge and understanding of the endocannabinoid system, the potential anti-inflammatory and analgesic effects of OEA and LEA lipids, as well as defining their self-assembly behaviour for the construction and application as a NP drug delivery system. In particular, these findings offer a novel delivery system for cannabinoid-administration and highlight promising application of cannabinoid-based medicines in the treatment of arthritis and other inflammatory mediated diseases.

REFERENCES

Abuchowski, A., van Es, T., Palczuk, N. C., & Davis, F. F. Alteration of immunological properties of bovine serum albumin by covalent attachment of polyethylene glycol. (1977). *J Biol Chem,* 252(11), 3578-3581.

Adamson Barnes, N. S., Mitchell, V. A., Kazantzis, N. P., & Vaughan, C. W. Actions of the dual faah/magl inhibitor jzl195 in a murine neuropathic pain model. (2016). *Br J Pharmacol,* 173(1), 77-87.

Agarwal, N., Pacher, P., Tegeder, I., Amaya, F., Constantin, C. E., Brenner, G. J., et al. Cannabinoids mediate analgesia largely via peripheral type 1 cannabinoid receptors in nociceptors. (2007). *Nat Neurosci,* 10(7), 870-879.

Ahmad, S. F., Ansari, M. A., Zoheir, K. M., Bakheet, S. A., Korashy, H. M., Nadeem, A., et al. Regulation of tnf-alpha and nf-kappab activation through the jak/stat signaling pathway downstream of histamine 4 receptor in a rat model of lps-induced joint inflammation. (2015). *Immunobiology,* 220(7), 889-898.

Ahn, K., Smith, S. E., Limatta, M. B., Beidler, D., Sadagopan, N., Dudley, D. T., et al. Mechanistic and pharmacological characterization of pf-04457845: A highly potent and selective fatty acid amide hydrolase inhibitor that reduces inflammatory and noninflammatory pain. (2011). *J Pharmacol Exp Ther,* 338(1), 114-124.

Aletaha, D., & Bluml, S. Therapeutic implications of autoantibodies in rheumatoid arthritis. (2016). *RMD Open,* 2(1), e000009.

Alexander, S. P. Therapeutic potential of cannabis-related drugs. (2016). *Prog Neuropsychopharmacol Biol Psychiatry,* 64, 157-166.

Alexis, F., Pridgen, E., Molnar, L. K., & Farokhzad, O. C. Factors affecting the clearance and biodistribution of polymeric nanoparticles. (2008). *Mol Pharm,* 5(4), 505-515.

Alhouayek, M., & Muccioli, G. G. Cox-2-derived endocannabinoid metabolites as novel inflammatory mediators. (2014). *Trends Pharmacol Sci,* 35(6), 284-292.

Ali, M., Vanniasinghe, A., Kumar, V., Barnett, R., Alberto, R., & Manolios, N. 99mtc-technetium labeling of antiarthritic peptides to evaluate homing and biodistribution at inflamed joints. (2011). *Nucl Med Biol,* 38(5), 751-756.

Alunno, A., Carubbi, F., Giacomelli, R., & Gerli, R. Cytokines in the pathogenesis of rheumatoid arthritis: New players and therapeutic targets. (2017). *BMC Rheumatology*.

Ambrosino, P., Soldovieri, M. V., Russo, C., & Taglialatela, M. Activation and desensitization of trpv1 channels in sensory neurons by the pparalpha agonist palmitoylethanolamide. (2013). *Br J Pharmacol,* 168(6), 1430-1444.

Anand, P., Whiteside, G., Fowler, C. J., & Hohmann, A. G. Targeting cb2 receptors and the endocannabinoid system for the treatment of pain. (2009). *Brain Res Rev,* 60(1), 255-266.

Anders, S., & Huber, W. Differential expression analysis for sequence count data. (2010). *Genome Biol,* 11(10), R106.

Annunziata, P., Cioni, C., Mugnaini, C., & Corelli, F. Potent immunomodulatory activity of a highly selective cannabinoid cb2 agonist on immune cells from healthy subjects and patients with multiple sclerosis. (2017). *J Neuroimmunol,* 303, 66-74.

Anseloni, V. C., Ennis, M., & Lidow, M. S. Optimization of the mechanical nociceptive threshold testing with the randall-selitto assay. (2003). *J Neurosci Methods,* 131(1-2), 93-97.

Ashfaq, U. A., Riaz, M., Yasmeen, E., & Yousaf, M. Z. Recent advances in nanoparticle-based targeted drug-delivery systems against cancer and role of tumor microenvironment. (2017). *Crit Rev Ther Drug Carrier Syst,* 34(4), 317-353.

Ates, M., Hamza, M., Seidel, K., Kotalla, C. E., Ledent, C., & Guhring, H. Intrathecally applied flurbiprofen produces an endocannabinoid-dependent antinociception in the rat formalin test. (2003). *Eur J Neurosci,* 17(3), 597-604.

Barrera, P., Blom, A., van Lent, P. L., van Bloois, L., Beijnen, J. H., van Rooijen, N., et al. Synovial macrophage depletion with clodronate-containing liposomes in rheumatoid arthritis. (2000). *Arthritis Rheum,* 43(9), 1951-1959.

Barrie, N., Kuruppu, V., Manolios, E., Ali, M., Moghaddam, M., & Manolios, N. Endocannabinoids in arthritis: Current views and perspective. (2017). *Int J Rheum Dis,* 20(7), 789-797.

Bartok, B., & Firestein, G. S. Fibroblast-like synoviocytes: Key effector cells in rheumatoid arthritis. (2010). *Immunol Rev,* 233(1), 233-255.

Bathon, J. M., Martin, R. W., Fleischmann, R. M., Tesser, J. R., Schiff, M. H., Keystone, E. C., et al. A comparison of etanercept and methotrexate in patients with early rheumatoid arthritis. (2000). *N Engl J Med,* 343(22), 1586-1593.

Battista, N., Di Tommaso, M., Bari, M., & Maccarrone, M. The endocannabinoid system: An overview. (2012). *Front Behav Neurosci,* 6, 9.

Bek, S., Bojesen, A. B., Nielsen, J. V., Sode, J., Bank, S., Vogel, U., et al. Systematic review and meta-analysis: Pharmacogenetics of anti-tnf treatment response in rheumatoid arthritis. (2017). *Pharmacogenomics J,* 17(5), 403-411.

Bello, A. E., Perkins, E. L., Jay, R., & Efthimiou, P. Recommendations for optimizing methotrexate treatment for patients with rheumatoid arthritis. (2017). *Open Access Rheumatol,* 9, 67-79.

Bernardi, A., Zilberstein, A. C., Jager, E., Campos, M. M., Morrone, F. B., Calixto, J. B., et al. Effects of indomethacin-loaded nanocapsules in experimental models of inflammation in rats. (2009). *Br J Pharmacol,* 158(4), 1104-1111.

Bjursell, M., Ryberg, E., Wu, T., Greasley, P. J., Bohlooly, Y. M., & Hjorth, S. Deletion of gpr55 results in subtle effects on energy metabolism, motor activity and thermal pain sensation. (2016). *PLoS One,* 11(12), e0167965.

Blake, D. R., Robson, P., Ho, M., Jubb, R. W., & McCabe, C. S. Preliminary assessment of the efficacy, tolerability and safety of a cannabis-based medicine (sativex) in the treatment of pain caused by rheumatoid arthritis. (2006). *Rheumatology (Oxford),* 45(1), 50-52.

Bonezzi, F. T., Sasso, O., Pontis, S., Realini, N., Romeo, E., Ponzano, S., et al. An important role for n-acylethanolamine acid amidase in the complete freund's adjuvant rat model of arthritis. (2016). *J Pharmacol Exp Ther,* 356(3), 656-663.

Boyd, B. J., Whittaker, D. V., Khoo, S. M., & Davey, G. Lyotropic liquid crystalline phases formed from glycerate surfactants as sustained release drug delivery systems. (2006). *Int J Pharm,* 318, 154-162.

Boyle, D. L., Soma, K., Hodge, J., Kavanaugh, A., Mandel, D., Mease, P., et al. The jak inhibitor tofacitinib suppresses synovial jak1-stat signalling in rheumatoid arthritis. (2015). *Ann Rheum Dis,* 74(6), 1311-1316.

Burstein, S. H. Ajulemic acid: Potential treatment for chronic inflammation. (2018). *Pharmacol Res Perspect,* 6(2), e00394.

Burstein, S. H., & Zurier, R. B. Cannabinoids, endocannabinoids, and related analogs in inflammation. (2009). *AAPS J,* 11(1), 109-119.

Burston, J. J., Sagar, D. R., Shao, P., Bai, M., King, E., Brailsford, L., et al. Cannabinoid cb2 receptors regulate central sensitization and pain responses associated with osteoarthritis of the knee joint. (2013). *PLoS One,* 8(11), e80440.

Bustamante, M. F., Garcia-Carbonell, R., Whisenant, K. D., & Guma, M. Fibroblast-like synoviocyte metabolism in the pathogenesis of rheumatoid arthritis. (2017). *Arthritis Res Ther,* 19(1), 110.

Butler, D. M., Malfait, A. M., Maini, R. N., Brennan, F. M., & Feldmann, M. Anti-il-12 and anti-tnf antibodies synergistically suppress the progression of murine collagen-induced arthritis. (1999). *Eur J Immunol,* 29(7), 2205-2212.

Cabral, G. A., & Griffin-Thomas, L. Emerging role of the cannabinoid receptor cb2 in immune regulation: Therapeutic prospects for neuroinflammation. (2009). *Expert Rev Mol Med,* 11, e3.

Cain, D. P., Saucier, D., & Boon, F. Testing hypotheses of spatial learning: The role of nmda receptors and nmda-mediated long-term potentiation. (1997). *Behav Brain Res,* 84(1-2), 179-193.

Cajanus, K., Holmstrom, E. J., Wessman, M., Anttila, V., Kaunisto, M. A., & Kalso, E. Effect of endocannabinoid degradation on pain: Role of faah polymorphisms in experimental and postoperative pain in women treated for breast cancer. (2016). *Pain,* 157(2), 361-369.

Cates, M. E. The isotropic ("sponge") to lamellar transition in dilute surfactant systems. (1991). *Phys. A Stat.Theor. Phys.,* 176, 187-199.

Chandrasekar, D., Sistla, R., Ahmad, F. J., Khar, R. K., & Diwan, P. V. Folate coupled poly(ethyleneglycol) conjugates of anionic poly(amidoamine) dendrimer for inflammatory tissue specific drug delivery. (2007). *J Biomed Mater Res A,* 82(1), 92-103.

Chemistry, R. S. o. (2015). Chemspider, search and share chemistry. http://www.chemspider.com/

Chen, L., Li, L., Chen, J., Li, L., Zheng, Z., Ren, J., et al. Oleoylethanolamide, an endogenous ppar-alpha ligand, attenuates liver fibrosis targeting hepatic stellate cells. (2015). *Oncotarget,* 6(40), 42530-42540.

Cheng, A. C. Interlamellar transition mechanism in model membranes. (1996). *M. J. Phys. Chem. B,* 100, 5608–5610.

Chinetti, G., Fruchart, J. C., & Staels, B. Peroxisome proliferator-activated receptors (ppars): Nuclear receptors with functions in the vascular wall. (2001). *Z Kardiol,* 90 Suppl 3, 125-132.

Chipkin, R. E., Latranyi, M. B., Iorio, L. C., & Barnett, A. Determination of analgesic drug efficacies by modification of the randall and selitto rat yeast paw test. (1983). *J Pharmacol Methods,* 10(3), 223-229.

Chiurchiu, V., Battistini, L., & Maccarrone, M. Endocannabinoid signalling in innate and adaptive immunity. (2015). *Immunology,* 144(3), 352-364.

Choy, E. H., Smith, C. M., Farewell, V., Walker, D., Hassell, A., Chau, L., et al. Factorial randomised controlled trial of glucocorticoids and combination disease modifying drugs in early rheumatoid arthritis. (2008). *Ann Rheum Dis,* 67(5), 656-663.

Chuang, S. Y., Lin, C. H., Huang, T. H., & Fang, J. Y. Lipid-based nanoparticles as a potential delivery approach in the treatment of rheumatoid arthritis. (2018). *Nanomaterials (Basel),* 8(1).

Clapper, J. R., Moreno-Sanz, G., Russo, R., Guijarro, A., Vacondio, F., Duranti, A., et al. Anandamide suppresses pain initiation through a peripheral endocannabinoid mechanism. (2010). *Nat Neurosci,* 13(10), 1265-1270.

Corcoran, L., Roche, M., & Finn, D. P. The role of the brain's endocannabinoid system in pain and its modulation by stress. (2015). *Int Rev Neurobiol,* 125, 203-255.

Coulon, D., Faure, L., Salmon, M., Wattelet, V., & Bessoule, J. J. N-acylethanolamines and related compounds: Aspects of metabolism and functions. (2012). *Plant Sci,* 184, 129-140.

Cox, M. L., Haller, V. L., & Welch, S. P. Synergy between delta9-tetrahydrocannabinol and morphine in the arthritic rat. (2007). *Eur J Pharmacol,* 567(1-2), 125-130.

Curtis, J. R., & Singh, A. J. The use of biologics in rheumatoid arthritis: Current and emerging paradigms of care. (2011). *Clin Ther,* 33(6), 679-707.

Dani, M., Guindon, J., Lambert, C., & Beaulieu, P. The local antinociceptive effects of paracetamol in neuropathic pain are mediated by cannabinoid receptors. (2007). *Eur J Pharmacol,* 573(1-3), 214-215.

Davis, M. E., Chen, Z. G., & Shin, D. M. Nanoparticle therapeutics: An emerging treatment modality for cancer. (2008). *Nat Rev Drug Discov,* 7(9), 771-782.

Deacon, R. M. J. Measuring motor coordination in mice. (2013). *J Vis Exp,* 75, 2609.

Decuzzi, P., Godin, B., Tanaka, T., Lee, S. Y., Chiappini, C., Liu, X., et al. Size and shape effects in the biodistribution of intravascularly injected particles. (2010). *J Control Release,* 141(3), 320-327.

Devane, W. A., Hanus, L., Breuer, A., Pertwee, R. G., Stevenson, L. A., Griffin, G., et al. Isolation and structure of a brain constituent that binds to the cannabinoid receptor. (1992). *Science,* 258(5090), 1946-1949.

Devchand, P. R., Keller, H., Peters, J. M., Vazquez, M., Gonzalez, F. J., & Wahli, W. The pparalpha-leukotriene b4 pathway to inflammation control. (1996). *Nature,* 384(6604), 39-43.

Di Marzo, V. Endocannabinoids: Synthesis and degradation. (2008). *Rev Physiol Biochem Pharmacol,* 160, 1-24.

Di Marzo, V. a. P., L. Why do cannabinoid receptors have more than one endogenous ligand? (2012). *Philos Trans R Soc Lond B Biol Sci,* 367(1607), 3216-3228.

Dobin, A., Davis, C. A., Schlesinger, F., Drenkow, J., Zaleski, C., Jha, S., et al. Star: Ultrafast universal rna-seq aligner. (2013). *Bioinformatics,* 29(1), 15-21.

Duffy, L., & O'Reilly, S. C. Toll-like receptors in the pathogenesis of autoimmune diseases: Recent and emerging translational developments. (2016). *Immunotargets Ther,* 5, 69-80.

El-Kady, I. M., & El-Masry, S. A. Pro-inflammatory and anti-inflammatory cytokines profile in rheumatoid arthritis patients. (2008). *Egypt J Immunol,* 15(1), 109-114.

Farrell, M., Buchbinder, R., & Hall, W. Should doctors prescribe cannabinoids? (2014). *BMJ,* 348, 27-37.

Feely, M. G., & O'Dell, J. R. Update on the use of conventional disease-modifying antirheumatic drugs in the management of rheumatoid arthritis. (2010). *Curr Opin Rheumatol,* 22(3), 316-320.

Fernandes, E. S., Russell, F. A., Spina, D., McDougall, J. J., Graepel, R., Gentry, C., et al. A distinct role for transient receptor potential ankyrin 1, in addition to transient receptor potential vanilloid 1, in tumor necrosis factor alpha-induced inflammatory hyperalgesia and freund's complete adjuvant-induced monarthritis. (2011). *Arthritis Rheum,* 63(3), 819-829.

Fernandes, J. C., Wang, H., Jreyssaty, C., Benderdour, M., Lavigne, P., Qiu, X., et al. Bone-protective effects of nonviral gene therapy with folate-chitosan DNA nanoparticle containing interleukin-1 receptor antagonist gene in rats with adjuvant-induced arthritis. (2008). *Mol Ther,* 16(7), 1243-1251.

Fichna, J., Salaga, M., Stuart, J., Saur, D., Sobczak, M., Zatorski, H., et al. Selective inhibition of faah produces antidiarrheal and antinociceptive effect mediated by endocannabinoids and cannabinoid-like fatty acid amides. (2014). *Neurogastroenterol Motil,* 26(4), 470-481.

Fimiani, C., Mattocks, D., Cavani, F., Salzet, M., Deutsch, D. G., Pryor, S., et al. Morphine and anandamide stimulate intracellular calcium transients in human arterial endothelial cells: Coupling to nitric oxide release. (1999). *Cell Signal,* 11(3), 189-193.

Fitzcharles, M. A., Baerwald, C., Ablin, J., & Hauser, W. Efficacy, tolerability and safety of cannabinoids in chronic pain associated with rheumatic diseases (fibromyalgia syndrome, back pain, osteoarthritis, rheumatoid arthritis): A systematic review of randomized controlled trials. (2016a). *Schmerz,* 30(1), 47-61.

Fitzcharles, M. A., Ste-Marie, P. A., Hauser, W., Clauw, D. J., Jamal, S., Karsh, J., et al. Efficacy, tolerability, and safety of cannabinoid treatments in the rheumatic diseases: A systematic review of randomized controlled trials. (2016b). *Arthritis Care Res (Hoboken),* 68(5), 681-688.

Fu, J., Oveisi, F., Gaetani, S., Lin, E., & Piomelli, D. Oleoylethanolamide, an endogenous ppar-alpha agonist, lowers body weight and hyperlipidemia in obese rats. (2005). *Neuropharmacology,* 48(8), 1147-1153.

Fu, W., & Taylor, B. K. Activation of cannabinoid cb2 receptors reduces hyperalgesia in an experimental autoimmune encephalomyelitis mouse model of multiple sclerosis. (2015). *Neurosci Lett,* 595, 1-6.

Fukuda, S., Kohsaka, H., Takayasu, A., Yokoyama, W., Miyabe, C., Miyabe, Y., et al. Cannabinoid receptor 2 as a potential therapeutic target in rheumatoid arthritis. (2014). *BMC Musculoskelet Disord,* 15, 275.

Galan-Rodriguez, B., Suarez, J., Gonzalez-Aparicio, R., Bermudez-Silva, F. J., Maldonado, R., Robledo, P., et al. Oleoylethanolamide exerts partial and dose-dependent neuroprotection of substantia nigra dopamine neurons. (2009). *Neuropharmacology,* 56(3), 653-664.

George, K. L., Saltman, L. H., Stein, G. S., Lian, J. B., & Zurier, R. B. Ajulemic acid, a nonpsychoactive cannabinoid acid, suppresses osteoclastogenesis in mononuclear precursor cells and induces apoptosis in mature osteoclast-like cells. (2008). *J Cell Physiol,* 214(3), 714-720.

Gonsiorek, W., Lunn, C., Fan, X., Narula, S., Lundell, D., & Hipkin, R. W. Endocannabinoid 2-arachidonyl glycerol is a full agonist through human type 2 cannabinoid receptor: Antagonism by anandamide. (2000). *Mol Pharmacol,* 57(5), 1045-1050.

Gonzalez-Aparicio, R., Blanco, E., Serrano, A., Pavon, F. J., Parsons, L. H., Maldonado, R., et al. The systemic administration of oleoylethanolamide exerts neuroprotection of the nigrostriatal system in experimental parkinsonism. (2014). *Int J Neuropsychopharmacol,* 17(3), 455-468.

Goppert, T. M., & Muller, R. H. Protein adsorption patterns on poloxamer- and poloxamine-stabilized solid lipid nanoparticles (sln). (2005). *Eur J Pharm Biopharm,* 60(3), 361-372.

Grabiec, U., & Dehghani, F. N-arachidonoyl dopamine: A novel endocannabinoid and endovanilloid with widespread physiological and pharmacological activities. (2017). *Cannabis Cannabinoid Res,* 2(1), 183-196.

Grove, M. L., Hassell, A. B., Hay, E. M., & Shadforth, M. F. Adverse reactions to disease-modifying anti-rheumatic drugs in clinical practice. (2001). *QJM,* 94(6), 309-319.

Guhring, H., Hamza, M., Sergejeva, M., Ates, M., Kotalla, C. E., Ledent, C., et al. A role for endocannabinoids in indomethacin-induced spinal antinociception. (2002). *Eur J Pharmacol,* 454(2-3), 153-163.

Gui, H., Liu, X., Liu, L. R., Su, D. F., & Dai, S. M. Activation of cannabinoid receptor 2 attenuates synovitis and joint distruction in collagen-induced arthritis. (2015). *Immunobiology,* 220(6), 817-822.

Guindon, J., LoVerme, J., De Lean, A., Piomelli, D., & Beaulieu, P. Synergistic antinociceptive effects of anandamide, an endocannabinoid, and nonsteroidal anti-inflammatory drugs in peripheral tissue: A role for endogenous fatty-acid ethanolamides? (2006). *Eur J Pharmacol,* 550(1-3), 68-77.

Haller, J., Goldberg, S. R., Pelczer, K. G., Aliczki, M., & Panlilio, L. V. The effects of anandamide signaling enhanced by the faah inhibitor urb597 on coping styles in rats. (2013). *Psychopharmacology (Berl),* 230(3), 353-362.

Heo, R., Park, J. S., Jang, H. J., Kim, S. H., Shin, J. M., Suh, Y. D., et al. Hyaluronan nanoparticles bearing gamma-secretase inhibitor: In vivo therapeutic effects on rheumatoid arthritis. (2014). *J Control Release,* 192, 295-300.

Hoes, J. N., Jacobs, J. W., Buttgereit, F., & Bijlsma, J. W. Current view of glucocorticoid co-therapy with dmards in rheumatoid arthritis. (2010). *Nat Rev Rheumatol,* 6(12), 693-702.

Hohmann, A. G. Spinal and peripheral mechanisms of cannabinoid antinociception: Behavioral, neurophysiological and neuroanatomical perspectives. (2002). *Chem Phys Lipids,* 121(1-2), 173-190.

Howlett, A. C., Bidaut-Russell, M., Devane, W. A., Melvin, L. S., Johnson, M. R., & Herkenham, M. The cannabinoid receptor: Biochemical, anatomical and behavioral characterization. (1990). *Trends Neurosci,* 13(10), 420-423.

Hu, C., & Ma, S. Recent development of lipoxygenase inhibitors as anti-inflammatory agents. (2018). *Medchemcomm,* 9(2), 212-225.

Huang, Q. Q., & Pope, R. M. The role of toll-like receptors in rheumatoid arthritis. (2009). *Curr Rheumatol Rep,* 11(5), 357-364.

Huggins, J. P., Smart, T. S., Langman, S., Taylor, L., & Young, T. An efficient randomised, placebo-controlled clinical trial with the irreversible fatty acid amide hydrolase-1 inhibitor pf-04457845, which modulates endocannabinoids but fails to induce effective analgesia in patients with pain due to osteoarthritis of the knee. (2012). *Pain,* 153(9), 1837-1846.

Hwang, J., Rodgers, K., Oliver, J. C., & Schluep, T. Alpha-methylprednisolone conjugated cyclodextrin polymer-based nanoparticles for rheumatoid arthritis therapy. (2008). *Int J Nanomedicine,* 3(3), 359-371.

Hwang, S. W., Cho, H., Kwak, J., Lee, S. Y., Kang, C. J., Jung, J., et al. Direct activation of capsaicin receptors by products of lipoxygenases: Endogenous capsaicin-like substances. (2000). *Proc Natl Acad Sci U S A,* 97(11), 6155-6160.

Ibrahim, M. M., Deng, H., Zvonok, A., Cockayne, D. A., Kwan, J., Mata, H. P., et al. Activation of cb2 cannabinoid receptors by am1241 inhibits experimental neuropathic pain: Pain inhibition by receptors not present in the cns. (2003). *Proc Natl Acad Sci U S A,* 100(18), 10529-10533.

Ibrahim, M. M., Porreca, F., Lai, J., Albrecht, P. J., Rice, F. L., Khodorova, A., et al. Cb2 cannabinoid receptor activation produces antinociception by stimulating peripheral release of endogenous opioids. (2005). *Proc Natl Acad Sci U S A,* 102(8), 3093-3098.

Inui, K., & Koike, T. Combination therapy with biologic agents in rheumatic diseases: Current and future prospects. (2016). *Ther Adv Musculoskelet Dis,* 8(5), 192-202.

Irby, D., Du, C., & Li, F. Lipid-drug conjugate for enhancing drug delivery. (2017). *Mol Pharm,* 14(5), 1325-1338.

Ishida, T., Nishiumi, S., Tanahashi, T., Yamasaki, A., Yamazaki, A., Akashi, T., et al. Linoleoyl ethanolamide reduces lipopolysaccharide-induced inflammation in macrophages and ameliorates 2,4-dinitrofluorobenzene-induced contact dermatitis in mice. (2013). *Eur J Pharmacol,* 699(1-3), 6-13.

Ishihara, T., Kubota, T., Choi, T., & Higaki, M. Treatment of experimental arthritis with stealth-type polymeric nanoparticles encapsulating betamethasone phosphate. (2009). *J Pharmacol Exp Ther,* 329(2), 412-417.

Israelachvili, J. N., Mitchell, D. J., & Ninham, B. W. J. Equations for the repulsion component of the lattice energy as derived from a direct minimisation of the total lattice energy. (1976). *Chem Soc Faraday Trans II* 72, 1525-1568.

Jacque, E., Tchenio, T., Piton, G., Romeo, P. H., & Baud, V. Rela repression of relb activity induces selective gene activation downstream of tnf receptors. (2005). *Proc Natl Acad Sci U S A,* 102(41), 14635-14640.

Jayamanne, A., Greenwood, R., Mitchell, V. A., Aslan, S., Piomelli, D., & Vaughan, C. W. Actions of the faah inhibitor urb597 in neuropathic and inflammatory chronic pain models. (2006). *Br J Pharmacol,* 147(3), 281-288.

Joris, I., Cuenoud, H. F., Doern, G. V., Underwood, J. M., & Majno, G. Capillary leakage in inflammation. A study by vascular labeling. (1990). *Am J Pathol,* 137(6), 1353-1363.

Jung, Y. S., Park, W., & Na, K. Temperature-modulated noncovalent interaction controllable complex for the long-term delivery of etanercept to treat rheumatoid arthritis. (2013). *J Control Release,* 171(2), 143-151.

Kalant, H. Medicinal use of cannabis: History and current status. (2001). *Pain Res Manag,* 6(2), 80-91.

Kamperidis, P., Kamalati, T., Ferrari, M., Jones, M., Garrood, T., Smith, M. D., et al. Development of a novel recombinant biotherapeutic with applications in targeted therapy of human arthritis. (2011). *Arthritis Rheum,* 63(12), 3758-3767.

Karlsson, J., & Fowler, C. J. Inhibition of endocannabinoid metabolism by the metabolites of ibuprofen and flurbiprofen. (2014). *PLoS One,* 9(7), e103589.

Katchan, V., David, P., & Shoenfeld, Y. Cannabinoids and autoimmune diseases: A systematic review. (2016). *Autoimmun Rev,* 15(6), 513-528.

Kelly, S., Chapman, R. J., Woodhams, S., Sagar, D. R., Turner, J., Burston, J. J., et al. Increased function of pronociceptive trpv1 at the level of the joint in a rat model of osteoarthritis pain. (2015). *Ann Rheum Dis,* 74(1), 252-259.

Keystone, E. C., Taylor, P. C., Drescher, E., Schlichting, D. E., Beattie, S. D., Berclaz, P. Y., et al. Safety and efficacy of baricitinib at 24 weeks in patients with rheumatoid arthritis who have had an inadequate response to methotrexate. (2015). *Ann Rheum Dis,* 74(2), 333-340.

Kinsey, S. G., Mahadevan, A., Zhao, B., Sun, H., Naidu, P. S., Razdan, R. K., et al. The cb2 cannabinoid receptor-selective agonist o-3223 reduces pain and inflammation without apparent cannabinoid behavioral effects. (2011a). *Neuropharmacology,* 60(2-3), 244-251.

Kinsey, S. G., Naidu, P. S., Cravatt, B. F., Dudley, D. T., & Lichtman, A. H. Fatty acid amide hydrolase blockade attenuates the development of collagen-induced arthritis and related thermal hyperalgesia in mice. (2011b). *Pharmacol Biochem Behav,* 99(4), 718-725.

Klein, T. W. Cannabinoid-based drugs as anti-inflammatory therapeutics. (2005). *Nat Rev Immunol,* 5(5), 400-411.

Kloza, M., Baranowska-Kuczko, M., Malinowska, B., Karpinska, O., Harasim-Symbor, E., Kasacka, I., et al. The influence of doca-salt hypertension and chronic administration of the faah inhibitor urb597 on kca2.3/kca3.1-edh-type relaxation in rat small mesenteric arteries. (2017). *Vascul Pharmacol,* 99, 65-73.

Kokkonen, H., Soderstrom, I., Rocklov, J., Hallmans, G., Lejon, K., & Rantapaa Dahlqvist, S. Up-regulation of cytokines and chemokines predates the onset of rheumatoid arthritis. (2010). *Arthritis Rheum,* 62(2), 383-391.

Koning, G. A., Schiffelers, R. M., Wauben, M. H., Kok, R. J., Mastrobattista, E., Molema, G., et al. Targeting of angiogenic endothelial cells at sites of inflammation by dexamethasone phosphate-containing rgd peptide liposomes inhibits experimental arthritis. (2006). *Arthritis Rheum,* 54(4), 1198-1208.

Kourbeti, I. S., Ziakas, P. D., & Mylonakis, E. Biologic therapies in rheumatoid arthritis and the risk of opportunistic infections: A meta-analysis. (2014). *Clin Infect Dis,* 58(12), 1649-1657.

Kozak, K. R., Gupta, R. A., Moody, J. S., Ji, C., Boeglin, W. E., DuBois, R. N., et al. 15-lipoxygenase metabolism of 2-arachidonylglycerol. Generation of a peroxisome proliferator-activated receptor alpha agonist. (2002). *J Biol Chem,* 277(26), 23278-23286.

Kozak, K. R., Prusakiewicz, J. J., Rowlinson, S. W., Prudhomme, D. R., & Marnett, L. J. Amino acid determinants in cyclooxygenase-2 oxygenation of the endocannabinoid anandamide. (2003). *Biochemistry,* 42(30), 9041-9049.

Krustev, E., Reid, A., & McDougall, J. J. Tapping into the endocannabinoid system to ameliorate acute inflammatory flares and associated pain in mouse knee joints. (2014). *Arthritis Res Ther,* 16(5), 437.

Kulkarni, C. V. Lipid self-assemblies and nanostructured emulsions for cosmetic formulations. (2016). *Cosmetics,* 3, 1-15.

Larsson, K. J. Cubic lipid-water phases: Structures and biomembrane aspects. (1989). *Phys Chem* (93), 7304-7314.

Larsson, K. J. Colloidal dispersions of ordered lipid-water phases. (1999). *Dispers Sci Technol,* 20, 27-34.

Lee, E. B., Fleischmann, R., Hall, S., Wilkinson, B., Bradley, J. D., Gruben, D., et al. Tofacitinib versus methotrexate in rheumatoid arthritis. (2014a). *N Engl J Med,* 370(25), 2377-2386.

Lee, H., Lee, M. Y., Bhang, S. H., Kim, B. S., Kim, Y. S., Ju, J. H., et al. Hyaluronate-gold nanoparticle/tocilizumab complex for the treatment of rheumatoid arthritis. (2014b). *ACS Nano,* 8(5), 4790-4798.

Lee, L., Buckley, C., Blades, M. C., Panayi, G., George, A. J., & Pitzalis, C. Identification of synovium-specific homing peptides by in vivo phage display selection. (2002). *Arthritis Rheum,* 46(8), 2109-2120.

Leon, L., Gomez, A., Vadillo, C., Pato, E., Rodriguez-Rodriguez, L., Jover, J. A., et al. Severe adverse drug reactions to biological disease-modifying anti-rheumatic drugs in elderly patients with rheumatoid arthritis in clinical practice. (2018). *Clin Exp Rheumatol,* 36(1), 29-35.

Li, H., Handsaker, B., Wysoker, A., Fennell, T., Ruan, J., Homer, N., et al. The sequence alignment/map format and samtools. (2009). *Bioinformatics,* 25(16), 2078-2079.

Li, P., Gong, P., Li, H., Perkins, E. J., Wang, N., & Zhang, C. Gene regulatory network inference and validation using relative change ratio analysis and time-delayed dynamic bayesian network. (2014). *EURASIP J Bioinform Syst Biol,* 2014, 12.

Lin, S., Khanolkar, A. D., Fan, P., Goutopoulos, A., Qin, C., Papahadjis, D., et al. Novel analogues of arachidonylethanolamide (anandamide): Affinities for the cb1 and cb2 cannabinoid receptors and metabolic stability. (1998). *J Med Chem,* 41(27), 5353-5361.

Lipsky, P. E., van der Heijde, D. M., St Clair, E. W., Furst, D. E., Breedveld, F. C., Kalden, J. R., et al. Infliximab and methotrexate in the treatment of rheumatoid arthritis. Anti-tumor necrosis factor trial in rheumatoid arthritis with concomitant therapy study group. (2000). *N Engl J Med,* 343(22), 1594-1602.

Liu, T., Zhang, L., Joo, D., & Sun, S. C. Nf-kappab signaling in inflammation. (2017). *Signal Transduct Target Ther,* 2.

Liu, Y. Z., Y.; Schmelzer, K.; Lee, T. S.; Fang, X.; Zhu, Y.; Spector, A. A.; Gill, S.; Morisseau, C.; Hammock, B. D. and Shyy, J. Y. J. The antiinflammatory effect of laminar flow: The role of pparγ, epoxyeicosatrienoic acids, and soluble epoxide hydrolase. (2005). *Proc Natl Acad Sci U S A. ,* 102(46), 16747-16752.

Lomazzo, E., Bindila, L., Remmers, F., Lerner, R., Schwitter, C., Hoheisel, U., et al. Therapeutic potential of inhibitors of endocannabinoid degradation for the treatment of stress-related hyperalgesia in an animal model of chronic pain. (2015). *Neuropsychopharmacology,* 40(2), 488-501.

Lotsch, J., Weyer-Menkhoff, I., & Tegeder, I. Current evidence of cannabinoid-based analgesia obtained in preclinical and human experimental settings. (2018). *Eur J Pain,* 22(3), 471-484.

Lowin, T., Apitz, M., Anders, S., & Straub, R. H. Anti-inflammatory effects of n-acylethanolamines in rheumatoid arthritis synovial cells are mediated by trpv1 and trpa1 in a cox-2 dependent manner. (2015). *Arthritis Res Ther,* 17, 321.

Lowin, T., Zhu, W., Dettmer-Wilde, K., & Straub, R. H. Cortisol-mediated adhesion of synovial fibroblasts is dependent on the degradation of anandamide and activation of the endocannabinoid system. (2012). *Arthritis Rheum,* 64(12), 3867-3876.

Luzzati, V. a. T., A. Lipid phases: Structure and structural transitions. (1974). *Annu. Rev. Phys. Chem. ,* 25, 79-94.

Maccarrone, M. Metabolism of the endocannabinoid anandamide: Open questions after 25 years. (2017). *Front Mol Neurosci,* 10, 166.

Maccarrone, M., Bab, I., Biro, T., Cabral, G. A., Dey, S. K., Di Marzo, V., et al. Endocannabinoid signaling at the periphery: 50 years after thc. (2015). *Trends Pharmacol Sci,* 36(5), 277-296.

Maccarrone, M., van der Stelt, M., Rossi, A., Veldink, G. A., Vliegenthart, J. F., & Agro, A. F. Anandamide hydrolysis by human cells in culture and brain. (1998). *J Biol Chem,* 273(48), 32332-32339.

Malek, N., Mrugala, M., Makuch, W., Kolosowska, N., Przewlocka, B., Binkowski, M., et al. A multi-target approach for pain treatment: Dual inhibition of fatty acid amide hydrolase and trpv1 in a rat model of osteoarthritis. (2015). *Pain,* 156(5), 890-903.

Malfait, A. M., Gallily, R., Sumariwalla, P. F., Malik, A. S., Andreakos, E., Mechoulam, R., et al. The nonpsychoactive cannabis constituent cannabidiol is an oral anti-arthritic therapeutic in murine collagen-induced arthritis. (2000). *Proc Natl Acad Sci U S A,* 97(17), 9561-9566.

Manolios N, C. S., Taylor J, et al. . T-cell antigen receptor transmembrane peptide modulate y-cell function and t-cell mediated disease. (1997). *Nat Med* 3, 84-88.

Matsuda, L. A., Lolait, S. J., Brownstein, M. J., Young, A. C., & Bonner, T. I. Structure of a cannabinoid receptor and functional expression of the cloned cdna. (1990). *Nature,* 346(6284), 561-564.

Maurelli, S., Bisogno, T., De Petrocellis, L., Di Luccia, A., Marino, G., & Di Marzo, V. Two novel classes of neuroactive fatty acid amides are substrates for mouse neuroblastoma 'anandamide amidohydrolase'. (1995). *FEBS Lett,* 377(1), 82-86.

McDougall, J. J. Arthritis and pain. Neurogenic origin of joint pain. (2006). *Arthritis Res Ther,* 8(6), 220.

McDougall, J. J., Muley, M. M., Philpott, H. T., Reid, A., & Krustev, E. Early blockade of joint inflammation with a fatty acid amide hydrolase inhibitor decreases end-stage osteoarthritis pain and peripheral neuropathy in mice. (2017). *Arthritis Res Ther,* 19(1), 106.

Mechoulam, R., Ben-Shabat, S., Hanus, L., Ligumsky, M., Kaminski, N. E., Schatz, A. R., et al. Identification of an endogenous 2-monoglyceride, present in canine gut, that binds to cannabinoid receptors. (1995). *Biochem Pharmacol,* 50(1), 83-90.

Melis, M., Carta, G., Pistis, M., & Banni, S. Physiological role of peroxisome proliferator-activated receptors type alpha on dopamine systems. (2013). *CNS Neurol Disord Drug Targets,* 12(1), 70-77.

Mi, Z., Lu, X., Mai, J. C., Ng, B. G., Wang, G., Lechman, E. R., et al. Identification of a synovial fibroblast-specific protein transduction domain for delivery of apoptotic agents to hyperplastic synovium. (2003). *Mol Ther,* 8(2), 295-305.

Milind, P., & Monu, Y. Laboratory models for screening analgesics. (2012). *International research journal of pharmacy,* 4(1), 15-19.

Mirsafian, H., Manda, S. S., Mitchell, C. J., Sreenivasamurthy, S., Ripen, A. M., Mohamad, S. B., et al. Long non-coding rna expression in primary human monocytes. (2016). *Genomics,* 108(1), 37-45.

Moghimi, S. M., & Hunter, A. C. Capture of stealth nanoparticles by the body's defences. (2001). *Crit Rev Ther Drug Carrier Syst,* 18(6), 527-550.

Moghimi, S. M., Hunter, A. C., & Murray, J. C. Long-circulating and target-specific nanoparticles: Theory to practice. (2001). *Pharmacol Rev,* 53(2), 283-318.

Mouslech, Z., & Valla, V. Endocannabinoid system: An overview of its potential in current medical practice. (2009). *Neuro Endocrinol Lett,* 30(2), 153-179.

Mulet, X. G., X.;Waddington, L. J.; Drummond, C. J. . Observation of intermediates in lamellar to cubic phase transformations of lipid nanoparticles. (2010). *Biophys. J.,* 98, 286a–287a.

Naor, D., & Nedvetzki, S. Cd44 in rheumatoid arthritis. (2003). *Arthritis Res Ther,* 5(3), 105-115.

Nakayama, T., Mutsuga, N., Yao, L., & Tosato G. Prostaglandin E2 promotes degranulation-independent release of MCP-1 from mast cells. (2006). J Leukoc Biol, 79(1):95-104.

Node, K., Huo, Y., Ruan, X., Yang, B., Spiecker, M., Ley, K., et al. Anti-inflammatory properties of cytochrome p450 epoxygenase-derived eicosanoids. (1999). *Science,* 285(5431), 1276-1279.

Noss, E. H., & Brenner, M. B. The role and therapeutic implications of fibroblast-like synoviocytes in inflammation and cartilage erosion in rheumatoid arthritis. (2008). *Immunol Rev,* 223, 252-270.

Nourshargh, S., & Alon, R. Leukocyte migration into inflamed tissues. (2014). *Immunity,* 41(5), 694-707.

Nunez, V., Alameda, D., Rico, D., Mota, R., Gonzalo, P., Cedenilla, M., et al. Retinoid x receptor alpha controls innate inflammatory responses through the up-regulation of chemokine expression. (2010). *Proc Natl Acad Sci U S A,* 107(23), 10626-10631.

O'Hearn, S., Diaz, P., Wan, B. A., DeAngelis, C., Lao, N., Malek, L., et al. Modulating the endocannabinoid pathway as treatment for peripheral neuropathic pain: A selected review of preclinical studies. (2017). *Ann Palliat Med,* 6(Suppl 2), S209-S214.

Ogawa, S., Lozach, J., Benner, C., Pascual, G., Tangirala, R. K., Westin, S., et al. Molecular determinants of crosstalk between nuclear receptors and toll-like receptors. (2005). *Cell,* 122(5), 707-721.

Okamoto, Y., Morishita, J., Tsuboi, K., Tonai, T., & Ueda, N. Molecular characterization of a phospholipase d generating anandamide and its congeners. (2004). *J Biol Chem,* 279(7), 5298-5305.

Onuora, S. Rheumatoid arthritis: Can tofacitinib be used as first-line monotherapy for ra? (2014). *Nat Rev Rheumatol,* 10(8), 443.

Overton, H. A., Babbs, A. J., Doel, S. M., Fyfe, M. C., Gardner, L. S., Griffin, G., et al. Deorphanization of a g protein-coupled receptor for oleoylethanolamide and its use in the discovery of small-molecule hypophagic agents. (2006). *Cell Metab,* 3(3), 167-175.

Ozdemir, B., Shi, B., Bantleon, H. P., Moritz, A., Rausch-Fan, X., & Andrukhov, O. Endocannabinoids and inflammatory response in periodontal ligament cells. (2014). *PLoS One,* 9(9), e107407.

Pacher, P., & Kunos, G. Modulating the endocannabinoid system in human health and disease--successes and failures. (2013). *FEBS J,* 280(9), 1918-1943.

Park, J., Fong, P. M., Lu, J., Russell, K. S., Booth, C. J., Saltzman, W. M., et al. Pegylated plga nanoparticles for the improved delivery of doxorubicin. (2009). *Nanomedicine,* 5(4), 410-418.

Parkkari, T., Salo, O. M., Huttunen, K. M., Savinainen, J. R., Laitinen, J. T., Poso, A., et al. Synthesis and cb1 receptor activities of dimethylheptyl derivatives of 2-arachidonoyl glycerol (2-ag) and 2-arachidonyl glyceryl ether (2-age). (2006). *Bioorg Med Chem,* 14(8), 2850-2858.

Pasut, G. V., F. M. State of the art in pegylation: The great versatility achieved after forty years of research. (2012). *J Control Release,* 161(2), 461-472.

Patti, F., Messina, S., Solaro, C., Amato, M. P., Bergamaschi, R., Bonavita, S., et al. Efficacy and safety of cannabinoid oromucosal spray for multiple sclerosis spasticity. (2016). *J Neurol Neurosurg Psychiatry,* 87(9), 944-951.

Pernia-Andrade, A. J., Kato, A., Witschi, R., Nyilas, R., Katona, I., Freund, T. F., et al. Spinal endocannabinoids and cb1 receptors mediate c-fiber-induced heterosynaptic pain sensitization. (2009). *Science,* 325(5941), 760-764.

Pertwee, R. G. The pharmacology of cannabinoid receptors and their ligands: An overview. (2006). *Int J Obes (Lond),* 30 Suppl 1, S13-18.

Petros, R. A., & DeSimone, J. M. Strategies in the design of nanoparticles for therapeutic applications. (2010). *Nat Rev Drug Discov,* 9(8), 615-627.

Philpott, H. T., O'Brien, M., & McDougall, J. J. Attenuation of early phase inflammation by cannabidiol prevents pain and nerve damage in rat osteoarthritis. (2017). *Pain,* 158(12), 2442-2451.

Piomelli, D., & Sasso, O. Peripheral gating of pain signals by endogenous lipid mediators. (2014). *Nat Neurosci,* 17(2), 164-174.

Pitzalis, C., Kelly, S., & Humby, F. New learnings on the pathophysiology of ra from synovial biopsies. (2013). *Curr Opin Rheumatol,* 25(3), 334-344.

Porter, A. C., Sauer, J. M., Knierman, M. D., Becker, G. W., Berna, M. J., Bao, J., et al. Characterization of a novel endocannabinoid, virodhamine, with antagonist activity at the cb1 receptor. (2002). *J Pharmacol Exp Ther,* 301(3), 1020-1024.

Premkumar, L. S., & Sikand, P. Trpv1: A target for next generation analgesics. (2008). *Curr Neuropharmacol,* 6(2), 151-163.

Quan, L., Zhang, Y., Crielaard, B. J., Dusad, A., Lele, S. M., Rijcken, C. J. F., et al. Nanomedicines for inflammatory arthritis: Head-to-head comparison of glucocorticoid-containing polymers, micelles, and liposomes. (2014). *ACS Nano,* 8(1), 458-466.

Rani Sagar, D., Burston, J. J., Woodhams, S. G., & Chapman, V. Dynamic changes to the endocannabinoid system in models of chronic pain. (2012). *Philos Trans R Soc Lond B Biol Sci,* 367(1607), 3300-3311.

Redmond, W. J., Gu, L., Camo, M., McIntyre, P., & Connor, M. Ligand determinants of fatty acid activation of the pronociceptive ion channel trpa1. (2014). *PeerJ,* 2, e248.

Richardson, D., Pearson, R. G., Kurian, N., Latif, M. L., Garle, M. J., Barrett, D. A., et al. Characterisation of the cannabinoid receptor system in synovial tissue and fluid in patients with osteoarthritis and rheumatoid arthritis. (2008). *Arthritis Res Ther,* 10(2), R43.

Ridgley, L. A., Anderson, A. E., & Pratt, A. G. What are the dominant cytokines in early rheumatoid arthritis? (2017). *Curr Opin Rheumatol,* 30(2), 207-214.

Robson, P. Human studies of cannabinoids and medicinal cannabis. (2005). *Handb Exp Pharmacol*(168), 719-756.

Romano, A., Coccurello, R., Giacovazzo, G., Bedse, G., Moles, A., & Gaetani, S. Oleoylethanolamide: A novel potential pharmacological alternative to cannabinoid antagonists for the control of appetite. (2014). *Biomed Res Int,* 2014, 203425.

Rosevear, F. B. The microscopy of the liquid crystalline neat and middle phases of soaps and synthetic detergents. (1954). *J Am Oil Chem Soc,* 31, 628–639.

Ross, R. A. Anandamide and vanilloid trpv1 receptors. (2003). *Br J Pharmacol,* 140(5), 790-801.

Ruiz-Medina, J., Flores, J. A., Tasset, I., Tunez, I., Valverde, O., & Fernandez-Espejo, E. Alteration of neuropathic and visceral pain in female c57bl/6j mice lacking the ppar-alpha gene. (2012). *Psychopharmacology (Berl),* 222(3), 477-488.

Ryberg, E., Larsson, N., Sjogren, S., Hjorth, S., Hermansson, N. O., Leonova, J., et al. The orphan receptor gpr55 is a novel cannabinoid receptor. (2007). *Br J Pharmacol,* 152(7), 1092-1101.

Sagnella, S. M., Conn, C. E., Krodkiewska, I., Moghaddam, M., & Drummond, C. J. Endogenous nonionic saturated monoethanolamide lipids: Solid state, lyotropic liquid crystalline, and solid lipid nanoparticle dispersion behavior. (2010a). *J Phys Chem B,* 114(4), 1729-1737.

Sagnella, S. M., Conn, C. E., Krodkiewska, I., Moghaddam, M., Seddon, J. M., & Drummond, C. J. Soft ordered mesoporous materials from nonionic isoprenoid-type monoethanolamide amphiphiles self-assembled in water. . (2009a). *Soft Matter,* 5, 4823-4834.

Sagnella, S. M., Conn, C. E., Krodkiewska, I., Moghaddam, M., Seddon, J. M., & Drummond, C. J. Soft ordered mesoporous materials from nonionic isoprenoid-type monoethanolamide amphiphiles self-assembled in water. (2009b). *Soft Matter,* 5, 4823–4834.

Sagnella, S. M., Conn, C. E., Krodkiewska, I., Moghaddam, M., Seddon, J. M., & Drummond, C. J. Ordered nanostructured amphiphile self-assembly materials from endogenous nonionic unsaturated monoethanolamide lipids in water. (2010b). *Langmuir,* 26(5), 3084-3094.

Salaga, M., Sobczak, M., & Fichna, J. Inhibition of fatty acid amide hydrolase (faah) as a novel therapeutic strategy in the treatment of pain and inflammatory diseases in the gastrointestinal tract. (2014). *Eur J Pharm Sci,* 52, 173-179.

Sancho, R., Calzado, M. A., Di Marzo, V., Appendino, G., & Munoz, E. Anandamide inhibits nuclear factor-kappab activation through a cannabinoid receptor-independent pathway. (2003). *Mol Pharmacol,* 63(2), 429-438.

Sanders, C. R. P., R.S. . Bicelles: A model membrane system for all seasons? . (1998). *Structure,* 6, 1227–1234.

Sasso, O., Bertorelli, R., Bandiera, T., Scarpelli, R., Colombano, G., Armirotti, A., et al. Peripheral faah inhibition causes profound antinociception and protects against indomethacin-induced gastric lesions. (2012). *Pharmacol Res,* 65(5), 553-563.

Sayd, A., Anton, M., Alen, F., Caso, J. R., Pavon, J., Leza, J. C., et al. Systemic administration of oleoylethanolamide protects from neuroinflammation and anhedonia induced by lps in rats. (2014). *Int J Neuropsychopharmacol,* 18(6).

Scanzello, C. R. Chemokines and inflammation in osteoarthritis: Insights from patients and animal models. (2017). *J Orthop Res,* 35(4), 735-739.

Schuelert, N., Johnson, M. P., Oskins, J. L., Jassal, K., Chambers, M. G., & McDougall, J. J. Local application of the endocannabinoid hydrolysis inhibitor urb597 reduces nociception in spontaneous and chemically induced models of osteoarthritis. (2011). *Pain,* 152(5), 975-981.

Schuelert, N., & McDougall, J. J. Cannabinoid-mediated antinociception is enhanced in rat osteoarthritic knees. (2008). *Arthritis Rheum,* 58(1), 145-153.

Schuelert, N., Zhang, C., Mogg, A. J., Broad, L. M., Hepburn, D. L., Nisenbaum, E. S., et al. Paradoxical effects of the cannabinoid cb2 receptor agonist gw405833 on rat osteoarthritic knee joint pain. (2010). *Osteoarthritis Cartilage,* 18(11), 1536-1543.

Scotter, E. L., Abood, M. E., & Glass, M. The endocannabinoid system as a target for the treatment of neurodegenerative disease. (2010). *Br J Pharmacol,* 160(3), 480-498.

Seddon, J. M. Structure of the inverted hexagonal (hii) phase, and non-lamellar phase transitions of lipids. (1990). *Biochim. Biophys. Acta* 1031, 1-69.

Seddon, J. M. T., R.H. Cubic phases of self-assembled amphiphilic aggregates. (1993). *Philos. Trans. Math. Phys. Eng. Sci. ,* 344, 377–401.

Seddon, J. M. Z., N.; Templer, R.H.; McElhaney, R.N.; Mannock, D.A. . An fd3m lyotropic cubic phase in a binary glycolipid/water system. (1996). *Langmuir,* 12, 5250–5253.

Seol, T. K., Lee, W., Park, S., Kim, K. N., Kim, T. Y., Oh, Y. N., et al. Effect of palmitoylethanolamide on inflammatory and neuropathic pain in rats. (2017). *Korean J Anesthesiol,* 70(5), 561-566.

Sharma, G., Saini, M. K., Thakur, K., Kapil, N., Garg, N. K., Raza, K., et al. Aceclofenac cocrystal nanoliposomes for rheumatoid arthritis with better dermatokinetic attributes: A preclinical study. (2017). *Nanomedicine (Lond),* 12(6), 615-638.

Shin, J. M., Kim, S. H., Thambi, T., You, D. G., Jeon, J., Lee, J. O., et al. A hyaluronic acid-methotrexate conjugate for targeted therapy of rheumatoid arthritis. (2014). *Chem Commun (Camb),* 50(57), 7632-7635.

Skaper, S. D., Facci, L., Barbierato, M., Zusso, M., Bruschetta, G., Impellizzeri, D., et al. N-palmitoylethanolamine and neuroinflammation: A novel therapeutic strategy of resolution. (2015). *Mol Neurobiol,* 52(2), 1034-1042.

Smart, D., Gunthorpe, M. J., Jerman, J. C., Nasir, S., Gray, J., Muir, A. I., et al. The endogenous lipid anandamide is a full agonist at the human vanilloid receptor (hvr1). (2000). *Br J Pharmacol,* 129(2), 227-230.

Smith, P. A., Selley, D. E., Sim-Selley, L. J., & Welch, S. P. Low dose combination of morphine and delta9-tetrahydrocannabinol circumvents antinociceptive tolerance and apparent desensitization of receptors. (2007). *Eur J Pharmacol,* 571(2-3), 129-137.

Snider, N. T., Nast, J. A., Tesmer, L. A., & Hollenberg, P. F. A cytochrome p450-derived epoxygenated metabolite of anandamide is a potent cannabinoid receptor 2-selective agonist. (2009). *Mol Pharmacol,* 75(4), 965-972.

Snipstad, S., Hak, S., Baghirov, H., Sulheim, E., Morch, Y., Lelu, S., et al. Labeling nanoparticles: Dye leakage and altered cellular uptake. (2017). *Cytometry A,* 91(8), 760-766.

Souhami, R. L., Patel, H. M., & Ryman, B. E. The effect of reticuloendothelial blockade on the blood clearance and tissue distribution of liposomes. (1981). *Biochim Biophys Acta,* 674(3), 354-371.

Spicer, P. T. Progress in liquid crystalline dispersions: Cubosomes. (2005). *Curr Opin Colloid Interface Sci* (10), 274-279.

Stankovic, A., Slavic, V., Stamenkovic, B., Kamenov, B., Bojanovic, M., & Mitrovic, D. R. Serum and synovial fluid concentrations of ccl2 (mcp-1) chemokine in patients suffering rheumatoid arthritis and osteoarthritis reflect disease activity. (2009). *Bratisl Lek Listy,* 110(10), 641-646.

Starowicz, K., & Przewlocka, B. Modulation of neuropathic-pain-related behaviour by the spinal endocannabinoid/endovanilloid system. (2012). *Philos Trans R Soc Lond B Biol Sci,* 367(1607), 3286-3299.

Staton, P. C., Hatcher, J. P., Walker, D. J., Morrison, A. D., Shapland, E. M., Hughes, J. P., et al. The putative cannabinoid receptor gpr55 plays a role in mechanical hyperalgesia associated with inflammatory and neuropathic pain. (2008). *Pain,* 139(1), 225-236.

Stockings, E., Campbell, G., Hall, W. D., Nielsen, S., Zagic, D., Rahman, R., et al. Cannabis and cannabinoids for the treatment of people with chronic non-cancer pain conditions: A systematic review and meta-analysis of controlled and observational studies. (2018). *Pain*.

Stuart, J. M., Paris, J. J., Frye, C., & Bradshaw, H. B. Brain levels of prostaglandins, endocannabinoids, and related lipids are affected by mating strategies. (2013). *Int J Endocrinol,* 2013, 436252.

Suardiaz, M., Estivill-Torrus, G., Goicoechea, C., Bilbao, A., & Rodriguez de Fonseca, F. Analgesic properties of oleoylethanolamide (oea) in visceral and inflammatory pain. (2007). *Pain,* 133(1-3), 99-110.

Sugiura, T., Kobayashi, Y., Oka, S., & Waku, K. Biosynthesis and degradation of anandamide and 2-arachidonoylglycerol and their possible physiological significance. (2002). *Prostaglandins Leukot Essent Fatty Acids,* 66(2-3), 173-192.

Suk, J. S., Xu, Q., Kim, N., Hanes, J., & Ensign, L. M. Pegylation as a strategy for improving nanoparticle-based drug and gene delivery. (2016). *Adv Drug Deliv Rev,* 99(Pt A), 28-51.

Sumariwalla, P. F., Gallily, R., Tchilibon, S., Fride, E., Mechoulam, R., & Feldmann, M. A novel synthetic, nonpsychoactive cannabinoid acid (hu-320) with antiinflammatory properties in murine collagen-induced arthritis. (2004). *Arthritis Rheum,* 50(3), 985-998.

Sun, L., Tai, L., Qiu, Q., Mitchell, R., Fleetwood-Walker, S., Joosten, E. A., et al. Endocannabinoid activation of cb1 receptors contributes to long-lasting reversal of neuropathic pain by repetitive spinal cord stimulation. (2017). *Eur J Pain,* 21(5), 804-814.

Szabo, A., Helyes, Z., Sandor, K., Bite, A., Pinter, E., Nemeth, J., et al. Role of transient receptor potential vanilloid 1 receptors in adjuvant-induced chronic arthritis: In vivo study using gene-deficient mice. (2005). *J Pharmacol Exp Ther,* 314(1), 111-119.

Talwar, R., & Potluri, V. K. Cannabinoid 1 (cb1) receptor--pharmacology, role in pain and recent developments in emerging cb1 agonists. (2011). *CNS Neurol Disord Drug Targets,* 10(5), 536-544.

Thomson, S. J., Askari, A., & Bishop-Bailey, D. Anti-inflammatory effects of epoxyeicosatrienoic acids. (2012). *Int J Vasc Med,* 2012, 605101.

Tsutsumi, H., Tanaka, T., Ohashi, N., Masuno, H., Tamamura, H., Hiramatsu, K., et al. Therapeutic potential of the chemokine receptor cxcr4 antagonists as multifunctional agents. (2007). *Biopolymers,* 88(2), 279-289.

Turcotte, C., Chouinard, F., Lefebvre, J. S., & Flamand, N. Regulation of inflammation by cannabinoids, the endocannabinoids 2-arachidonoyl-glycerol and arachidonoyl-ethanolamide, and their metabolites. (2015). *J Leukoc Biol,* 97(6), 1049-1070.

Turner, R. A. Central stimulants in screening methods in pharmacology,. (2009). *Academic press Elsevier,* 1(178-189).

Ueda, N., Tsuboi, K., Uyama, T., & Ohnishi, T. Biosynthesis and degradation of the endocannabinoid 2-arachidonoylglycerol. (2011). *Biofactors,* 37(1), 1-7.

van der Heijden, J. W., Oerlemans, R., Dijkmans, B. A., Qi, H., van der Laken, C. J., Lems, W. F., et al. Folate receptor beta as a potential delivery route for novel folate antagonists to macrophages in the synovial tissue of rheumatoid arthritis patients. (2009). *Arthritis Rheum,* 60(1), 12-21.

Vanniasinghe, A. S., Manolios, N., Schibeci, S., Lakhiani, C., Kamali-Sarvestani, E., Sharma, R., et al. Targeting fibroblast-like synovial cells at sites of inflammation with peptide targeted liposomes results in inhibition of experimental arthritis. (2014). *Clin Immunol,* 151(1), 43-54.

Vincenti, M. P., & Brinckerhoff, C. E. Transcriptional regulation of collagenase (mmp-1, mmp-13) genes in arthritis: Integration of complex signaling pathways for the recruitment of gene-specific transcription factors. (2002). *Arthritis Res,* 4(3), 157-164.

Walitt, B., Klose, P., Fitzcharles, M. A., Phillips, T., & Hauser, W. Cannabinoids for fibromyalgia. (2016). *Cochrane Database Syst Rev,* 7, CD011694.

Walker, J. M., & Huang, S. M. Endocannabinoids in pain modulation. (2002). *Prostaglandins Leukot Essent Fatty Acids,* 66(2-3), 235-242.

Wang, X., Li, J., Wang, Y., Cho, K. J., Kim, G., Gjyrezi, A., et al. Hft-t, a targeting nanoparticle, enhances specific delivery of paclitaxel to folate receptor-positive tumors. (2009). *ACS Nano,* 3(10), 3165-3174.

Wang, Z. Y., McDowell, T., Wang, P., Alvarez, R., Gomez, T., & Bjorling, D. E. Activation of cb1 inhibits ngf-induced sensitization of trpv1 in adult mouse afferent neurons. (2014). *Neuroscience,* 277, 679-689.

Ware, M. A., Adams, H., & Guy, G. W. The medicinal use of cannabis in the uk: Results of a nationwide survey. (2005). *Int J Clin Pract,* 59(3), 291-295.

Ware, M. A., & Tawfik, V. L. Safety issues concerning the medical use of cannabis and cannabinoids. (2005). *Pain Res Manag,* 10 Suppl A, 31A-37A.

Warheit, D. B. Debunking some misconceptions about nanotoxicology. (2010). *Nano Lett,* 10(12), 4777-4782.

Weissig, V., Pettinger, T. K., & Murdock, N. Nanopharmaceuticals (part 1): Products on the market. (2014). *Int J Nanomedicine,* 9, 4357-4373.

Wilder, R. L. Integrin alpha v beta 3 as a target for treatment of rheumatoid arthritis and related rheumatic diseases. (2002). *Ann Rheum Dis,* 61 Suppl 2, ii96-99.

Williams, A., Goodfellow, R., Topley, N., Amos, N., & Williams, B. The suppression of rat collagen-induced arthritis and inhibition of macrophage derived mediator release by liposomal methotrexate formulations. (2000). *Inflamm Res,* 49(4), 155-161.

Xu, R., Zhang, G., Mai, J., Deng, X., Segura-Ibarra, V., Wu, S., et al. An injectable nanoparticle generator enhances delivery of cancer therapeutics. (2016). *Nat Biotechnol,* 34(4), 414-418.

Yang, L., Guo, H., Li, Y., Meng, X., Yan, L., Dan, Z., et al. Oleoylethanolamide exerts anti-inflammatory effects on lps-induced thp-1 cells by enhancing pparalpha signaling and inhibiting the nf-kappab and erk1/2/ap-1/stat3 pathways. (2016). *Sci Rep,* 6, 34611.

Yang, Y. H., Rajaiah, R., Ruoslahti, E., & Moudgil, K. D. Peptides targeting inflamed synovial vasculature attenuate autoimmune arthritis. (2011). *Proc Natl Acad Sci U S A,* 108(31), 12857-12862.

Yao, B. B., Hsieh, G. C., Frost, J. M., Fan, Y., Garrison, T. R., Daza, A. V., et al. In vitro and in vivo characterization of a-796260: A selective cannabinoid cb2 receptor agonist exhibiting analgesic activity in rodent pain models. (2008). *Br J Pharmacol,* 153(2), 390-401.

Zhang, L., & Granick, S. How to stabilize phospholipid liposomes (using nanoparticles). (2006). *Nano Lett,* 6(4), 694-698.

Zhang, L., Gu, F. X., Chan, J. M., Wang, A. Z., Langer, R. S., & Farokhzad, O. C. Nanoparticles in medicine: Therapeutic applications and developments. (2008). *Clin Pharmacol Ther,* 83(5), 761-769.

Zhang, L., Kajiwara, H., Kuboyama, N., & Abiko, Y. Reduction of cxcr4 expression in rheumatoid arthritis rat joints by low level diode laser irradiation. (2011). *Laser Ther,* 20(1), 53-58.

Zhao, Y., Liu, Y., Jing, Z., Peng, L., Jin, P., Lin, Y., et al. N-oleoylethanolamide suppresses intimal hyperplasia after balloon injury in rats through ampk/pparalpha pathway. (2018). *Biochem Biophys Res Commun,* 496(2), 415-421.

Zhou, H., Yang, W. S., Li, Y., Ren, T., Peng, L., Guo, H., et al. Oleoylethanolamide attenuates apoptosis by inhibiting the tlr4/nf-kappab and erk1/2 signaling pathways in mice with acute ischemic stroke. (2017a). *Naunyn Schmiedebergs Arch Pharmacol,* 390(1), 77-84.

Zhou, H. F., Chan, H. W., Wickline, S. A., Lanza, G. M., & Pham, C. T. Alphavbeta3-targeted nanotherapy suppresses inflammatory arthritis in mice. (2009). *FASEB J,* 23(9), 2978-2985.

Zhou, H. F., Yan, H., Hu, Y., Springer, L. E., Yang, X., Wickline, S. A., et al. Fumagillin prodrug nanotherapy suppresses macrophage inflammatory response via endothelial nitric oxide. (2014). *ACS Nano,* 8(7), 7305-7317.

Zhou, J., Ren, T., Li, Y., Cheng, A., Xie, W., Xu, L., et al. Oleoylethanolamide inhibits alpha-melanocyte stimulating hormone-stimulated melanogenesis via erk, akt and creb signaling pathways in b16 melanoma cells. (2017b). *Oncotarget,* 8(34), 56868-56879.

Zogopoulos, P., Vasileiou, I., Patsouris, E., & Theocharis, S. E. The role of endocannabinoids in pain modulation. (2013). *Fundam Clin Pharmacol,* 27(1), 64-80.

Zou, S., & Kumar, U. Cannabinoid receptors and the endocannabinoid system: Signaling and function in the central nervous system. (2018). *Int J Mol Sci,* 19(3).

Zurier, R. B. Prospects for cannabinoids as anti-inflammatory agents. (2003). *J Cell Biochem,* 88(3), 462-466.

Zurier, R. B., Rossetti, R. G., Lane, J. H., Goldberg, J. M., Hunter, S. A., & Burstein, S. H. Dimethylheptyl-thc-11 oic acid: A nonpsychoactive antiinflammatory agent with a cannabinoid template structure. (1998). *Arthritis Rheum,* 41(1), 163-170.

APPENDIX 1: NMR traces

NMR traces of synthesised peptides are shown below.

Figure A1.1 NMR Ole-PEG2000-Succ, showing correct peptide structure with mass of 2364.

Figure A1.2 NMR of Ole-PEG2000-HAP, shows populations of correct mass to charge ratios with mass of 3682.

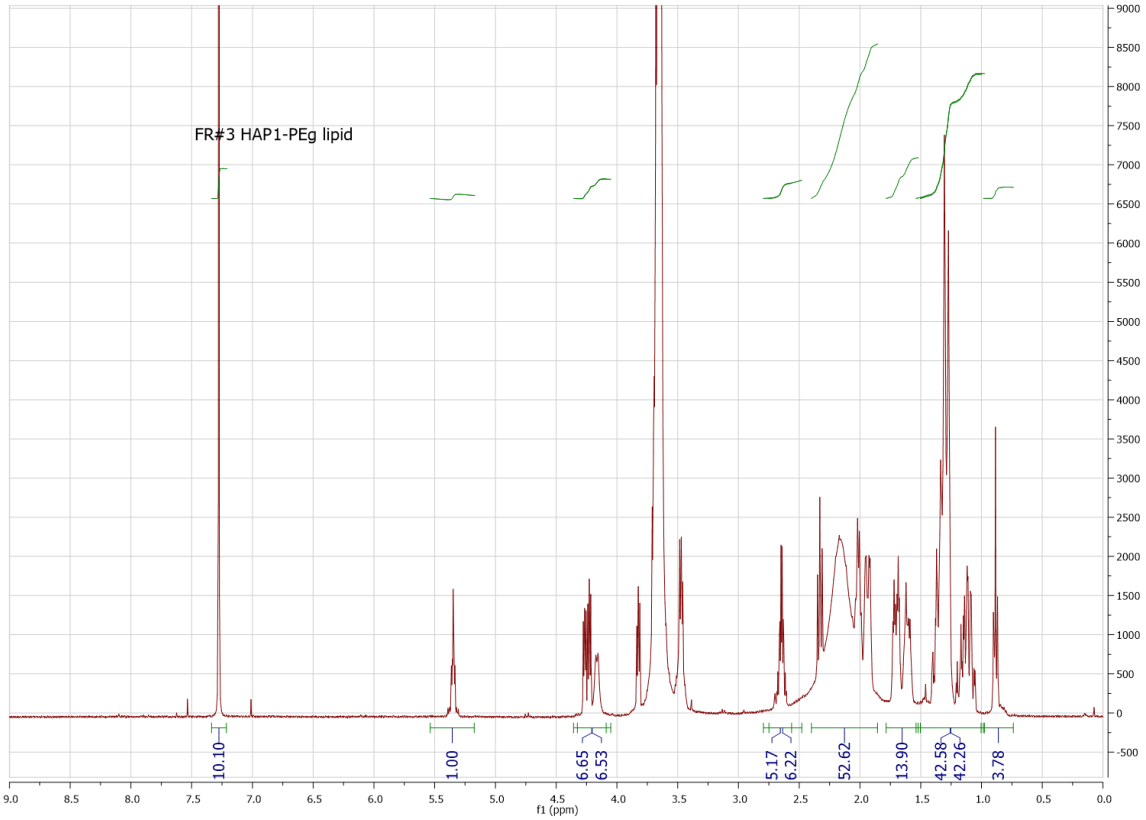

Figure A1.3 NMR analysis of synthesised LEA shows populations of correct mass to charge ratios with mass 323.52.

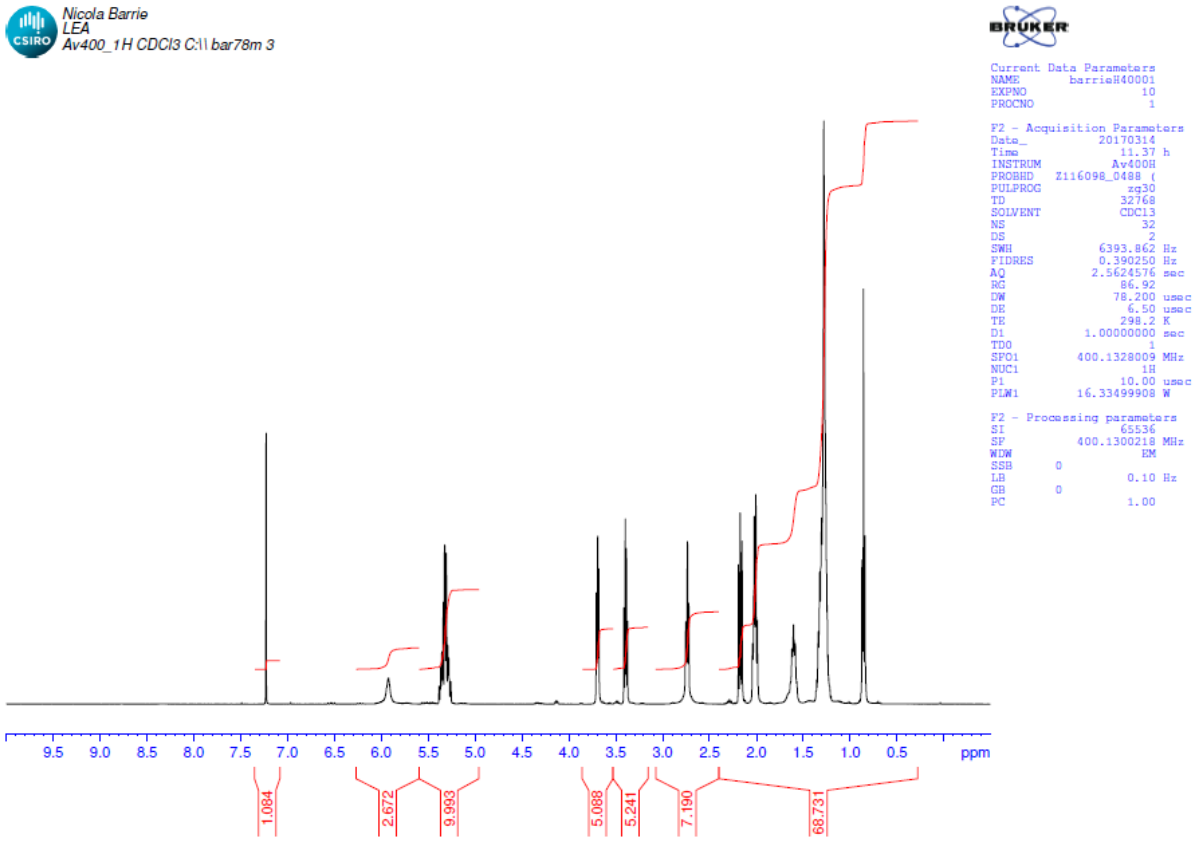

Figure A1.4 NMR analysis of synthesised OEA shows populations of correct mass to charge ratios with mass of 325.54

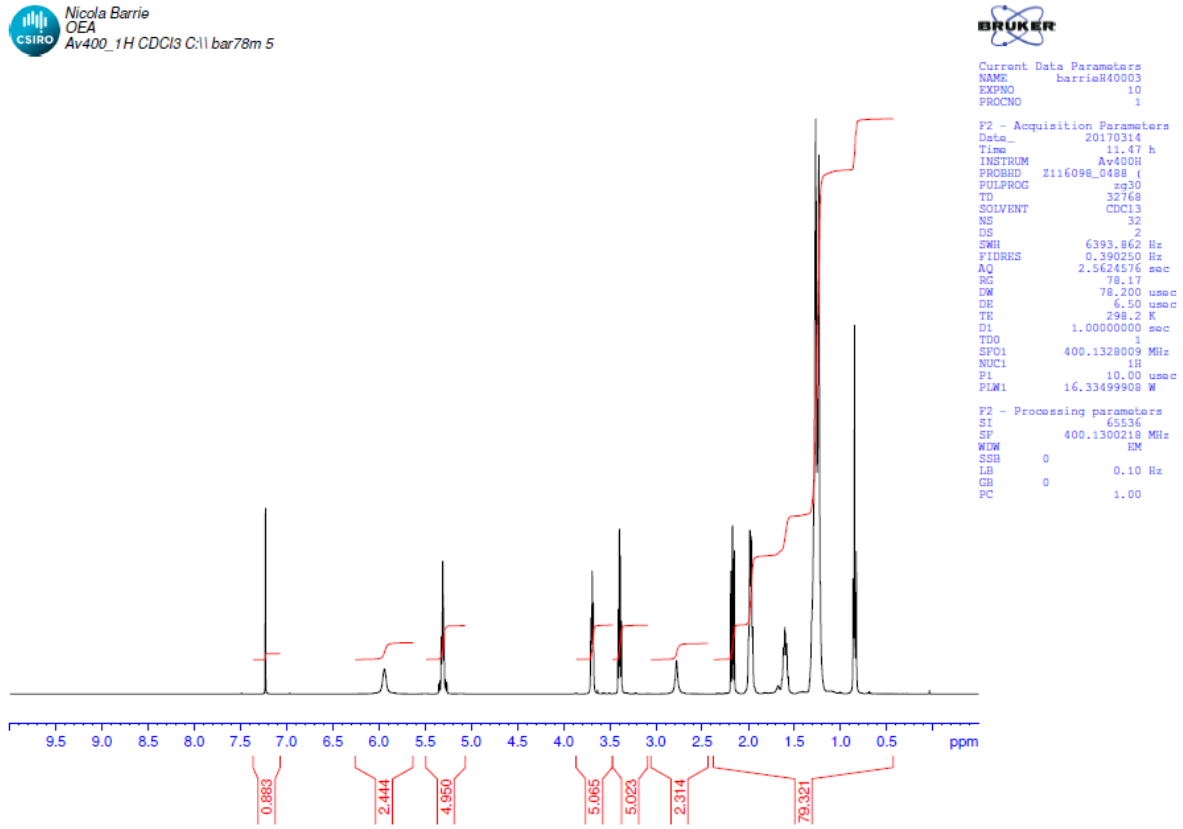

Figure A1.5 NMR analysis of synthesised ɣ-LEA shows populations of correct mass to charge ratios with mass 321.52

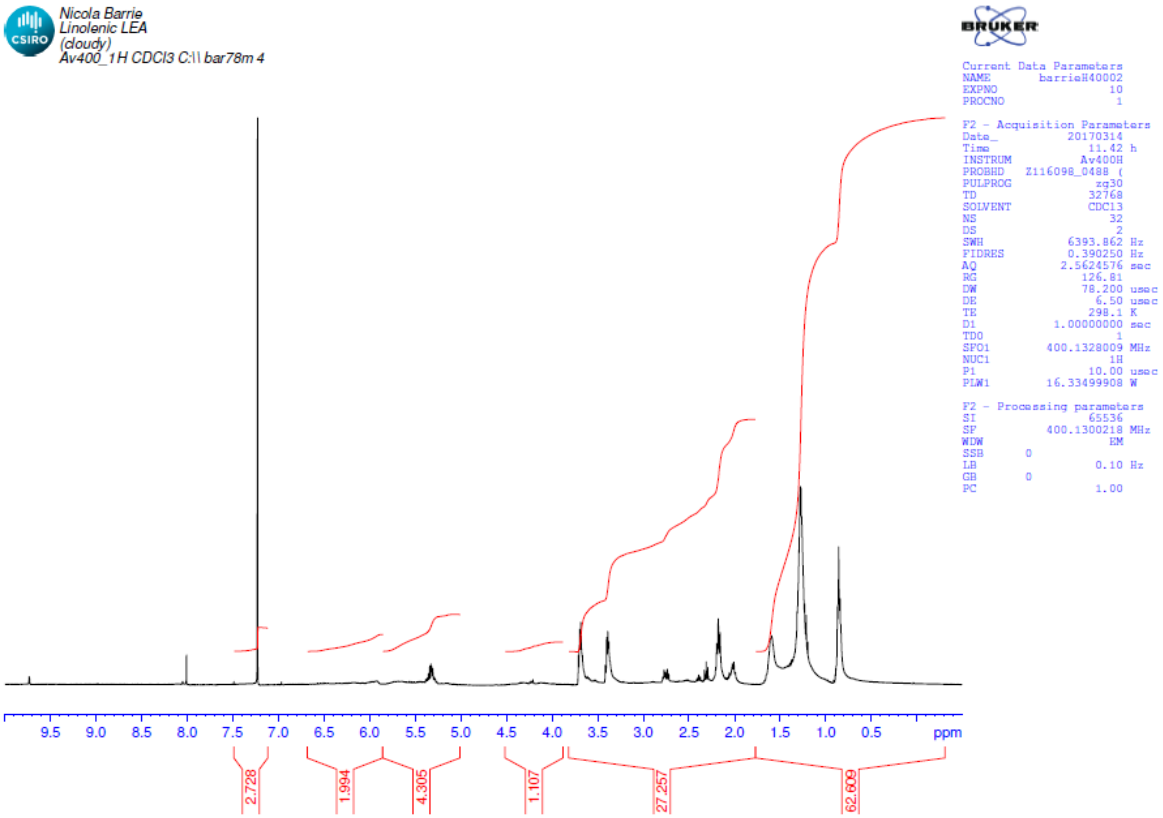

APPENDIX 2: Mass specs and HPLC traces of fully deprotected peptides

Figure A2.1 Fully deprotected homing peptide HAP-1 weighed at 1336, as shown by **(A)** MS and **(B)** HPLC

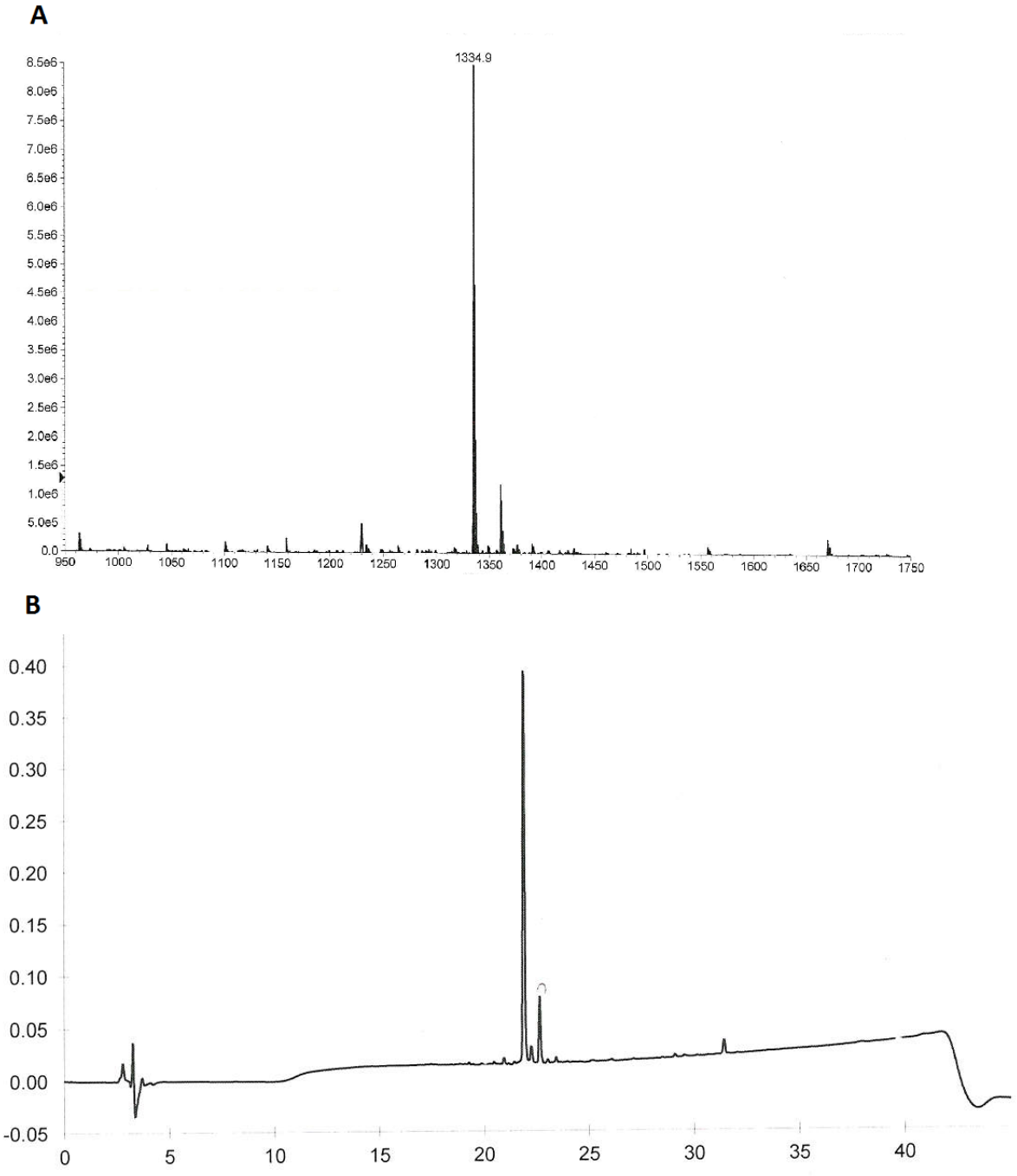

Figure A2.2 Fully deprotected homing peptide sHAP-1 weighed at 1336, as shown by **(A)** MS and **(B)** HPLC

A

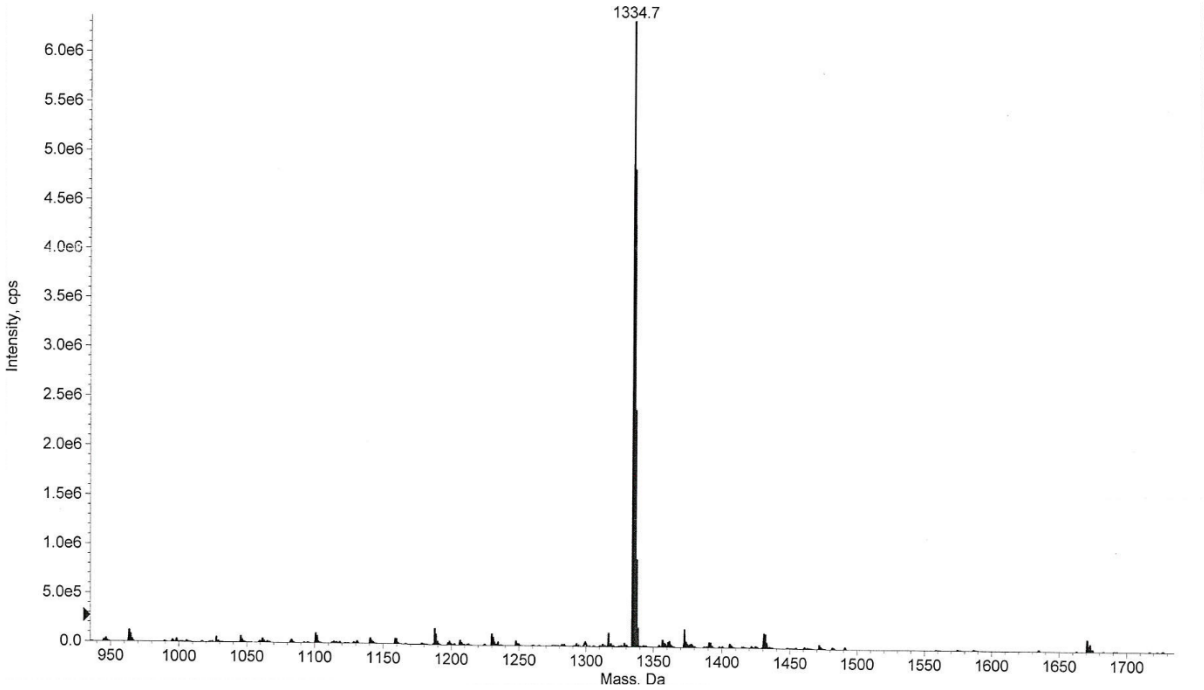

B

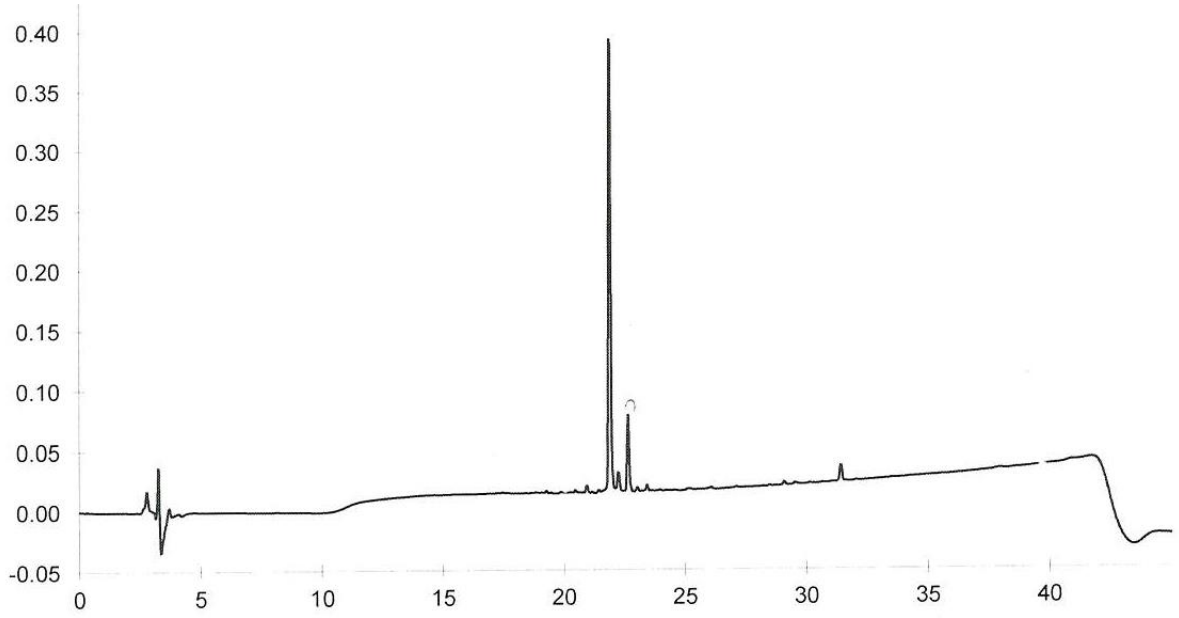

APPENDIX 3: **RNA-seq aw read counts and quality statistics**

Figure A3.1 Summary of raw read count and gene expression statistics for significant and non-significant gene counts.

Groups	Total read count	FDR <0.05 TRUE	FDR <0.05 FALSE	*LFC > 0 (up)	LFC < 0 (down)	Outliers	Low counts
RA-TNF vs RA-UT	28288	9944	7968	4116, 15%	3852, 14%	10, 0.04%	10366, 37%
RA-NP vs RA-UT	28288	9898	5941	2998, 10%	3052, 11%	10, 0.04%	12439, 44%
RA-TNF/NP vs RA-UT	28288	10110	8320	4164, 15%	4156, 15%	10, 0.04%	9848, 35%
RA-TNF/NP vs RA-TNF	28288	10556	7874	3710, 13%	4164, 15%	10, 0.04%	9848, 35%
OA-TNF vs OA-UT	27438	13766	2013	1219, 4.4%	794, 2.9%	137, 0.5%	11522, 42%
OA-TNF/NP vs OA-UT	27438	11499	5282	2484, 9.1%	2798, 10%	137, 0.5%	10520, 38%
OA-TNF/NP vs OA-TNF	27438	12846	3935	1669, 6.1%	2266, 8.3%	137, 0.5%	10520, 38%

* log fold change (LFC)

MA-scatter plots of RNA-seq data

Figure A3.2 MA-scatter plots of microarray spot statistics implementing shrinkage estimators; **(A)** DESeq2 **(B)** Shrunken log2 fold change (LFC) **(C)** Ashr and **(B)** Apeglm.

The x-axis represents the mean of normalised counts. Plot symmetry around the mean, indicates normalisation is fine with equal number of upregulated and downregulated genes. Shrunken LFC is based on DESeq2 original shrinkage estimator: an adaptive Normal distribution as a prior. Ashr is an adaptive shrinkage estimator from the Ashr package (Stephens 2016), DESeq2 can use ashr option to fit a mixture of normal distributions to form the prior. Apeglm is an adaptive t prior shrinkage estimator from Apeglm package.

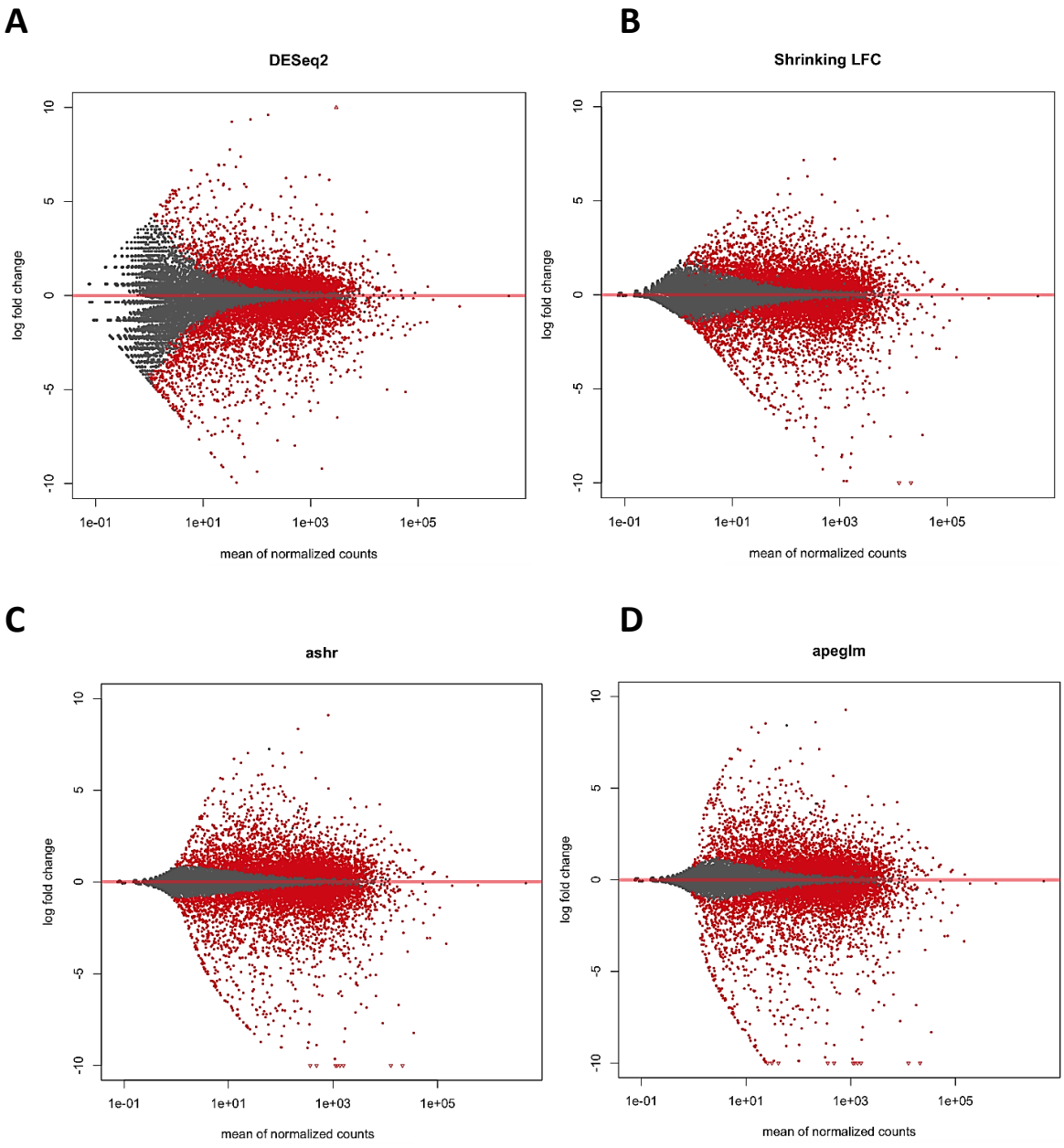

Figure A3.3 MA-scatter plots of microarray spot statistics implementing shrinkage estimators; **(A)** DESeq2 **(B)** Shrunken log2 fold change (LFC) **(C)** Ashr and **(B)** Apeglm.

The x-axis represents the mean of normalised counts. Plot symmetry around the mean, indicates normalisation is fine with equal number of upregulated and downregulated genes. Shrunken LFC is based on DESeq2 original shrinkage estimator: an adaptive Normal distribution as a prior.

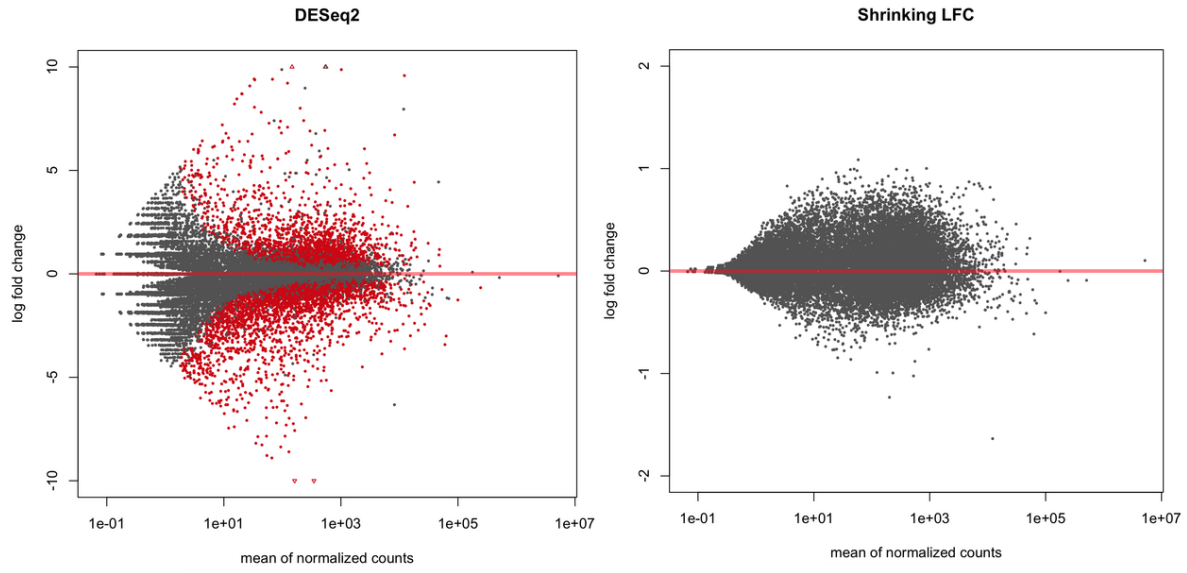

APPENDIX 4: Top 10 DE genes based on comparison of RNA-seq treatment groups

Figure A4.1 Top 10 DE genes based on comparison of RNA-seq data between TNF-α treated (RA-TNF) and non-treated (RA-UT) RA-FLS cells.

Gene	Description	Log2 FC	FDR	Role in RA
Top 10 DE genes				
IBSP	integrin binding sialoprotein	13.357	1.88E-28	bone remodelling
CXCR4	C-X-C motif chemokine receptor 4	12.839	1.2E-25	CXCR4-CXCL12 interaction plays a crucial role in the accumulation of T cells in the RA synovium (Tsutsumi et al., 2007; Zhang et al., 2011)
CXCL5	C-X-C motif chemokine ligand 5	11.767	5.19E-170	Promotes angiogenesis
CCL20	C-C motif chemokine ligand 20	11.706	3.92E-57	Enhance osteoblast-mediated osteoclast genesis
IL1RN	interleukin 1 receptor antagonist	11.65	7.9E-22	Inhibits IL-1 signalling
CXCL8	C-X-C motif chemokine ligand 8	11.523	0	enhance osteoblast-mediated osteoclast genesis
MMP3	matrix metallopeptidase 3	11.189	1.81E-39	breakdown of ECM
IL23A	interleukin 23 subunit alpha	10.157	1.12E-16	Differentiation of Th17 cells, osteoclastogenesis through RANKL expression
CXCL10	C-X-C motif chemokine ligand 10	10.155	1.25E-16	recruit Th1 cells into RA ST
C15orf48	chromosome 15 open reading frame 48	9.887	5.55E-21	protein coding

Figure A4.2: Top 10 DE genes based on comparison of RNA-seq data between TNF-α and NP treated cells (RA-TNF/NP), and TNF-α treated (RA-TNF) RA-FLS cells.

Gene	Description	Log2 FC	FDR	Type(s)
Top 10 top-regulated genes				
SERPINB2	serpin family B member 2	10.458	5.3E-118	other
MRGPRX3	MAS related GPR family member X3	-9.952	1.03E-15	G-protein coupled receptor
TLR2	toll like receptor 2	-9.64	1.1E-14	transmembrane receptor
HSPA6	heat shock protein family A (Hsp70) member 6	9.603	1.32E-19	enzyme
IL36B	interleukin 36 beta	9.366	3.25E-14	cytokine
HSPA7	heat shock protein family A (Hsp70) member 7	9.241	1.78E-13	other
CX3CL1	C-X3-C motif chemokine ligand 1	-9.204	2.14E-292	cytokine
FOXI1	forkhead box I1	-9.128	4.9E-13	transcription regulator
NOS2	nitric oxide synthase 2	-8.597	1.78E-11	enzyme
ANO9	anoctamin 9	-8.584	1.35E-15	ion channel

Figure A4.3: Top 10 DE genes based on comparison of RNA-seq data between NP treated (RA-NP), and untreated (RA-UT) RA-FLS cells.

Gene	Description	Log2 FC	FDR	Type(s)
Top 10 top-regulated genes				
MMP3	metalloproteinase 3	8.826	2.02E-24	peptidase
RPS4Y1	ribosomal protein S4, Y-linked 1	8.195	6.05E-14	other
NLGN4Y	neuroligin 4, Y-linked	7.446	1.27E-08	enzyme
ZFP	zinc finger protein, Y-linked	7.150	2.85E-07	other
MMP1	metalloproteinase 1	7.148	2.81E-271	peptidase
TXLNGY	taxilin gamma pseudogene, Y-linked	7.002	1.78E-13	other
IL1RN	Interleukin 1 receptor antagonist	6.783	4.89E-08	cytokine
LINC-PINT	long intergenic non-protein coding RNA, p53 induced transcript	6.532	1.94E-09	other
TFPI2	tissue factor pathway inhibitor 2	6.521	1.14E-49	other
DDX3Y	DEAD-box helicase 3, Y-linked	-8.597	2.25E-12	enzyme

Figure A4.4: Log2FC and FDR values for candidate signalling genes in RA-FLS treated groups.

		RA-TNF vs RA-UT		RA-TNF/NP vs RA-TNF		RA-NP vs RA-UT	
Gene	**Name**	**Log2FC**	**FDR**	**Log2FC**	**FDR**	**Log2FC**	**FDR**
AKT1	Serine/threonine-protein kinase	0.6319	8.01E-15	0.1771	0.0481	0.3764	1.11E-05
SOCS4	Suppressor of cytokine signaling 4	0.2855	0.0292	0.2726	0.0337	0.0372	0.8433
STAT3	Signal transducer and activator of transcription 3	0.5900	4.93E-15	-1.7089	5.65E-112	-0.5846	7.23E-14
STAT1	Signal transducer and activator of transcription 1	0.5610	0.0002	-1.3746	4.92E-22	-0.7473	5.69E-07
JAK2	Janus kinase 2	1.4219	2.29E-26	-2.3457	2.58E-63	-0.2986	0.0744
JAK3	Janus kinase 3	3.3021	1.31E-59	-4.8323	3.74E-70	-0.6367	0.0381
TLR2	Toll like receptor 2	7.6736	1.94E-12	-9.6404	1.10E-14	-1.9213	0.3674
TLR3	Toll like receptor 3	0.1570	0.3186	-3.1333	1.18E-69	-1.0438	3.05E-14
TLR4	Toll like receptor 4	-1.2391	5.14E-18	-1.3763	2.87E-17	-1.0557	1.21E-13
RXRB	Retinoid X receptor B	-0.3404	0.1780	0.1401	0.6397	-0.0915	0.7657
RXRA	Retinoid X receptor A	-0.0426	0.7933	-0.2269	0.0781	-0.2444	0.0582
RXRG	Retinoid X receptor G	-0.1062	0.9694	-2.2083	0.4417	-3.2309	0.1239
LXR-a	Liver X receptor	-0.5896	0.0223	0.1842	0.5692	-1.5676	1.20E-09
LXR	Liver X receptor	0.5326	0.0002	0.0677	0.7248	0.1425	0.4385
PPARA	Peroxisome proliferator-activated α	1.1205	1.06E-29	-0.4717	2.03E-06	0.0993	0.4822
PPARG	Peroxisome proliferator-activated ɣ	1.0725	4.14E-06	-1.7309	8.44E-13	0.4007	0.1532
PPARD	Peroxisome proliferator-activated δ	0.5348	4.74E-05	1.4956	8.29E-37	0.5789	1.08E-05

Figure A4.5: Log2FC and FDR values for candidate endocannabinoid synthesis and degradation genes in RA-FLS treated groups.

		RA-TNF vs RA-UT		RA-TNF/NP vs RA-TNF		RA-NP vs RA-UT	
Gene	**Name**	**Log2FC**	**FDR**	**Log2FC**	**FDR**	**Log2FC**	**FDR**
NAT	N-acyltransferase 1	-0.5824	0.0807	0.1707	0.6881	0.0604	0.8923
ABHD4	α/β-hydrolase domain 4	-0.7182	3.56E-16	-0.2895	0.0034	-0.1495	0.1451
NAPEPLD	N-acyl phosphatidylethanolamine-specific phospholipase D	-0.6701	1.25E-06	0.3250	0.0341	-0.2711	0.0656
GDE1	Glycerophosphodiesteras	-0.6449	1.88E-19	0.1571	0.0597	-0.6327	4.07E-19
FAM213B	Family with sequence similarity 213 Member B	-0.2202	0.2478	1.4201	4.71E-23	0.6736	5.48E-06
PTPN22	Non-receptor protein tyrosine phosphatase 22	-0.1481	0.5042	2.3253	5.09E-56	1.1179	1.28E-13
PLCG1	Phospholipase C gamma	0.1122	0.3653	0.4418	6.73E-06	0.2110	0.0584
PTGES2	Prostaglandin E synthase 2	0.5400	0.0003	0.5593	3.33E-05	0.4348	0.0046
COX2	Cyclooxygenase-2	6.8501	0	-0.1832	0.0550	3.5068	1.38E-164
CP450	Cytochrome P450 monooxygenases	-0.3344	0.8340	2.3979	0.0194	2.8107	0.0013
LOX	Lipoxygenase	-2.2046	2.84E-179	-1.9594	7.30E-128	-0.4505	2.52E-08
FAAH	Fatty acid amide hydrolase	-0.6481	0.3064	0.0153	0.9847	-0.6813	0.2776

APPENDIX 5: NP regulation of main signalling pathways regulated in RA in FLS cells

Red - upregulated genes, green - down regulated genes; blue - pathway is predicted to be downregulated, orange – pathway predicted to be upregulated.

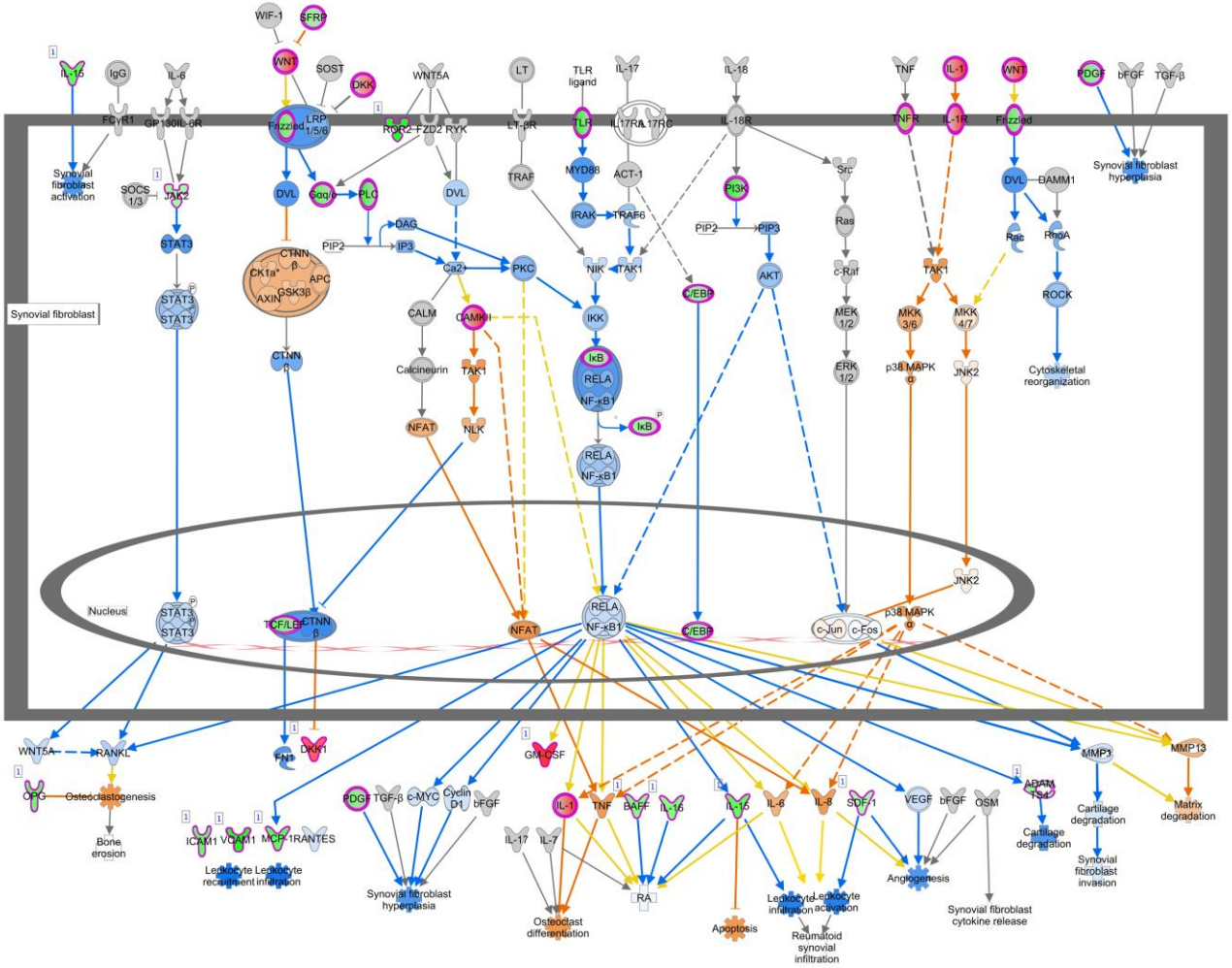

APPENDIX 6: **Analyte curve information**

Figure A6.1 LEGENDplex™ Rat Th Cytokine Panel (13-plex), Analyte curve information.

Analyte	CV	R2	Slope	Intercept	MinDC	MaxDC	Fit State	Fit Formula
A4.IL-10	0.71%	0.99	0.49	3.62	4.07	85576	Good	4-P.log(6.10, 9.01, 0.67, 8.06)
A5.IFN-Y	0.15%	1	1.28	0	1.18	314433	Good	4-P.log(6.20, 11.27, 1.01, 7.24)
A6.CXCL1/KC	0.2%	1	1.62	0	1.92	165502	Good	4-P.log(6.18, 11.92, 1.13, 6.45)
A7.CCL2/MCP	0.29%	1	1.62	0	1.79	182389	Good	4-P.log(6.18, 11.72, 1.17, 6.57)
A8.TNF-α	0.83%	1	1.59	0	2.61	68229	Good	4-P.log(6.18, 11.85, 1.12, 5.80)
A10.GM-CSF	0.27%	1	1.19	0.81	2.53	236495	Good	4-P.log(6.30, 11.71, 0.88, 6.87)
B2.IL-18	0.42%	1	1.14	1.87	1.72	173683	Good	4-P.log(6.36, 12.23, 0.78, 6.49)
B3.IL-12p70	0.39%	1	1.43	0	1.94	157889	Good	4-P.log(6.19, 12.55, 0.90, 7.01)
B4.IL-1B	1.28%	0.99	1.52	0	2.92	47875	Good	4-P.log(6.23, 11.16, 1.23, 5.89)
B5.IL-17A	0.64%	1	1.57	0	2.17	126716	Good	4-P.log(6.25, 12.66, 0.98, 7.25)
B6.IL-33	0.36%	1	1.06	1.03	1.89	153237	Good	4-P.log(6.55, 12.16, 0.75, 7.85)
B7.IL-1a	0.61%	1	1.63	0	2.36	107813	Good	4-P.log(6.51, 12.35, 1.12, 7.49)
B9.IL-6	0.47%	1	1.01	0.4	1.91	155264	Good	4-P.log(6.59, 12.05, 0.74, 8.87)

APPENDIX 7: Clinical application of nanotherapeutic agents in arthritic diseases

Figure A7.1 Current nanocarrier system in the treatment of rheumatoid arthritis. Table taken from (Chuang et al., 2018)

Therapeutic Classification	Drugs/Agents	Nanocarrier System	Mean Size (nm)	Delivery/Target	Model	Reference
NSAIDs	Indomethacin	Polymeric micelles	240	EPR	AIA	(Bernardi et al., 2009)
	Aceclofenac	Lysine-liposomes	-	EPR	AIA	(Sharma et al., 2017)
	Indomethacin	Folate-PEG-PAMAM dendrimer	<100	Folate receptor (macrophages)	Patients	(Chandrasekar et al., 2007)
	Indomethacin	Lipid microspheres	150	EPR	AIA	(Suk et al., 2016)
Glucocorticoids	Dexamethasone	Liposomes	96	EPR	AIA	(Quan et al., 2014)
	Methylprednisolone	Cyclodextrin polymer	27	EPR	CIA	(Hwang et al., 2008)
	Dexamethasone	RGD-PEG liposomes	100	Endothelials	AIA	(Koning et al., 2006)
DMARDs	Methotrexate	Stealth-type polymeric NP	51–116	EPR	AIA	(Ishihara et al., 2009)
	Methotrexate	PEGylated liposomes	210–260	EPR	AIA	(Williams et al., 2000)
	Clodronate	Liposomes	120–160	Macrophages	AIA	(Barrera et al., 2000)
Biological agents	Etanercept	TMN complex	250	EPR	CIA	(Jung et al., 2013)
	Anakinra	Folate-chitosan DNA nanoparticles	110	Macrophages	AIA	(Fernandes et al., 2008)
	Tocilizumab	Hyaluronate-gold NP	64	IL-6R$^+$ cells	CIA	(Lee et al., 2014b)

Therapeutic Classification	Drugs/Agents	Nanocarrier System	Mean Size (nm)	Delivery/Target	Model	Reference
Others inhibitor	γ-secretase inhibitor	Hyaluronan NP	255	Macrophages	CIA	(Heo et al., 2014)
	Fumagillin	Perfluorocarbon nanoparticle	250	$\alpha_V\beta_3$ integrin activated cells	K/BxN mouse model	(Zhou et al., 2009)

AIA: adjuvant-induced arthritis; CIA: collagen-induced arthritis; EPR: enhanced permeability and retention; PEG-PAMAM: poly(ethylene glycol) conjugates of anionic dendrimer; RGD-PEG: RGD peptide-polyethylene glycol; TMN: temperature-modulated noncovalent interaction.

Figure A7.2 Clinical application of nanotherapeutic agents in arthritic diseases. Table taken from (Chuang et al., 2018)

Patent	Lipid Nanocarrier	Advantage Function
US 20150174069 A1	Dexamethasone sodium phosphate liposome	There is about a 10% reduction in one or more symptoms of arthritis
WO 2003000190 A2	Glycosaminoglycans liposome	It provides good efficacy in treatment of osteoarthritis
CN 104688721 A	Paclitaxel liposome	The gel achieves a treatment effect and pain of a patient suffering from RA
US 20090232731 A1	Cationic liposome	It provides reduction of the infiltration of mononuclear cells into the synovial tissue, pannus development and cartilage erosion
US 20160000714	Curcumin solid lipid particles	It provides suppression of cyclooxygenase 2 (COX-2) expression
WO 2017025588 A1	Cyclosporine solid lipid particles	It prevents transcription of interleukin 2, thereby decreasing activation and proliferation of T lymphocytes.
US 8715736 B2	Nanostructured Lipid Carriers	It provides efficient skin permeation at the inflammatory site in RA
CN 102225205 B	Tripterine nanostructured lipid carrier	It provides inhibition of rheumatoid arthritis inflammation